CONDITIONS REQUIRED FOR SPINNING CONTINUOUS FIBRES FROM CELLULOSE NANO-FIBRILS.

ZURINE HERNANDEZ

A thesis submitted in partial fulfilment of the requirements of Edinburgh Napier University, for the award of Doctor of Philosophy.

Forest Product Research Institute

School of Engineering and the Built Environment

Edinburgh Napier University

Edinburgh, Scotland, United Kingdom

March 2012

ABSTRACT

The thesis describes a programme of work to develop a novel cellulose based fibre. The most important innovative step in this work lies in the manufacture of the fibre from a chiral nematic suspension of plant based cellulose nano-fibrils. In the course of the project a number of key steps have been addressed in the development process. These included:

- Developing a method for extraction of nano-fibrils from wood and cotton based pulp and filter paper;
- Development of concentrated chiral nematic suspensions of the nano-fibrils suitable for extrusion (spinning);
- Spinning a continuous fibre or filament;
- Fibre characterization.

A key objective of the work was to understand the factors that could contribute to nematic order of the nano-fibrils in the fibre and produce a high strength fibre.

The fibres developed showed reasonably good strength potential and good stiffness properties with the best fibres having a tenacity of between 40 and 100 cN/tex and an initial modulus of 5000-6000 cN/tex. These values fall midway between lyocell and Kevlar. Two patents have to date been published based upon the developments described in this work (Turner *et al.,* 2010, 2011). However, the work highlighted a number of gaps in current knowledge that prevented development of the full potential strength properties of these fibres. These included:

- Incomplete knowledge of the gel conditions required to achieve complete alignment of the fibrils in the spinning process;
- Challenges in being able to draw the fibre sufficiently during spinning to produce target fibre diameters of 5-10μm;
- The linear density of the spun fibres had a key impact on fibre strength. It was only when linear density values dropped below 1 tex (1g/km) that a significant increase in fibre strength occurred. Factors that had an important impact on linear density included solids content of the suspension, zeta potential, extrusion

rate and fibre drying temperature. All these factors relate directly to the mobility of the cellulose nano-fibrils and their subsequent ability to align under flow during spinning.

The thesis can be seen as a first phase in an ongoing process to develop a new approach to the manufacture of cellulose based industrial textile fibres.

DECLARATION OF THE AUTHOR

I hereby declare that the research activities carried out at Edinburgh Napier University over the course of this project were unless stated in the text developed and coordinated by me. Due to the extent and scale of the project it was impossible for one person to carry out all the technical work. In a number of cases, once I had developed and refined a technique then a member of the technical support team was delegated the responsibility to generate the base data. I would like to acknowledge the contribution of a number of technical staff who assisted in the development of data in the following activities:

- Hydrolysis, washing, centrifugation and tubing work;
- Sample analysis (solids content, zeta potential, acid group content, pH and particle size distribution);
- Scanning Electron Microscope pictures;
- Three roll mill mixing;
- Water conductivity;
- Fibre testing.

All fibre spinning activities were carried out by myself with the help and support of my director of studies Philip Turner.

Simon Turner took an important lead in developing the phase behavior studies. Although I was involved through the coordination of this work I do not claim this work as my own, but it was included in the thesis as it formed an important, integral part of the overall study.

…….
ZURINE HERNANDEZ (Candidate)

……..
Date

ACKNOWLEDGEMENTS

It is a pleasure to thank the many people who made this thesis possible.

First and foremost I offer my sincerest gratitude to my Director of studies, Dr. Philip Turner for his active support, constructive guidance, technical advice and his personal assistance during this research. I am most grateful to the opportunity he offered me with this project. I attribute the level of my Thesis degree to his persistent encouragement and effort and without him this thesis would not have been completed or written. One simply could not wish for a better supervisor.

The author is grateful to Edinburgh Napier University and especially to Alan Davidson as director of the Advanced Material Centre for the use of the specialized equipment needed to conduct this investigation when this project was only a dream. Furthermore, I am grateful for the assistance I have received from the technician Bill Brownlee and his practical know-how.

Thanks are due to Professor Callum Hill, Tom Dobbie and the technical staff: Andrea Lavado, Sarah Jarvie, Holly Allan, Dominic O'Rourke, Tommaso Locatelli, Dongyang Sun, Sheila Patrick and Stephen McClatchy for their great assistance and their effort that have contributed to the project and have made my time happier in the university.

Thanks to Edinburgh Napier University for sponsoring my research studies. Thanks also go to Sappi and Edinburgh Napier University for the broader research funding for this project.

This research would not have happened without the love and support of my family, especially to my parents, Mr. Rafael Hernandez and Mrs. Lucia Garcia and my brother Mr. Unai Hernandez for the unconditional encouragement throughout my years living far from them. Feeling that they were always there made me feel safe to move confident through this time, for this I am truly grateful. They have been, always, my pillar, my joy and my guiding light, and I thank them. I would like to express my deepest gratitude to my partner Mr. Eneko Zaldibar for his unfailing patience and kindness, who has given to me strength when I needed it and for being the best!

Thanks to all the friends that have been along with me during all this time and have shared with me the experience of the PhD and living in Scotland. Many thanks to Andres, Gracia, Naren and Smuga.

Finally, I would like to thank my office colleagues, Natalie Wager, Aamir Muhammad and Zaihan and I wish you all the best in your present studies and future careers.

TABLE OF CONTENTS

TABLE OF FIGURES

LIST OF TABLES

GLOSSARY

Aspect ratio: of a particle describes the proportional relationship between its width and its height.

Bohemite: a soft, orthorhombic mineral, hydrous aluminum oxide, AlO(OH) that is a chief component of some bauxites.

Chitin: A tough, protective, semitransparent polysaccharide forming the principal component of arthropod exoskeletons and the cell walls of certain fungi.

Crossover strain rate: If a Maxwell viscoelastic model is used, the crossover strain rate is equal to the reciprocal of the average relaxation time and is related to the weight average molecular weight of the polymer molecules.

Degree of polymerisation (DP): The number of structural units in the average polymer molecule in a particular sample.

Die swell: When a spinning solution is forced out of a spinneret at high pressure, it has a tendency to increase in diameter since it is no longer constrained circumferentially. This increase in diameter is called die swell and the amount by which this occurs is related to the viscosity of the solution, the *relaxation time* and flow rate.

Dry (jet) spinning: The fibre is extruded from the die into an air gap. If the fibre then passes into a liquid coagulation bath, this is referred to as dry-jet wet spinning.

Hencky strain (ε_h): The Hencky strain is defined as $\ln(L/L_o)$ where L is the final length of the sample whose original length is L_o.

Herman's orientation factor (f_c): This describes the orientation of polymers with respect to the fibre axis. A value of 1.0 represents perfect orientation, and a value of zero is random orientation.

Maxwell viscoelastic model: The Maxwell model is represented by the linear connection of a spring and damper in series.

Mercerised cellulose: Mercerisation alters the chemical structure of the cotton fibre. The structure of the fibre inter-converts from alpha-cellulose to a thermodynamically more favourable beta-cellulose polymorph. Mercerising results in the swelling of the cell wall of the cotton fibre. This causes increase in the surface area and reflectance, and gives the fibre a softer feel.

Molecular weight: Molecular weight is a measure of the sum of the atomic weights of the atoms in a molecule. It is the ratio of the mass of that molecule to 1/12 of the mass of carbon-12 and is a dimensionless number.

Molecular weight is often used interchangeably with molecular mass in chemistry, but there is a difference between the two. Molecular mass is a measure of mass and molecular weight is a measure of force acting on the molecular mass.

Persistence length: A property of rigid rod molecules in a lyotropic solution or suspension. In the molecular context, as the length of the molecule increases, it will inevitably exhibit some ability to distort. The persistence length is the effective rigid length of the molecule.

RCF: Relative Centrifuged Force. This value is used as an alternative expression to that of revolutions per minute (r.p.m.) as it also takes into consideration the length of the rotor arm. An RCF value in one centrifuge is directly comparable to that in another centrifuge of a different size.

Regenerated cellulose: Cellulose obtained in a changed form by chemical treatment (as of a cellulose solution or derivative)

Relaxation time: Rod-like molecules or crystallites can be aligned by shear, elongation, or some other force. When the aligning force is removed, the rods will return to an equilibrium state. The time taken for this to occur is the relaxation time.

Shear rate: The rate of change of shear strain per unit time (unit s^{-1})

Shear strain (γ): Relative deformation in shear, often abbreviated to shear.

Spin draw ratio, draw down ratio (DDR), or draw ratio: A fibre or film can be stretched immediately after formation. In fibre formation the ratio between the velocity of the fibre jet exiting the spinneret to the velocity of the fibre take up on the spool is the draw down ratio. Where DDR is greater than 1, there is an extensional stress on the fibre, which can aid molecular alignment.

Thixotropic: is the property of some gels that are thick under normal conditions but become thin when shaken, agitated, or otherwise stressed. They then take a fixed time to return to a more viscous state.

Trouton ratio: The ratio between the effective extensional viscosity and the shear viscosity at a strain rate equal to the shear rate and is a good measure of the deviation from Newtonian behaviour of a solution.

Wet spinning: The fibre exits from the spinneret and precipitation of the polymeric material occurs because of reaction with a liquid in a coagulation bath.

Dry spinning: The fibre exits from the spinneret and directly into a fibre drier.

1 INTRODUCTION

1.1 General

Wood fibres are constructed from a complex, multilayered composite of lignin and polysaccharides (Fig 1.1). High strength, crystalline cellulose nano-fibrils contribute stiffness and strength to the wood fibre in the form of a skeletal structure. It should be noted that crystalline cellulose whilst offering high levels of stiffness and strength is also a relatively brittle material, a constraint, which is resolved in a cell wall through the inclusion of amorphous polysaccharides, and lignin, which binds the cellulose skeleton together and creates a flexible structure.

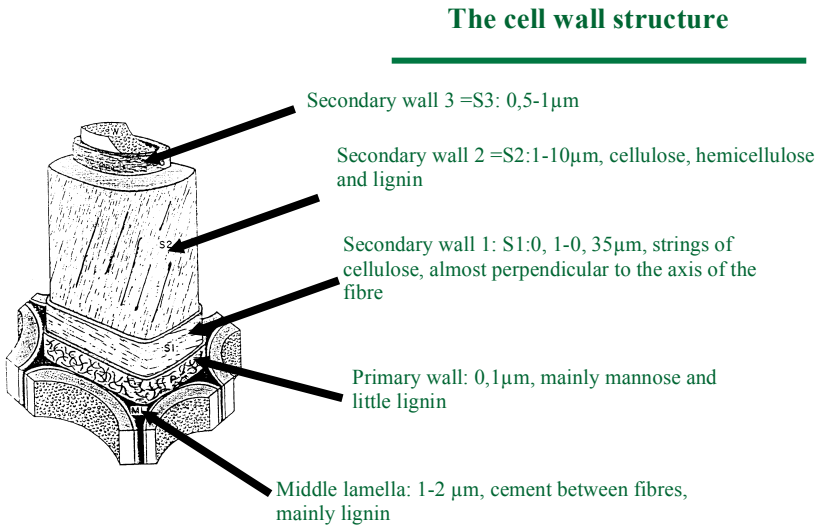

Figure 1.1: The cell wall structure.

Cellulose is an organic compound with the formula $(C_6H_{10}O_5)_n$, a polysaccharide consisting of a linear chain of several hundred to over ten thousand β(1→4) linked D-glucose units. The chemical structure of the cellulose is presented in Figure 1.2.

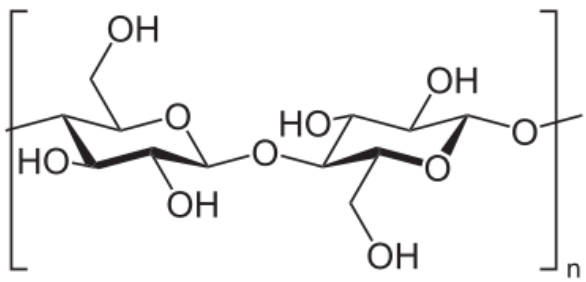

Figure 1.2: Cellulose chemical composition.

Cellulose is a straight chain polymer and the molecule adopts an extended and rather stiff rod-like conformation, aided by the equatorial conformation of the glucose residues. The multiple hydroxyl groups on the glucose from one chain form hydrogen bonds with oxygen atoms on a neighbouring chain, holding the chains firmly together side-by-side and forming "*crystallites"* or "*microfibrils"* with high tensile strength and stiffness. This strength is important in cell walls, where the microfibrils are meshed into a carbohydrate matrix, conferring rigidity to plant cells. Lignin is a complex polyphenolic compound, which forms an integral part of the cell walls of woody plants and trees. Lignin fills the spaces in the cell wall between cellulose, hemicellulose, and pectin components. It is covalently linked to hemicellulose and, therefore, crosslinks different plant polysaccharides, conferring mechanical strength and flexibility to the cell wall and by extension the plant as a whole.

Figure 1.3, which shows an image of a spruce fibre alongside an enlarged image showing the crystalline skeletal structure in the secondary wall (S2) after removal of amorphous polysaccharides and lignin.

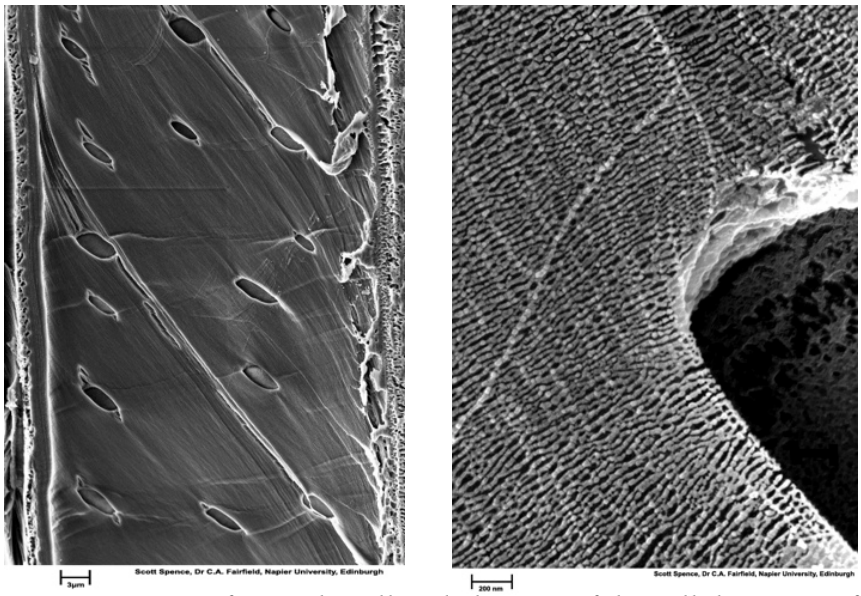

Figure 1.3: Images of a single cell and close up of the cellulose nano-fibril skeletal structure of the S2 layer after removal of amorphous polysaccharides and lignin.

It has been shown by a number of workers that it is possible to extract these high strength, natural "nano-fibres" from conventional Kraft and Sulphite pulps used for paper making and derivative products such as viscose and lyocell (Fig 1.4 shows an example of mechanical dissociated cellulose nano-fibrils).

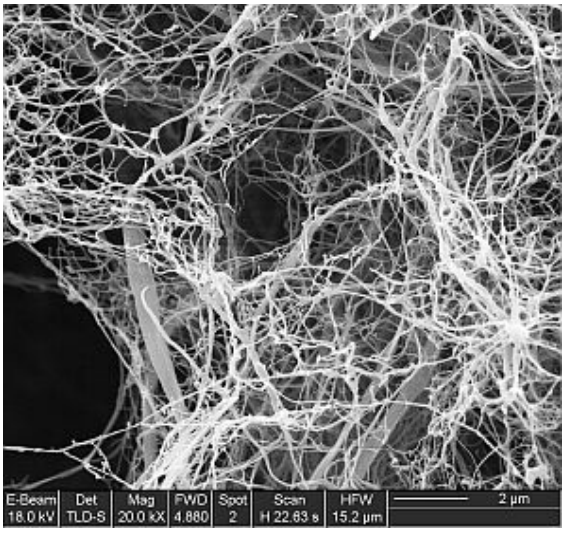

Figure 1.4: Dissociated cellulose nano-fibrils

Crystalline cellulose has a very high strength to weight ratio and thus appears to be an attractive resource for high performance materials. Table 1.1 shows comparative data on the stiffness and strength of cellulose compared with some alternate materials. Strength is almost double that of steel. When combining structural performance with the fact that cellulose is based on a renewable resource, the argument for investigating the potential of this material becomes compelling. In the first instance it makes sense to focus on high value markets such as automotive and aerospace industries. If successful, there should then be a number of spin offs in lower value industries as economies of scale and manufacturing costs in general decline.

Comparison of mechanical properties for cellulose versus other materials.		
Material	Strength, MPa	Stiffness, GPa
Cellulose crystal	7500	145
Aluminum	620	73
Steel	4100	207
Graphite	1700	250

Table 1.1: Commercially important materials (Eichhorn et al., 2001).

A relatively crude form of crystalline cellulose (microcrystalline cellulose or MCC) has been used for a number of small-scale non-structural applications within the pharmaceutical industry in drugs such as aspirin. In the last 3 years, researchers like Zimmermann *et al.,* 2004 have begun exploring the potential to incorporate crystalline cellulose fibrils (from wood and other plant material) in model materials in order to evaluate their strength potential. Until now, published studies (referred in more detail in the literature review) have been based upon thin films manufactured for academic study. No one has yet developed an industrial scale process to extract "intact" cellulose nano-fibrils and use them as building blocks in the manufacture of a new material. Until now, industrial chemical processes have focused on a complete breakdown of the chemical structure to molecular level and then re-engineered the molecular structure to form derivative materials such as viscose, lyocell, cellulose ethers or acetate.

The focus of this thesis lies in the development of a new fibre constructed from cellulose nano-fibrils. The end goal was to develop a fibre that could utilize the strength properties of crystalline cellulose through nematic alignment of all the fibres so that they could hydrogen bond together into a continuous crystalline structure. Such a film could theoretically have strength properties exceeding that of Kevlar, which is an organic fibre in the aromatic polyamide family with strength values of 200 cN/tex.

2 LITERATURE REVIEW

2.1 Introduction

This review forms part of a research programme to evaluate the potential to develop high strength continuous fibres from cellulose nano-fibrils. Prior work (*Pers. Com. By P. Turner*) has shown that under the right conditions, cellulose nano-fibrils can be induced to aggregate into substantial crystalline structures. Figure 2.1 indicates the structure of a typical cellulose structure in the S2 layer at 50 000 times magnification. The average diameter of the cellulose fibrils is of the order of 20 nm. Figure 2.2 (50 000 times magnification) indicates the structure of cellulose, which has aggregated after being mechanically milled with a hammer mill. The diameter of these crystalline structures is of the order of 1000 nm. The observation suggests that the high local pressure generated from the hammer mill was adequate to compress the cellulose fibrils together whilst simultaneously providing sufficient heat to overcome the latent heat of crystallization of cellulose (the quantity of heat liberated or absorbed per mol when a substance passes into the crystalline state) which as been determined as 25.8 cal/g and 27.4 cal/g by Calvet and Hermans (2003) and Dale and Tsao (1982) respectively.

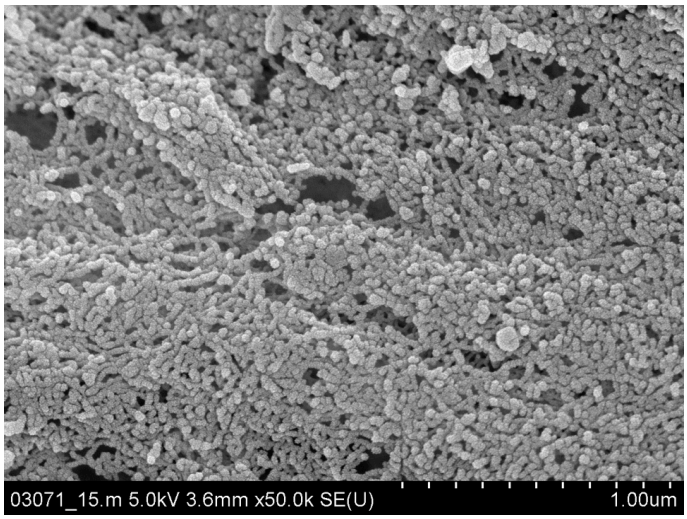

Figure 2.1: FEG-SEM image of cellulose structure in the S2 layer in its natural form at 50 000x magnification.

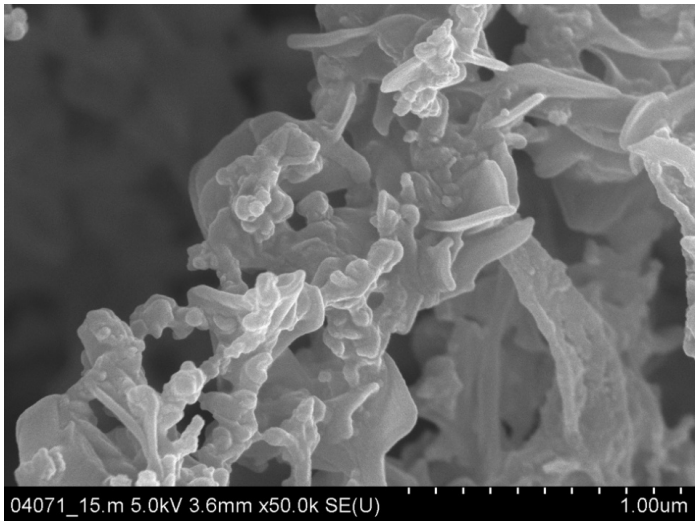

Figure 2.2: Cellulose aggregation after mechanical milling.

One of the objectives of the project was to understand the conditions required to replicate the aggregation process in a controlled way that will allow us to convert individual cellulose nano-fibrils into continuous crystalline fibre. In order to do this a hypothesis was developed that states it should be possible to exploit the lyotropic properties of colloidal suspensions of cellulose nano-fibrils and axially align fibres in a nematic phase to ensure maximum fibril interaction prior to crystallization and minimize defects in the macro fibre structure. Theory suggests that nematic order requires that the fibrils are of a rigid rod like structure with an aspect ratio of around 10 or higher (Donald *et al.,* 2002). If a nematic phase needs to be induced it is essential that the phase behaviour of the cellulose nano-fibril suspensions and conditions required to ensure fibril alignment are properly understood. In a further process step the right conditions in which the solvent can be removed from the suspension and ensure the fibres remain aligned to allow fibres to hydrogen bond together (crystallise) as effectively as possible, with minimum dislocations between the fibres, have to be understood and created. This requires a study of the various options available for fibre spinning and processing. The object of the current review was to identify prior research that could assist in forming the research programme, which was targeted at addressing the following:

- The most appropriate options for extraction of cellulose nano-fibrils;
- Study of their behaviour in colloidal suspensions;
- Identify the most appropriate approach to spin fibres in a way that would induce nematic order amongst fibrils within the spun fibre;

2.2 Extraction of cellulose nano-fibrils

Cellulose consists of linear β 1→4 linked glucose chains, which organize in a supramolecular structure. This supramolecular structure includes amorphous and crystalline regions (recent reviews include Krässig 1996, Atalla 1999, Hon and Shiraishi 2001). The crystalline regions are normally of the order of a few nano-meters (nm) in diameter but can be from 50 nm up to several micro-meters (μm) long. Because of their shape i.e. their high aspect ratio, they can be regarded as nano-fibres. The amorphous regions of the cellulose between fibrils are more accessible to acid hydrolysis. By the degradation of the amorphous regions with a suitable acid treatment it is possible to extract these nano-crystals in the form of independent fibrils. Acid hydrolysis has long been used in cellulose analysis to obtain the 'level-off degree of polymerisation (DP) as a measure for cellulose crystallinity (Davidson 1943, Battista *et al.,* 1956).

The size of the cellulose nano-fibres is strongly related to the size of the crystalline regions in the cellulose (Marchessault *et al.,* 1961, Battista 1975). It has been reported that the preparation conditions have only a minor influence on the size (Dong *et al*., 1998). Therefore the biomass source is important in influencing their characteristics (length, diameter, flexibility, etc.). Typical sizes of cellulose nano-cellulose nano-fibrils from different biomass sources are given in Table 2.1. It is worth noting that a number of published sources of cellulose such as nano-fibrils like Tunicin are obtained from rather exotic organisms, which make them expensive and only available in small amounts. However, they do have a very high aspect ratio, which makes them useful as model fibres for research purposes.

Cellulose nano-whisker source	**Size [nm]**	**Reference**
Valonia	20 x (100-2000)	Sugiyama *et al.,* 1984, Hanley *et al.,* 1992, Imai *et al.,* 1998
Micrasterias denticulata	5 x (60-80) x several 1000	Kim et al 1996, Hanley *et al.,* 1997
Cladophora *sp.*	40 x 4000	Nishiyama *et al.,* 1997
Bleached softwood Kraft pulp Bleached spruce Kraft pulp	(3-5) x 180 ± 75 5 x 6 x 180-280	Araki *et al.,* 1998 Orts *et al.,* 1998
Whatman CF11 cellulose powder	(5-10) x (100-150)	Araki *et al.,* 2000
Sulphite pulp (acetylation grade) Dissolving pulp	7.4 x 46.0 n.d.	Rånby 1951 Edgar and Gray 2001, 2003

Cotton filter paper (Whatman No. 1)	7 x (100-300, diameter 115)	Dong *et al.,* 1997, 1998
	~17 x 170	Ebeling *et al.,* 1999
	10 x 200 ± 70	Fleming *et al.,* 2000
	15 x 255	De Souza Lima *et al.,* 2003
Cotton linters	2-5 diameter; L/d 20-100	Sassi *et al.,* 1997
Tunicin (*Microcosmus fulcatus*)	(10-20) x (100 - several 1000)	Favier *et al.,* 1995
Tunicin (*Halocynthia roretzi*)		
	16 x 1160	De Souza Lima *et al.,* 2003
	d: 8.8 x 18.2 x 1000	Sugiyama *et al.,* 1992, Terech *et al.,* 1999, Goussé *et al.,* 2002
Sinapis alba	(3-4) x (300-4000, d1200)	Sprey and Bochem 1991

Table 2.1: Dimensions of cellulose nano-fibrils from different sources (n.d.: no details given).

Chitin is another alternative resource for polysaccharide nano-fibres (Marchessault *et al.,* 1959). Their sizes are also primarily dependent on the organism from which they are prepared. They vary between 15 nm (length) x 240 nm (diametre), 10 nm x 150 nm and 18 nm x 2200 nm for crab shell (Gopalan Nair and Dufresne 2003a), squid pen (Paillet and Dufresne 2001) and Rifita (Morin and Dufresne 2002), respectively. It has been demonstrated that they have similar properties to those from wood (Li *et al.,* 1996, 1997, Gopalan Nair and Dufresne 2003b, Gopalan Nair *et al.,* 2003).

Since work on the extraction of cellulose nano-fibrils from wood and other plant materials was first published in the late 1940's the number of papers on the subject has proliferated. However, most processes described, are variants on a relatively small number of themes. This current review focuses on those key processes that have been described and could assist in achieving the goals of the project. The review identifies the most appropriate approach for the proposed work in the extraction and further processing of cellulose nano-fibrils into continuous fibre.

The literature differentiates the extraction of cellulose nano-fibrils into two key approaches. The first involves chemical treatment of various plant fibres through acid hydrolysis. The earliest work led to the development of what is termed microcrystalline

cellulose (MCC). MCC typically has an aspect ratio of about 3 and is widely used as a rheology control agent and as a binder in the pharmaceutical industry. Hydrolysis under the right conditions however, can lead to cellulose nano-fibrils with improved aspect ratios of between 10 and 100. It is this category of fibrils that have been found to have stable liquid crystal properties in suspension. This approach formed the focus of the current research. The second approach to the extraction of cellulose nano-fibrils involves the use of mechanical processes. These processes produce what is commonly referred to as microfibrillated cellulose (MFC). MFC has an aspect ratio ranging from 50 to 1000 and is extensively investigated for its reinforcing potential in composite materials (Janardhnan and Sain 2006). This approach is reviewed for the purpose of background and explains why it was unsuitable for the type of product envisaged in this thesis.

2.2.1 Acid hydrolysis extraction of cellulose nano-fibrils and their behaviour in colloidal suspension.

The glycosidic linkage in cellulose (Fig. 1.2) is susceptible to acid-catalyzed hydrolysis under suitable conditions. The mechanism of the reaction (Fig. 2.3) comprises three stages: rapid protonation of the glycosidic oxygen atom, slow transfer of the positive charge to C-1 with consequent formation of a carbinium ion and fission of the glycosidic bond, and rapid attack on the carbonium ion by water to give the free sugar residue and to re-form the hydroxonium ion. The second stage is rate-determining, which means that the ease with which the carbonium ion (I) can be formed influences the overall rate of the reaction.

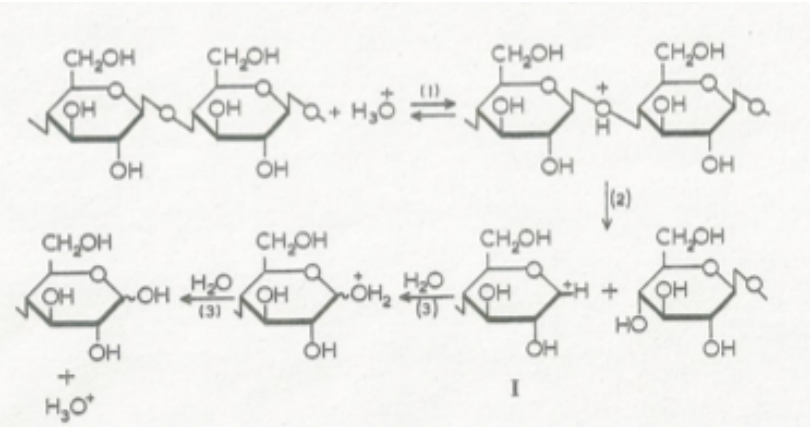

Figure 2.3: The diagram shows where acid cleavage and where sulphate groups attaches. (Nevell and Zeronian, 1985)

In practice, the hydrolysis process is not random but preferentially targets amorphous, rather than crystalline regions of cellulose, which are more accessible. Figure 2.4 shows how the crystalline regions are connected to each other by amorphous regions (A, B and C). As the acid attacks these amorphous regions, the individual crystalline regions (crystalline nano-fibrils) are released into suspension.

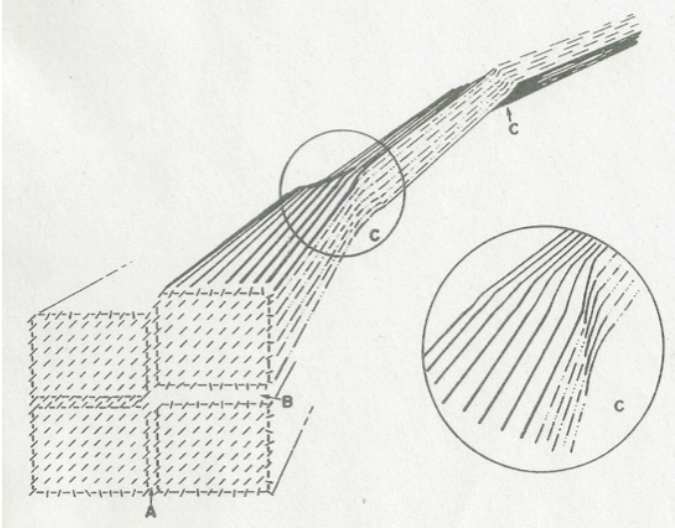

Figure 2.4: A schematic representation of the elementary fibril, (A) coalesced surfaces of high order, (B) readily accessible disordered surfaces, and (C) readily accessible surfaces on strain-distorted, tilt-twist regions. (Nevell and Zeronian, 1985)

In addition to the acid cleavage reaction, which occurs with acids such as sulphuric acid and hydrochloric acids, sulphuric acid also interacts in an esterification reaction (usually with the C6 carbon) to form a $-CH_2-OSO_3^-$ group resulting in a charged glucose unit. When this reaction occurs across the surface of a nano-fibril, a charged fibril results. This electrical charge is measured as zeta potential of the nano-fibril suspension, with increasing levels of esterification leading to increasing electrical charge and increasing levels of repulsion between fibrils within the suspension. Zeta potential thus has an important impact on the stability of the colloidal suspension of cellulose nano-fibrils. Apart from the level of esterification, zeta potential can be controlled by the addition of counterions such as calcium chloride to the bulk suspension. This approach is discussed in Section 9.6.3. However as discussed in Section 11.2.1 challenges were observed in controlling the zeta potential precisely, due to the unstable nature of the suspension.

Unlike sulphuric acid, in the case of HCl hydrolysed cellulose, no further reaction takes place after cleavage, resulting a neutrally charged suspension of nano-fibrils. The lack

of charged particle prevents the formation of stable liquid crystal colloidal suspensions. This issue is discussed in more detail in Section 9.6.

When considering the characterisation of the cellulose after hydrolysis to determine the extent of breakdown into individual fibrils, a number of techniques can be applied. The most common qualitative tool used throughout this thesis was electron microscopy (Rånby, 1949; Rånby and Ribi, 1950; Rånby 1951). However, a number of additional quantitative analytical tools are referred to in the literature review. The most commonly used tools include X-ray diffraction (Ingersol, 1946, Howsmon, 1949) and Solid State NMR (Larsson *et al.*, 2007).

Rånby and Ribi (Rånby, 1949; Rånby and Ribi, 1950; Rånby 1951) were the first to produce stable colloidal suspensions of cellulose crystals by sulphuric acid hydrolysis of cellulose fibres. Electron microscope images of the dried suspensions showed rod like structures of the order of 50-60nm long by 5-10 nm wide. Electron diffraction from the rods demonstrated that they had the same crystal structure as the original fibres (Rånby 1951). Development of the acid degradation of cellulose by Battista (1950) and Battista *et al.* (1961) using hydrochloric acid led to the production of MCC (Most grades of MCC are made using hydrochloric acid) and led to industrial scale applications for example in the pharmaceutical (Johansson *et al*., 1995, Westermarck *et al.,* 1999) and food industry (McClements and Demetriades 1998). The size of MCC particles is in the range of 1 micron (O'Neil *et al.*, 2003) because single nano-crystals are not completely dissociated. Aspect ratio is not highlighted as of great importance for MCC, but by a suitable mechanical treatment (e.g. sonification) MCC can be further degraded to separate out single nano-cellulose nano-fibrils (Rånby, 1951). Only recently a procedure to prepare ultra fine MCC in the range of 0.1 micron was patented (Colliopoulos *et al.,* 1998) but even here aspect ratio was not highlighted as of major importance.

The paper by Battista (1950) included a review of earlier work. A number of important observations, which are particularly relevant to the current project, are summarised below:

Battista and Coppick (1947) demonstrated that on prolonged mild hydrolysis, the basic degree of polymerisation (DP) of most native cellulose structures tended to level off at

much higher values (225 to 275) than was the case for regenerated cellulose structures (40 to 80). Under relatively mild sulphuric acid hydrolysis conditions, Nickerson and Habrle (1947) noted differences in the limiting D.P. values for native, mercerised and regenerated cellulose, respectively and suggested that the levelling-off DP on drastic hydrolysis might correspond to the average crystallite length. Roseveare *et al*. (1948) suggested that the limiting DP on hydrolysis of regenerated cellulose might correspond to the average length of a chain passing through one crystalline and one disordered region. On the basis of X-ray data, Ingersol (1946) proposed that relatively mild hydrolysis might cause the crystallisation of cellulose chains simultaneously with chain splitting. Howsmon (1949) published moisture regain, weight loss and X-ray data, showing that the drop in moisture regain and the sharpening of the x-ray diagram could not be explained by the very small loss in weight, due presumably to the removal of amorphous cellulose. Howsmon compared physical and chemical methods for characterising cellulose fine structures and proposed that hydrolytic methods give high values for the crystallinity of cellulose because additional crystallisation of the chains occurs on hydrolysis.

Brenner *et al.* (1948) came to a similar conclusion on the basis of specific volume and density measurements made on hydrolyzed cellulose. In later work, using improved x-ray techniques to follow changes in crystallinity on hydrolysis, Hermans and Weidinger (1949) obtained data to confirm further the belief that with regenerated cellulose, crystallisation of the cellulose occurs simultaneously with chain splitting on acid hydrolysis.

This background work was followed up by Battista (1950) who highlighted the importance of time, temperature and acid concentration of the hydrolysis of the fine structures of both native and regenerated cellulose. Comprehensive data on weight loss and degree of polymerisation were obtained for a wide variety of celluloses, which were subjected systematically to hydrolysis under mild and drastic hydrolysing conditions.
Combined data on weight loss and degree of polymerisation demonstrated that the mechanism of crystallisation and hydrolysis are interdependent. It was suggested that conditions of mild hydrolysis, during which 1, 4 glycosidic bonds are split at a relatively slow rate, favour the formation of longer, less acid-soluble crystallised material. Drastic conditions of hydrolysis, on the other hand promoted the formation of very short, more acid-soluble crystalline material.

A mechanism was proposed to explain these findings that could have important implications for this work. Under relatively mild hydrolysis conditions, only a small number of 1, 4 glycosidic bonds of the accessible cellulose chains are split per unit time. This makes crystal growth possible, and longer segments of cellulose chains in the amorphous phase of the fine structure can "crystallise" before further chain splitting takes place, giving rise to a progressively less accessible fine structure, which is resistant to further hydrolysis. However, when hydrolysis conditions are drastic, the splitting of the 1, 4 glycosidic bonds proceed so rapidly that only very short segments of cellulose chains are available for crystallisation. Battista submitted the hypothesis that the solubility of short-chain crystalline areas, formed simultaneously with drastic hydrolysis should be greater than under mild hydrolysis conditions and that this would explain the larger loss in weight that was observed.

Mukherjee and Woods (1953) described a method of preparing an aqueous suspension of cellulose crystallites by hydrolysis using strong sulphuric acid (952 gm./l.) at 30 or 40°C for 24 hours. This method has become a standard for most work on the preparation of cellulose nano-fibrils using sulphuric acid although subsequent workers have moved towards shorter hydrolysis times with varying temperature and acid concentration combinations.

In 1959 Marchessault *et al.*, used the approach of Mukherjee and Woods (1953) to produce a suspension of crystallite particles from 20g of purified chitin from crab shells using 750 ml of 2.5 N hydrochloric acid under reflux for 1 hour. The resulting sediment was then passed through a homogenizer. From this treatment, a stable isotropic suspension was obtained. Electron micrographs of the stable suspension illustrated the presence of rod-like particles. Analysis of suspensions using a polarising microscope at concentrations of 13-15 % indicated birefringence suggestive of an ordered liquid crystal phase. In the presence of salts this concentration was still greater.

In 1961 Battista *et al.* issued a patent for the purification of cellulose, which resulted in the production of a stable dispersion of cellulose crystallites, which could be used to produce continuous film on glass or a thixotropic gel above 3% cellulose suspensions. Hydrochloric acid was chosen as the preferred acid as it produced crystallites of high purity that are readily washed free of acids. It was found that the yield with sulphuric

acid was as much as 30% lower than with hydrochloric acid under comparable conditions. Battista claimed that sulphuric acid was less desirable than hydrochloric acid because it tends to produce sulphated cellulose crystallites with up to 2% sulphur being introduced. It was noted that the sulphated cellulose crystallites were relatively difficult to free of excess acid.

Since the work by Battista, workers have reported a number of different approaches to the extraction of cellulose nano-fibrils from a variety of sources, including bacterial cellulose (Araki and Kuga, 2001; Roman and Winter, 2004), microcrystalline cellulose (Araki *et al.*, 1999), sugar beet primary cell wall cellulose (Dinand *et al.*, 1999), cotton (Dong *et al.*, 1998), tunicate cellulose (Favier *et al.*, 1995), softwood pulp (Revol *et al.*, 1992; Araki *et al.*, 1998; Beck-Candanedo *et al.*, 2005) and eucalyptus pulp (Beck-Candanedo *et al.*, 2005). It is interesting that no one has since reported the negative concerns of Battista around the use of sulphuric acid hydrolysis. Indeed, the sulphate groups were later found to have an important influence on the phase behaviour of colloidal suspensions and the chiral nematic suspensions that were subsequently discovered. It will become clear from the rest of this review of acid hydrolysis processes that the extraction method and subsequent phase behaviour of cellulose nano-fibril suspensions are inextricably linked.

Marchessault *et al.* (1959) and Hermans (1963) demonstrated that the nano-crystal suspensions displayed liquid crystalline order. However, it was not until several decades later that Revol *et al*. (1992) showed that aqueous cellulose nano-crystal suspensions extracted using sulphuric acid formed a stable chiral nematic liquid crystalline phase above a critical concentration of fibrils. The method described for acid hydrolysis was based upon that of Mukherjee and Woods (1953). Suspensions of cellulose nano-fibrils were prepared from bleached Kraft wood pulp from black spruce. 0.5 g of air-dried pulp was treated with 5 ml sulphuric acid (65% by weight) at 70°C for 30 minutes. The samples were then washed with distilled water by successive dilution and centrifugation until the supernatant was turbid at a pH ranging from 1 to 3. The suspension was dialyzed for at least 2 days against distilled water and then brought to a concentration of 1.5% to 3.5% by weight. Yields were of the order of 50-60% due to significant hydrolysis of the pulp. The suspensions were further dispersed with an ultrasonic treatment in a Branson Sonifier (Model 350) for one minute, resulting in colloidal

suspensions, which above a critical concentration exhibited a stable chiral nematic structure.

In this work TEM studies indicated that the crystallite length ranged from 100 to 200 nm with width averages of 5 nm giving an aspect ratio of 20 to 40. Domains of parallel orientation extended over several micrometers. Electron diffraction patterns corresponded to native cellulose 1 crystal structure and indicated that the molecular axes and hence the rods were close to parallel. It was noted that theoretical treatments of phase equilibrium of rod-like particles in suspension by Onsager (1949) and Flory (1956) predicts that above a critical concentration that depends primarily on the aspect ratio of the rods, phase separation occurs. Aspect ratios of 20 to 40 should correspond to volume fraction of 0.2 to 0.5 (Flory, 1956). However, Revol *et al.* (1992) observed phase separation at a volume fraction of only 0.01 to 0.02. They concluded that the stability of the suspensions was probably due to an interaction between electric double layers resulting from ionization of sulphate esters formed on the cellulose micro-fibrils during the acid treatment. They also concluded that the presence of charge on the rods would also increase their effective diameter resulting in a lower volume fraction for the phase separation. The authors expressed surprise at observing a chiral nematic phase. Cellulose and its derivatives readily form chiral nematic phases at the molecular level. It was therefore concluded that the chirality of the cellulose chains must somehow be transferred to the crystallites. Possibly as a helical geometry or helical charge distribution.

The studies by Revol *et al.* (1992) were extended to look at a broader range of reaction conditions with a follow up paper by Revol *et al.* (1994) using both Whatman grade 1 filter paper and a bleached softwood Kraft pulp. The cellulose was disintegrated in a Wiley mill to pass a 20 mesh screen and then treated with 64 wt. % sulphuric acid at times ranging from 10 minutes at 70°C to 3 hours at 45°C. The suspension was then diluted 10 fold with distilled water to halt the hydrolysis concentrated by centrifugation and then dialysed until the water outside the dialysis membrane was neutral. The suspension was treated with a mixed-bed ion exchange resin and dispersed by an ultrasonic treatment after Revol (1992) and the properties of a range of suspensions were recorded.

On standing, the suspensions separated into an upper isotropic and a lower anisotropic, birefringent phase. The concentrations were measured gravimetrically before and after evaporation of the water. The sulphur content of the fibrils, measured by elemental analysis, was in the range 0.5-1% sulphur by dry weight, depending on the hydrolysis conditions. The cellulose fibrils making up the suspension were of the order of 100nm to 200nm long by 5nm wide. This was confirmed using TEM. Electron diffraction patterns corresponded to the native cellulose 1 crystal structure. Samples of these suspensions for optical microscopy were sealed in a flat-sided glass capillary, 4 mm wide with an optical path length of 0.4 mm.

The precise dimensions of the fibrils and the critical concentration necessary to form an ordered suspension were sensitive to the source of cellulose, the hydrolysis conditions and the ionic strength. When a suspension at a concentration just below the critical concentration was allowed to evaporate, small ordered regions formed, to give a lower ordered region and an upper isotropic suspension. As previously, the crystallites were reported to be stabilised in suspension by the sulphate groups on their surface. The chiral nematic liquid crystalline phase formed at concentrations above about 5% by weight in salt free suspensions.

The findings of Revol *et al.* (1992 and 1994) were supported by the work of Onsager, 1949 and Odijk, 1986 who reported that the transition from isotropic to anisotropic phase in liquid crystal systems is governed by four key parameters. These include:

- The length and diameter (aspect ratio) of the particles;
- The distribution of particle sizes (polydispersity);
- The surface charge of the particles;
- Ionic strength of the system.

The first three parameters depend on the particle properties that are determined by the conditions of preparation. If the phase separation is carried out in pure water, the ionic strength will also be determined by concentration and surface charge of the rods (Manning and Zime, 1965). Theory suggests that under the right conditions such as large aspect ratio, low polydispersity and sufficient inter-fibril repulsion; these suspensions should align in a nematic phase. One of the questions is; can in practice the nematic order be achieved?

In the right conditions stiff rod-like molecules and structures can exhibit ordered structures when in solution. Lyotropic suspensions of cellulose nano-fibrils have been observed, and this has also recently been demonstrated for carbon nanotubes (Song and Windle 2005). The degree of alignment in a lyotropic system can be defined by a molecular ordering parameter (*S*). The ordering parameter represents a statistical measure of the average orientation of the molecules with reference to the director. The director being the direction towards which all the molecules are biased. If there is perfect alignment of the molecules, *S* has the value of 1, and if there is no alignment *S*=0 (Donald *et al.,* 2002) (Fig. 2.5).

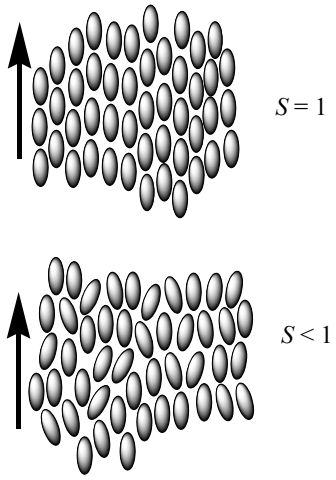

Figure 2.5: *Showing lyotropic systems with ordering parameter (S) of 1 and less than 1. Arrow shows the director.*

At a macroscopic level, molecular alignment occurs within domains with disinclinations formed at domain boundaries. These occur over length scales of 1 to 10 μm. As a result there is a distribution of director directions. In consequence a liquid crystal will often exhibit no orientation on a macroscopic scale, even though there is spontaneous ordering at a molecular level (Fig. 2.6).

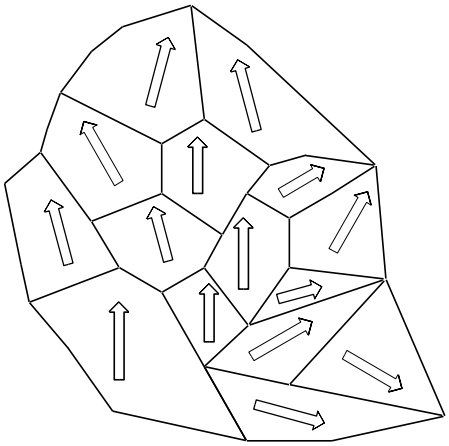

Figure 2.6: *Illustration of several domains in a liquid crystal with the director for each domain shown.*

In the case of cellulose nano-fibril lyotropic suspensions, there is the added complication of the chiral nematic ordering, but there is still a director associated with such structures. Ordering requires both molecular orientation within domains and director orientation of the domains.

Various techniques can be used to characterise the molecular ordering in these solutions, such as X-ray scattering, neutron scattering, UV dichroism and birefringence, although optical methods can be confused by other physical effects. Hongladarom *et al*. (1996) noted that there were often inconsistencies in determination of molecular orientation in sheared lyotropic solutions and used birefringence, X-ray scattering and neutron scattering on the same systems.

In addition to looking at phase behaviour, workers have looked at alternative approaches to achieving fibril alignment. Sugiyama *et al*. (1992) demonstrated that Tunicin micro-crystals extracted using the method published by Revol *et al.,* 1992 could be aligned in what appeared to be nematic phase when exposed to a strong magnetic field of 7T over a three hour exposure period. Electron micrographs clearly showed axial alignment of the fibrils and the findings were also confirmed through electron diffraction and x ray diffraction experiments.

The work on phase behaviour of sulphonated cellulose nano-fibril suspensions was extended by Dong *et al*. (1996) to further test the work of Onsager (1949), Flory (1956) and Odijk (1986) for cellulose nano-fibrils suspensions. The work involved a detailed

study of the effects of ionic strength on the isotropic-chiral nematic phase transition. The paper provides a theoretical background to the phase behaviour of cellulose nano-fibrils in suspension. An early theory was developed by Onsager (1949) and Flory (1956) who predicted that for neutral, perfect rigid rods, the critical concentration for ordered phase formation would depend only on the axial ratio of the rod (L/D). However, for charged particles, the electrostatic interaction has an important impact on the free energy of the system. However, even taking this effect into account, Onsager's theory could not predict the phase separation accurately. Stroobants *et al.* (1986) and Odijk (1986) modified Onsager's theory by introducing two additional factors that included a way to estimate the increased effective diameter and a twisting factor due to electrostatic repulsion (Sato and Teramator, 1991). They demonstrated that for a system with excess added monovalent electrolyte, the effects of electrostatic interactions on phase separation would include an increased effective diameter and that electrostatic repulsion favoured a perpendicular, rather than parallel orientation of particles, which could be viewed as a twisting action between rods. Dong *et al.*, 1996 found that these additional factors led to a theoretical prediction closely aligned with experimental observations. This paper forms an important milestone in the understanding of phase behaviour for cellulose nano-fibril suspensions and demonstrated the importance of electrostatic repulsion and ionic concentration on phase behaviour.

A phase transition diagram was shown by Dong *et al.* (1996) for a cellulose crystallite suspension in pure water extracted from Whatman No1 filter paper using the method described by Revol *et al.* (1994) with 64% sulphuric acid at 45°C for 1 hour. When the total cellulose concentration was below 4.55%, the suspension displayed a single isotropic phase. As the total concentration rose above this critical point, the suspension became biphasic with an upper isotropic and a lower anisotropic phase. The volume of the anisotropic phase increased with increase in fibril concentration up to 13.13%, after which the isotropic phase disappeared completely and the whole suspension was anisotropic. The suspension concentrations in the biphasic and anisotropic phase were measured and did not remain constant in the biphasic region as expected for neutral rods but increased with increasing total suspension concentration. The results resembled theoretical curves for the effect of polydispersity on the phase separation of neutral particle systems (Buining and Lekkerkerker, 1993). However, the polydispersity effect alone could not explain the difference in the co-existing concentrations in the biphasic region. The change in isotropic and anisotropic concentrations with increasing

suspension concentration was mainly ascribed to the change of ionic strength in the aqueous medium as the concentration of charged crystallites increased making it difficult to keep a constant ionic strength.

In order to prepare suspensions with a relatively constant ionic strength, a sample of the cellulose suspension was dialyzed exhaustively against 0.01M HCl solutions and a concentrated suspension was obtained with a measured pH of 1.61. A range of concentrations was then prepared by diluting this concentrated suspension with HCl solution to get a final pH of 1.61 for all the samples. The phase separation was examined for this series of solutions with constant hydrogen ion concentration and a further phase diagram produced. Relatively good linearity was obtained for the plot of volume fraction against total concentration. It was observed that a higher suspension concentration was required to form an ordered phase in these solutions than in distilled water. The extrapolation of the results gave the critical concentrations for phase transition. From isotropic to biphasic and from biphasic to anisotropic the critical values were weight concentrations of 10.7% and 15.8%, respectively. The co-existing concentrations were also measured for the controlled pH system and it was found that the concentrations are much less sensitive to the suspension concentration. More interestingly, the concentration difference between the isotropic and anisotropic phase was much larger.

The addition of salt to a biphasic system did not significantly change the concentration of particles in each phase but greatly changed the relative proportions of each phase.

A further study reported in the paper involved the determining the effect of added electrolyte HCl, NaCl and KCl, at concentrations from 0 to 2.5mM, on the phase separation of cellulose suspensions at a constant suspension concentration. The phase equilibrium was found to be very sensitive to added electrolyte with the volume fraction of the anisotropic phase in the biphasic samples decreasing dramatically with increasing electrolyte concentration. It was at the same time noted that the concentration of the isotropic and anisotropic phase increased only slightly. For a given total suspension concentration, an increase in the concentration of the isotropic and anisotropic phase can only occur if the relative proportions of each phase change. Thus an increase in suspension concentration was observed in both phases. It was noted that the different electrolytes had exactly the same effect on suppressing anisotropic phase formation.

Chiral nematic mesophases possess a structure in which the alignment of the molecules or rods is at a slight angle to one another to create a helicoidal structure. The helicoidal structure is described by a pitch p (or its inverse, the twist) and the corresponding handedness of the twist. Pitch is the distance between two layers that have the same orientation. Dong *et al.*, 1996 concluded that particle geometry and ionic strength were the most important factors governing phase separation. With increasing total suspension concentration or increasing ionic strength, co-existing concentrations in both isotropic and anisotropic phases increased, but the chiral nematic pitch of the anisotropic phase decreased. For a biphasic sample at a fixed total concentration of crystallites, increasing the amount of added electrolyte decreased anisotropic phase formation, but the co-existing concentrations in both phases were only slightly increased. A relatively good agreement was obtained between theoretical predictions and experimental results for the pure suspension.

This work was extended by Revol *et al.* (1997) who patented the production of chiral nematic films with "advantageously optically properties". They demonstrated that the colour of reflected polarized light is "tunable" since the final pitch varies depending on processing variables such as the length of the micro-fibrils, the salt content and the source of the cellulose micro-fibrils. The preferred hydrolysing acid was sulphuric acid due to the attachment of the charged sulphate groups esterified onto the crystallites which offers a more stable suspension compared with other acids. It was proposed that other charged groups such as phosphates or nitrates could have a similar effect. This patent was followed up with a paper on the same subject (Revol *et al.*, 1998).

The work on magnetic alignment of cellulose suspensions carried out by Sugiyama *et al.,* 1992 was revisited by Revol *et al.*, 1994 and Dong and Gray 1997, they were not able to observe a nematic phase but stated that the crystallites exhibited an alignment with their long axes perpendicular to the direction of the field. Since the particles re-oriented across, rather than along the field, the field does not untwist the chiral nematic structure, but rather lines up the chiral nematic axis along the direction of the magnetic field. The process of magnetic alignment occurred over a period of hours to days due to the viscosity of the crystallite suspensions and therefore, applications in such areas as liquid crystal displays is thought to be unlikely (Flemming *et al.*, 2001). The paper by Dong and Gray (1997) also reported that in suspensions above a critical concentration,

the crystallites from filter paper were oriented in a chiral helicoidal arrangement that persisted over dimensions of the order of millimeters. Under an electron microscope, fibrils with this arrangement would have appeared nematic. Personal communications with D. Gray revealed that they have never observed a pure nematic phase. The findings of Sugiyama *et al*. (1992) therefore need to be revisited.

Li *et al.* (1997) confirmed that the surface charge due to sulphonation is strong enough to prevent fibrils from coagulating and that as sulphonation increased the repulsive forces between particles also increased. These repulsive forces can be reduced or cancelled out by the ionic concentration of the solution in which the suspension is dispersed (Dong *et al.*, 1996)). The understanding of the impact of counter-ion was further investigated by Dong and Gray (1997) who contrary to their previous work (Dong *et al.,* 1996) observed that the nature of the counter-ion in suspension affected the critical concentration of at which the suspension transformed from isotropic to chiral nematic phase equilibrium. After fibril extraction from Whatman No.1 filter paper using the method described by Dong *et al.* (1996), suspensions were prepared with a range of counter-ions. Suspensions with H^+ counter-ions formed an ordered phase at the lowest concentration of fibrils. For inorganic counter-ions, the critical concentration for ordered phase formation increased in the order $H^+ < Na^+ < K^+ < Cs^+$. For organic counter-ions, the critical concentration was found to increase with increasing counter ion size, suggesting that the equilibrium is governed by a balance between hydrophobic attraction and steric repulsion forces. The nature of the counter-ions also influenced other properties of the suspensions such as their stability, the temperature dependence of the phase separation and of the chiral nematic pitch and the redispersibility of dried samples made from the suspensions.

Yoshiharu *et al.* (1997) looked at the problem by taking a 4% suspension of cellulose fibrils from the cell wall of a green algae extracted using the sulphuric acid hydrolysis method described by Marchessault *et al.* (1959). A 20 ml portion of the suspension was put into a 50ml glass vial with an inner diameter of 3.6 cm. The vial was kept horizontal and rotated around its centre at 500r.p.m. at room temperature. A layer was formed around the inside of the vial which when dried in a warm air flow produced a highly anisotropic film (confirmed by SEM and x-ray diffraction). It was concluded that shear flow could be used as a mechanism for aligning the fibril suspensions. In the same paper, the influence of electrolyte concentration was examined by washing the

suspension repeatedly with centrifugation and dialysis to neutrality. The neutral suspension did not form an oriented gel layer. Addition of a small amount of electrolyte (NaCl or acid) immediately raised the viscosity and enabled the formation of the gel layer again. Increase in viscosity is in line with Araki *et al*. (1998) but appears to be in conflict with Dong and Gray (1997) who indicated that anisotropic behaviour is promoted by the absence of electrolyte. However, it may support the hypothesis that some electrolyte may be useful in reducing the repulsive forces between fibrils that tend to force a twist in the fibril suspension. Two much electrolyte cancels out the repulsive forces leading to aggregation of the fibrils and preventing fibril alignment of any description, resulting in an isotropic suspension.

Ebeling *et al.*, 1999, carried out similar work to that of Yoshiharu *et al.* (1997) and reported similar alignment of microcrystals along the flow plane using small angle x-ray scattering.

One of the most useful papers for the work in this thesis (Dong *et al.*, 1998) builds on the paper by Dong *et al.* (1996), reporting a detailed study of the effect of hydrolysis time and temperature on the properties of cellulose nano-fibrils and their phase behaviour. Extraction of cellulose nano-fibrils is a heterogeneous acid diffusion process that almost certainly contributes to a relatively heterogeneous particle size distribution. A wide range of particle sizes makes the theoretical prediction of phase separation much more difficult. More than one ordered phase has been predicted in some theories (Abe and Flory, 1978; Semenov and Khokhlov, 1988). Orientational order in long rods is predicted to be greater than shorter ones. As seen in earlier work, the longer rods preferentially form an anisotropic phase. A fractionation thus accompanies the phase separation. Odijk and Lekkerkerker (1985) have predicted the fractionation ratio in a system of bi-disperse rod-like polymers, but polydisperse systems are more complex.

The work by Dong *et al.* (1998) involved looking at the preparation of several suspensions with different acids. Only suspensions hydrolysed by sulphuric acid were found to form an ordered phase at a concentration above a certain critical value. Although cellulose nano-fibrils were successfully made using hydrochloric acid and phosphoric acid, they were not able to observe any chiral nematic phase with these suspensions.

Hydrolysis conditions must be mild enough to avoid complete hydrolysis to cellulose. Based on the work by Revol *et al.* (1994) the best concentration of sulphuric acid was found to be in the range of 60-70%. In this work on the impact of temperature, time, the concentration of sulphuric acid and the ratio of the filter paper to acid were fixed at 64 % (w/v) and 1:8.75g/ml, respectively. After the hydrolysis, the suspension was further dispersed by an ultrasound treatment (typically 5 min at full power) with a Sonifier cell disrupter 350 with standard tip (Branson Sonic Power Co.).

At low temperature (26°C) an 18 hour reaction time was required to produce micro-crystallites that could form an ordered suspension. With a time of 1 hour, the cellulose was not broken down sufficiently and yielded large fragments of cellulose fibres, which were visible, by optical microscopy. No chiral nematic phase was formed by these larger fragments of cellulose. At 65°C the hydrolysis could not be controlled easily and side reactions occurred leading to a yellow colouration after about 10 minutes, which subsequently turned black after an hour. At 45°C, the hydrolysis proceeded smoothly and yielded an ivory white suspension with a yield of 44% after 1 hour reaction. A chiral nematic phase was observed with this sample. Temperature was then fixed at 45°C in order to investigate the impact of time in more detail. The properties of the cellulose nano-fibrils were characterised by particle length, surface charge and the ability to form an anisotropic phase.

Times ranged from 10 to 240 minutes. As time increased the total sulphur content and the fibril surface charge increased. Conversely the length of the fibrils decreased. The decline from almost 400 nm length at 10 minutes to 170 nm after 1 hour was rather rapid after which the length seemed to stabilise.

Looking at the effect of sonification, particle size decreased for the first 5 minutes after which it stabilised. The reduction in apparent particle size was attributed to the further dispersion of particle aggregates. The surface charges on the particles were not influenced by different levels of sonification.

When it came to looking at the impact of preparation conditions on phase separation (on deionised suspensions) it was found that the critical concentration for anisotropic phase formation was the highest (7.1%) for the shortest hydrolysis time of 20 minutes and

dropped off rapidly to a lowest value of 4.2% as the time increased to 1 hour. The concentration stabilised at this level for hydrolysis times as long as 4 hours. The lower concentration indicates that the suspension has greater propensity to form an ordered chiral nematic suspension. It was proposed that the sharp drop in concentration was due to the break up of coarse aggregates of cellulose (330 nm long at 20 mins.) to give more uniform, thinner crystallites. The increase in total surface area resulting from this breakdown also leads to an increase in total surface charge. The increase in axial ratio and surface charge lead to a rapid decrease in the concentration required for ordered phase formation that reached a minimum after about 40-50 minutes. Further hydrolysis produced little further increase in surface charge but particle dimensions (and aspect ratio) continued to decrease.

The final area of work that they looked at in this paper was fractionation. Using the tendency of longer fibrils to form an anisotropic phase first, they were able to separate out fibrils with different dimensions distributions. When looking at fibril suspensions from two anisotropic phases and one isotropic phase (from the same sample) under TEM they couldn't see any clear distinctions in fibril size due to the variation involved. However, with the use of image analysis on 600 fibrils from each sample, differences in average length and size distribution were observed. However the breadth of distribution in the different samples was still quite large. Conclusions from this work included the following:

- More work was required to optimise the preparation and fractionation of these materials;

- Chiral nematic ordering was found to be highly dependent upon the hydrolysis and preparation conditions. Anisotropic phase formation only occurs when an appropriate size is reached. The particle size, surface charge and polydispersity of the fibrils changed with the degree of hydrolysis;

- It is important to determine an optimal hydrolysis time that breaks cellulose down to its basic crystalline unit. Shorter times mean aggregates containing some amorphous material. Longer times simply shorten the fibrils as the crystalline material is attacked;

- A more uniform fibril dimension would lead to greater propensity to assemble in a chiral nematic and perhaps nematic structure. It could be that the polydispersity and aspect ratios observed to date are not adequate to form a nematic phase. Theoretically, nematic order could be achieved if fibrils have adequate aspect ratio and/or uniformity.

Looking at hydrolysis with alternative acids in more detail, Araki *et al*. (1998) reported that the hydrolysis of native cellulose by 4N hydrochloric acid hydrolysis gave a stable suspension of cellulose micro-crystals. As part of this work they investigated the flow properties of cellulose nano-fibril suspensions. Fibrils extracted using both hydrochloric acid and sulphuric acid were compared. Sulphuric acid extraction was carried out using the method described by Revol *et al.* (1992). Ten grams of Kraft pulp was treated with 100ml of 65% (w/w) H_2SO_4 at 70°C for 10 minutes with continuous stirring. The sample was then repeatedly washed with centrifugation (1600g, at 100°C for 5 mins.) until a pH of 1-3 was achieved. Hydrochloric acid extraction involved 175 ml of 4N HCl mixed with 5g. of Kraft pulp at 80°C for 225 minutes. The suspension was then repeatedly centrifuged to achieve a pH of 4. In both cases the suspensions were dialysed against distilled water and then sonicated with a rod-type sonicator for 1 min.

The HCl treated suspension contained only a small amount of weak acid groups, but still formed a stable colloid at the very low ionic strength attained by dialysis. Its colloidal stability was however much lower than the H_2SO_4 treated sample.

The viscosity of the H_2SO_4 treated suspension was much lower than that treated with HCl and remained constant over time. The HCl suspension viscosity decreased with time (thixotropic) at higher concentrations but increased (anti-thixotropy) at very low concentrations. Thixotropy of the HCl-treated suspension indicates the effect of significant inter-particle aggregation, which forms in static conditions and is destroyed by shear flow. The behaviour at lower concentrations suggests that the increased inter-particulate distances reduce the contribution of aggregation to thixotropic and that conversely the interaction between particles may be enhanced by their mutual alignment due to shear flow. Both cellulose suspensions showed shear-thinning behaviour. HCl treated suspension declined very rapidly with shear rate. However, it started at much higher levels than the H_2SO_4 treated material and even at high shear rates was still three

times higher than H_2SO_4 treated cellulose without shear. By contrast H_2SO_4 treated cellulose showed only weak shear-rate dependence although this might have been different at higher concentrations.

Orts *et al.* (1995) demonstrated that shearing of a suspension could produce a high degree of orientation, but the orientation could not be achieved in a solid material. Subsequent work by Orts *et al.* (1998) confirmed a shear induced nematic phase. The stability of the nematic phase was found to be dependent on the characteristics of the nano-fibrils. Viscous suspensions derived from long micro-fibrils (280 nm) remained aligned for hours after shearing while samples with shorter micro-fibrils (180 nm) relaxed quickly. They also observed that cellulose nano-fibrils that had been fractionated to give a lower polydispersity more readily formed a chiral nematic phase at a lower concentration than more disperse suspensions. It was also observed that tobacco mosaic virus which has a lower polydispersity formed an anisotropic phase at lower concentrations. This is in line with the hypotheses postulated by Onsager (1949) and Stroobants *et al.* (1986).

In follow up to the work by Araki *et al.* (1998) and Araki *et al*. (1999) repeated the observation that the viscosity of hydrochloric acid hydrolysed suspension was several fold higher than that of a suspension prepared by sulphuric acid from the same material. The difference in viscosity between the two suspensions was ascribed to the different surface charges that governs the inter-particular forces, which meant that hydrochloric acid extracted cellulose nano-fibril suspensions, did not form a chiral nematic phase. Surface charge impacts on viscosity, since aligned fibres in the chiral nematic phase flow more readily than those in a random (isotropic) orientation. In addition, surface charge prevents aggregation of the fibrils, which would otherwise resist inter-fibril flow. To confirm the influence of surface charge, they introduced sulphate groups to HCl hydrolysed cellulose crystals by secondary treatment with sulphuric acid. Treatment for two hours at 60^0C gave an acid group content of 60 mmol/Kg, which drastically reduced the viscosity to a level approaching that of sulphuric acid hydrolysed suspension (acid group content of 84 mmol/Kg) whilst treatment at 40°C (acid group content of 53 mmol/Kg) gave an intermediate viscosity. The results indicated that the viscosity behaviour is strongly affected by the surface charge in a range around 50-60 mmol/Kg. The paper offers a potential alternative method to that of sulphuric acid for preparing cellulose nano-fibrils suspensions, which may offer useful control over levels of surface

charge. Araki *et al.* (2000) followed up their research in the area of post sulphation of cellulose nano-fibrils with an investigation of the phase behaviour of these alternatively treated suspensions. By examining the properties of these suspensions with various surface charge levels they found a new birefringent high viscosity glassy phase between 2.8 and 7.1% solid content that was different from the normal chiral nematic phase. It was claimed that this was similar to that reported for bohemite suspensions reported by Buining *et al.* (1994). This is a potentially important observation that needs validation since the glass phase behaviour of bohemite rods reported by Buining *et al.* (1993) was described as nematic.

It is interesting to note that Heux *et al.* (2000) reported evidence of chiral nematic ordering of cellulose nano-fibril suspensions in organic media when stabilized by a surfactant. This was followed up with a US Patent by Heux *et al.* (2005). This may well open up new opportunities for spinning continuous fibres in organic solvents.

One of the more interesting papers was published by Araki and Kuga (2001) who claimed to be the first to have observed a nematic phase in a cellulose microcrystal suspension extracted from bacteria. The work was carried out using commercial food-grade bacterial cellulose that was disintegrated using a homogeniser and thoroughly washed with deionised water by filtration. The material was then treated with 65% sulphuric acid at 70^{o}C for 30 minutes and then purified by repeated centrifugation (1600g, 5 mins.) and dialysis following the method described by Revol *et al*. (1992). The suspension was concentrated up to approximately 3% solid content by osmotic compression using cellulose tubing and 10% poly (ethylene glycol) solution followed by 2-3 min sonification. This stock solution was diluted with distilled water or NaCl solution to make the desired cellulose concentration (0.2-1.5%) and electrolyte concentrations (0-1mM). Phase separation of the suspension was examined between crossed polarizer's.

The length of the cellulose fibrils ranged from 0.1 to several micrometres, typically being 1-2 micrometres. The cross section of the fibrils was of the order of 10 x 50 nm giving an aspect ratio of 50-100. As reported by Revol *et al.*, 1992; Dong *et al.*, 1996 and Orts *et al.*, 1998), the microcrystals were stabilised in suspension by the negative charge of sulphate groups introduced by the acid treatment. Sulphate content, determined by conductiometric titration was 5 mmol/kg. At low solid contents (<0.2%)

the fibril suspension without electrolyte was isotropic at rest. At solids contents of 0.4-1.5%, the suspension showed birefringence with iridescent domains indicating some alignment of the fibrils. When the suspension was concentrated up to 3%, it became highly viscous, appeared turbid through crossed polarizer and showed immobilized birefringence patterns described as a glassy phase. This was observed to be much lower than in some of their previous studies with cotton-derived micro-crystals at 2-7%. However, the birefringent glassy-like state was not in equilibrium and showed phase separation into isotropic and anisotropic phases after 1 week of standing. This observation is similar to that of other cellulose micro-crystal suspensions (Revol *et al.*, 1992; Dong *et al.,* 1996 and Orts *et al.*, 1998). The particle concentration for phase separation was 0.3-1.2% for the bacterial cellulose compared to 5-10% for cotton and wood cellulose microcrystals (Orts *et al.*, 1998). This was almost certainly due to the higher aspect ratio. The anisotropic phase of the bacterial cellulose suspension under polarization microscope showed many birefringent patterns, apparently due to shearing motion during injection into the flat cell. After 1 day this specimen developed a schlieren texture with typical disinclination points and many small birefringent spheroids, called tactoids. Most of the tactoids disappeared after 1 week, leaving the schlieren pattern, which is associated with a nematic phase.

Introduction of small amounts of electrolyte caused substantial changes in the appearance and phase separation behaviour of the bacterial cellulose suspension: its viscosity decreased and the phase separation became much faster forming a clear boundary within 1 day and reaching equilibrium within 2 days. The presence of electrolyte also decreased the volume of the anisotropic phase significantly. Under a polarisation microscope this phase exhibited chiral nematic order.

It was claimed that the results demonstrated the importance of the approach to suspension preparation. The same nano-crystal suspension formed a chiral nematic phase when prepared by dialysis after acid hydrolysis but formed a nematic phase when prepared by dilution with distilled water after osmotic compression. The differences were explained with reference to previous studies (Revol *et al.*, 1992; Dong *et al.*, 1996; Orts *et al.*, 1998), which suggested that the crystalline cellulose has a geometric twist or a helical distribution of surface charge that leads to chiral nematic order. The explanation for a nematic phase in the absence of electrolyte was explained to be due to an increase in particle diameter due to surface charge, which effectively makes the rods

straight and smooth. Addition of electrolyte could cause a shrinkage of the effective particle size due to shielding of the surface charge. This would lead to the exposure of the twisted morphology and the formation of chiral nematic order. From their work they couldn't exactly determine the threshold NaCl concentration for the chiral nematic transition, but estimated it to be of the order of 0.01mM. The second question to be explained was why only the bacterial cellulose formed a nematic phase since wood and cotton derived nano-crystals have not been observed to form a nematic phase even after extensive desalination. It was suggested that it could be due to the greater length and aspect ratio and flat, ribbon like cross section. Interestingly, they limited their work to the biphasic region and didn't look at higher concentrations to determine the point at which the suspensions become completely anisotropic.

The theory of a twisted cellulose nano-fibril needs further examination. Araki and Kuga (2001) conclude that a twist in the cellulose nano-fibril explains the chiral nematic structure of the suspension. However, they make no mention of the hypothesis by Stroobrants *et al.* (1986) who built on the model by Onsager (1949) in which they developed a quantitative model for the impact of electrostatic repulsion which causes both an increase in effective fibril diameter and a twist in a fibril suspension based on the fact that that electrostatic repulsion between fibrils favours perpendicular rather than parallel orientation of the particles. Apart from entropy favouring disorder, the repulsive forces offer an additional factor favouring random orientation of fibrils at low suspension concentrations. The logical conclusion from this hypothesis is that fibrils with a lower surface charge will more easily align in a nematic phase at lower concentrations. This would suggest that the Araki-Kuga hypothesis of inherent fibril twist, as an explanation of chiral nematic behaviour is perhaps unnecessary. The earlier paper by Araki *et al.* (1999) on post sulphation of HCl extracted cellulose nano-fibrils offers a potential mechanism for controlling the level of surface charge but they did not appear to have made the connection. In addition to the work by Stroobrants and his co-workers, the earlier model developed by Onsager (1949) makes it clear that aspect ratio is a critical factor in the formation of a nematic phase. Araki and Kuga (2001) conclude that the large aspect ratio of bacterial cellulose is likely to be an important factor in the observed nematic ordering of the cellulose crystals. However, they do not refer to the fact that Onsager's model predicts it (even though they quoted the Onsager work in their paper).

Work by Kimura *et al.* (2005) extended the work on magnetic alignment by Dong and Gray, 1997. They confirmed that the chiral nematic axis aligns parallel to a static magnetic field. However, they found that a rotating magnetic field (5T for 15 hours) could bring about the unwinding of the helical axis to form a nematic-like alignment. However, once the external field is removed the orienting effect is lost and the system will relax to a state of thermodynamic equilibrium. The rate at which this relaxation occurs is key to maintaining the orientation in the fibre once it has been formed but before it is fixed through a drying process. The large magnets used to align fibrils, plus the slow fibril orientation times observed suggest magnetic alignment may not be a useful commercial option for aligning fibrils in an industrial fibre spinning process. It is therefore important to consider alternatives such as shear alignment as demonstrated by Orts *et al.* (1995).

Song and Windle (2005) observed the formation of a nematic phase in a multi-walled carbon nanotube suspension (average length/diameter of 31 nm/976 nm giving an aspect ratio of 31) at a concentration of 5.3% and observed that a more polydisperse suspension (but with a higher average aspect ratio) exhibited a larger biphasic window with the nematic phase forming at a higher concentration of 6.5%. The results suggest that homogeneity is more important than aspect ratio.

It should be noted that in the majority of papers, one of the key processes for neutralising the cellulose nano-fibril suspension after extraction with acid involves the use of dialysis. Song and Windle (2005) published an alternative, more efficient approach for acid treated carbon nanotubes. The process involved the filtering of the carbon nano tube suspension with water over a 400nm pore membrane (PTFE) until the water passing through the filter had a pH of between 6 and 7.

In 2005 Beck-Candanedo *et al.* published results on the effect of hydrolysis reaction time and acid to pulp ratio on dimensions of nano-crystals and their suspension properties from eucalyptus and black spruce pulp. They found that the properties of colloidal suspensions produce by sulphuric acid hydrolysis (after Revol *et al.*, 1992) of eucalypt and black spruce pulps were essentially the same. Typical cross section dimensions clustered around 5nm with lengths of around 147 nm. They found that for a fixed acid to pulp ratio longer hydrolysis times for black spruce pulp led to shorter cellulose nano-fibrils. Battista (1950) demonstrated that longer hydrolysis times under

low acid to pulp ratios gave longer nano-fibrils. This was to some extent supported by the findings of Beck-Candanedo *et al.* (2005) who found that a higher acid to pulp ratio led to a decrease in nano-fibril dimensions. It was also noted that shorter reaction times resulted in lower surface charge and sulphur content and that the surface charge of nano-fibrils is highly sensitive to heat. An increase in temperature can cause de-esterification of the sulphate groups on the surface of the fibrils.

It was noted that chiral nematic pitch decreased from ~20 to ~10 micrometers with increasing cellulose concentration over a specific range from 7-13% wt.%. This appears, on first analysis to be counter intuitive, since an increase in concentration from low levels leads to an increasing level of anisotropy in the biphasic region until a chiral nematic phase is reached (Dong *et al.,* 1996). This is supported by liquid crystal theory (Donald *et al.*, 2002). The findings of Beck-Candanedo *et al.* (2005) suggest that there is an optimum concentration beyond which level of alignment starts to decrease.

The model of Doi and Edwards (1986) is often used when discussing the rheological behaviour of lyotropic liquid crystals. The theory considers the effect of length and concentration of rod-like molecules upon behaviour and considers the isotropic and nematic phase as well as the transition between these two states.

The model considers a solution of rods of length L, diameter d, and with a number per unit volume of c. The model describes three regimes:

- $c << 1/L^3$ At low concentrations, there is essentially no interaction between the rods;
- $c \approx 1/L^2d$ At this concentration, the Onsager condition for the formation of a liquid crystalline phase is met and spontaneous alignment occurs;
- $1/L^3 < c < 1/L^2d$ In this concentration range the motion of the rods is severely impeded by mutual entanglement.

Thus, the viscosity rises rapidly in the mid-range of concentration before decreasing dramatically when the lyotropic phase is formed.

Pitch was found to increase with nano-fibril length. This finding is supported by the work of Grelet and Fraden (2003) on mutant virus suspensions. Liquid crystalline theory (Donald *et al.,* 2005) suggests that longer rods show less tendency to form

twisted chiral nematic structures (at the same volume fraction of fibres) i.e. longer rods show a greater tendency to align in a parallel (untwisted) arrangement. This supports the findings of Araki and Kuga (2001) for high aspect ratio bacterial cellulose. It is important to combine this knowledge with the findings of (Dong *et al.*, 1996) in that the suspensions showed a tendency to align and increase the pitch when the ionic strength is decreased.

One of the key objectives of the project was to spin fibres in the nematic phase; this requires removal of the solvent with minimum disruption to the fibril alignment. Intuitively, higher concentrations of the fibres during the spinning process should be preferable. One objective was to determine the maximum concentration obtainable. Orts, (1998) states that increasing concentrations of cellulose nano-fibril suspensions become increasingly gel like and exhibit higher viscosities. "It is difficult to imagine processing such gels without altering the structure by shear". Their data suggests that the chiral nematic phase is disrupted under increasing shear rate and that micro-fibrils exhibit nematic ordering with the fibrils aligned parallel to the flow direction. These findings offered an interesting avenue of investigation within this research project.

Qizhou *et al*. (2005 and 2006) supported the conclusions of past work on the impact of shear by stating that chiral nematic mesophases are concentration dependent and strongly influenced by shear rate. Stating that when the shear rate is high enough, the polymer chains or rods will orient along the shear direction. The chiral nematic structure changes to a flow-aligned nematic-like phase and the dependence of viscosity on concentration decreases. However, it was noted that chiral nematic domains remain dispersed within the suspension.

2.2.2 Alternative techniques to assist in the extraction of cellulose nano-fibrils

In parallel with the development of acid hydrolysis methods, scientists have reported both mechanical and enzymatic breakdown processes.

Microfibrillated cellulose is a form of expanded high volume cellulose, obtained through a mechanical homogenisation process. A number of workers have reported developments in this area with a number of patents being filed.

Turbak *et al.* (1983) patented a process to produce microfibrillated cellulose (MFC), which they claimed to have properties "distinguishable from all previously known celluloses". Key benefits of the MFC claimed included:

- No substantial chemical change or degradation of the starting cellulose material. Using acid hydrolysis destroys a significant part of the cellulose resulting in lower yields;

- In MCC, most of the desirable, amorphous, reactive part of the fibres is removed leaving the microcrystals. *This is a positive point for most of the intended applications for MFC but for the application proposed in this research the presence of amorphous cellulose and hemicellulose is undesirable;*

- The MFC had a vastly increase surface area, greatly improved absorption characteristics and improved reactivity and binding capability. The MFC had a water retention value of over 280% and a rate of degradation increase by hydrolysis at 60^{o}C in one molar hydrochloric acid at least twice as great as highly beaten pulp. *This is an interesting observation as it offers an option to consider the pre-treatment of pulp prior to acid hydrolysis to improve the yield and/or aspect ratio of cellulose nano-fibrils in the acid hydrolysis process*[1].

The MFC was produced with a high pressure homogenizer of a type, which is commercially used to produce emulsions and dispersions. In this patent, a liquid suspension or slurry of cellulose (4-7% cellulose) heated to 80°C was introduced into a Manton-Gaulin™ homogeniser[2] and brought to a pressure of 5-8000 psi (34,450 kPa - 55,120 kPa). In such a device, energy is applied to a low viscosity suspension by a high velocity flow through a restricted area. The heart of the device was a homogeniser valve and valve-seat assembly, which is attached to the discharge end of a high pressure pump. A liquid suspension enters the valve assembly at high pressure and low velocity. As the liquid advances to a small diameter orifice formed in the close clearance area between the valve and valve seat there is a very rapid increase in velocity up to as high

[1] When combining this with the theories of Battista (1950) in which he recommended mild hydrolysis conditions to increase crystallinity we may find additional improvements.
[2] Turbak did not make any specific recommendations but referred to an article by Rees (1974) on homogenizers for chemical processing.

as 700 ft/second. As the suspension emerges between the valve and valve seat it impinges on an impact ring surrounding the orifice and this results in a high velocity decelerating impact. The orifice must be small enough to create the required shearing action but must be larger than the fibre diameter. The slurry was repeatedly passed through the homogeniser (typically 10 to 20 times) until it formed a stable cellulosic suspension.

The key point of this approach was that it does not separate out individual fibres but rather produces a network of long, flexible interconnected micro-fibrils.

In the case of conventional cellulosic pulps, drying is known to reduce the chemical reactivity and water absorbency of the pulps. It is also known that certain additives can be used to reduce the inter-fibre bonding that occurs on drying. Debonding agents were generally cationic surfactants such as fatty acid quaternary amines and have been added to pulps before drying to reduce the energy required to defiber pulp sheets. Herrick (1984) improved on the patent by Turbak *et al.* (1983) with a further patent using the same principle. It was found that adding specific compounds to never dried cellulosic pulp significantly reduced costs in the microfibrillation process. Recommended additives included polyhydroxy compounds including carbohydrates, other than cellulose itself, such as glycols, sugars, and carbohydrate gums starches. It should be noted that both these patents have now expired.

In 1984, an enzymatic hydrolysis method was patented by Zabriskie as an alternative method of producing MCC for tablet making. The patent claimed the use of cellulose enzymes such as a commercially available cellulase of *Trichoderma viridie*. It was claimed that endo-glucanase activity, which is unable to hydrolyse crystalline cellulose in the absence of exo-glucanase activity, selectively removes the amorphous regions of the cellulose particles. In this way the selectivity of the cellulose for amorphous cellulose is enhanced. Enzymatic hydrolysis was carried out at 50°C at a pH of between 4 and 5, using buffering agents such as citric acid. It was found that a hydrolysis time of 5 hours or greater produced a product suitable for tablet formation. It was found that cellulose powders could be produced with a crystalline cellulose content of up to 75% compared with 78%, which is the normal value for MCC produced by the acid hydrolysis process. *This doesn't support the claim that enzymatic treatment is more selective. However, an overall assessment of the patent suggests that whilst it was at*

the time focussed on the production of an alternative to MCC, it is certainly worth further investigation as an option for the preparation of cellulose nano-fibrils.

Dinand *et al.,* 1999 lodged a further patent based upon similar principles to Turbak *et al.* (1983) but with a focus on sugar beet fibrils. The key difference over prior art was the use of a pre-treatment of pulp with acid or basic hydrolysis to extract pectin's and hemicelluloses followed by a further alkaline extraction process to remove unwanted cellulose.

Taniguchi and Okamara (1998) reported on a "new process" to microfibrillate pulp fibres using a small commercial grinder with a specially designed disk (super-grinding), manufactured by Masuko Corp, Japan. The MFC produced had fibrils with diameters in the range of 20 to 90 nm. However, the study did not provide a size distribution of the fibrils produced or evaluate the aspect ratio of the fibrils.

Zimmermann *et al.*, 2004 reported on the use of cellulose nano-fibrils for polymer reinforcement. The paper looked at two methods for extraction of the fibrils.

The first involved mechanical separation. The process involved dispersing sulphite pulp in deionised water. The suspension was then treated with an ultra-turrax (FA IKA; 24000 r.p.m. for 8 hours) to separate the fibril bundles from the cell wall. The fibrils were then further dispersed and homogenised using a micro fluidizer M-100y (FA Microfluidics; 1000 bar, 60 min).

Once the fibres had been separated they were characterised using SEM and TEM. Mechanical dispersion led to fibril structures with diameters between 20 and 100 nm and estimated lengths of several tens of micrometers. The fibrils were found to strongly interact and agglomerate creating a web like network of fibrils.

The second involved 5g of oven dried pulp in 200 ml of sulphuric acid (10 wt.%) and stirred at 60°C for 16 hours. The resulting suspension was centrifuged (5000 r.p.m.) and washed several times in deionised water. Afterwards the solution was neutralised with sodium hydroxide (0.1N) and homogenised with a micro fluidizer M-100y (FA Microfluidics; 1000 bar, 60 mins.) in the same way as the mechanically separated fibres.

Chemical breakdown with sulphuric acid combined with mechanical dispersion resulted in finer fibril structures with diameters below 50 nm. The fibrils were also shorter than mechanically extracted fibres but their length was still in the range of micrometers. They observed that these finer and shorter fibrils interacted to a lower extent, and did not form the strong network of fibrils observed in the mechanically extracted fibrils.

The key observations from this work include the following:

- The chemically extracted fibrils did not agglomerate to the same extent as the mechanically extracted fibrils due to their shorter length and due to the surface charging with sulphate groups, which leads to repulsion between fibrils. This latter concept was not mentioned in the paper but is extensively covered in the papers looking at sulphuric acid hydrolysis discussed in this review;

- The chemically extracted fibrils were notably longer than those described by previous workers using acid hydrolysis. This could be due to the source of pulp, which is acknowledged as a source of variation. However it could also be linked to the much milder acidic conditions used as originally suggested by Battista (1950) who indicated that milder conditions of hydrolysis would lead to longer cellulose crystallites;

- The mechanically extracted cellulose fibrils varied enormously in diameter compared with chemically extracted fibrils, indicating incomplete separation of individual fibrils in some instances;

- The mechanically extracted cellulose fibrils are very long and flexible. This could be the result of a number of issues. The fibrils have hydrogen bonded together suggesting longer fibrils (not possible to determine actual length of crystalline regions) or amorphous regions between crystalline regions have not been broken down. Possibly a combination of both. *The long flexible fibres obtained in this work are highly suitable for the production of gels or thickening agents but the level of cross-linking would not be suitable for the formation of lyotropic suspensions. However it may be possible to carry out a gentle acid hydrolysis on the mechanically extracted fibrils to cut the fibres into shorter, stiffer rods. It is proposed that this form one of the lines of investigation in*

optimising fibril length whilst ensuring stiffness and suitability for lyotropic suspension.

In 2005 Sain and Bhatnager filed a patent for the production of MFC (provisional patent filed in 2003). The invention describes a process in which pulp fibres are frozen with liquid nitrogen and then a high impact was applied to break the cell walls. This was followed by high pressure defibrillation by passing 2% of the crushed suspension through a high pressure defibrillator (a "PANDA 2K" BY NIRO SOAVI^{R} unit), which subjected the treated suspension to high pressure flow with high turbulence and shear. The resulting suspension after 30 minutes contained nano-fibrils in the range of 5-120 nm diameter (and high aspect ratios) after which it was defibrillated further at 0-150 MPa pressure. The results are very much in line with other MFC processes such as that described by Zimmermann *et al.*, 2004. There was inadequate information within the patent to compare the cost effectiveness of the process with other prior art.

In 2005, Chakraborty *et al.* claimed a new method of preparing cellulose micro-fibrils using high shear refining and cryocrushing. The approach involved passing fibres at a consistency of 10% through a PFI refiner for 125 000 revolutions (no other refining information was provided). It was claimed that the refiner produced high shear capable of forming individual micro-fibrils at the surface of the fibre bundles. However, this step was not suitable for effectively isolating these micro-fibrils into individual entities. The refined fibres were subsequently immersed in liquid nitrogen to freeze the water content in the fibres. The fibres were then subjected to high impact grinding with a cast iron pestle and mortar under the surface of the liquid nitrogen. The majority of fibrils had diameters in the desired range of 0.1 to 1 micrometer with lengths of up to several micrometers, with a considerable degree of entanglement that mirrored the observations of Zimmermann *et al.,* 2004. At these dimensions the majority of the fibres where unlikely to be individual cellulose crystallites but large aggregates of fibril bundles. It is clear that further processing of the fibrils would be required if they were to be used in lyotropic suspensions.

Following on from the patent by Zabriskie (1984) work on the enzymatic extraction of cellulose nano-fibrils was extended by Janardhnan and Sain (2006) who combined an enzymatic and mechanical approach to the isolation of cellulose micro-fibrils. They started with the assumption that a mechanical process to separate the micro-fibrils is

very energy intensive. The objective of the work was to investigate and establish an enzymatic chemistry that would partially or completely break down the hydrogen bonds between micro-fibrils making their isolation more energy efficient. The process used for micro-fibril extraction was the same as that published the previous year by Chakraborty *et al.* (2005). Interestingly no mention was made of this paper despite that fact that Mohini Sain was a co-author on both papers. The fungus OS1, isolated in the laboratory from Elm tree infected with Dutch elm disease was used as the source of enzyme for the fibre treatment. The work was exploratory in nature but concluded that the fungus treatment was shown to have a significant impact on the defibrillation characteristics of the fibres and offered an improvement/refinement in the process of isolating of cellulose nano-fibrils. Fibril characteristics were very similar to those of Zimmermann, 2004, and the comments regarding the pros and cons of their findings are equally valid for this work. The findings suggest that enzymatic breakdown may be worth considering in future when considering optimisation of the cellulose nano-fibril extraction process but is not considered as part of the critical path in the first phase of the current research project.

In 2007 Zuluaga *et al.* published work in which they investigated the extraction of cellulose micro-fibrils from banana farming residues. The work described the extraction of cellulose crystallites from banana rachis using chemical and mechanical treatments. Chemical treatment involved 80% (v/v) acetic acid and 70% (v/v) nitric acid at 120°C for 15 minutes. After washing, the cellulose was sonicated for 15 minutes at 45 kHz. Mechanical treatment involved a peroxide alkaline bleaching followed by mechanical homogenisation for 2 hours using a Manton Gaulin homogeniser following the method described by Turbak *et al.* (1983) and Dufresne *et al.,* 1997. The mechanical process resulted in suspensions of long thin interconnected micro-fibrils. The chemical process resulted in shorter cellulose crystallites of about 5 nm diameter with an aspect ratio of around 100. These findings were comparable to those published by Zimmermann *et al.*, 2004 who compared chemical and mechanical breakdown processes. What is particularly interesting in the paper by Zuluaga *et al.*, 2007 was the use of x-ray diffraction diagrams on dry films of the two cellulose fibril sources and compared with a mat of bacterial cellulose. The mechanically broken down cellulose indicated high levels of amorphous cellulose relative to the chemically process cellulose. This would be expected as it is known that mechanical treatment leaves amorphous material intact. The x-ray diffraction pattern generated by bacterial cellulose indicated that it was of

higher crystallinity than that processed through acid hydrolysis. This suggests that the long crystallites produced (high aspect ratios) are not totally crystalline and may include amorphous regions (dislocations) within them. The paper demonstrated the usefulness of x-ray diffraction as a tool in evaluating the level of crystallinity within the cellulose structure, which will be useful in comparing different extraction, processes as well as evaluating larger, continuous fibres spun from cellulose nano-fibrils.

2.2.3 Size of the basic cellulose crystalline unit

A good deal of attention has been dedicated to the extraction of cellulose nano-fibrils from wood and other sources of cellulose. However, one of the more fundamental questions relates to the actual size of the most basic cellulose fibril. A number of authors have referred to an average diameter that ranges from 5 to 20 nm. Many authors have stated that the typical micro-fibril found in wood is around 20nm, but that it is actually constituted from smaller crystalline sub units of 4 to 5 nm in diameter. The issue is an important one as the objective of this work is to extract the most basic building block with maximum crystallinity. The hypothesis that 20 nm diameter micro-fibrils are not a completely crystalline units could cause problems if correct, as any large scale fibre that are produced from such units would have a large number of inherent defects. Sugiyama *et al.* (1984) published a paper on the use of TEM in which they looked at a cellulose micro-fibril of Valonia macrophysa. A typical fibril was found to be 20 nm in diameter and made up of a uniform structure of 0.54nm lattice lines (presumably individual cellulose chains). The lattice lines were visible for more than 50 nm in the longitudinal direction and formed a continuous single set of lattice lines across the 20 nm diameter. No breaks in the lattice structure were observed. Their conclusion was that the observations ruled out the existence of either smaller crystalline sub-elements in the transverse direction or periodicity in the longitudinal direction as proposed by earlier workers. This observation confirms the work on acid hydrolysis in which many workers have observed 20 nm diameter fibrils that cannot be broken down further without total dissolution. However, other workers have extracted fibrils of the order of 5 nm diametre or have observed smaller subunits using methods such as solid state Nuclear Magnetic Resonance (NMR) (Larsson *et al.*, 2007). This suggests that there may well be differences in the crystalline structure in different sources of cellulose.

The other issue arising from the TEM work by Sugiyama *et al.* (1984) is that there is a method to allow us to visualise the levels of crystallinity within individual nano-fibres and the continuous fibres (and the levels of amorphous material) when we attempt to merge cellulose nano-fibrils into supramolecular structures. This method could be an important addition to tools such as x-ray diffraction.

According to this review nano-fibril dimensions are determined to some extent by the nature of the cellulose source and the degree of crystallinity which both vary from species to species (Battista, 1955; Marchessault *et al.,* 1961). Algal and tunicate fibrils are highly crystalline (Belton *et al.*, 1989; Sassi and Chanzy, 1995; Terech *et al.*, 1999; de Sousa Lima and Borsali, 2002) and yield nano-fibres up to several micrometers in length. By contrast wood micro-fibrils have a lower crystallinity (Hermans, 1951; Sjostrom, 1981; Fengel *et al.*, 1984) and on the whole have been reported to yield much shorter nano-fibrils (Fengel *et al.,* 1984).

The extraction of cellulose nano-fibrils with different acids affects the suspension properties: hydrochloric acid hydrolysis yields cellulose fibrils with minimal surface charge (Araki *et al.*, 1999) whereas sulphuric acid provides highly stable aqueous suspensions, due to the presence of charged sulphate groups (Rånby, 1949). Nano-fibrils with minimum surface charge form suspensions at much higher viscosities and do not form a chiral nematic phase. Above a critical suspension concentration, charged cellulose nano-fibrils form a chiral nematic phase (Onsager, 1949; Marchessault *et al.*, 1959; Revol *et al.*, 1992; Revol *et al.*, 1994, Dong *et al.*, 1998; Araki *et al.*, 1998; Araki *et al.*, 2000). The concentration varies dependent upon aspect ratio, polydispersity, surface charge and ionic concentration of suspension. It is possible that understanding these factors in more detail could play an important role in unlocking the door to the creation of nematic suspensions.

Acid hydrolysis conditions are known to affect the properties of nano-fibrils. Dong *et al.,* 1998 reported that a longer reaction time leads to shorter nano-crystals under constant hydrolysis conditions. However, Battista (1950) demonstrated that milder hydrolysis conditions over longer periods led to longer nano-fibril length due to crystallisation of amorphous regions. This work needs to be revisited with a more comprehensive study of the impact of reaction conditions. Some of the longer fibres

reported by workers such as Zimmerman *et al.* (2004) may contain significant amounts of amorphous cellulose that bond multiple crystalline units in a chain.

2.3 Shear mechanisms as an approach to alignment of cellulose nano-fibrils.

Araki and Kuga (2001) claimed that they are the only team to have observed nematic phase behaviour in static suspensions of cellulose nano-fibrils. In their work only bacterial cellulose with its high aspect ratio resulted in a nematic phase, under very specific conditions and only after allowing several days for the suspension to stabilise. This on the surface suggests that it may be possible to spin a continuous fibre in which all the cellulose fibrils are aligned to the main axis of a fibre. However, the work by Orts *et al.* (1995 and 1998), Yoshiharu *et al.* (1997), Ebeling *et al.* (1999) and Qizhou *et al.* (2005 and 2006) has shown that high shear can lead to alignment of the fibrils. This raises the question as to the most practical mechanism to induce shear. Appaw (2004) offers a good overall summary of the rheology of cellulosic liquid crystalline solutions.

It was reported by Appaw (2004) that under high rate flow, the chiral nematic mesophase aligns along the flow direction and uncoils to form a nematic structure (sometimes referred to as a pseudo-nematic phase). Upon cessation of flow, the chiral nematic phase will reform and the molecular orientation will decrease. This is due to the driving force for the liquid crystalline solution to form the more thermodynamically stable chiral nematic structure. Orts *et al.* (1998) demonstrated this with cellulose nano-fibril suspensions and showed that the rate of relaxation is dependent upon the aspect ratio of the fibres and the shear rate used in the first instance.

Appaw (2004) gave a useful summary of the concentration dependence of viscosity. Isotropic solutions and suspensions give a monotonic increase in shear viscosity with increasing concentration. The viscosity increases to a maximum when the biphasic region is approached. Upon formation of an anisotropic phase the viscosity begins to decrease. After which viscosity increases exponentially as the concentration continues to increase. However, Zugenmaier (1994) found that the correlation of the viscosity maximum with the formation of the anisotropic phase was only valid when the shear rate was low. At a higher shear rate, high viscosity solutions shift to a lower value. When the shear rate is high enough to cause shear-induced orientation (pseudo-nematic

phase) the viscosity maximum disappears and a monotonic increase of viscosity vs. concentration is observed. This indicates that under these conditions, the viscosity of the nematic or pseudo-nematic mesophase is less sensitive to concentration than that of the chiral nematic phase.

Anisotropic suspensions of cellulose nano-fibres demonstrate a similar viscosity-concentration relationship. The viscosity vs. concentration curve has a maximum, which disappears at high shear rates, Bercea and Navard (2000).

Onogi and Asada (1980) proposed the universal existence of three shear flow regimes to describe the viscosity of polymer liquid crystals: a shear thinning regime at low shear rates (I), a Newtonian plateau at intermediate shear rates (II) and another shear thinning regime at high shear rates (III) (Fig. 2.7). The commonly used method of describing how flow affects rheology is to use a logarithmic plot of viscosity against flow rate, viscosity against flow stress, or flow stress against shear rate.

In practice region (II) is seldom distinct for thermotropic systems, whereas region I is sometimes not seen in lyotropic systems. In the latter case, this has been attributed to the inability of instruments to make accurate measurements at sufficiently low shear rates.

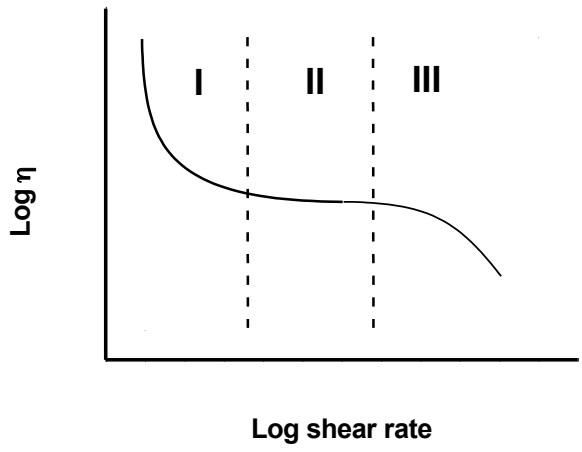

Figure 2.7: Plot of viscosity against shear rate for a liquid crystal polymer.

It is generally considered that the behaviour in region I is related to the presence of defects in the liquid crystalline structure which have a large effect upon viscosity at low

shear rates. The behaviour in region I can thus be attributed to the re-orientation of the directors associated with the multiple domains. At low shear rates, the director undergoes a continuous chaotic rotation (tumbling). This distorts the director field, which responds to this motion by creating defects to decrease the elastic free energy (Keates *et al.,* 1996).

However, it was proposed that some polymer liquid crystal systems do not show all regimes because not every regime lies in the accessible shear rate range. It is important to determine the shear flow properties of cellulose nano-fibril suspensions in identifying optimal conditions for fibril alignment.

Li *et al.* (1996) noted the existence of the electroviscous effect, which is observed, with suspensions of charged rods. This is influenced by: (i) the ability of the diffuse layer of ions surrounding the charged rods to resist distortion, (ii) the electrostatic repulsion between neighbouring rods. Such effects are more pronounced in concentrated suspensions. Adding salt suppresses the electrical double layer and reduces viscosity of the suspension.

Lyotropic solutions exhibit elasticity as well as viscosity. The elasticity of lyotropic solutions arises because the stress field increases the alignment of molecules relative to the director, as discussed above. Release of the applied stress allows the system to relax to the equilibrium state. If the strain of the system is coupled to molecular orientation, then the strain will also relax. This is thought to be related to the existence of pleated structures found in many fibres spun from lyotropic solution. This was first observed by using transmission electron microscopy of Kevlar™ fibres (Dobb *et al.,* 1977). In rheological experiments, it is nearly always associated with strain relaxation. In Kevlar fibres (Fig. 2.8) it has been shown that the bands correspond to a ‘pleated sheet’ structure with radial symmetry. These banded structures are characteristic of liquid crystalline polymers. Romo-Uribe and Windle (1999) have shown that there is a threshold molecular weight below which banded structures are not seen. Whether such a phenomenon would be observed in a fibre made of nano-crystals is not known.

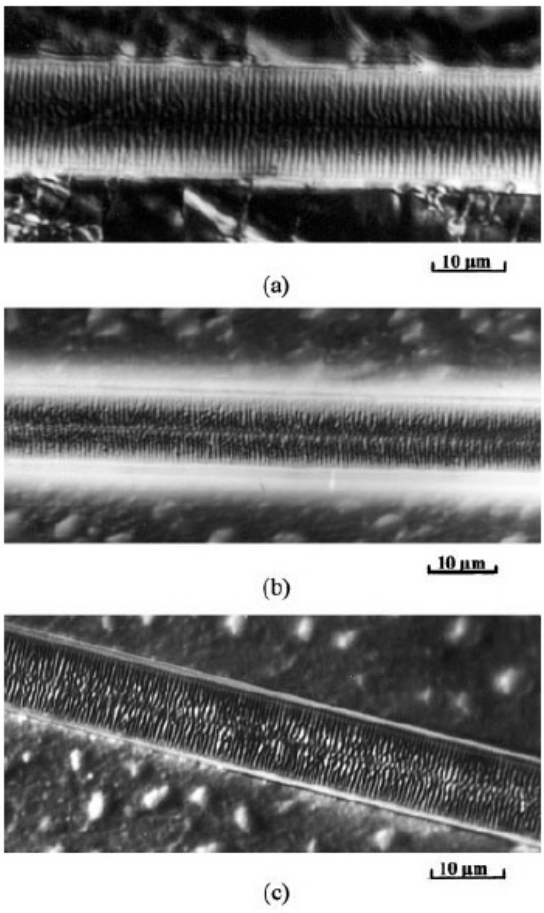

Figure 2.8: Pleated structures visible in etched Kevlar fibres (Shahin, 2003).

The understanding of rheology under conditions of flow is clearly important in the processing of lyotropic solutions. According to Donald *et al.* (2002) there is not, as yet, a full theoretical understanding of the response of liquid crystals to flow fields. In a theoretical description it is necessary to consider not only the orientation of molecules (or nano-particles) within a domain, but also the polydomain nature of the liquid crystal polymer. It is also important to understand the viscoelastic behaviour of the system.

2.4 Fibre spinning

An alternative approach to shear induction includes spinning of fibres from nano-fibril suspension under pressure. When the material used to make the fibres is polymeric in nature it is desirable to align the polymer backbone with the long axis of the fibre, in order to maximise tensile strength. Alignment can take place during the fibre spinning process, but there is additional advantage to forming an aligned mixture prior to spinning.

The spinning of cellulose nano-fibrils from a lyotropic suspension of cellulose nano-crystals involves the following stages:

- Ensuring that the suspension is fully dispersed and exhibits an ordered (chiral nematic) structure;
- Forcing the suspension through a small diameter orifice creating the shear forces required for unwinding the chiral twist to create nematic order along the fibre axis;
- Annealing the long fibre to create efficient hydrogen bonding networks between the nano-crystals.

Fibres spun from lyotropic solution normally exhibit good internal alignment. Such fibres are spun by forcing the anisotropic solution through a spinneret, either directly into a coagulation bath (wet spinning) or through a hot air drier (dry spinning). The dry spinning process was subjected to a theoretical analysis by Ohzawa *et al.* (1969) and Brazinsky *et al.* (1975).

The fibre spinning process requires knowledge of the extensional rheology of the lyotropic solution. This is a subject that is not nearly so well understood as other rheological phenomena. The subject of extensional viscosity is discussed by Barnes *et al.* (1997), who describe the 'state of the art' as it was in 1987. In 1998 Collier *et al.* noted that the measurement of elongational rheology was in its infancy. Donald *et al.* (2002) do not consider this subject in any great depth compared with other aspects of the rheology of liquid crystalline polymers.

Barnes *et al.* (1997) note that during processing, any abrupt change in geometry will result in a flow having an extensional component. This is particularly so, when there is a sudden constriction in an orifice, as with a spinneret. The flow characteristics in such a situation cannot be predicted from knowledge of the shear viscosity only. A very important property is whether the material to be used for spinning is tension thickening, or tension thinning. During the spinning of a threadline, there will inevitably be small disturbances resulting in changes to the fibre cross section and it is important that these are suppressed rather than magnified. If the diameter of the threadline decreases at a point, the extensional strain rate will be higher in this region. If the polymeric solution is tension thinning, then the velocity in this part of the threadline increases, so that the region becomes thinner again. Tension thickening has the opposite effect and stabilises the process. In this context it is worth noting the work of Batchelor (1970, 1971) who

showed that the extensional viscosity of systems containing slender particles could be very high, depending upon the aspect ratio of the particles.

One of the problems with this area is the difficulty of making accurate measurements although as noted later, Collier *et al.* (1998) claimed to have solved this by the use of a special die configuration. Barnes *et al.* (1997) state that in the case of stiff systems, the problem is 'not one of exposing the sample to uniaxial extensional flow, but rather of maintaining it for a sufficient time for the stress (in a controlled strain rate experiment) or the strain (in a controlled stress experiment) to reach a steady state, thus enabling the *steady* extensional viscosity η_E to be determined'. From the purely pragmatic point of view, this probably does not matter if the fibre spinning process is sufficiently rapid that a steady state is not achieved in any case.

Of the various devices used for measuring extensional rheological properties, the spin line rheometer appeared to be the most relevant for the work described in this thesis. However, Barnes *et al.* (1997) note that it is very difficult to interpret the data in terms of an extensional viscosity. The problem is that although the flow down the threadline may be constant when velocity is considered, this will not be the case when strain rate is considered. Even if the strain rate is constant over a section of the threadline, there is the problem of 'memory' of conditions experienced in the spinnerette.

There are no reports in the literature of using cellulose nano-fibril suspensions for the production of continuous fibre, nor any studies of the extensional rheology of cellulose nano-fibril suspensions.

The prediction is that an increase in fibre aspect ratio will have a strong influence on extensional viscosity as is shown in Figure 2.9, where the viscosity for an aspect ratio of 4 is arbitrarily assigned the value of 1. However, increasing the volume fraction does not influence the elongational viscosity strongly (Fig. 2.10). The conclusion is that higher aspect ratio fibrils have a much higher impact of extensional viscosity (the ability of the fibre to draw down) than solids content.

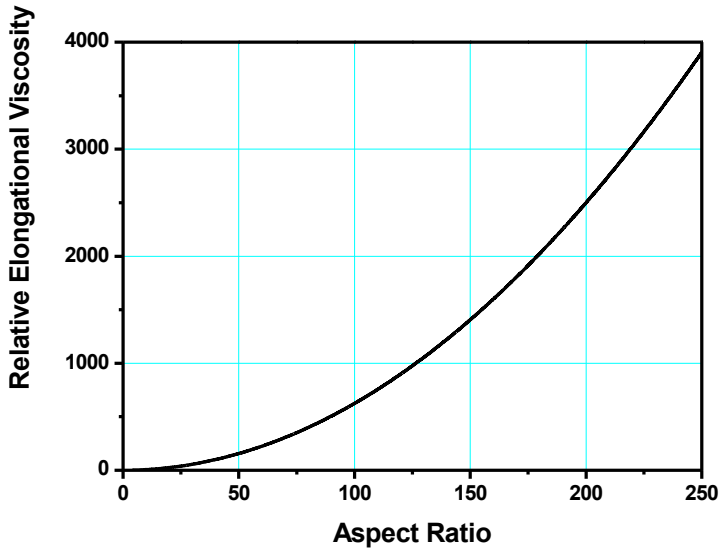

Figure 2.9: Relationship between relative elongational viscosity and fibre aspect ratio. Petrie (1999).

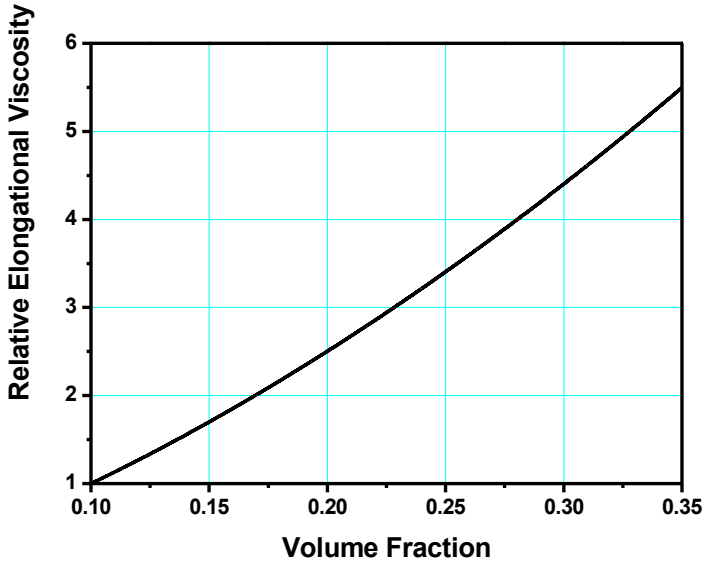

Figure 2.10: Relationship between relative elongational viscosity (arbitrarily set at 1 for a volume fraction of 0.1) and volume fraction. Petrie (1999).

A good example of cellulose spinning technology is the lyocell process in which dissolved cellulose is spun from a very high viscosity solution. The fibres are spun through a 50-80 micrometer spinneret at high pressures between 100 and 150 bar at temperatures of 90°C - 120°C. To avoid a rapid expansion of the fibre diameter as it emerges from the spinneret under high pressure shown in Figure 2.11, the fibre is then drawn at very high speed to ensure that the crystalline units that are formed within the

fibre remain aligned until after they have passed through a coagulation bath. Higher performance tyre chord fibres are drawn at up to 80m/minute to maximise alignment and subsequent strength. Fibres such as Formate have strength properties of up to 140cN/tex. Cellulose in this process also has a higher degree of polymerisation (longer cellulose chain length), which also ensures better inter chain bonding and subsequently higher strength.

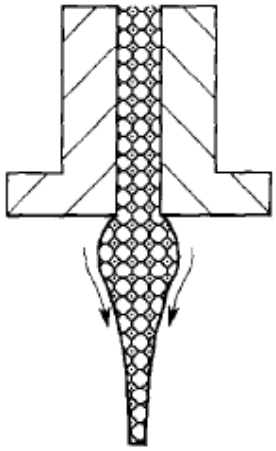

Figure 2.11: Diagram of fibre spinning showing die swell.

One of the key design elements of the spinneret is the hyperbolic curve to the entrance of the spinneret, which allows smooth flow of the cellulose into a relatively long narrow tube (minimum 50 micrometres) without inducing turbulent flow. As the cellulose is forced through the tube under high pressure the induced shear forces align the cellulose chains in a nematic phase.

The rheology of nematic polymer solutions is well documented, both in terms of experiments and theories (Larson 1999). This knowledge has been utilised effectively in the processing of lyotropic suspensions of cellulose to produce products such as lyocell. A key question surrounds whether the shear dynamics of aqueous suspensions of cellulose nano-fibrils, will be the same as lyotropic polymer solutions. Bercea and Navard (2000) investigated the effects of shear-induced orientation in the isotropic and chiral nematic phase. The behaviour of chiral nematic suspensions at around 3% cellulose nano-fibrils appeared to be comparable to that of nematic polymer solutions. However, a shear induced nematic phase was not reported. The paper did not go far enough in looking at the high levels of concentration and shear that are typical in the spinning of lyocell and so it was not possible to make direct comparisons. Their

preliminary data did however indicate that similar characteristics to liquid crystal polymer solutions might be expected at the higher concentrations and shear rates. This needs to be investigated, as it could be an important factor determining the success of the proposed research programme.

It may be that it is not critical to achieve optimal phase behaviour prior to processing if sufficient shear can be induced to untwist the chiral nematic structure prior to spinning. However, there are potentially hundreds if not thousands of process scenarios that need to be considered in achieving the optimal spinning conditions. It is apparent that a full understanding of all the issues is not realistically achievable within the constraints of this body of work. It is anticipated that this could form an important part of subsequent process development.

3 EXPERIMENTAL WORK

3.1 Introduction

The number of potential variables in a proposed research programme could be substantial. To simplify things sulphuric acid hydrolysis was chosen as the basic method of extraction of cellulose nano-fibrils as it introduces electrostatic stabilisation of the suspension and the spontaneous formation of a chiral nematic phase above a critical concentration.

From the literature review it was possible to draw a number of indications as to what would make a good cellulose nano-fibril suspension for the purposes of spinning continuous, high strength internally aligned fibres.

The ideal suspension should theoretically contain:

- Fibrils with high aspect ratio;
- Fibrils with low polydispersity;
- Solutions with zero or low ionic strength;
- A surface charge on the fibrils to prevent aggregation. However, this needs to be managed as too high a surface charge may interfere with interfibril bonding;
- An optimal concentration for maximum alignment, which will be dependent upon the above factors.

An important objective of the research was to test this hypothesis and to determine in more detail the relative impact of aspect ratio, polydispersity, surface charge and ionic concentration on the characteristics of the suspension and end product characteristics.

A second challenge was to determine what other factors could assist in moving beyond the chiral nematic stage and induce nematic order. Araki and Kuga (2001) showed that nematic order could be achieved using bacterial cellulose nano-fibrils with a high aspect ratio when the conditions within suspension are carefully controlled. However the time scales for this were too long to be practical on work limited to high aspect ratio cellulose.

An alternative approach is to physically align the fibrils. The key objective of the programme was to investigate shear induced nematic alignment. Like all suspensions of rigid rod particles, cellulose nano-fibrils have to align under flow (Ebeling *et al.,* 1999). The objective was to determine the critical suspension concentration and shear rate combination (the maximum in the viscosity vs. concentration curve vanishes at high shear rates). Brecea *et al.* (1996) and Brecea and Navard (2000) found that cellulose nano-fibril suspensions show fast inception and relaxation when compared to conventional liquid crystalline polymer solutions.

The hypothesis of this thesis is that orientation of a chiral nematic suspension of cellulose nano-fibrils in a fibre should be theoretically possible by shearing of the fibril suspension as it is forced through a spinneret orifice and by drawing of the fibre after formation. The relative importance of these two variables will be considered. Although it is possible to obtain a lyotropic suspension of cellulose nano-fibrils by appropriate processing, ensuring axial alignment of the fibrils in the drawn fibre involves more than altering the alignment of the twisted chiral nematic state. As noted in the literature review, the lyotropic suspension will contain many domains each with its own director. Thus the alignment process requires alignment of the rods in each domain, plus alignment of the directors to form a monodomain fibre. The focus of this work was to determine if full alignment of the fibrils could be achieved in reality.

Although alignment of the cellulose nano-fibrils can be achieved by using shear and that this may improve the flow properties through a spinneret, the literature review indicates that the behaviour of the suspension under extension is perhaps of equal or more importance in terms of achieving good alignment of cellulose nano-fibrils in a continuous fibre. The variables in the spinning process that require study are diameter and geometry of exit die, flow rate through die, suspension concentration, aspect ratio, surface charge on the fibrils, pH of solvent, temperature and draw down ratio.

3.2 Developing a method for preparation of cellulose nano-fibril gels from Whatman No4 filter paper.

3.2.1 Ball Milling

The primary cellulose source used in preliminary investigations was Whatman No4 filter paper, which has a cellulose content of 99%. Whatman No4 was selected as it was standard form of cellulose of high purity. For uniform hydrolysis to take place it was important to have a small, relatively uniform particle size in the region of 0.8mm. This was achieved by cutting individual sheets of filter paper and then grinding them in a Fritsch ball-mill at 450r.p.m. for twenty minutes. After milling the powder was passed through an 850 micron sieve. The un-sieved coarser material was then discarded. Figure 3.1 shows a picture of the three forms of cellulose from paper through to powder.

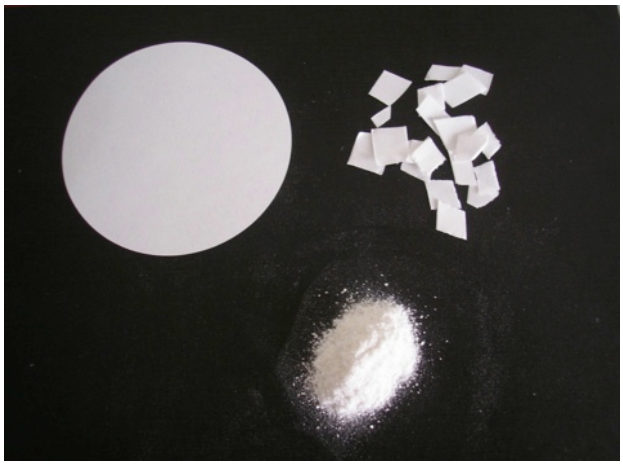

Figure 3.1: Three forms of cellulose from paper through to powder.

3.2.2 Establishment of hydrolysis conditions

The objective of this work was to identify the acid concentration that produced free unaggregated cellulose nano-fibrils, with low levels of amorphous cellulose. The recommendations of Revol *et al.* (1992) were used as a starting point. 140 grams batches of powder obtained from ball milling were hydrolysed using sulphuric acid. Acid concentration was varied from 10% to 60%, at a constant temperature of 46^{o}C and time of 75 minutes. The powder, at a concentration of 10% (w/w) of the acid was hydrolysed under constant stirring using a hotplate/magnetic stirrer (Figure 3.2).

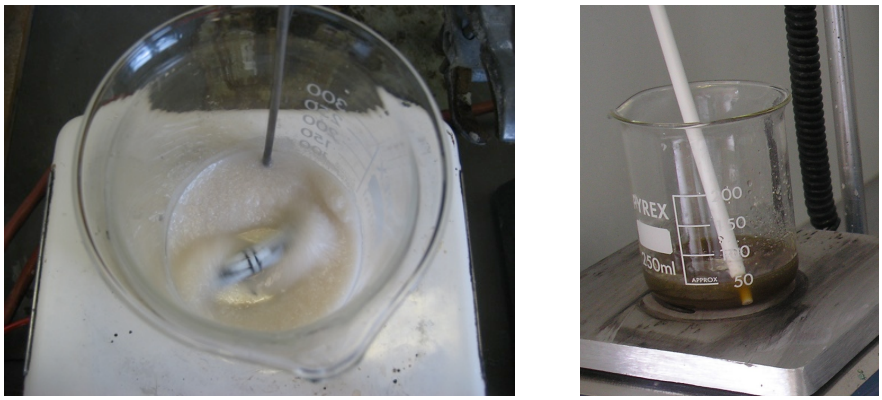

Figure 3.2: Hydrolysis of filter paper under 52.5% acid concentration at 46°C.

Hydrolysis was stopped by addition of deionized water (10 times the volume of the original acid plus cellulose). The main differences in the hydrolysed suspensions were the viscosity and the colour (Fig. 3.3).

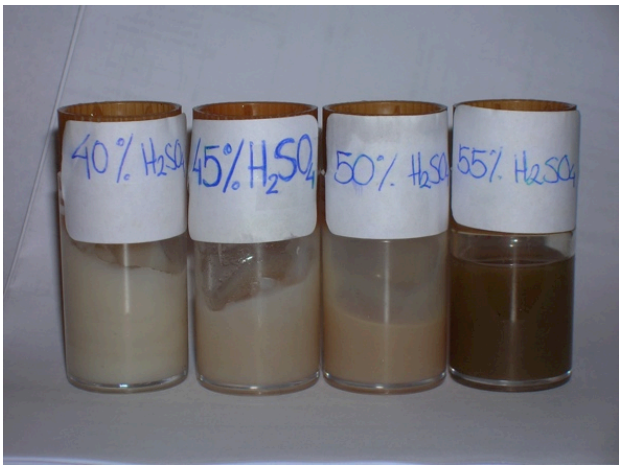

Figure 3.3: The image shows the different colours of the solutions under different acid concentrations. The lighter colours are in solutions with low acid while the colour darkened at high acid concentrations.

Field Emmission Gun Scanning Electron Microscopy (FEG-SEM) was an important tool for the characterisation of cellulose suspensions as it can operate at very low energy levels. Conventional electron microscopes typically operate with an electron beam in the 30KV range. When looking at plant based material such as a cell wall or cellulose nano-fibrils it is very difficult to go magnifications of 20 000 x or higher due to electron beam damage. Typically the plant material will be destroyed within a matter of seconds. Using the FEG-SEM at Edinburgh Napier University it was possible to work with energy levels at below 1KV. This allowed the use of high magnifications of up to

250 000x when looking at crystalline cellulose. However, it was observed that amorphous polysaccharides are still sensitive to the electron beam at these low energy levels and some visible damage could be observed within a relatively short period of time (less than 1 minute) even at magnifications as low as 10 000x.

After checking the samples from each concentration in the FEG-SEM it was found that acid concentration that gave discrete nano-fibrils relatively free of amorphous material was between 50% and 55% H_2SO_4. Having narrowed the range of acid concentrations, the process was repeated to determine the optimal acid concentration, which was found to be 52.5% (Fig. 3.4). 52.5% acid solution gave the most discrete nano-fibrils. The lower concentration contained amorphous material, which had not been completely broken down by hydrolysis. Concentrations above 52% also appeared to contain more amorphous material, which is assumed to be due to break down of crystalline material as a result of too high concentration. The darker colour found at 55% and higher concentration was thought to be overhydrolysed leading to excessive damage.

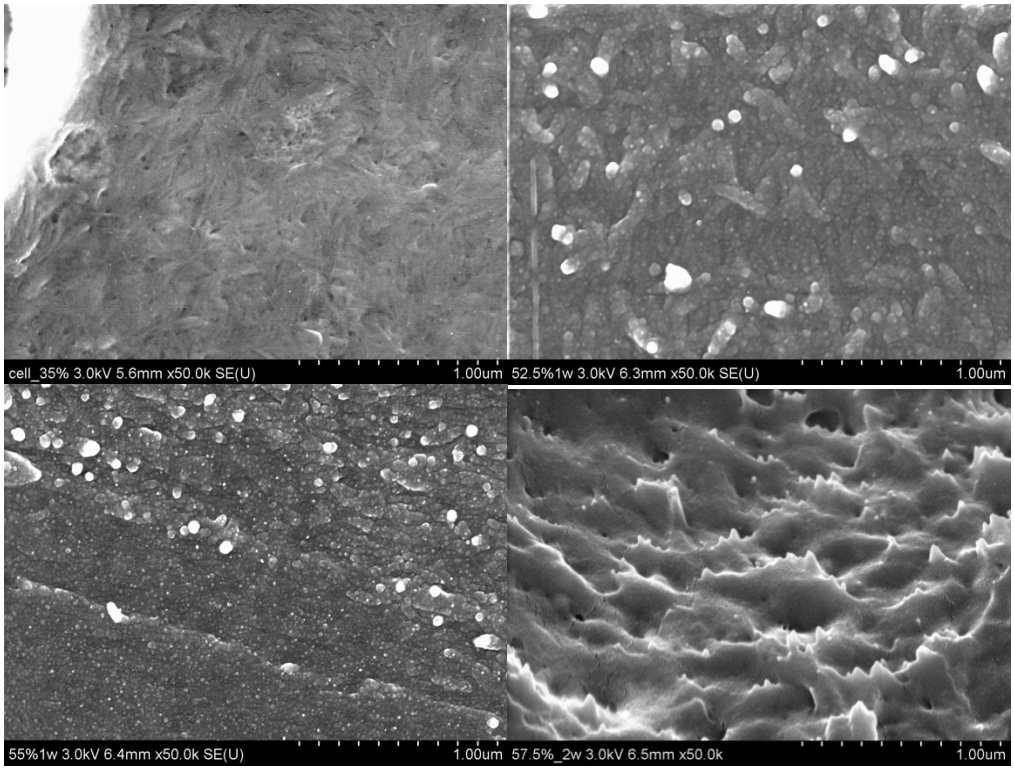

Figure 3.4: FEG-SEM pictures at 50,000 magnification of solutions under different acid concentrations before washing and centrifugation (from 50% to 57.5%).

These results support findings in the literature (Battista, 1950), which highlight the importance of hydrolysis conditions that have an important impact on the dimensions of cellulose nano-fibrils. The wrong conditions can lead to either inadequate breakdown of the cellulose into separate fibrils or complete destruction of the crystalline structure.

3.2.3 Washing and centrifugation

After determining the most appropriate acid concentration, the next step was to look at the impact of the number of centrifugation stages on fractionation of the nano-fibril suspensions. This was done to remove surplus acid, and to remove fibrillar debris and amorphous material broken down during the hydrolysis. Each centrifugation was for 1hour at 17 000 RCF (relative centrifugal force) for a total of 5 hours centrifugation.

After hydrolysis and washing stages, a field emission scanning electron microscope (FEG-SEM) was used to carry out a visual assessment of the nano-fibril size distribution and to qualitatively determine levels of amorphous cellulose still present in suspension. Each sample was prepared by placing a drop of suspension on a standard aluminum SEM stub which was subsequently dried at room temperature before being coated with around 5 to 10 nanometers of gold using a Emitech sputter coater. The coated samples were then examined at magnifications ranging from 5 000x to 50 000x. In carrying out this study a total of six washes was used. All images reproduced in this study are shown at 25000x magnification using the FEG-SEM.

1st Wash

After the hydrolysis the liquid was separated into 6 bottles (of 500 ml each) and placed in a Sigma 6K 15 centrifuge. The first centrifugation ran for one hour at 9 600 r.p.m. (17 000 RCF). After this time there were two different phases formed, an acidic solution (wash water) and a concentrated cellulose gel pellet of approximately 20% solids content. The surplus water was then poured off and the remaining gel assessed using the FEG-SEM before being re-diluted and washed of additional cycles.

Figure 3.5 shows FEG-SEM of the structure of the gel formed after the first wash. The cellulose nano-fibrils appeared to form a strong domain structure. However, it is quite

difficult to discriminate individual fibrils. This is thought to be due to the presence of amorphous cellulose and fine fibriliar debris at this stage.

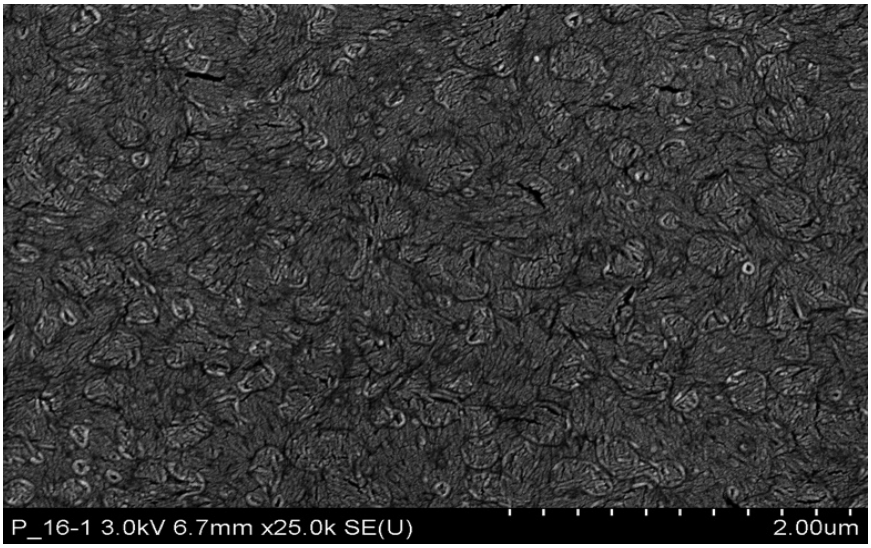

Figure 3.5: FEG-SEM image of filter paper cellulose nano-fibrils suspension after the first wash.

Figure 3.6 shows a FEG-SEM image of the remaining acidic solution. It is not possible to identify individual cellulose nano-fibrils. Some structure can be seen in the image but this is clouded by what is thought to be largely amorphous cellulose and fibrilar debris that is too small to discriminate at this magnification (25,000x). The dry mass content of this wash water was around 13% indicating that a large amount of cellulose is lost in the first wash.

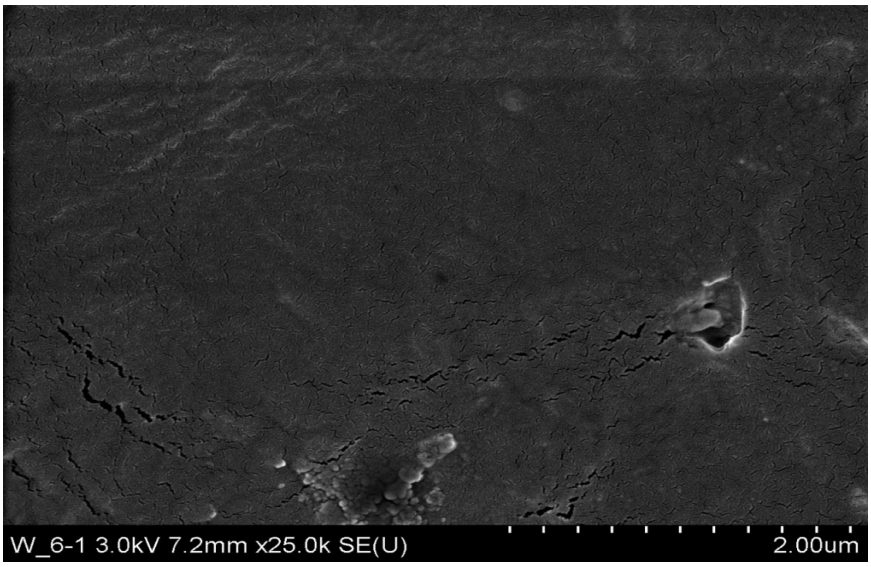

Figure 3.6: FEG-SEM image of wash water (remaining acidic solution) after the first wash.

2nd Wash

The gel pellet was re-suspended in 250ml of de-ionized water and subsequently centrifuged again for one hour and the cellulose gel pellet and wash water re-evaluated. Figure 3.7 shows the structure of the cellulose gel after the second wash. The cellulose nano-fibril structure was clearer than after the first wash. It is thought that this was due to the extraction of much of the amorphous cellulose and fine fibrilar debris during the second centrifugation. Figure 3.8 shows an image of the wash water after the second wash. It looked comparable to that of Figure 3.6 and is still thought to comprise largely of amorphous cellulose and fine fibrilar debris. The dry mass of this wash water was significantly reduced from that of the first wash at around 1.5%. The assumption regarding the amorphous character of the material was supported by the fact that it was highly unstable under the electron beam. It was extremely difficult to capture an image before it is destroyed. This problem was not observed to the same degree with the crystalline nano-fibrils, which were more resistant to electron beam damage.

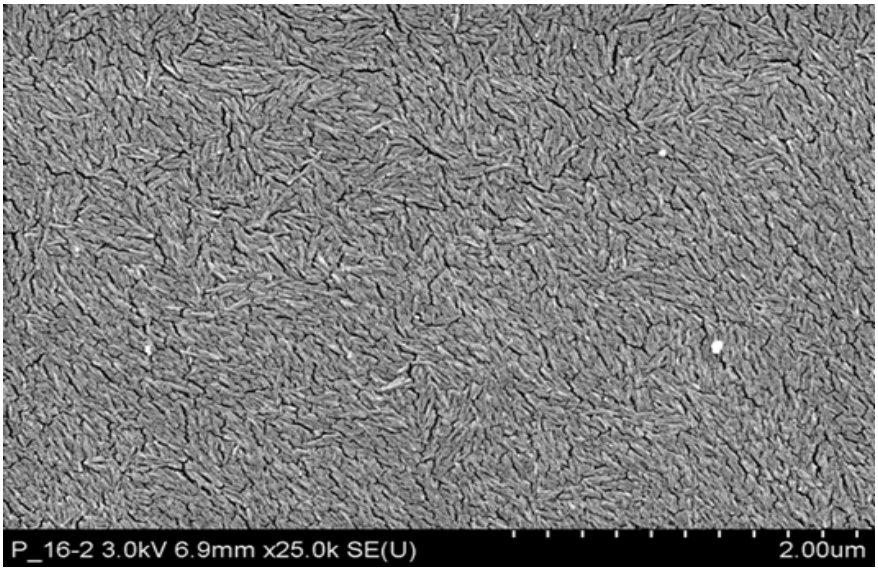

Figure 3.7: FEG-SEM image of filter paper cellulose nano-fibrils suspension after the second wash.

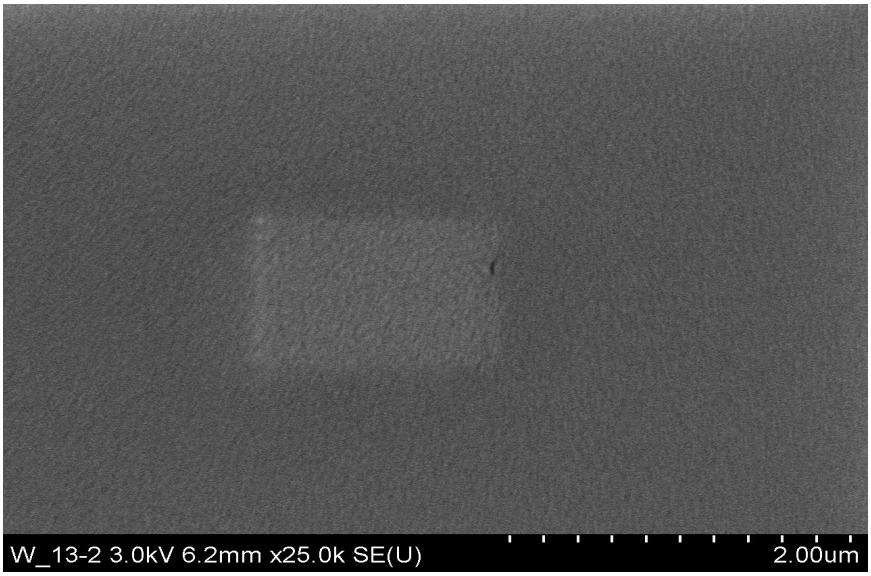

Figure 3.8: FEG-SEM image of wash water after the second wash.

3rd Wash

After the third wash the gel structure under the FEG-SEM (Fig. 3.9) did not appear to be similar to that of the second wash. However, the image of the wash water from this centrifugation (Fig. 3.10) had more structure to it than in the previous wash water. This may be due to the elimination of most of the amorphous cellulose in the previous wash. It was possible to observe what appears to be a small amount of amorphous material and some of the larger debris and cellulose nano-fibrils. At this stage the amount of dry matter in the wash water was around 1%.

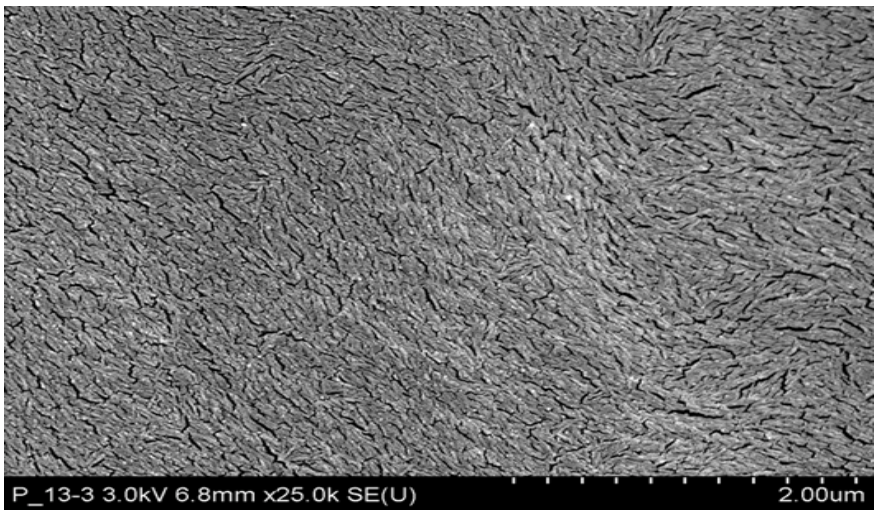

Figure 3.9: FEG-SEM image of filter paper cellulose nano-fibril suspension after the third wash.

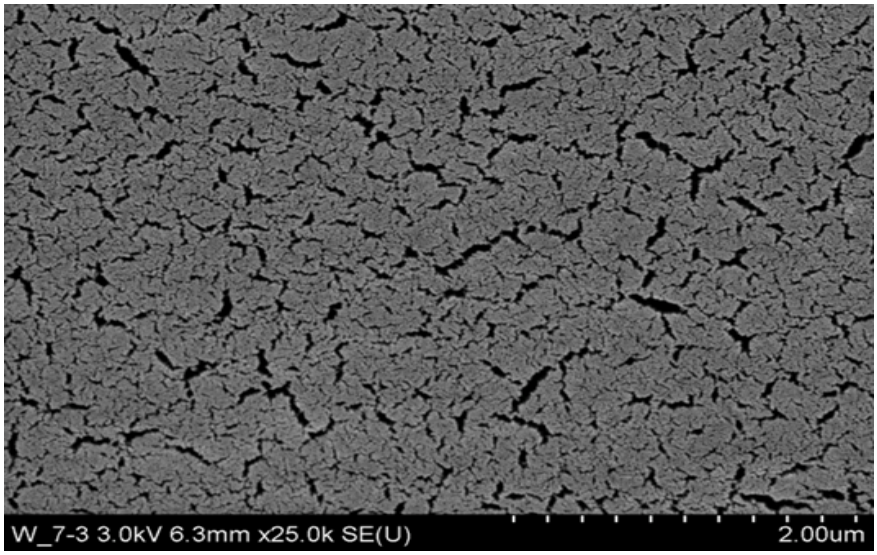

Figure 3.10: FEG-SEM image of wash water after the third wash.

4th Wash

After the 4th wash the cellulose nano-fibrils were easier to discriminate (Fig. 3.11) with the majority of the fine debris removed from the suspension and from here on the better quality nano-fibrils were started being lost as it can be seen in the wash water (Fig. 3.12). It was observed that the dry mass percentage of the wash water from the 4th wash was less than 1%.

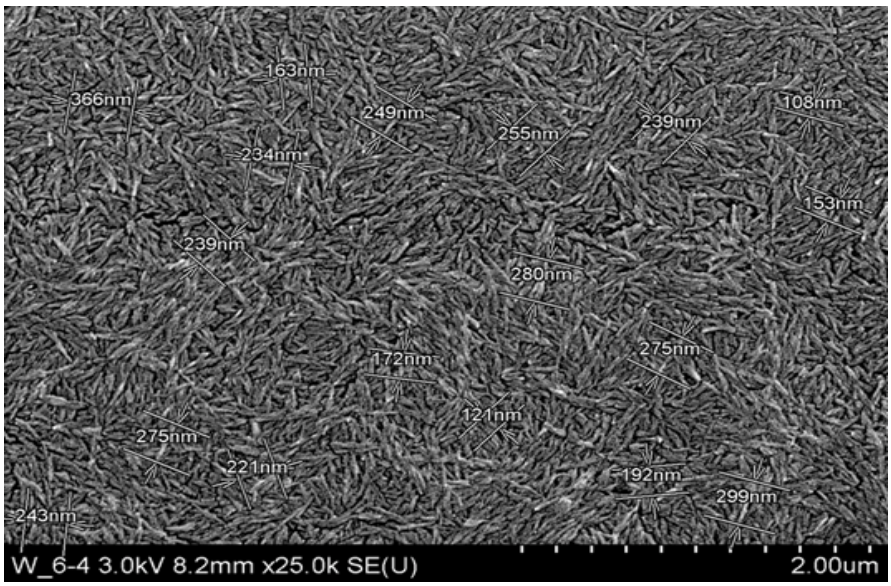

Figure 3.11: FEG-SEM image of filter paper cellulose nano-fibril suspension after the forth wash.

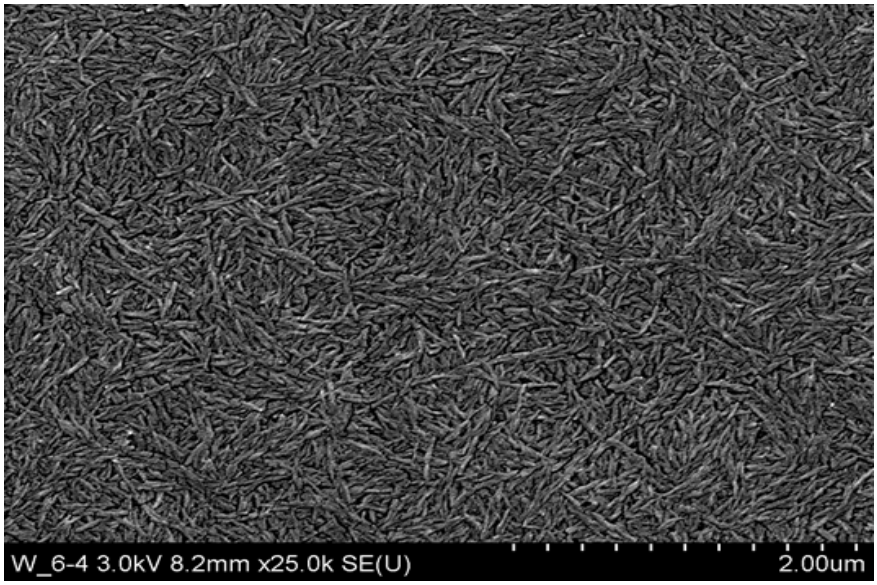

Figure 3.12: FEG-SEM image of wash water after the fourth wash.

5th Wash

After the 5th wash the nano-fibril structure of the gel (Fig. 3.13) does not appear different from that of the previous wash (Fig. 3.11). As with the previous wash water (Fig. 3.12), the wash water after the 5th wash (Fig. 3.14) appeared very similar to that of the gel indicating the loss of nano-fibrils.

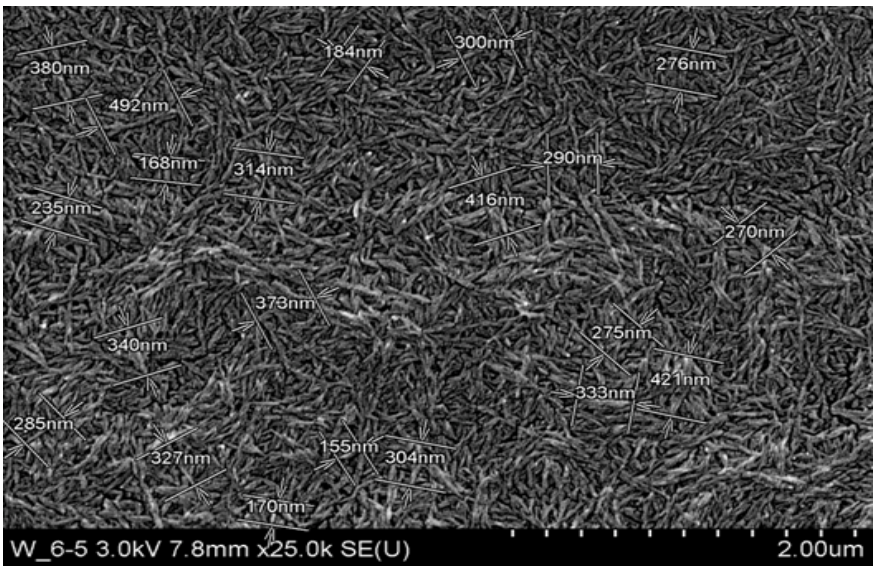

Figure 3.13: FEG-SEM image of filter paper cellulose nano-fibril suspension after the fifth wash.

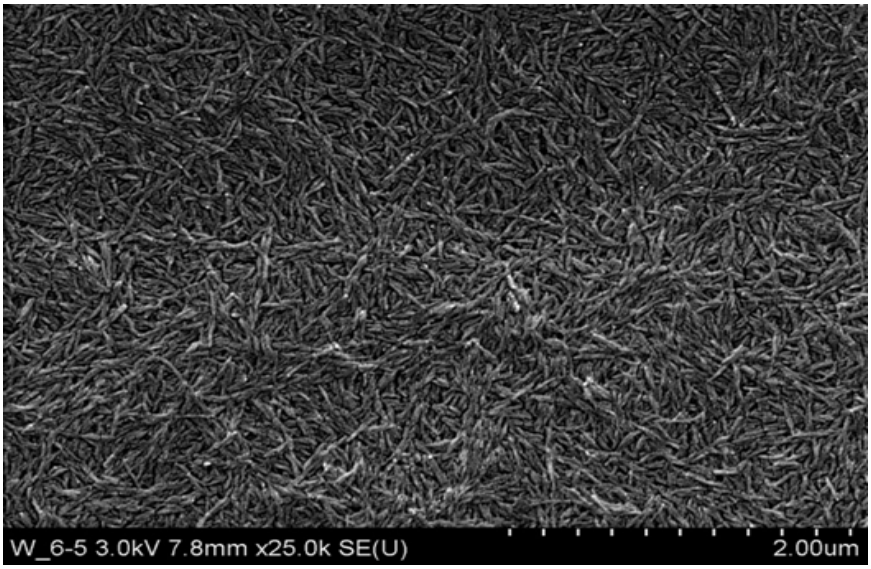

Figure 3.14: FEG-SEM image of wash water after the fifth wash.

6th Wash

Images of the gel appeared to be the same as those from the 5th wash and were therefore not shown.

3.2.4 pH values after the different washes and size distribution

Figure 3.15 indicates the change in pH of the wash water from the first dilution of the original acid hydrolysis (0) through to the fourth (final wash). After washing stages of 0 through to 4, centrifugation time was 1 hour.

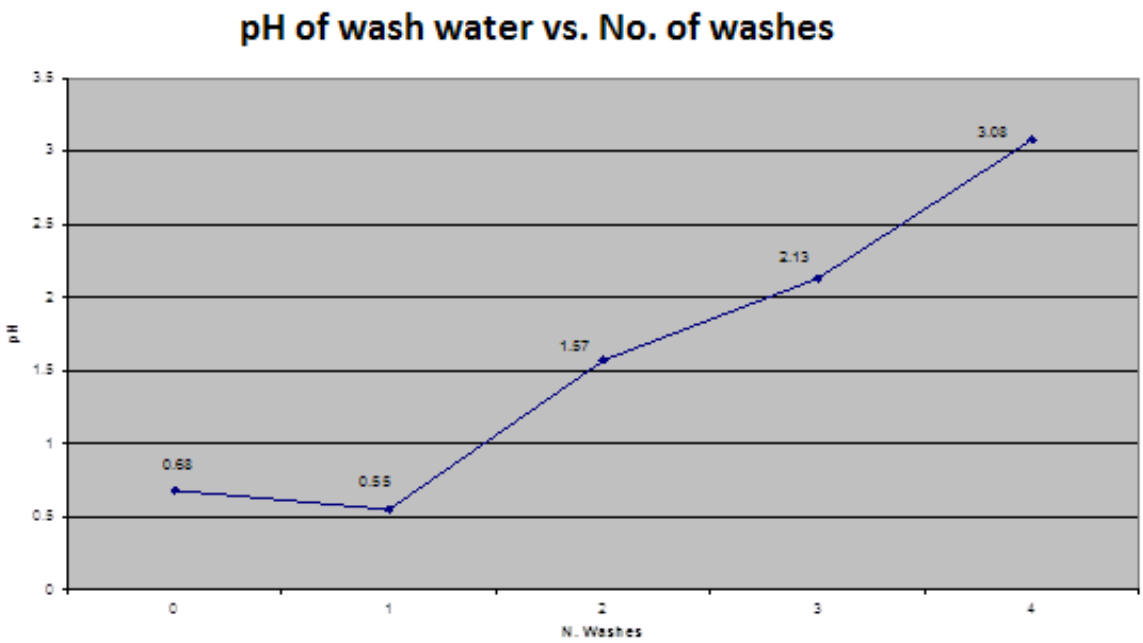

Figure 3.15: pH change of the wash water with number of washes after initial acid hydrolysis.

In order to determine differences between the nano-fibril distribution after the different washes, a study was carried out in which the length of 25 fibres from each image were measured and a graph plotted showing average length and standard deviation (Fig. 3.16). There was a slight (non-significant) trend of increasing average length of nano-fibrils from the first (125 nm) to the 5th and 6th wash (160 nm). However, the data does not give any insight into what can be seen visually between wash 3 and wash 4 where some changes in length distribution were expected. Interestingly, the total variation in nano-fibril length between washes did not appear to change, with a standard deviation of around 70 nm. It is possible that this was due to lack of attention to the small fibrillar debris that was almost certainly present in the earlier washes. It was concluded that this approach whilst giving some indications of fibril size distribution was inadequate for ongoing characterization studies. A decision was taken to establish five washes to remove as much acid as possible and for fractionation purposes.

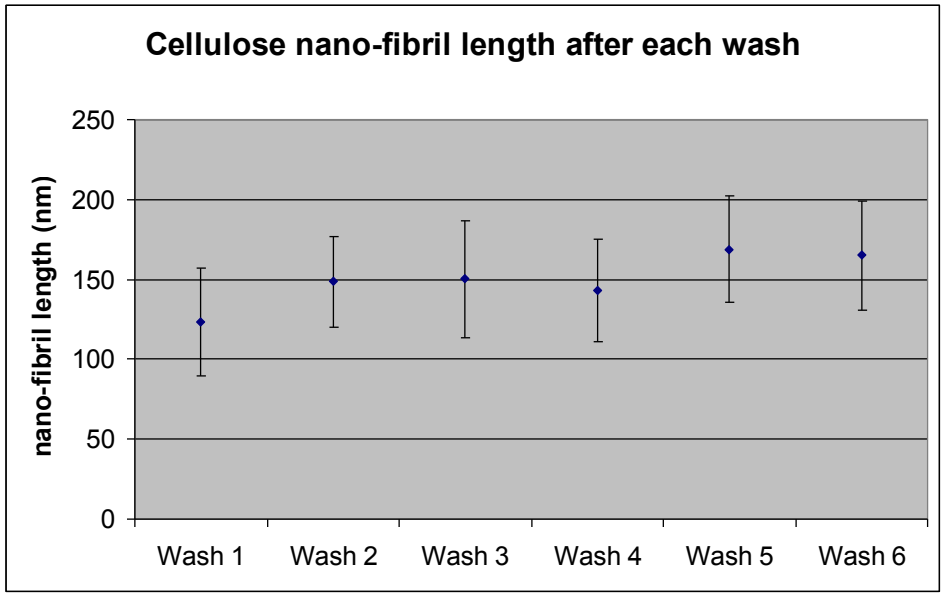

Figure 3.16: Average length and standard deviation of cellulose nano-fibrils in the extracted gel after each wash and subsequent centrifugation.

3.2.5 Discussions for dialysis

After 5 washing/centrifugation stages, the subsequent gel was still very acidic (pH ≤1) and needed further processing. Dialysis was identified in the literature as a critical step in removing excess acid. After the 5th wash the nano-fibril suspension were placed in 15mm diameter visking tubing with a cut off of 12-14KDa. The dialysis tubes were then stored in a bucket and dialysed against running tap water. At this stage in the investigation the level of dialysis required was not clear. One week appeared to be sufficient to stabilize the pH of the suspensions. Figure 3.17 shows the pH change with time, where the solution reached neutral values after five days in dialysis. However it should be noted that this dialysis time was only observed with relatively small amounts of nano-fibrils per bucket. As volumes increased the dialysis time to neutrality increased and required an alternative approach, which will be discussed in Section 9.

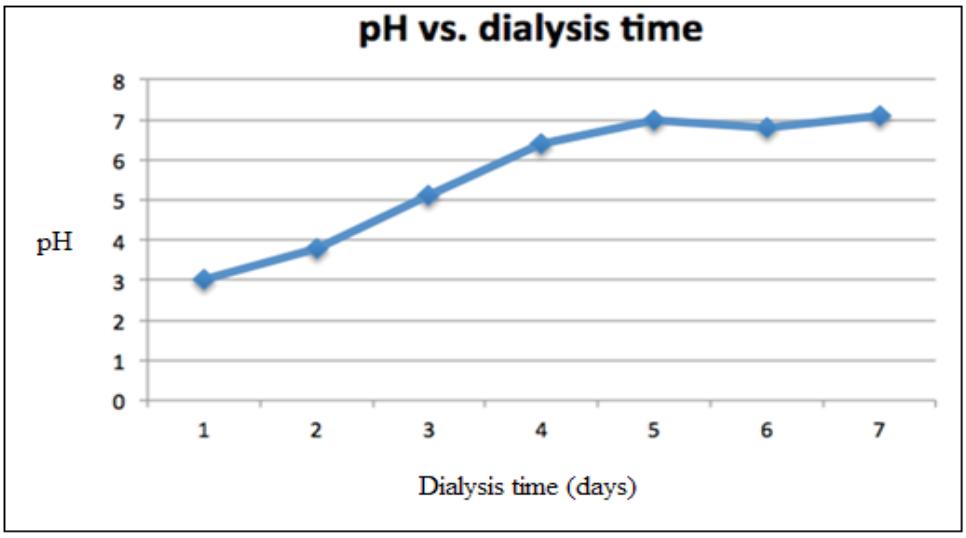

Figure 3.17: pH values for a nano-fibril suspension in dialysis (tap water) for periods of 1 to 7 days.

3.2.6 Summary of conditions required for cellulose nano-fibril gel preparation using Whatman No4 filter paper.

The final conditions established for Whatman No4 filter paper preparation were as follows:

- 52.5% sulphuric acid (w/w) at a temperature of 46°C for 75 minutes;
- The hydrolysis suspension was concentrated by centrifugation at an RCF value of 17 000 for 1 hour. The concentrated cellulose was then repeatedly (5 times) washed and re-concentrated using deionised water followed by a centrifugation for 1 hour;
- After the 5th wash the cellulose preparations were sonicated for 20 minutes (in two 10minute bursts to avoid overheating) to disperse any aggregates and then re-centrifuged to produce the concentrate form;
- After washing and sonication the cellulose suspension was dialysed against running tap water at around 2-5% concentration using visking dialysis tubing with a molecular weight cut-off of 12,000 to 14,000 Daltons, for at least 1 week.

- After dialysis the material was concentrated by centrifugation (RCF value -17 000) for an extended period of 10 hrs. to produce a concentrated gel.

3.3 Methodology for preparation of bacterial cellulose nano-fibrils

As part of this initial study a second source of cellulose nano-fibrils from bacteria was also considered for evaluation as a potential raw material for studies. Bacterial cellulose was chosen for it's high aspect ratio with lengths reported by Sugiyama *et al.,* 1984, Hanley *et al.,* 1992, Imai *et al.,* 1998 at up to 2000 nm with a diameter in the same range as wood based cellulose at around 20 nm. It was thought that this could be used as a model nano-fibril to test the impact of extremes of aspect ratio on the subsequent spinning of continuous fibre. The source of bacterial cellulose selected was Nata de Coco as it is readily available as a food stuff imported from Thailand. The cellulose is prepared as gel cubes saturated with a coconut based syrup, which needs to be removed as part of the preparation process by washes with deionised water.

After a first wash to remove the syrup the bacterial cellulose was sonicated with an "IKA T25 ultra-Turnax" for 15 min at speed No.6. Another four more washes of 4h each were required using strong stirring. When the bacterial cellulose was completely clean (free of additives) it was centrifuged (Sigma 6k 15) for 1h at 9 600 r.p.m. (17 000 RCF) to separate the water from the cellulose. The solids content of the resulting cellulose gel was then determined to establish the correct level of sulphuric acid concentration to be added for the next stage of the process, which included acid hydrolysis. In most cases the water content was around 95% so a 70% sulphuric concentration was used. Hydrolysis was carried out for 90 minutes at 46°C. As the filter paper, acid treatment was required in order to sulphate the surface of the fibrils to allow formation of a stable liquid crystal suspension.

After hydrolysis the same procedure as with filter paper was followed with a series of washes followed by centrifugation. Figure 3.18 shows an image at 25K magnification, at this stage the fibrils were still contaminated with non-crystalline material.

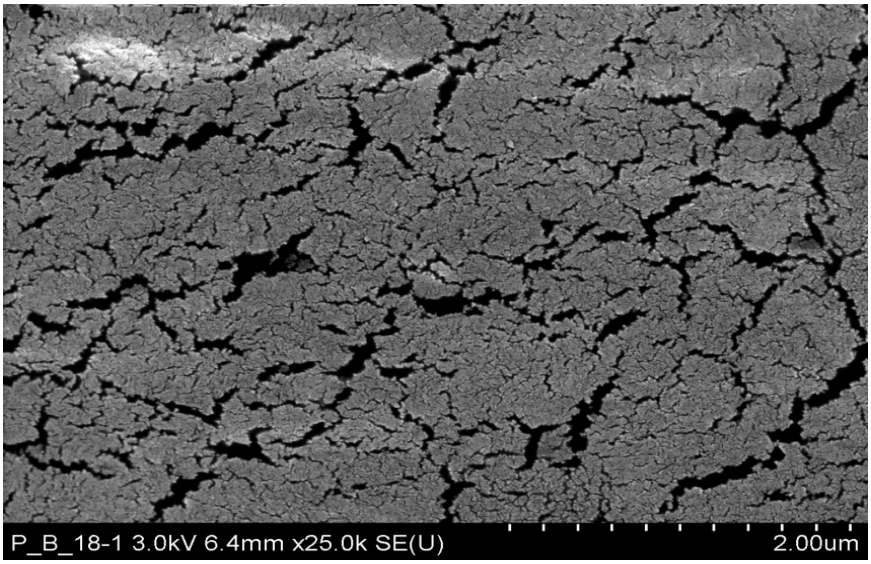

Figure 3.18: FEG-SEM image of bacterial cellulose nano-fibrils suspension after the first wash.

After the second wash the cellulose nano-fibrils were clearly discernable but still not without contamination (Fig. 3.19).

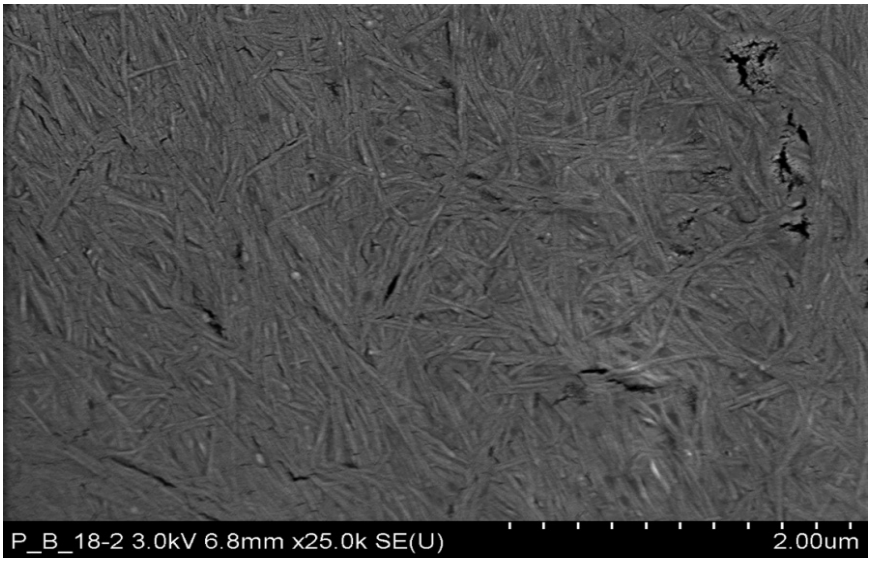

Figure 3.19: FEG-SEM image of bacterial cellulose nano-fibrils suspension after the second wash.

After the third wash debris and amorphous material was still observable amongst the fibrils (Fig. 3.20).

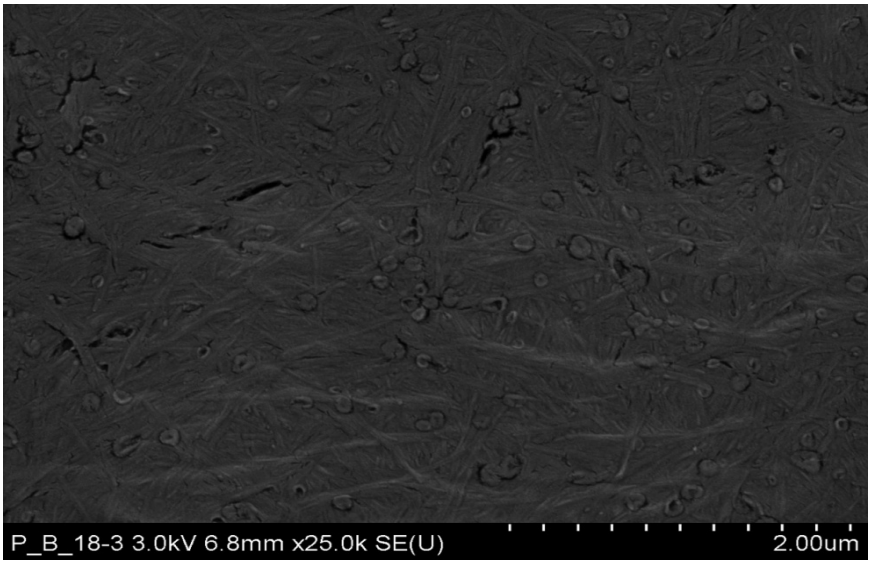

Figure 3.20: FEG-SEM image of bacterial cellulose nano-fibrils suspension after the third wash.

After the fourth wash (Fig. 3.21) it looked as if all of the fine debris had been removed and the structure of the fibrils appeared to be more uniform.

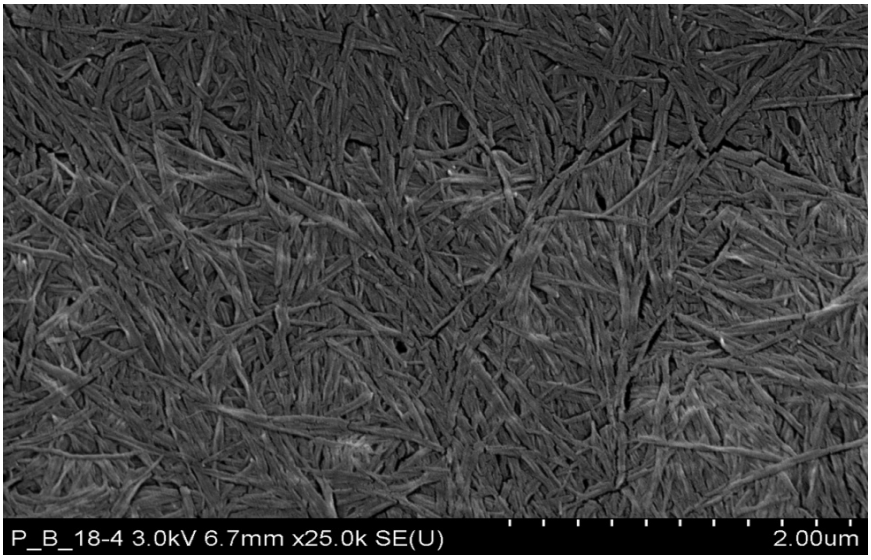

Figure 3.21: FEG-SEM image of bacterial cellulose nano-fibrils suspension after the fourth wash.

After the fifth wash (Fig. 3.22) the structure of the fibrils appeared to be sharper suggesting that residual amorphous material and debris had been removed from the gel.

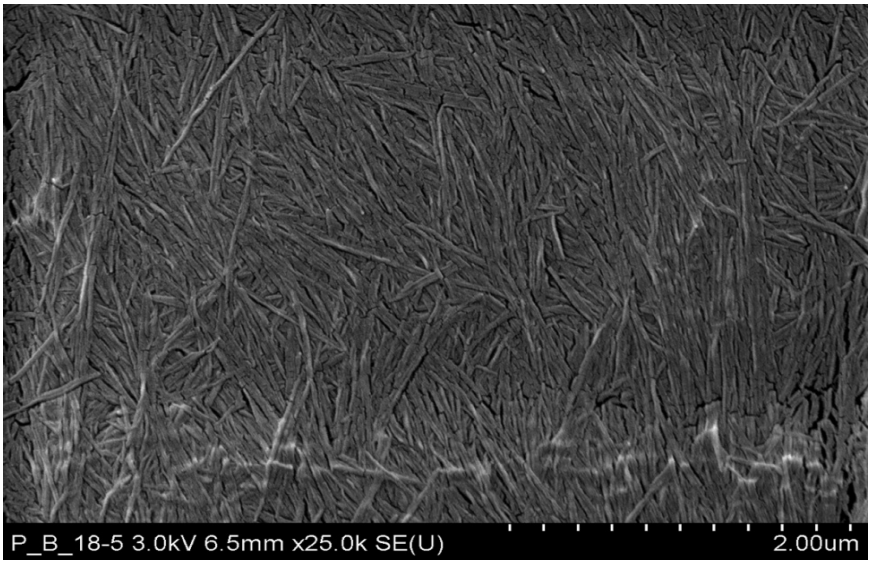

Figure 3.22: FEG-SEM image of bacterial cellulose nano-fibrils suspension after the fifth wash.

It was not possible to measure fibrils after the first wash due to the extent of contamination. Figure 3.23 shows an increase in the average length of nano-fibrils between the second and third wash but as with the previous starting materials the variation was large, meaning that the differences were not significant. There appeared to be no differences in average fibril length after wash 3. The graph also shows a clear increase in the average length of cellulose nano-fibrils compared with that of filter paper after wash 3. It can also be observed that the standard deviation of the bacterial fibril length was much higher at 400 nm. This bacterial cellulose was used in later spin trials reported in Section 10.3.

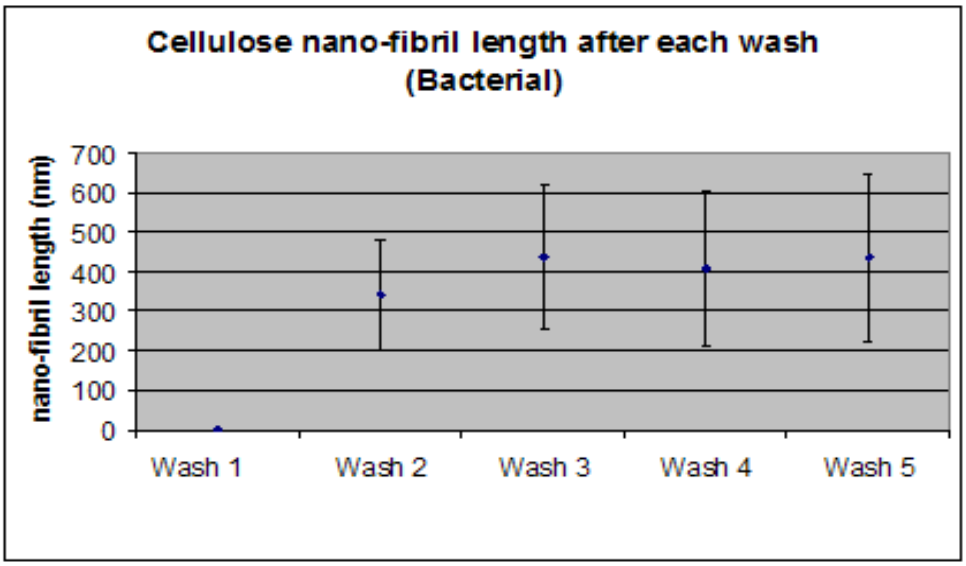

Figure 3.23: A graph of average length of cellulose nano-fibrils using FEG- SEM after each of the fibre washes. NOTE: There were not visible nano-fibrils after the first wash.

4 ASSESSMENT OF METHOD FOR DETERMINING NANO-FIBRIL SIZE DISTRIBUTION

As part of an ongoing process to better understand and characterize the cellulose nano-fibril suspensions, a new approach to size distribution assessment and surface charge determination was identified. In earlier studies, the electron microscope was used to measure nano-fibril size distribution. This approach was time consuming and because the method used manual measurement of each nano-fibril there was a limit to the number of fibrils that could be practically measured. The approach gave comparative data for different sources of nano-fibrils. However, it limited the statistical validity of the results. In addition the method was not good at discriminating fibrillar debris.

When it came to looking at surface charge it was measured indirectly through measurement of acid group content in the suspension using conductiometric titration. It was not known how good the correlation was between acid group content and the actual surface charge on the fibril surfaces.

4.1 Zetasizer

A laboratory instrument known as a Zetasizer (Malvern, Nano ZS) was reported as being theoretically capable of measuring both size distribution and surface charge. This was evaluated for its suitability in characterizing the nano-fibril suspension developed in this investigation.

The Malvern Instruments Zetasizer Nano (Fig. 4.1) is a Dynamic Light Scattering (DLS) measurement device used for characterising particle size and zeta potential. In DLS the speed at which particles are diffusing due to Brownian motion is measured. The instrument measures the particles as they rotate. This assuming a spherical object, the diameter of which theoretically relates to fibril length. For this reason information like aspect ratio or particle's diameter cannot be measured through this method.

Figure 4.1: Zeta-size nano ZS.

The second value that can be determined from the Zetasizer is zeta potential. Zeta potential is a measure of the charge that a particle achieves within a specific medium. It can be used as a predictor for colloid stability. If all the particles in a colloid have the same charge there will be repulsion effects, with the magnitude of this repulsion affecting colloid stability. The Zeta potential for stability is generally taken as being ±30mV. If the zeta potential is higher than 30mV (positive or negative) then this is a good indicator of stability (see figure 4.2). Below 30mV the particles will generally begin to aggregate. Zeta potential is pH dependent, decreasing (generally) as the pH approaches neutrality. Zeta potentials will generally be positive at low pH and negative at high pH.

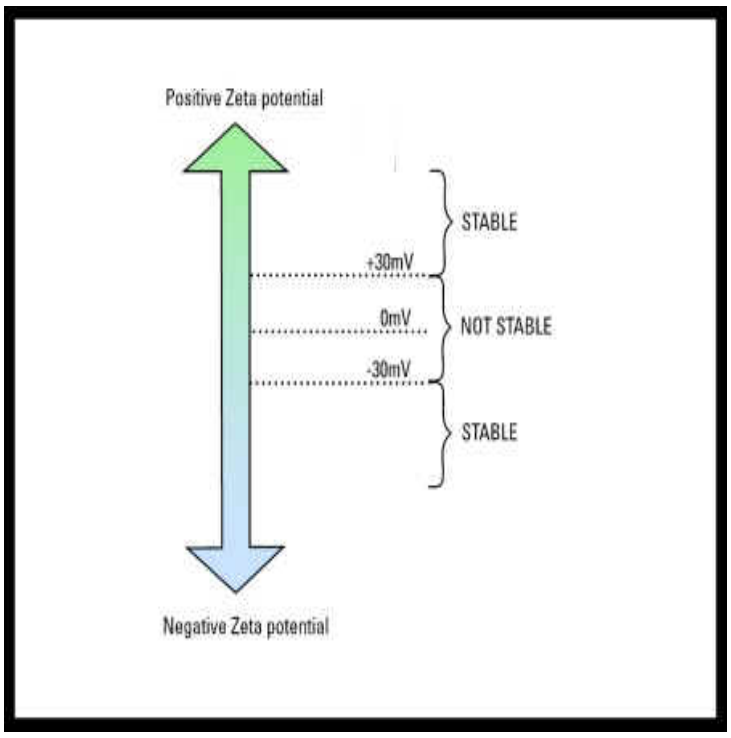

Figure 4.2: Zeta potential and colloid stability (Malverm commercial catalogue).

4.2 Experimental work

A small study was developed to assess the Zetasizer accuracy to measure the particle size distribution of the cellulose nano fibrils. For that, two industrial pulps viscose (α92) and acetate (α96) grade pulp preparations were evaluated for nano-fibril size distribution, manually using a SEM and automatically using a Zetasizer. The preparation process for these two pulps is described in Section 5. Distribution data is a composite of values from 3 separate preparations. The different methods were expected to give slightly different results since the zetasizer values gave an approximate determination of fibre length based on the diameter of a sphere resulting from fibre rotation and such proved to be the case with different overall size distribution. However, the mean values for fibril length (Fig. 4.3 and Fig. 4.4) were comparable at 150nm for Acetate and 180nm for the viscose grade pulp source. In both methods the ranking of the two samples stayed the same. Based on this result, it was concluded that the Zetasizer could be used as a routine tool for measuring the length distribution of cellulose nano-fibrils.

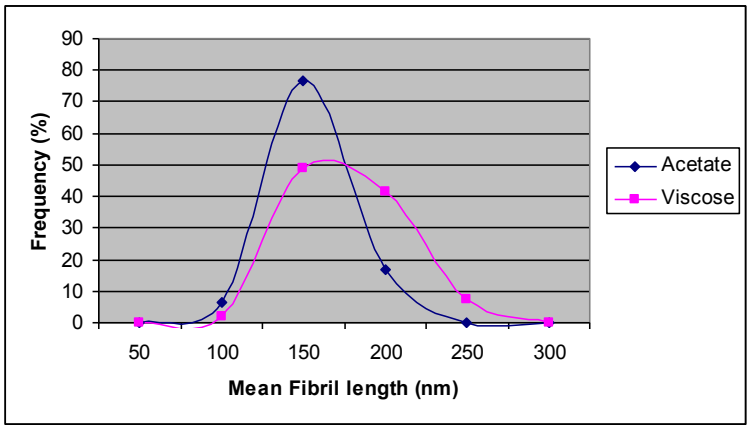

Figure 4.3: 92α viscose and 96α acetate grade nano-fibril size distribution comparation using the FEG-SEM.

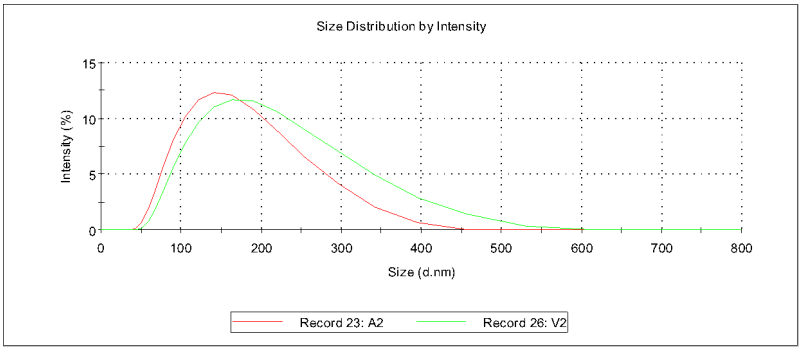

Figure 4.4: 92α viscose and 96α acetate grade nano-fibril size distribution comparation using the Zetasizer. (V2 =viscose and A2 = acetate).

4.2.1 Development of an optimal method for measuring fibril length using the Zetasizer.

Following on from the initial assessment to determine if the Zetasizer could be used as a tool to measure fibril length, a series of further investigations were carried out to determine optimum conditions for its use.

Cellulose nano-fibril suspensions from four different sources of cellulose were prepared using standard acid hydrolysis conditions described for Whatman No4 filter paper (Section 3.2.6). The samples were then dialysed against tap water for one week. Samples were then measured using the Zetasizer both before and after sonication for thirty minutes at 3400 r.p.m. (IKA, T25-D Ultra- TURRAX).

Results of the findings on Size distribution and zeta potential are shown in Table 4.1.

Sample number	Sample Identity	Average particle size (length) before sonication (nm)	Average particle size (length) after sonication (nm)
1	Northwood	164	84.5
2	Enopine	197	118.4
3	Cotton	301	239.2
4	Bacterial	547	470.6

Table 4.1: Average particle size before/after sonication for some industrial pulps.

From table 4.1 it can be seen that sonication to disperse the particles had an effect on the average particle size determination. This is also shown in Fig. 4.5 and Fig. 4.6, which show the distribution of particle lengths.

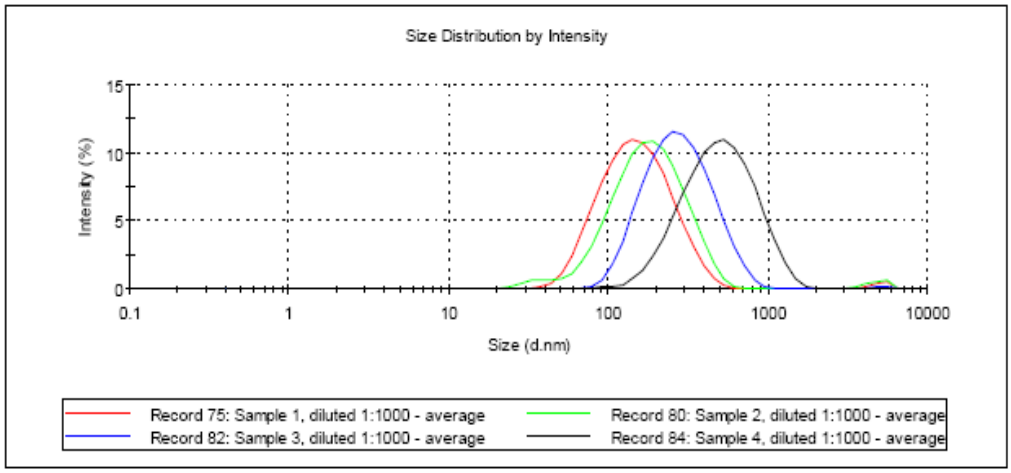

Figure 4.5: Size distribution of all 4 samples without sonication. Sample number identities are shown in table 4.1.

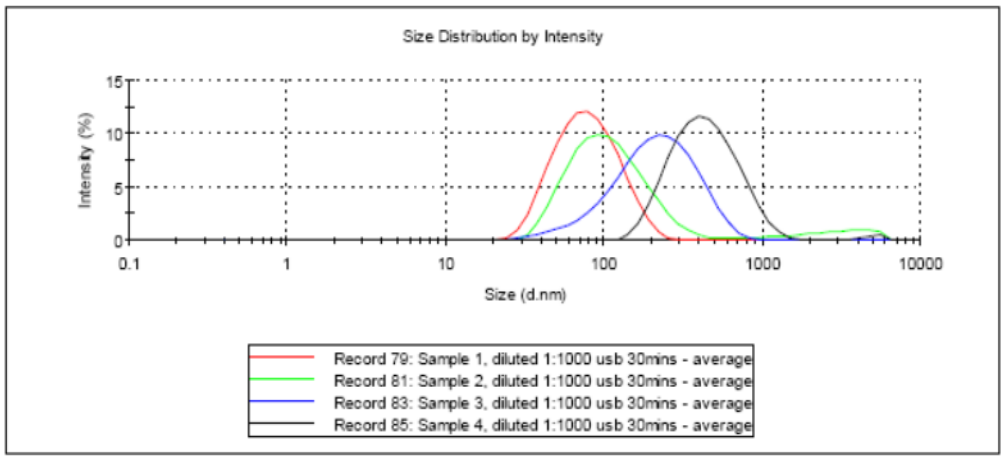

Figure 4.6: Size distributions of all 4 samples following sonication. Sample number identities are shown in table 4.1.

What was interesting is that there is a long tail on the distribution of Enopine and bacterial cellulose. Figure 4.6 shows a shift in the size distribution, indicating the impact of sonication. It is postulated that sonication leads to dissociation of aggregated nano-fibrils. It is however possible that sonication can also lead to break down of the fibrils. The graph below (Figure 4.7) shows the effect of increasing lengths of sonication time on a single sample (Sample 1). It can be seen that there was no significant difference in fibril length between 20 minutes and 30 minutes of treatment

suggesting that breakdown is not occurring. Until this point 20 minutes sonication was used in the preparation process. These results suggested that this set of conditions could be used as a standard in future studies.

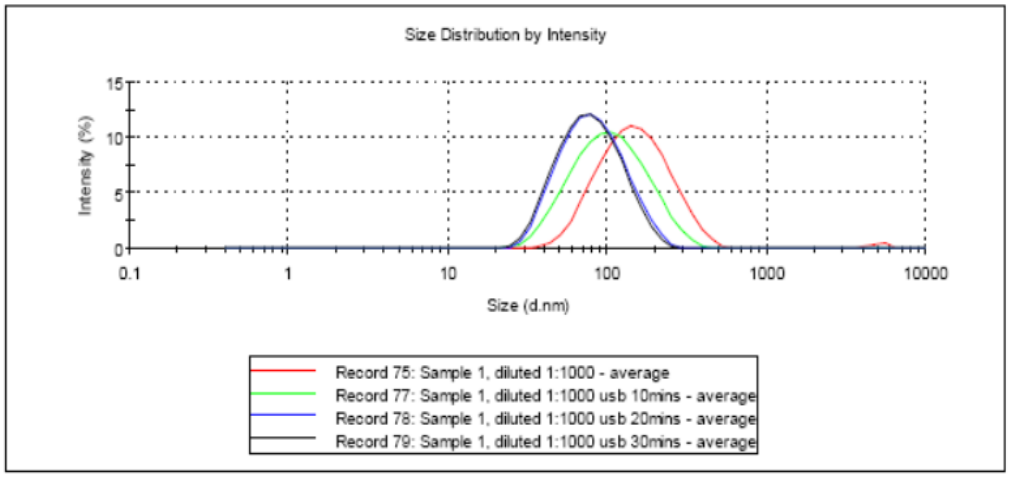

Figure 4.7: Effect of sonication (for 10, 20 or 30 mins.) on particle size for sample 1.

Table 4.2 shows the actual zeta potential values for the four samples measured. All the samples exhibited similar zeta potentials, in the range of -34 to -37mV. This would indicate that the colloid suspensions should be stable.

Sample number	Sample Identity	Zeta potential (mV)
1	Northwood	-36.9 *(0.7)*
2	Enopine	-36.4 *(0.5)*
3	Cotton	-34.0 *(0.2)*
4	Bacterial	-35.1 *(0.2)*

Table 4.2: Zeta potential of some industrial pulps. Standard deviations in parentheses.

Figure 4.8 shows the actual zeta potential values for the four samples measured.

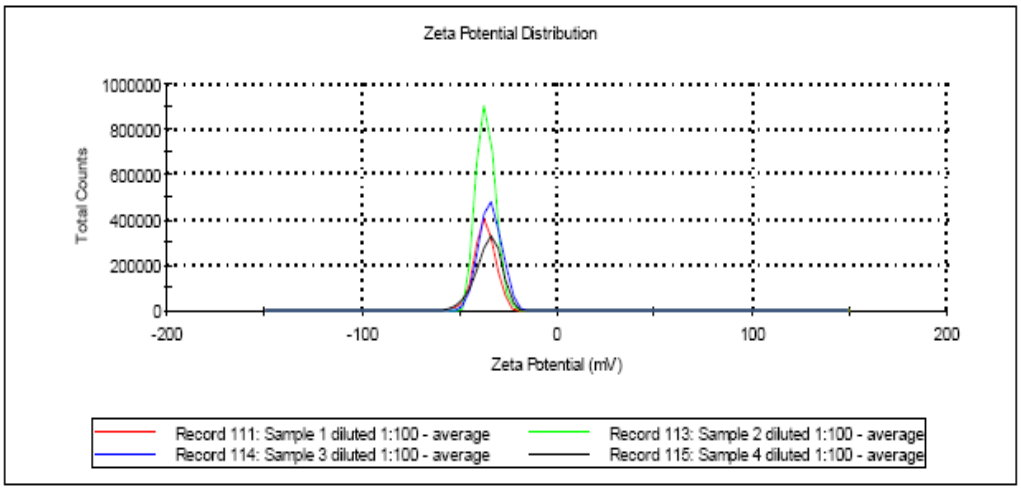

Figure 4.8: Zeta potential of samples.

4.2.2 Conclusions for Zetasizer evaluation

The results indicate that the Zetasizer was particularly well suited to characterization of particle size distribution and surface charge and provided a tool that can be used to efficiently determine both, the length distribution and zeta potential of cellulose nano-fibril suspensions.

5 IDENTIFICATION OF AN ALTERNATIVE SOURCE OF CELLULOSE TO WHATMAN No4 FILTER PAPER.

5.1 Introduction

The objective of this study was to identify an industrial pulp that could be used as an alternative to filter paper. This was required for later work in which the hydrolysis process was scaled up and significantly larger volumes of cellulose were required for spinning studies and filter paper was not considered as a practical and economic option. In addition, due to the extent of commercial interest in this project. It was also considered necessary to develop a process that was more closely matched to an industrially available cellulose resource.

5.2 Experimental work

5.2.1 Ball milling

A number of industrial pulps were hydrolysed in a manner similar to that for Whatman No4 filter paper, but due to the tougher characteristics of the pulp they had to be ground in the ball mill for a longer period of 40 minutes.

An initial evaluation of some industrial pulps highlighted in Table 5.1 was carried out to screen for the most appropriate material for ongoing optimization studies. Initial findings showed that it was possible to extract nano-fibrils successfully from all the industrial pulps. However, there were differences in the ease with which it was possible to produce what appeared to be a consistent gel. It is worth noting that the biggest challenge was with Ecocel, a mixture of softwood and hard wood followed by Ardennes, a mixed hardwood pulp. In both cases the extracted gels formed two separate layers after washing and concentration with centrifugation. It is possible that this was due to the mix of species used in the pulp. However, it should be noted that in earlier development work with Whatman No4 cellulose, similar characteristics were observed.

		Viscosity cm^3/g
Ardennes	Mixed hardwood	487
Viscose (92α)	Eucalyptus grandis	607
Acetate (96α)	Eucalyptus grandis	611
Northwood	Canadian Softwood	650
Terrace Bay	Canadian Softwood	693
Södra gold	Scand.SW	612
Enopine	Scand.SW	597
Laja	Radiata Pine	620
Ecocell tcf	Sulphite (80% spruce/20%beech)	822

Table 5.1: Summary of some of the pulp types used. The viscosity values given are those provided by the manufacturer.

Figure 5.1 shows the fibril distribution of different pulps measured using the Zetasizer after the fourth wash. Figure 5.2 shows the change after the 5th wash. What was most striking was that after the fourth wash Enopine had a fibril length distribution comparable to that of bacterial cellulose. This was unexpected as it proved to be an outliner compared with the other industrial pulps. The results showed, clear differences between different commercial pulps and justify the exploration of fibre resource as a source of variation in the manufacturing process. This knowledge could help play an important role in determining the most appropriate commercial pulp resources for the manufacture of cellulose nano-fibrils, if fibril length proves to be an important factor in the fibre manufacturing process.

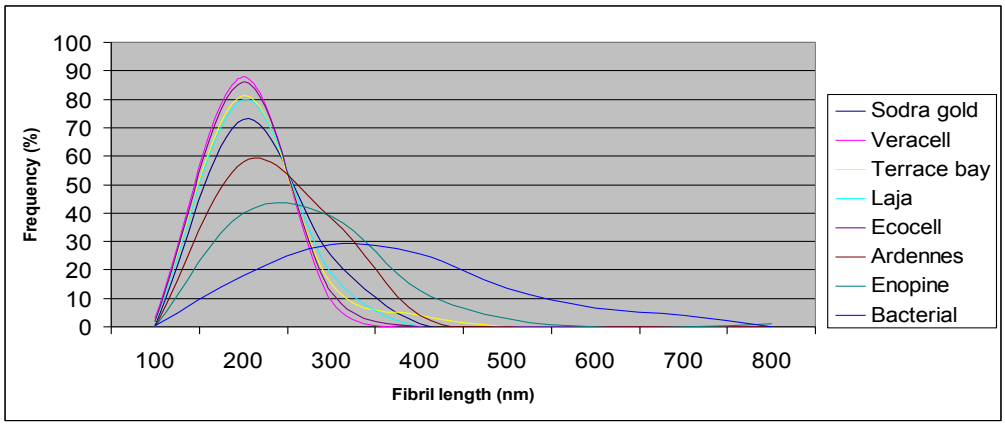

Figure 5.1: Fibril distribution for different industrial pulps after the fourth washes.

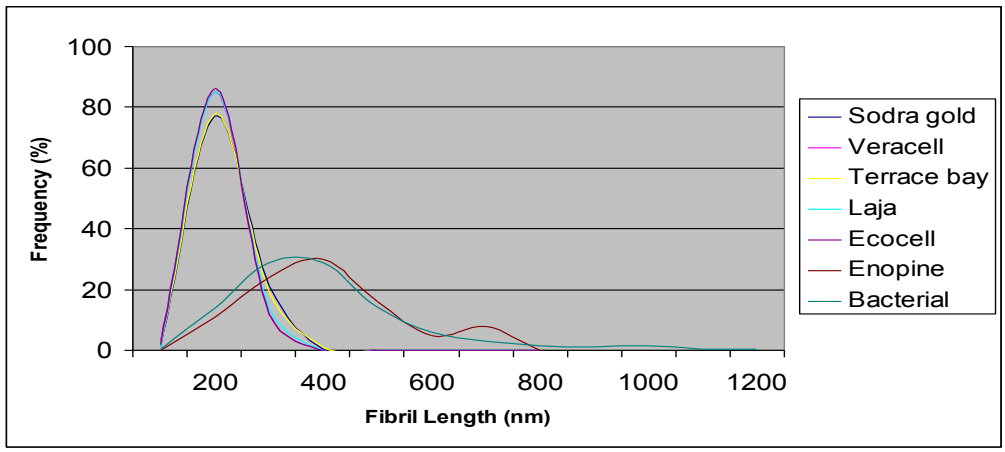

Figure 5.2: Fibril distribution for different industrial pulps after the fifth washes. Note that Ardennes is missing due to lost data.

5.2.2 Optimization of hydrolysis of industrial pulps

Notably the viscose (92α) and acetate (96α) grade pulps were similar to cotton to process. Out of these two pulps, the 92α cellulose viscose grade pulp was slightly easier to process than the acetate grade pulp and had slightly longer fibril lengths. So a decision was taken to focus on the production of viscose grade pulp and to use it as a benchmark industrial pulp so it was selected for ongoing optimization studies.

A set of standard hydrolysis conditions were established of 51% sulphuric acid concentration at 46°C for 60 minutes. As with Whatman No4 the next step involved an evaluation of the washing and centrifugation steps.

Figure 5.3 shows an image of the fibrils from viscose pulp after the first wash. As with earlier trials with Whatman No4 and bacterial cellulose, it was not possible to see individual fibrils due to the large amount of amorphous material present; the electron beam damaged the substrate explaining the cracked appearance of the surface.

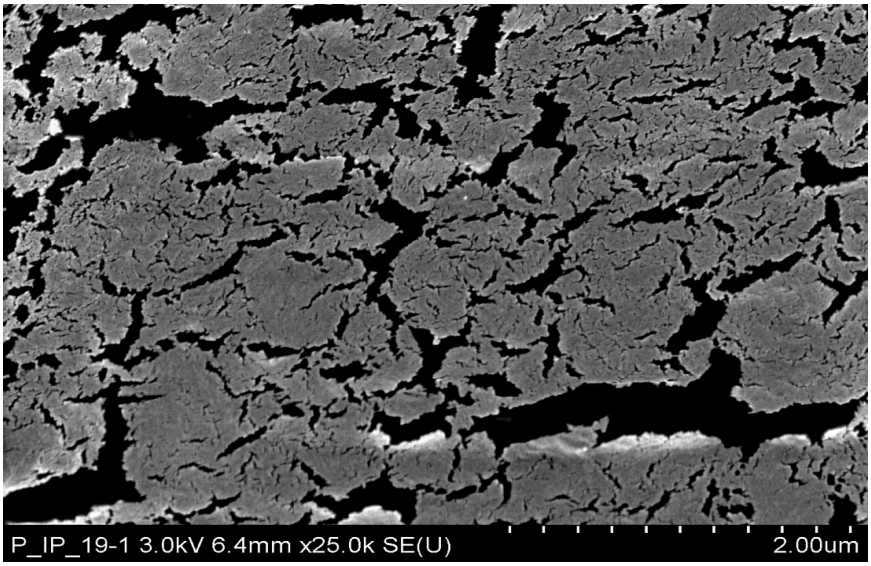

Figure 5.3: FEG-SEM image of 92α viscose cellulose nano-fibrils suspension after the first wash.

After the second wash it was possible to see individual nano-fibrils (Fig. 5.4):

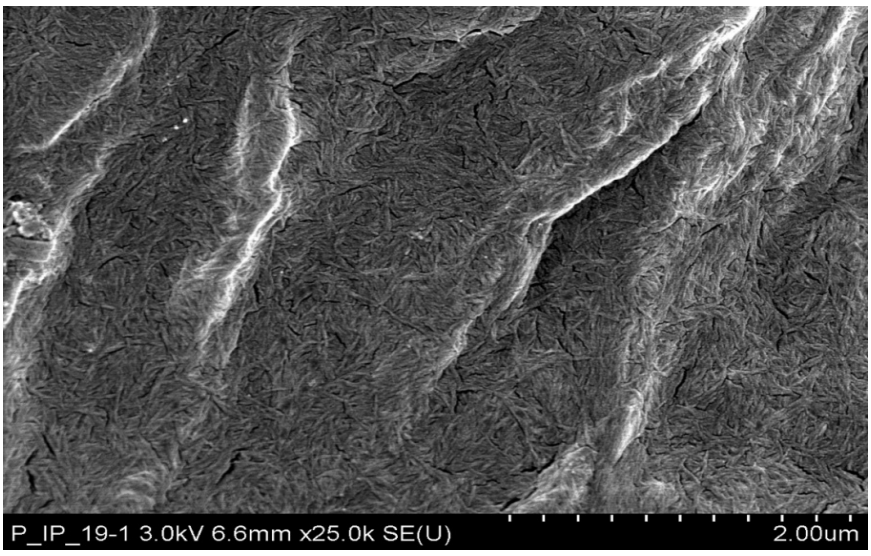

Figure 5.4 FEG-SEM image of 92α viscose cellulose nano-fibrils suspension after the second wash.

There did not appear to be any visual differences between the nano-fibrils from the second (Fig. 5.4) and third wash (Fig. 5.5).

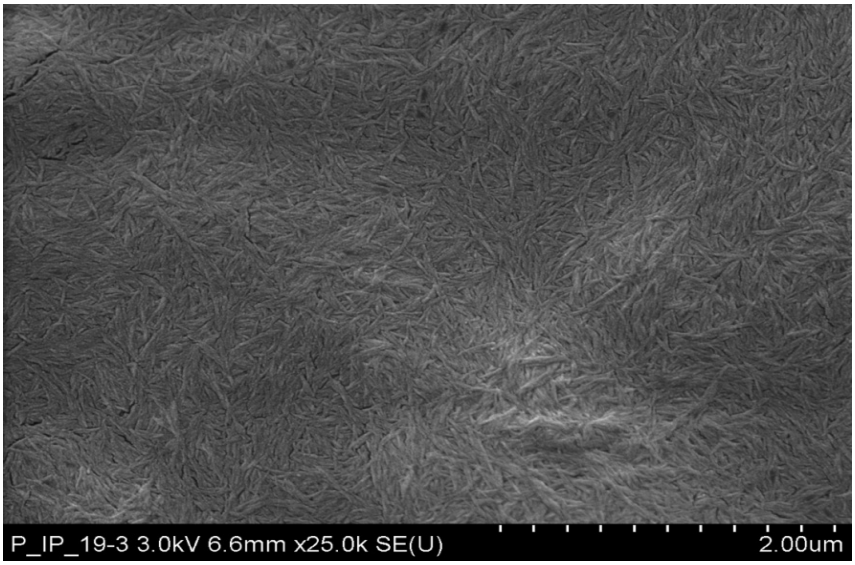

Figure 5.5: FEG-SEM image of 92α viscose cellulose nano-fibrils suspension after the third wash.

The nano-fibrils in the gel from the fourth wash (Fig. 5.6) appeared to be sharper than in figure 5.5, probably due to the removal of any residual amorphous material and fine debris.

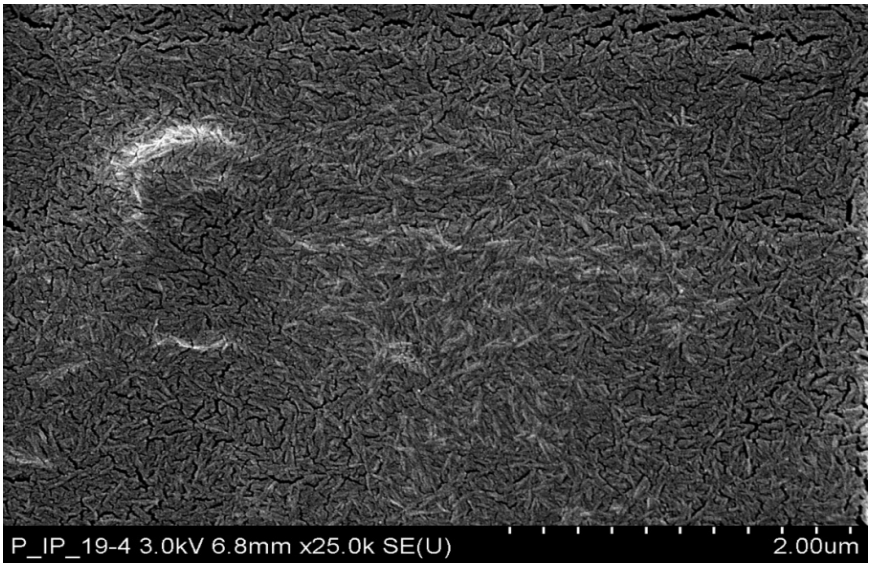

Figure 5.6: FEG-SEM image of 92α viscose cellulose nano-fibrils suspension after the fourth wash.

There appeared to be no change in the structure of the gel after the fifth wash (Fig. 5.7) suggesting no further benefit from additional fractionation. Figure 5.8 actually shows a slight decrease in average fibril length after the 5th wash using the FEG-SEM method, however, it was not significant. It was interesting to note that the average length of fibrils for the viscose grade pulp was longer (200 nm) compared with that from Whatman No4 filter paper at 150nm (Fig. 3.15).

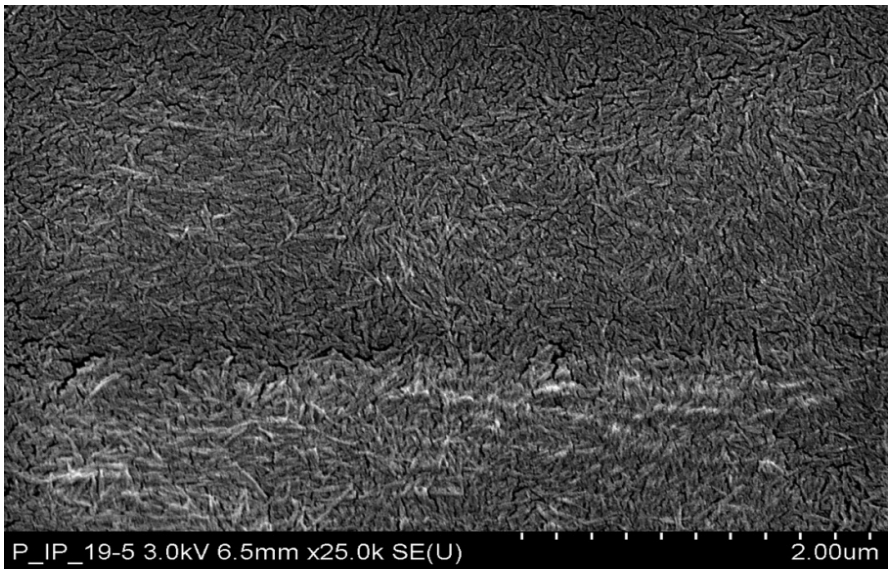

Figure 5.7 FEG-SEM image of 92α viscose cellulose nano-fibrils suspension after the fifth wash.

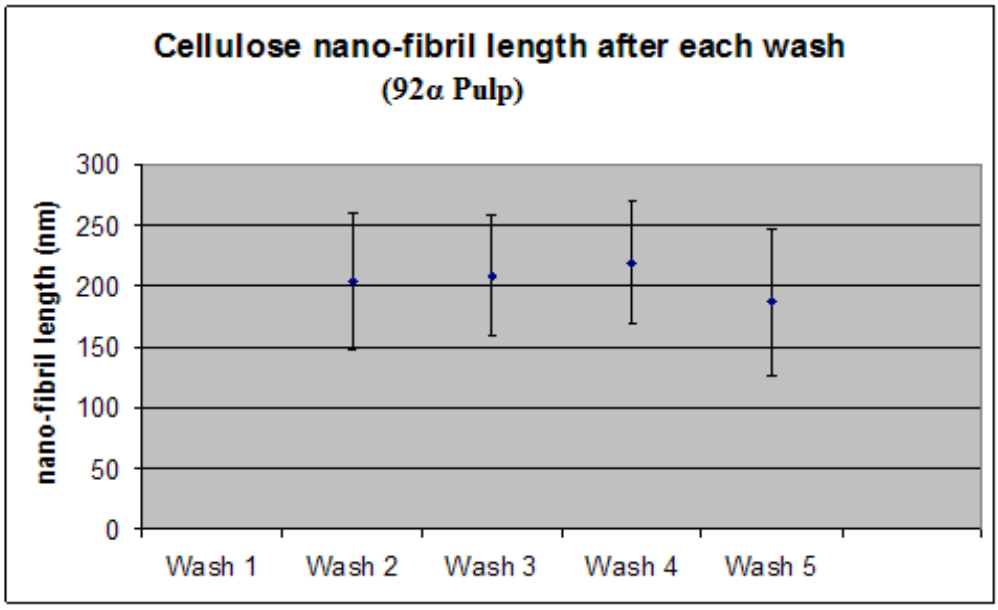

Figure 5.8: Average length and standard deviation of cellulose nano-fibrils in the extracted gel after each wash and subsequent centrifugation determined using the FEG-SEM.

5.2.3 Comparison of processing conditions for Whatman No.4 and 92α cellulose Industrial pulp.

The overall processing conditions for the two sources of cellulose were similar with hydrolysis time being shorter with slightly lower acid concentration for the 92α cellulose viscose grade pulp (Table 5.2). The number of centrifugation and washing steps was the same for both sources of cellulose. So a decision was taken to focus on the production of viscose grade pulp and to use it as a benchmark industrial pulp so it was selected for ongoing optimization studies.

	Whatman No.4	Viscose
Acid concentration	52.5% H_2SO_4	51% H_2SO_4
Temperature	46°C	46°C
Time	75 mins	60 mins

Table 5.2: Summary of hydrolysis conditions for Whatman No4 filter paper and 92α cellulose viscose grade pulp.

6 DEVELOPMENT OF THE FIBRE SPINNING PROCESS

6.1 Methodology

At the start of this project there was no published or established method for the spinning of a continuous fibre from cellulose nano-fibrils. As a result, a number of alternative approaches were tried as part of a developmental process.

The first step in the process was to extrude fibres from a hypodermic syringe on to a highly polished steel plate. The fibres were then allowed to air dry and then analysed using FEG-SEM to see how the nano-fibrils within the fibres were aligned. The gel was produced from Whatman No4 following the conditions established in section 3.2.6. It was concentrated for 24 hours at 17 000 RCF in a Sigma centrifuge to get a 20% solid content gel.

In some subsequent fibres it was possible to orient the surface fibres over short distances with improved flow of the fibril suspensions. These fibres were exposed to very high pressure (25 ton press) at 150°C to see if it was feasible to induce mass aggregation (crystallisation).

The fibres produced were relatively large (around 1mm diameter). FEG-SEM analysis of the fibres highlighted a chiral nematic twisted structure (Fig. 6.1), which resulted in multiple layers within the fibre. This structure resulted in a large numbers of defects (both within each layer and between layers). FEG-SEM images indicated that when the fibrils were aligned over short distances up to 500 nm they fused into a continuous, smooth surface. However, where the fibrils changed direction because of the chiral nematic twist in the gel there were very clear surface defects, which even the high pressures where unable to smooth out.

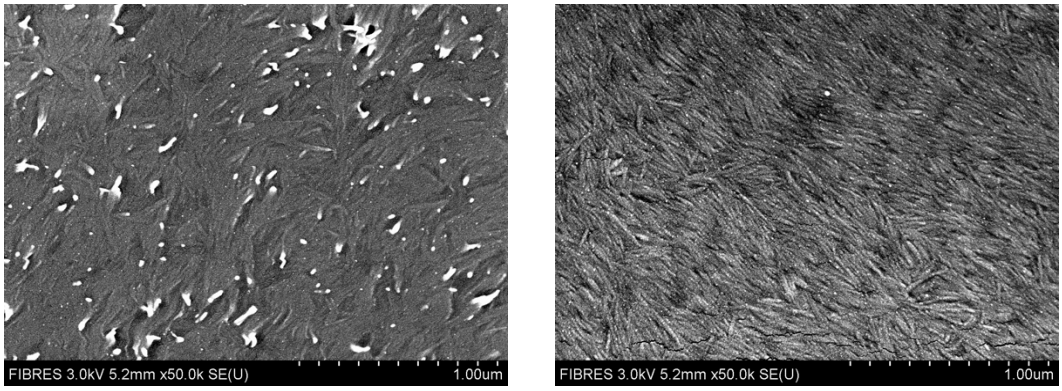

Figure 6.1: FEG-SEM photographs at 50 000x magnification. On the right the fibre was spun from a hypodermic syringe on to a highly polished steel plate. On the left the same process was done, however the fibre was subsequent pressed under 25 tons.

From this initial study it was apparent that to produce a high strength fibre a nematic phase (a linear alignment of the fibres) was needed. It was therefore critical to understand the conditions required to induce better alignment (ideally a nematic phase) before any fibres worth testing could be produced.

6.2 Manual injection against rotational cylinder

Based on the twisted chiral structure of fibres on a static plate, it was decided that fibres should be extruded onto a rotatory heated roller to see if better alignment could be induced as the fibre was drawn from the needle. A relatively basic spinning process using a lathe was developed to test the importance of draw speed on fibril alignment. The fibres were extruded manually from a syringe with a 250 micron needle onto a rotating drum (diameter of 150 mm), which was heated to 100^{o}C to facilitate rapid drying. Different rotational speeds were testing, from 600 to up 1600 r.p.m.

It was found that at slow drawing speeds fibril alignment was more or less random (Figure 6.2, FEG-SEM image at 50 000x). However under fast drawing conditions, a degree of fibril alignment was observed (Figure 6.3, FEG-SEM image at 50 000x).

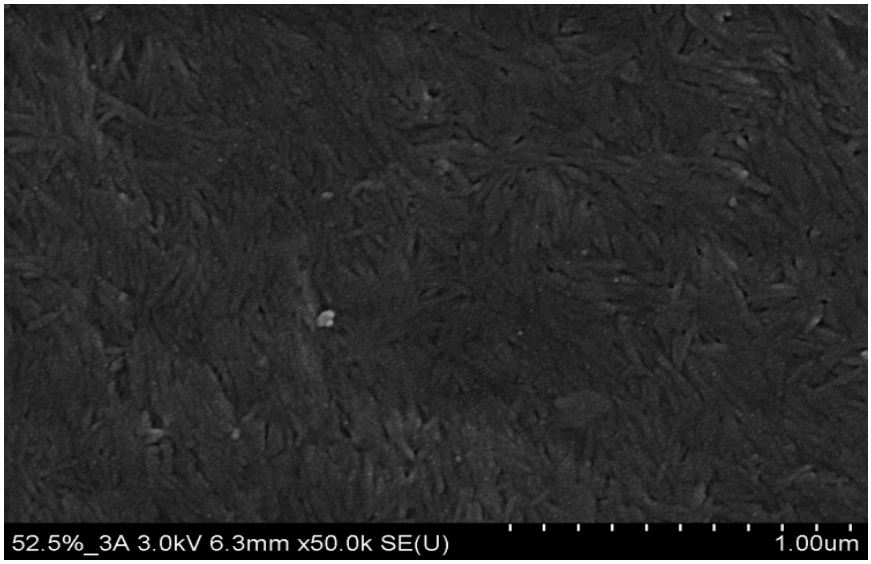

Figure 6.2: FEG-SEM image of slow spun fibre (600 r.p.m.) showing random orientation of surface fibres.

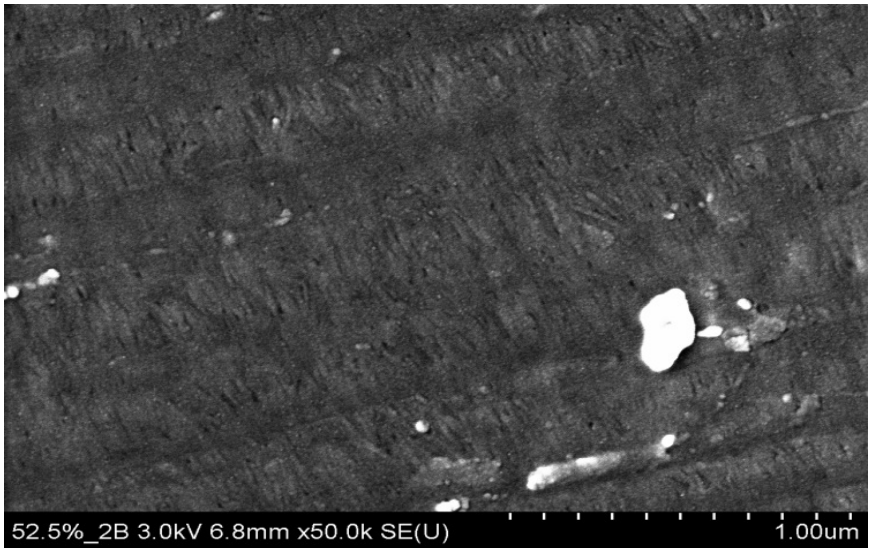

Figure 6.3: FEG-SEM image of fast spun fibre (1600 r.p.m.) showing oriented surface fibres. Note Horizontal marks on the surface are caused by striations on the drum on which the fibres were spun and are not a function of the spinning process.*

The decision to heat the drum was key in order to get a thinner fibre as the rapid drying resulted in fibre stretch and extension of the fibre leading to improved alignment. This can be seen in figure 6.4.

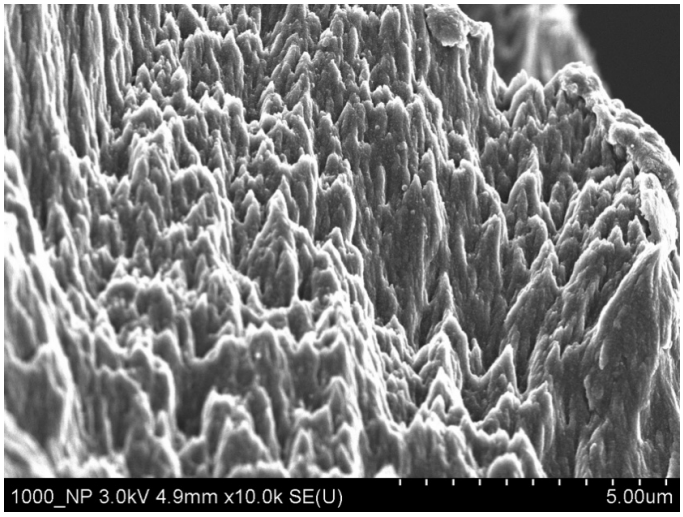

Figure 6.4: Surface of a fractured fibre spun at 1 000 r.p.m. at 100°C temperature. The fibrils appeared to be aligned along the axis of the fibre.

Key challenges to improve the spun fibres included the following:

- Reducing fibril diameter. Initial fibres were around 250 microns due to constraints on the needle diameter available. The objective was to reduce the fibre diameter significantly to assist in the minimizing defects and increase the rate at which drying of fibres takes place;
- Increase the rate of draw to improve alignment of nano-fibrils even further;
- Increase the viscosity of the fibril suspensions to improve rate of drying;
- FEG-SEM measurements of fibres to determine level of fibril alignment;
- Producing a consistent diameter fibre as spinning carried out by hand from a syringe resulted in a variable fibre diameter making the finer fibres difficult to spin in a continuous uniform diameter. This was achieved through the introduction of an automated syringe pump.

6.3 Modification to the spinning process using a syringe pump attached to a lathe

6.3.1 Methodology

A special jig was constructed to hold a syringe pump so that the syringe could spin fibre directly onto the drum that was attached to a high speed lathe. The system is illustrated in Figure 6.5 and 6.6. This set up offered better control over injection speeds that led to a more uniform fibre.

Figure 6.5: Overview of syringe pump attached to lathe.

Figure 6.6: Close up showing needle almost in contact with a heated drum onto which the cellulose fibres were injected. The heated drum gives rapid drying of the fibres, which leads to extensional alignment of the cellulose nano-fibrils.

6.3.2 Results

Fibres formed under various flow rates were spun using a standard gel of 20% solids content manufactured from Whatman No4 filter paper at a pH = 3.08 prepared as described in Section 3.2.6. Table 6.1 outlines details of the three rates of flow that were used. The table also gives predicted fibre diameters. Manual handling of the fibres indicated clear improvements in fibre strength with increasing draw down ratio. As predicted, the fibre diameter decreased with increasing draw down ratio.

The syringe pump was calculated to give three different delivery rates of 9.6, 6.4 and 3.2 ml/min. Given that ID of syringe needle was 0.025 cm r = 0.01 cm, the fibre flow rate was calculated by:

$$(\text{Delivery rate})/(\pi r^2)$$

The diameter (d) of the take up drum was 8.7 cm. The linear velocity at the surface of the drum was:

$$d\pi \times \text{rpm}$$

For a take-up drum rotating at 1600 rpm

Actual delivery rate (ml/min)	Exit speed (cm/min)	Take up speed (cm/min)	DDR calculated	Fibre diameter (microns)
9.6	30554	43737	1.43	140
6.4	20369	43737	2.15	93
3.2	10185	43737	4.29	46

Table 6.1: Shows the three rates of flow used to spin fibres on the lathe.

6.3.2.1 Characterization of the cellulose fibres

Two samples were sent to Cambridge University Materials Department for mechanical testing:

1. Cellulose Fiber spun @ 1600 rpm with a 9.6 mL/min solution feed rate: CelF 10
2. Cellulose Fiber spun @ 1600 rpm with a 3.2 mL/min solution feed rate: CelF 3

i. Mechanical testing

Fibre characteristics measured included tensile strength (tenacity) and stiffness (Initial modulus). A FAVIMAT fibre tester was used to carry out the mechanical testing. The machine was a single fibre tensile tester with two additional measuring systems located in the tensile testing section. The highly sensitive load cell enabled accurate adjustment of specific pre-tensions, as well as the measurement of extremely low tensile forces

when determining fibre crimp properties. Tensile testing with the FAVIMAT produced the following data: breaking force, extension to failure, Initial modulus, tenacity and a continuous force/elongation-curve.

The effect of variations in the testing parameters was investigated. Figure 6.7 and 6.8 show the change in the tenacity and modulus of fibers with respect to testing sample length (in mm).

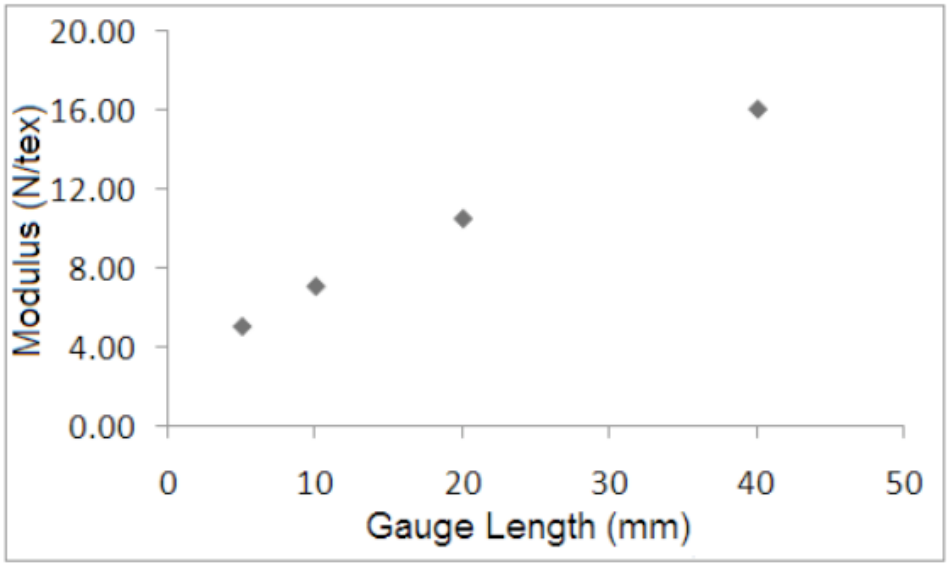

Figure 6.7 Initial modulus variation with respect to gauge length.

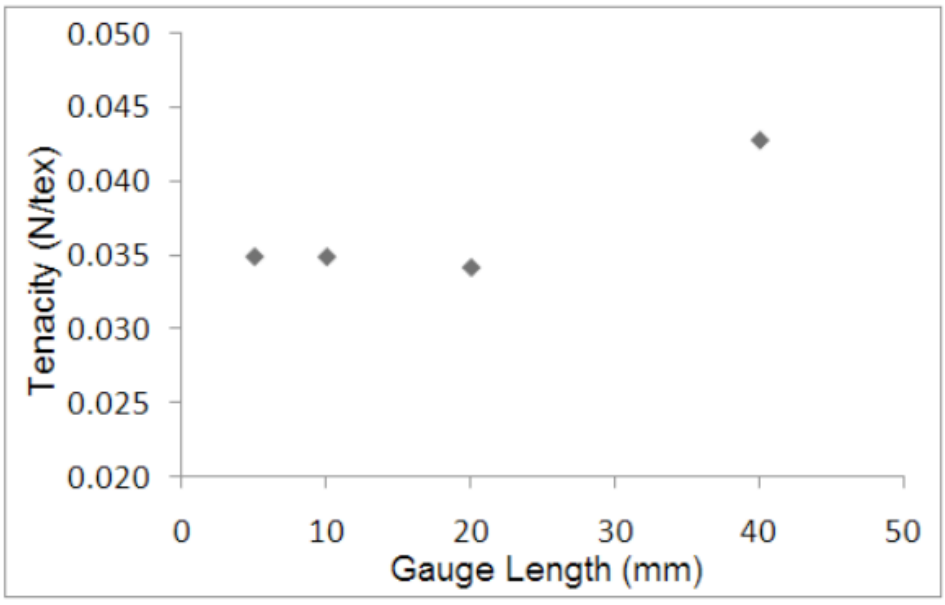

Figure 6.8: Tenacity variation with respect to gauge length.

From figure 6.7, it can clearly see that for a given fibre, as the gauge length increased the average modulus of the fibers increased gradually. On the other hand, tenacity values did not show this dependency for 5mm, 10mm and 20 mm lengths (Figure 6.8). A 20% increase in the tenacity was observed for 40 mm gauge length.

Fibre alignment inside the Favimat instrument was an important issue, mis-alignment between the grips was more apparent as the gauge length decreased and resulted in a decrease in the mechanical values. This may be an explanation as to why the larger gauge length gave better properties. As a result of this preliminary work a gauge length of 40 mm was selected to avoid the mis-alignment problems.

In addition to the gauge length, hard and soft rubber grips (Fig. 6.9) were tested for clamping the samples and a pressure optimization study was carried out in order to avoid fibre damage on the grips.

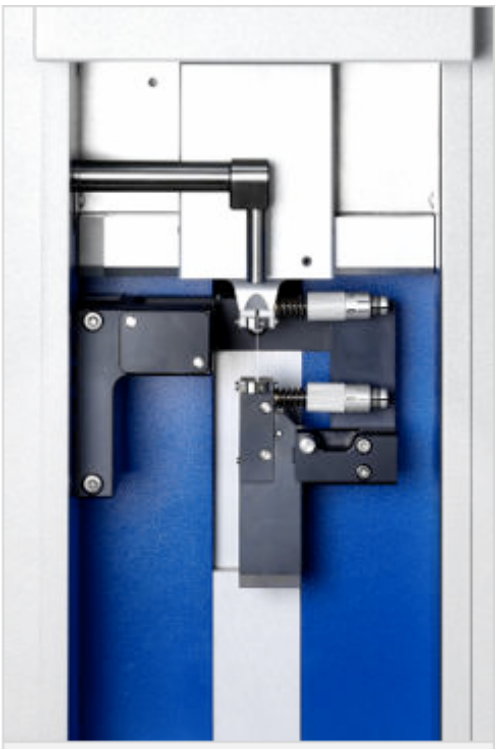

Figure 6.9: Rubber grips for clamping the fibre.

The testing system was optimized by using soft rubber grips at 40 mm testing distance with 0.07% elongation.

Linear densities of the fibres were measured by two techniques: weighing and vibroscopy. For the weighing method a Sartorius balance accurate to 6 decimal places was used.

The vibroscopic method was available as a capability within the Favimat equipment. The Favimat automatically determines the linear density of single fibres using the vibration method (according to ASTM D 1577). With this testing method the resonance frequency of the sample was measured at constant gauge length and known pre-tension; the data obtained was then used for calculating the linear density according to the following formula:

$$T_t = F_V / (4 \cdot f^2 \cdot L^2)$$

T_t = linear density
F_V = pre-tensioning force
f = resonance frequency
L = test section length

The gravimetric approach was the more accurate method and two different fibre batches showed that the vibroscopic technique introduced unacceptable errors into calculation of fibre properties. As a result, all fibres tested were weighed to determine linear density prior to testing and these values were used for calculation of tenacity and Initial modulus.

6.3.2.2 Results

Table 6.2 shows the results of two batches of fibres measured after processing according to table 6.1. In the first sample, CelF10 produced at the higher feed speed of 9.6 ml/min, ten fibres were measured giving an average linear density of 4.5 tex with individual values ranging from 3 to 10.9 tex. The second batch of fibre CelF3 was produced using the lowest feed speed (3.2 ml/min) onto the heated roller. The average linear density was significantly lower at 2.6 tex with a range of values from 1.38 to 4.49 tex. In both fibre batches a large variation in dtex was observed indicating variability in the fibre spinning process.

Sample	m (mg)	L (mm)	tex (g/1000m)	dtex (g/10000m)	AVG dtex
CelF 10-1	0.2435	24.64	9.88	98.82	45.21
CelF 10-2	0.0641	20.88	3.07	30.70	
CelF 10-3	0.0683	23.58	2.90	28.97	
CelF 10-4	0.0358	20.27	1.77	17.66	
CelF 10-5	0.3352	30.62	10.95	109.47	
CelF 10-6	0.0634	18.58	3.41	34.12	
CelF 10-7	0.0330	10.60	3.11	31.13	
CelF 10-8	0.1386	46.02	3.01	30.12	
CelF 10-9	0.0798	23.71	3.37	33.66	
CelF 10-10	0.0733	19.55	3.75	37.49	
CelF 3-1	0.0533	29.59	1.80	18.01	26.63
CelF 3-2	0.1243	27.67	4.49	44.92	
CelF 3-3	0.1486	71.99	2.06	20.64	
CelF 3-4	0.1135	26.82	4.23	42.32	
CelF 3-5	0.0248	17.96	1.38	13.81	
CelF 3-6	0.1279	57.72	2.22	22.16	
CelF 3-7	0.0638	26.00	2.45	24.54	

Table 6.2:Linear density measurement (weighing method).

		L.D. (tex)	Tenacity (cN/tex)	Initial Modulus (cN/tex)
CelF10	Favimat	5.41	3 ± 1.1	1214 ± 656
	Balance	4.52 ± 3.16	2 ± 0.2	803 ± 337
CelF3	Favimat	3.52	11 ± 5	1873 ± 635
	Balance	2.66 ± 1.21	16 ± 7	1989 ± 698

Table 6.3:Tenacity and initial modulus values for both batches of material.

Table 6.3 shows the mean (and range) of values for tenacity and Initial modulus calculated using both the vibroscopic and gravimetric approach. The tenacity for the faster feed speed (CelF10) was 2cN/tex using the gravimetric approach whilst initial modulus was 803cN/tex. It was interesting to note that the lower linear density fibre (CelF3) had a significantly higher mean tenacity (16cN/tex) and Initial modulus (1989cN/tex).

6.3.2.3 Photographs of fibres spun on the lathe

Figure 6.10 shows the smooth upper surface of a spun fibre (CelF 10), at a magnification of 10 000x. This image also shows what appear to be aligned fibrils below the surface exposed by the fracture on the bottom left corner.

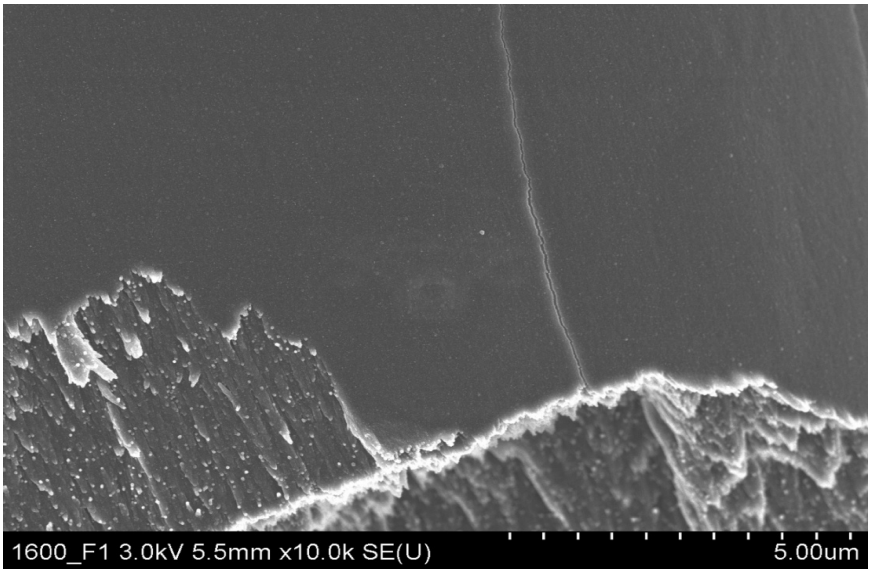

Figure 6.10: FEG-SEM image of a large fractured area close to the surface of the fibre.

Figure 6.11 shows aligned fibrils in the core of the same fibre. What is perhaps more interesting is the structure of the fracture. The fibrils did not break as individual fibrils but as larger aggregates with some measuring over 500 nm.

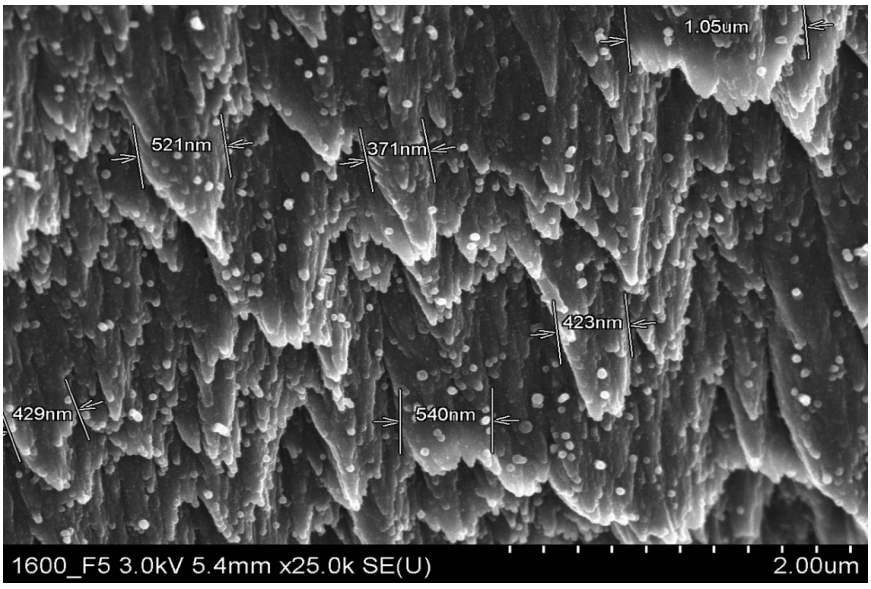

Figure 6.11: FEG-SEM image of aligned fibrils in the core of the fibre spun at a 9.6 ml/min.

The approach to spinning selected had some key limitations:

1. The fibre was spun onto a heated drum. As a result the part of the fibre in contact with the drum was flattened prior to drying (Fig. 6.12);

2. The drum, which had visible smooth surface, had defects at the micron scale, which led to defects in the flattened fibre in the form of striations;
3. It appears that as the fibre come into contact with the heated surface, the rapid volatilisation of water led to cavitation in the fibre. The holes in the underside of the fibre can be seen in figure 6.12;
4. Once the wet fibre come into contact with the heated surface it led to differential flow of nano-fibrils within the fibre. In fibre sample CelF3 with a feed rate of 3.2 ml/min it was possible to see two different components to the fibre. The top right of the fibre (Fig. 6.13) is slightly out of focus, however it is possible to see the linear flow (nematic alignment) of the fibrils. At the edges of the fibre that were in contact with the drum it is possible to see turbulent flow, analogous to eddies at the bank of a stream where the nano-fibrils were dragged by the drum prior to drying.

All these factors contributed to the production of a fibre with less than its full potential and with significant variation in linear density, tenacity and Initial modulus as it was shown in table 6.3.

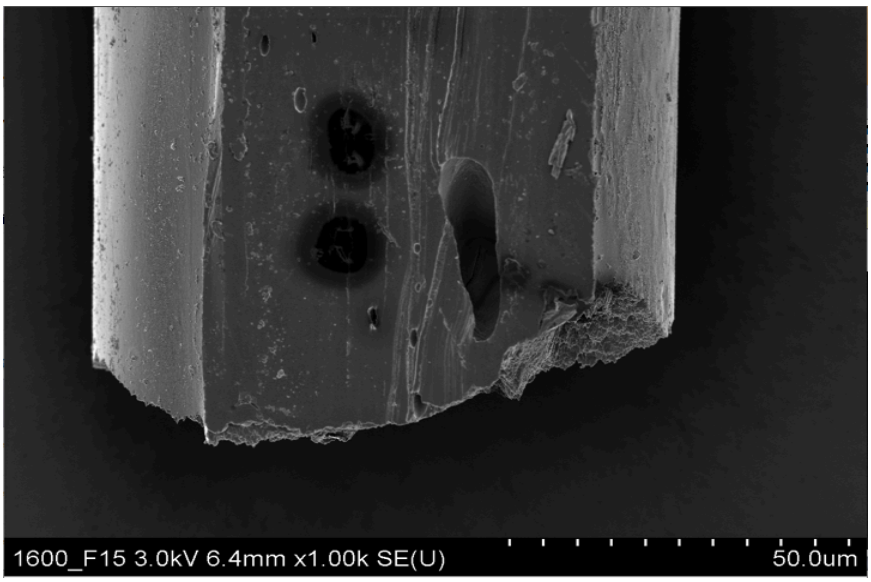

Figure 6.12: FEG-SEM image showing defects on the fibre's surface in contact with the drum.

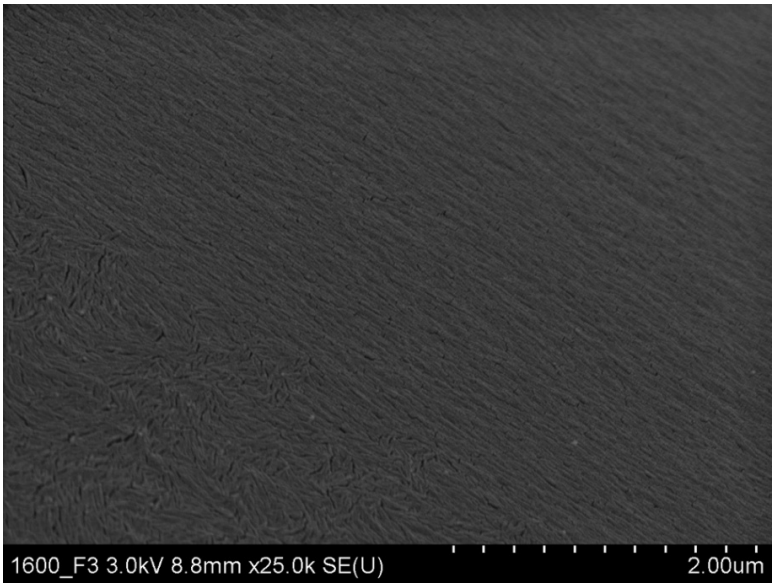

Figure 6.13: FEG-SEM image (at 25000x) of the surface for a spun fibre at 3.2 ml/min where boundaries between the turbulent and linear flow can be seen.

6.3.3 Conclusions from preliminary spinning.

This preliminary spinning work had shown that it was possible to produce a continuous fibre from a liquid crystal suspension of cellulose nano-fibrils. However, it was clear that an alternative route to spinning the fibre was required. The new approach identified involved the use of a customized spin-line rheometer, which is discussed in Section 6.4.

6.4 Establishment of a new spinning process with a spin line rheometer

6.4.1 Introduction

As part of the process to develop an alternative fibre spinning process a project was started to design, commission and test a spin-line rheometer that was customized to meet the requirements of the project. The rheometer consisted of a main frame (Fig. 6.14, bottom left) with a moving head and a piston (top left) which was used to extrude a gel through a 15 mm diameter (50 ml volume) bore which was contained within a temperature controlled jacket (top right). The piston speed was computer controlled to ensure a controlled extrusion rate from a needle (or die) screwed into the base of the rheometer bore (Fig. 6.14, top right and Fig. 6.15). The rheometer bore was manufactured from Hastalloy to ensure resistance to corrosion from the acidic gels. Between the needle and a take up wheel (bottom right) was a 600 mm air gap (with

space to fit a fibre drier). The take up wheel could be set at the same rate as the fibre extrusion speed or could be controlled to increase at a faster rate to permit different levels of draw on the extruded fibre.

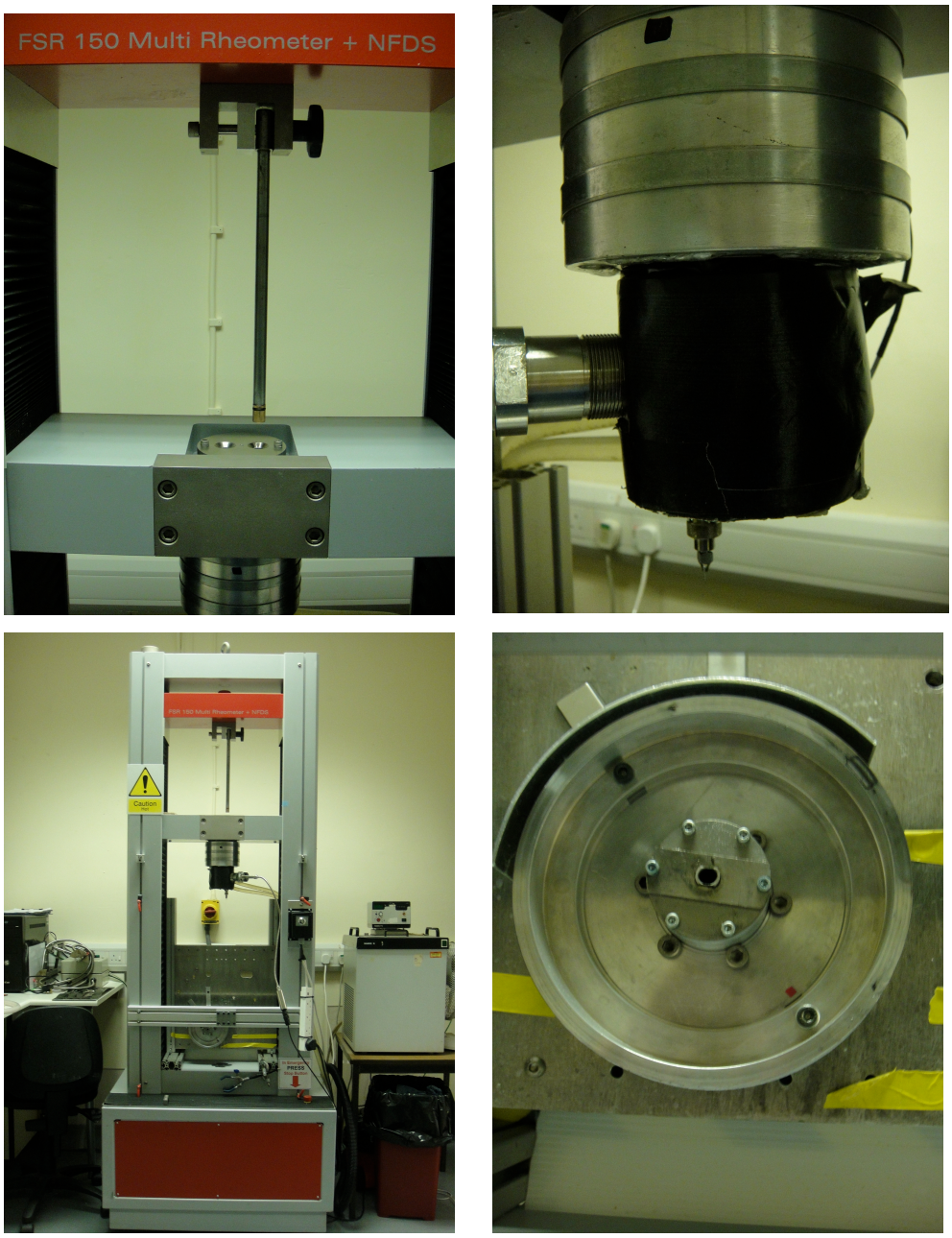

Figure 6.14: More detailed pictures of the rheometer. Top left: piston with the twin bore where the gel is feed. Top right: barrel with needle attached. Bottom left: rheometer general view. Bottom right: take up wheel.

The dryer (Fig. 6.15) used to dry the fibres during the spinning process consisted of a cylindrical tube of aluminium split into two halves longitudinally with a 15 mm internal diameter and 375 mm length. A 500W cartridges heater was inserted in each of the two halves of the aluminium block to raise temperatures up to 550°C. The aluminium block

had external insulation to reduce heat loss and to minimize the health and safety hazard. The top and the bottom of the internal heater cylinder extended 40 mm outside the main aluminium block to allow a more gradual heat gradient and to minimise thermal shock to the fibre to be dried.

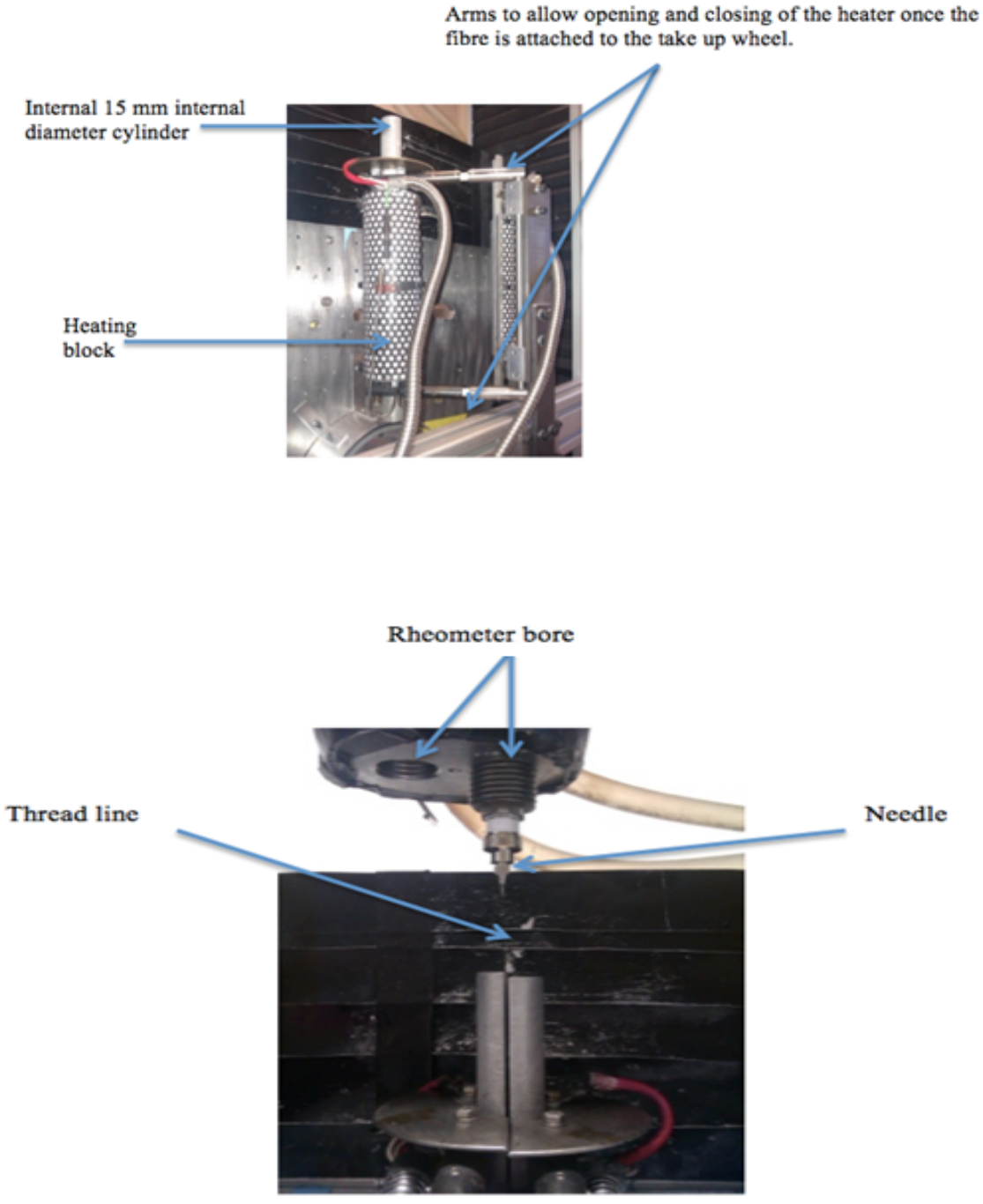

Figure 6.15: The dryer used to dry the fibres during spinning.

6.4.2 Experimental work

6.4.2.1 Phase 1: Initial challenges

During initial trials on the new spinning facility, two problems were quickly identified. At this stage the gels were produced from Whatman No4 filter paper following the conditions established in Section 3.2.6 resulting in a final gel with pH3 and a 20% solids content after concentrating it for 10 hours.

The first problem observed was linked to the viscosity of the material. At room temperature the viscosity was similar to that of Vaseline. When the gel was mixed or decanted from one container to another it was impossible to avoid the incorporation of air bubbles into the media. Bubbles caused problems in the spinning process when they burst out of the die, resulting in either fracture of the fibre or major defects. The issue was resolved by centrifugation (10 minutes at 17 000RCF) of the material in the syringe used to inject the gel into the bore of the spin-line rheometer.

The second problem related to the wet strength of the gel as it was extruded from the die. With the earlier lathe setup there was a small air gap (approximately 1 cm) between the die and the hot drum onto which the fibre was spun. The new system had a much larger gap of 600 mm to allow for drying of the fibre prior to collection on the take up wheel. The gap was required to dry the fibre prior to being wound onto a take up reel. Before spinning could take place, a "wet" leader fibre had to be drawn from the die and attached to the take up reel. The take up wheel and the feed speed from the die were then ramped up to an acceptable extrusion (spinning) speed once fibre spinning had stabilized the take up wheel was accelerated further to achieve the draw down ratio required to stretch the fibre and get extensional alignment of the fibrils. This draw down led to a thinning of the fibre. In such a system, as diameter decreases, surface area to volume ratio increases leading to more rapid drying and strength formation.

In the first trials it was found that the wet strength of the gel was insufficient to form a long leader that would allow attachment to the take up reel, a constraint that had not been experienced before. It was found that very minor differences in viscosity amongst the gel samples had an impact on wet strength. In practice, the maximum leader length achievable with 20% solids content varied from around 1cm to 5cm. To increase wet strength to an acceptable level it was important to increase viscosity still further.

Subsequent trials using larger centrifuge times showed that it was possible to increase wet strength significantly. In principle, the highest possible viscosity was preferable as there would be less moisture to remove from the gel and it would ensure the strongest possible wet fibre prior to draw down and collection on the take up wheel. This in turn should theoretically ensure fewer problems with potential breakage during spinning. However, too high a viscosity could, it was thought, also lead to potential problems in the subsequent alignment of the nano-fibrils during spinning.

6.4.2.2 Phase 2: Improving wet fibre strength

The following studies were carried out to look at the impact of dialysis time (which should theoretically impact on inter fibril repulsion) and centrifugation time on gel concentration.

After 24 hours centrifugation of a gel prepared according to the process described in Section 3.2.6 at 9 600 r.p.m. (17 000 RCF) compared with the previous gel, which was spun for 10 hours, a significant increase in viscosity was noted. However there was only a very slight increase in solids content from 20% to 21% solids. The pH of the gel was 3.5 and the average acid group content 12.98 mmol/Kg with a standard deviation of 4.4. The wet strength of the fibre was around 23 cm.

Looked at extending dialysis time reported in Section 7.4 from 1 to 3 weeks. This resulted in the following:

1. An increase in pH from 3.5 to 4.2;

2. The solids content went up to 40% after the same time in centrifugation compared with 1 week of dialysis, which gave 20-21% solids. The viscosity was significantly higher than previously, approaching the consistency of a soft candle wax. The structure of the gel looked similar to that of marble;

3. The gel was noticeably tackier and the gel wet strength increased from about 23 cm (after 1 week dialysis) to over 1 meter after 3 weeks. As a result of the improvements in gel consistency and viscosity it was possible to successfully

extrude a continuous fibre. The hypothesis for the improved viscosity of the gel is that surplus acid and surface sulphate groups on the nano-fibrils were significantly reduced allowing the fibrils to pack more closely (hence the increase in solids content). This hypothesis was supported by an increase in pH to 4.2 and a lower average acid group content of 8.8 mmol/Kg measured using conductiometric titration compared with the previous value of 12.98 mmol/Kg. In addition, it is believe that the lower standard deviation of 2.7 for acid group content at least in part related to a noticeable improvement in gel structure and consistency.

Figure 6.16 shows a photograph of a 100 micron diameter fibre being pulled from a 250 micron needle. The picture shows that the fibre had sufficient strength to be fed onto a take up reel, which would then be used to draw the fibre down to smaller diameters. Figure 6.17-6.19 shows electron micrographs of the same fibre, which was allowed to air dry after extrusion. Figure 6.17 shows that the fibre surface was smooth and free of mayor defects. Figure 6.18 shows a close up of the fibre surface indicating a reasonable degree of alignment of the nano-fibrils. The surface structure was mirrored by the internal structure in figure 6.19. It should however be noted that there was some twist to the structure indicating chiral nematic order.

Figure 6.16: 100 micron wet fibre spun being drawn by hand from the die.

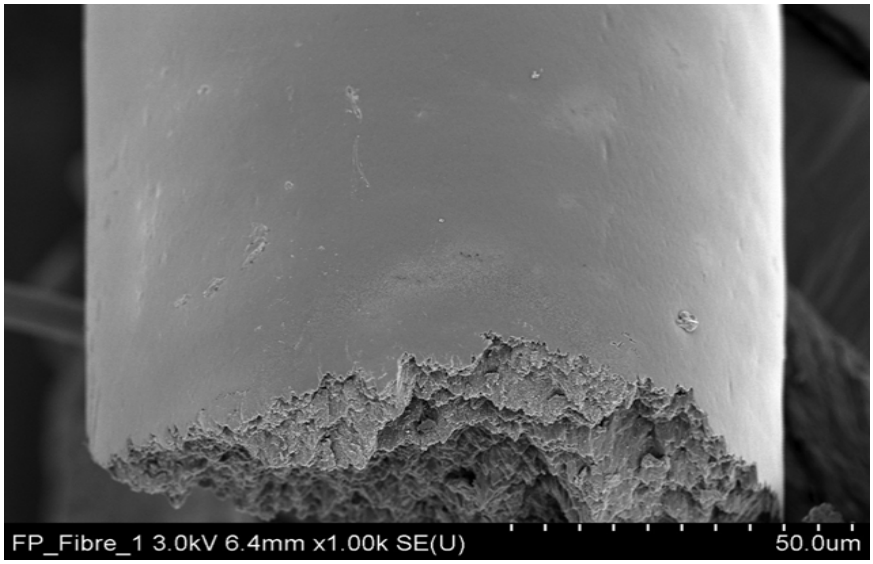

Figure 6.17: FEG-SEM image at 1 000x magnification of the smooth surface of a 100 micron spun fibre, which was hand drawn and allow to air dry.

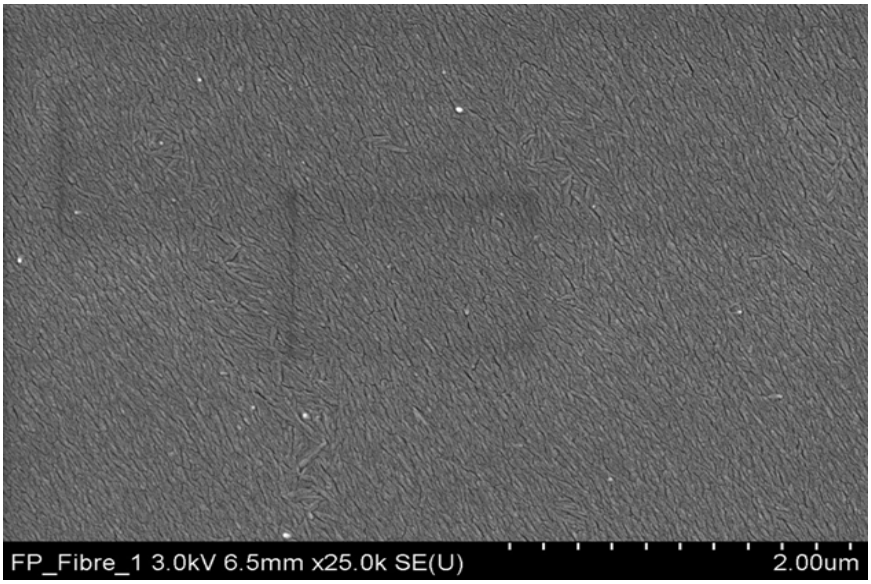

Figure 6.18: FEG-SEM image at 25 000x magnification of the surface of fibre showing reasonably good orientation of nano fibrils along the fibre axis but not yet fully aligned.

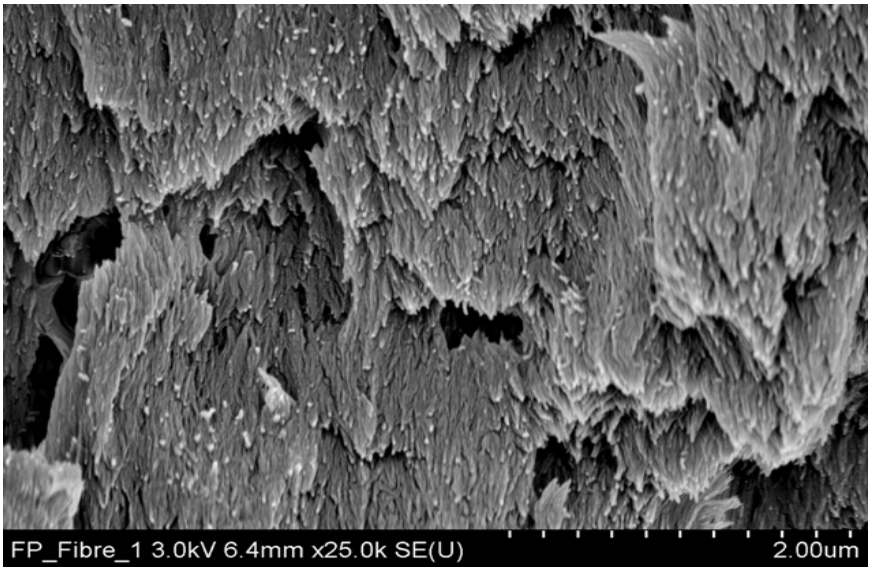

Figure 6.19: FEG-SEM image at 25 000x magnification of cross section of fibre showing already good alignment of core fibres.

6.4.3 Conclusions

The main hypothesis for the improved viscosity of the gel is that surplus acid and mobile sulphate groups contained in the bound water layer surrounding the nano-fibrils were removed allowing the fibrils to pack more closely (hence the increase in solids content). This hypothesis was supported by an increase in pH from 3.5 to 4.2 and a lower average acid group content from 12.98mmol/kg to 8.8 mmol/kg. In addition, it was believed that the lower standard deviation of 2.7 for acid group content at least in part related to a qualitative improvement in gel consistency that was observed.

Viscosity level for spinning gels was achieved that had acceptable wet strength. This was an important step forward.

The viscosity of the gel was highly dependent upon the level of acidity, which was thought to be related to the degree of sulphonation of the nano-fibrils. It also appeared that the variability of surface charge within the suspension had a very important role to play in the consistency of gel structure. The objective of the next step of the study was to better understand how to control the consistency of gels as effectively as possible (Section 10).

7 ONGOING DEVELOPMENT AND OPTIMISATION OF THE NANO-FIBRIL GEL PREPARATION PROCESS

Good progress had been made in the development of a fibre spinning process. However, it was thought that more work was required to better understand how to control the gel preparation process to produce the best possible gels for spinning. As part of this investigation a number of changes were made to the preparation of cellulose nano-fibrils as described below.

7.1 Pulp preparation

It was found that Whatman No4 was not fully mixing into the acid at the beginning of the hydrolysis process. The mixture was becoming difficult to stir and there was a concern that the powder was not being fully hydrolysed as a result of this. In order to obtain a more thorough hydrolysis, sheets of industrial pulp and filter paper were first shredded using an industrial office shredder (Rexel). After shredding, the cellulose fibre was balled milled using a (Fritsch Pulverisette 5). The milling time varied depending on the type of material being milled. 92α cellulose grade pulp was extended from 40 minutes to 1hour, and Whatman No4 was extended from 20 to 30 minutes. These revised conditions produced a more consistent particle size, which reflected in a higher yield of particles passing through 250 micron sieve.

There was a further problem associated with the use of the new ball mill. Ceramic balls were initially used to grind the cellulose. However, this proved problematic due to ceramic debris contaminating the cellulose nano-fibrils. The problem was solved through the use of stainless steel balls.

Following this, the resulting powder was sieved through a 250-micron sieve. This removed some of the larger clumps of paper previously observed when using an 850 micron sieve. These changes promoted more even mixing during the subsequent hydrolysis stage. The previous conditions led to powder aggregation, leading to un-hydrolyzed material at the end of the end of the centrifugation procedure.

7.2 Acid Preparation prior to hydrolysis

In earlier work, it was noted that whilst adding sulphuric acid to the water (previously at ambient temperature), the solution was increasing to over 100ºC. It was felt that this would result in volatilization of acid and a potential source of variation in acid concentration during acid preparation. The problem was eliminated by preparing the acid solution in a beaker surrounded by crushed ice. The acid was added to water, slowly whilst monitoring the temperature to ensure that it remained below 80ºC. After mixing, the acid solution was cooled rapidly by the ice to 20^{o}C, reducing the overall preparation time to less than fifteen minutes.

7.3 Hydrolysis

The earlier hydrolysis studies were carried out on a hot plate, using an integrated temperature controller to monitor and maintain the solution at 46^{o}C throughout the process. The length of time of the hydrolysis of Whatman No.4 was 75 minutes. The amount of acid used was ten times the weight of the powder to be hydrolysed (acid:cellulose ratio of 10:1). However, it was noted that there were variations in the temperature of the hydrolysis during the procedure, with temperatures fluctuating three to six degrees from the required temperature throughout the process. To ensure a more consistent temperature during hydrolysis, the previously used hot plate was replaced with a temperature controlled water bath which proved more efficient at controlling temperature, ensuring better heat transfer. In addition the temperature control of the water bath was very consistent, varying at the most by 1ºC. Using the water bath, the temperature stabilised rapidly and remained constant throughout the hydrolysis. Scanning electron microscope images of the nano-fibrils after hydrolysis at different times showed that the time of the hydrolysis of Whatman No.4 could be reduced from 75 minutes to 65 minutes due to the more effective temperature control. Tests also showed that decreasing the weight of the powder added to the acid by ten grams (10:0.9)produced more favourable results, as the hydrolysis was less viscous and therefore stirred more efficiently, resulting in a more thorough hydrolysis.

The SEM images (see Fig. 7.1 and 7.2) indicated that nano-fibrils extracted using the new hydrolysis process appeared subjectively to be more readily discriminated suggesting more effective hydrolysis with less damage to the nano-fibrils.

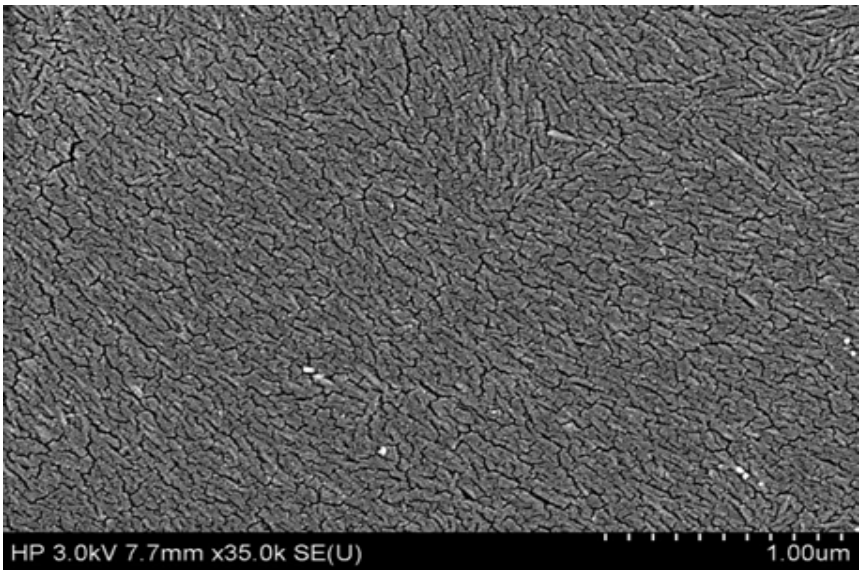

Figure 7.1: Hot Plate Cotton Hydrolysis.

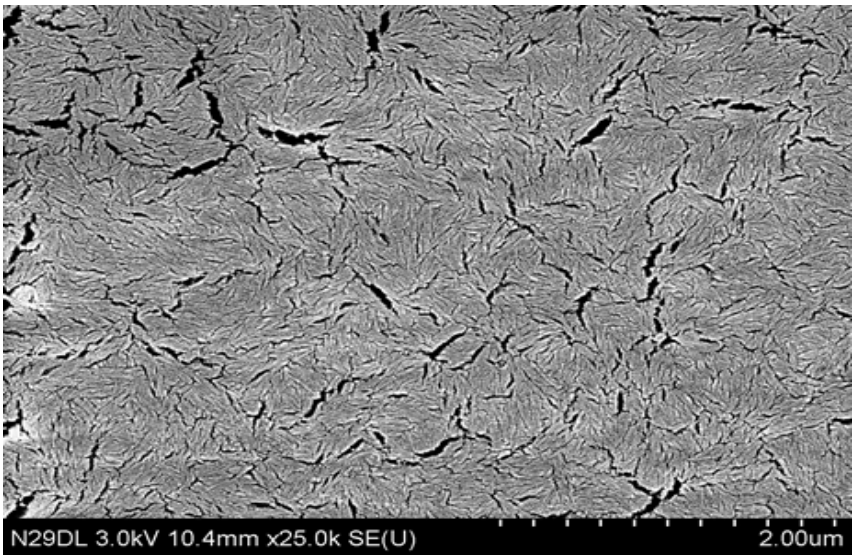

Figure 7.2: Water Bath Cotton Hydrolysis.

In addition to the above measures, it was found that the introduction of a "Swivel" impeller stirrer as opposed to the previously used "U shape" (see Fig. 7.3) resulted in improved hydrolysis with the time taken for the powder to completely dissolve, reducing from 4 minutes to less than one minute. A notable increase in the viscosity of the hydrolysed suspensions was also observed indicating the more effective release of cellulose nano-fibrils.

Figure 7.3: Stirring paddles: 1-"U" shape Stirrer; 2- Swivel impeller. (Fisher Scientific)

7.4 Tap water dialysis

Dialysis of hydrolysed gels using continuous running tap water introduced counterions, which appeared to give the type of properties required for spinning to form a stable thread. However, the variation in counterions in tap water led to apparent variation in the rheological properties of the gels under otherwise constant conditions preventing precise control of the spinning process and producing the type of fibres require on a consistent basis. This section described work carried out to understand the impact of the tap water dialysis process on cellulose nano-fibrils gel properties.

7.4.1 Time dependency of gel pH dialysed with tap water

The first step of the investigation involved an evaluation of a stock of 92α cellulose pulp that was in dialysis for up to 89 days. The objective was to determine the impact of dialysis time on pH of the suspensions to the point of neutrality and at the same time test pH stability after dialysis. A second objective was to determine if it was possible to over dialyse the suspensions and reduce zeta potential to a level that could lead to destabilization of the colloidal suspension.

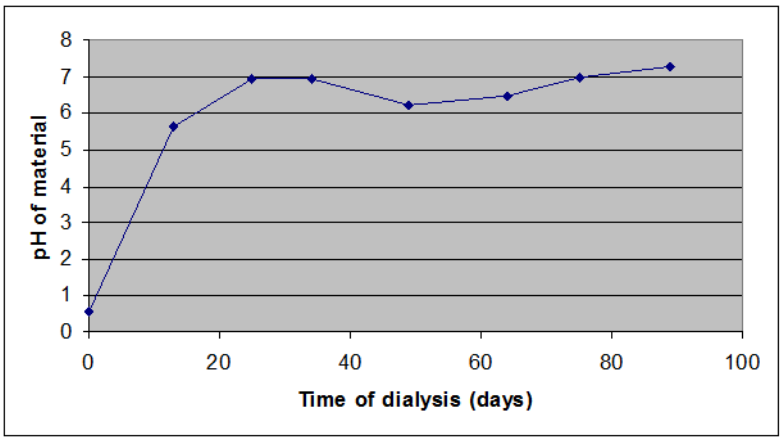

Figure 7.4: Dialysis time vs. pH for cellulose nano-fibrils gel after tap water dialysis.

Figure 7.4 illustrates the change in pH with dialysis time, pH 5 was reached at around 14 days and pH7 at around 3 weeks after which point it levels off. It is not clear why there was a slight decrease followed by a subsequent increase after 4 weeks. This may be due to variability in different suspensions and/or variation in the counterion composition within the tap water over time.

A study was undertaken to track changes in suspension pH with time after removal from dialysis and storage of the suspensions in a sealed container. Three samples that had been in dialysis for different lengths of time were tested. Figure 7.5 shows that pH was not completely stable after removal of the suspensions from dialysis. After 13 days in dialysis the suspension was particularly unstable suggesting freely available sulphate groups on the surface of fibrils or in the bound water layer around the fibrils, which move into solution over time. However, stability appeared to improve with increased dialysis time.

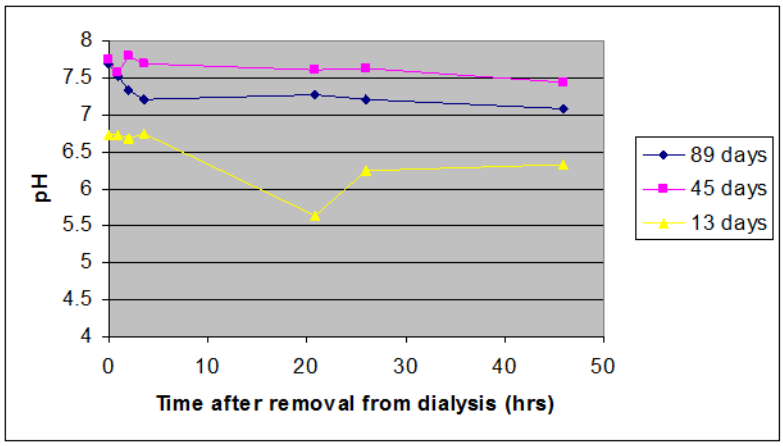

Figure 7.5: pH Stability after removal of suspension from dialysis at different dialysis times.

These results show that long-term dialysis increased the pH of the suspension into the basic (7.5+) range of the scale. This was almost certainly due to counterions from the tap water used for the dialysis.

7.4.2 Impact of tap water dialysis and centrifugation times on solids content and pressure during spinning

High speed centrifuges were required to remove water from cellulose nano-fibril suspensions to get viscosities high enough to achieve the high gel strengths required to allow spinning.

As part of the process to improve gel viscosities a new higher speed centrifuge (Thermo Scientific Sorvall RC 6^{+}) capable of working at over 20 000 RCF was purchased. It was found that it was possible to achieve 40% solids content after 26 hours compared to 35% solids content after 49 hours with the previous centrifuge (Sigma 6K 15).

The objective of this study was to determine the combine impact of tap water dialysis and centrifugation times on solids content and its subsequent impact on rheometer pressures during spinning. In this study 92α cellulose was hydrolysed under standard conditions and subsequently dialysed using a continuous flow of tap water for a range of times. The suspensions were then centrifuged for either 26, 30 or 35 hours at 20 000 RCF in a Thermo Scientific Sorvall RC 6^{+} in 50ml conical centrifuge tubes.

After centrifugation, each of the cellulose gels was mixed by hand with a spatula for at least 10 minutes prior to final degassing with a 10 minutes centrifugation at 17 000 RCF ready for study. The objective of mixing was to eliminate variation in solids content and nano-fibril distribution, which resulted from concentrating the gels during centrifugation.

7.4.2.1 Results and discussions

Figure 7.6 shows the impact of solids content against dialysis time from 3 days to 4 weeks after 26 hours centrifugation. The values were derived from an average of at least five 2-3g subsamples of a single larger sample of around 50g of concentrated gel. An overall trend of increasing average solids content was observed with dialysis time with a significant difference in solids content between the two extremes. It is suggested that the differences in solids content could be explain by higher surface charge being present on the cellulose nano-fibrils and within the bound water layer after 3 days dialysis. These surface charges being gradually removed with increasing dialysis time.

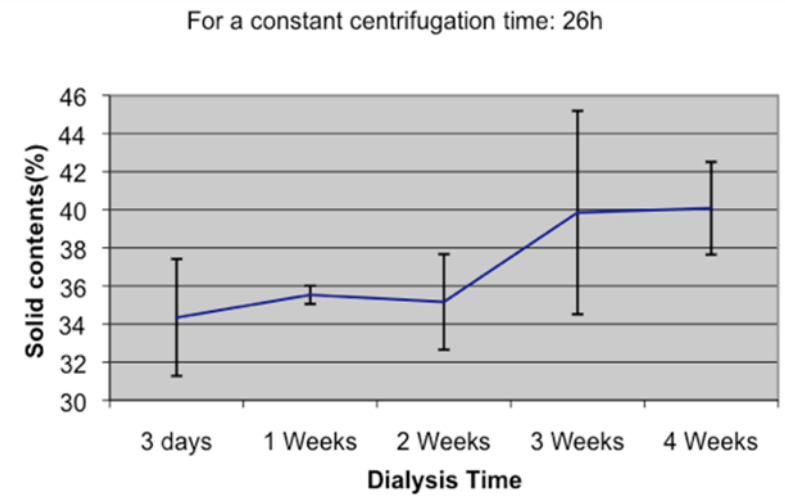

Figure 7.6: Solid content evolution for a constant centrifugation time of 26h.

The second observation to be made from figure 7.6 is the large range of standard deviation values for solids content due to the heterogenity of the gel (the gel was not properly mixed), which is also seen in subsequent centrifugation times in figure 7.7 and 7.8. The reasons for this were thought to be inadequate mixing which is discussed in more detail in Section 10.2.2.

Figure 7.7, representing 30 hours centrifugation time, showed no significant differences between the extremes of 3 days and 6 weeks dialysis. It is interesting that there was a significant dip in solids content after two weeks dialysis. It is suggested that variation in counterion type and content of the tap water over time was responsible for this anomaly.

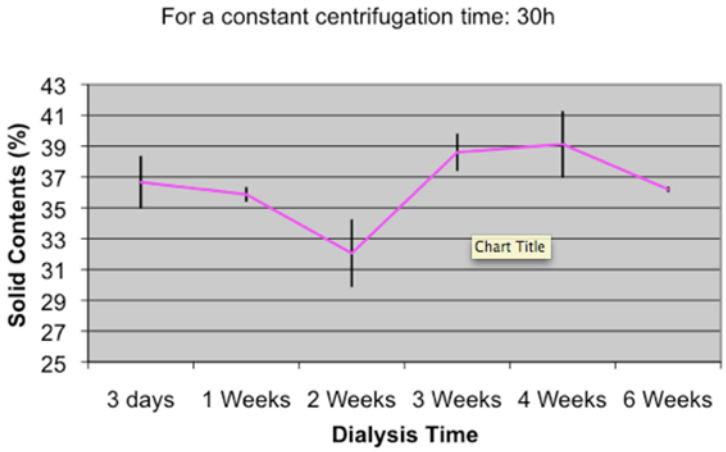

Figure 7.7: Solid content evolution for a constant centrifugation time of 30h.

Figure 7.8 indicates results after 35 hours centrifugation. This graph again showed a big variation in solids content but far more consistent average values for solids content across the range of dialysis times. This is emphasized in figure 7.9, where mean values for the three graphs are shown together. It was interesting to note that there was no significant difference in solids content between 26, 30 and 35 hours centrifugation after 4 weeks dialysis. However, the figure illustrates how the gap widened between 35 hours and the lower centrifuge times when exposed to the shorter dialysis times. It is suggested that these observations were due to differences in repulsive forces between nano-fibrils at the lower dialysis times as a result of surface charge and counter ions present in the gel. However, these repulsive forces were overridden by the higher centrifugal forces.

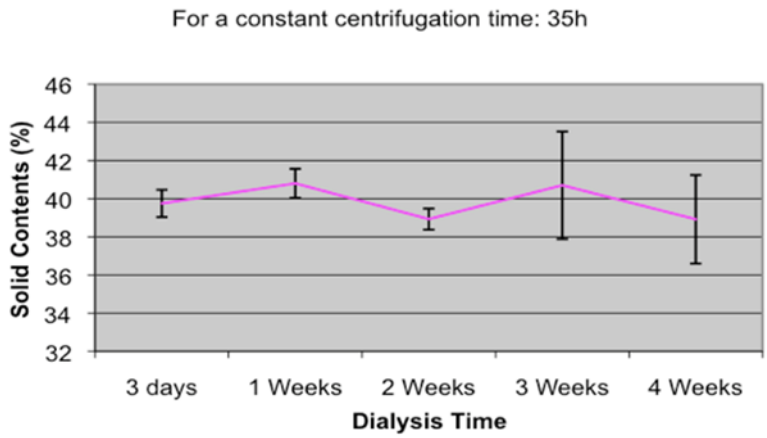

Figure 7.8: Solid content evolution for a constant centrifugation time of 35h.

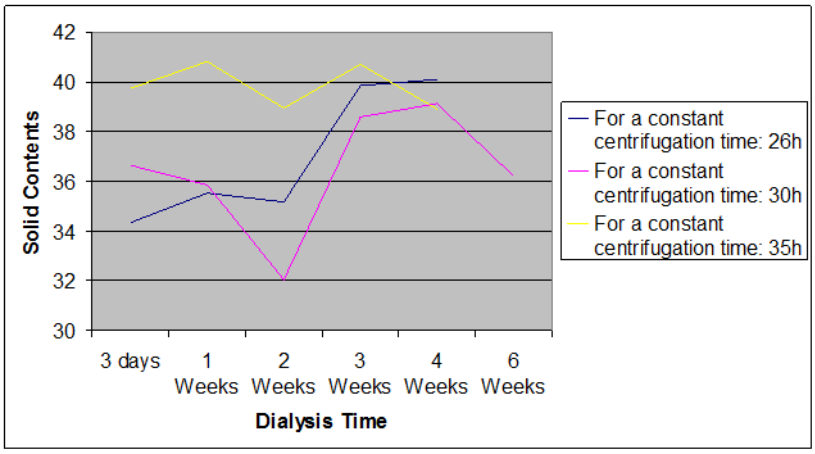

Figure 7.9: Difference in solids content between 26, 30 and 35 hours centrifugation after 4 weeks dialysis.

It was clear from these results that due to the extremely viscous nature of the gels, that the mixing process required a rethink. The standard mix with a spatula was distributive in nature (mixing at the macro level) to break up the large scale differences between the top and bottom on the gel in the centrifuge but no amount of standard mixing was breaking down some of the higher density gel aggregates and evenly dispersing the cellulose nano-fibrils.

To address the dispersive mixing requirement a test was carried out in which a gel (Sample V160) was split in two. The first half was run through the rheometer with a 250 micron needle attached without any mixing creating huge pressure variations, see figure 7.10. The second half was first passed through a 500 micron zero die attached to the rheometer. This process had the effect of breaking up the gel structure and extruding

it into a highly aerated vermicelli type structure with a large surface area that could be more easily mixed. This process was repeated twice combined with distributive mixing with a spatula and then decanted into a centrifuge tube for final concentration and removal of air pockets. The effect on pressure variation was equally significant with a greatly reduced variation in pressure (Fig. 7.11) during the spinning process and no fibre breakage from the 250 micron needle as it was extruded.

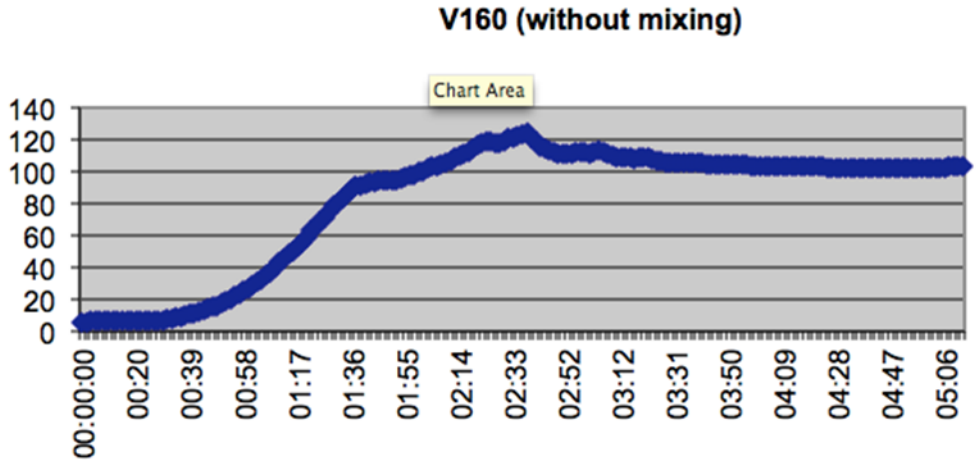

Figure 7.10: Pressure variation for a non-mixed gel.

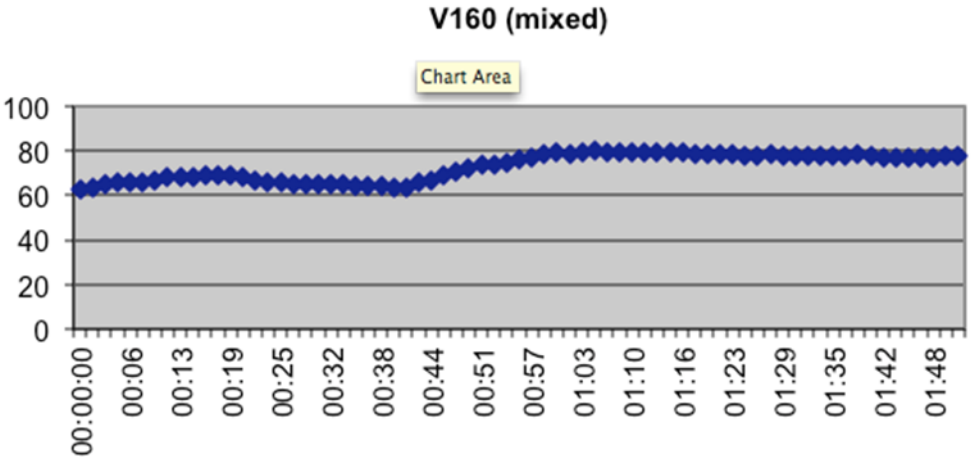

Figure 7.11: Pressure variation for a mixed gel.

The variation in mean solids content highlighted in figure 7.9 suggests that something other than dialysis and centrifuge time is having an effect on solids content. In addition there was no overall correlation between pressure at the die exit and solids content (Fig. 7.12). This is counter intuitive suggesting that something more complex is occurring. Figure 7.13 gives a breakdown of the data into individual centrifuge times. It is interesting to note that all the 26-hour values exhibited low pressures even though solids

contents were as high as 40%. Even taking these data out of the graph there is still no correlation within the remaining data. This suggests that tap water dialysis is playing an addition role, having a significant impact on the overall structure of the gel and the way in which the nano-fibrils interact.

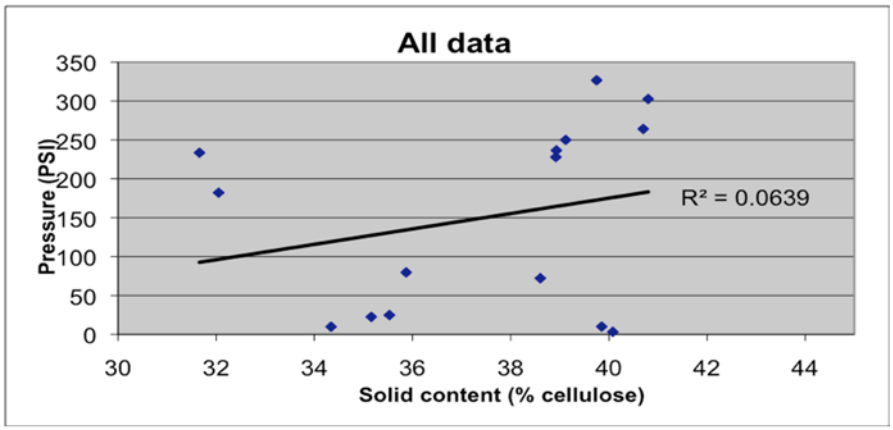

Figure 7.12: The correlation between solids content and pressure at the die exit.

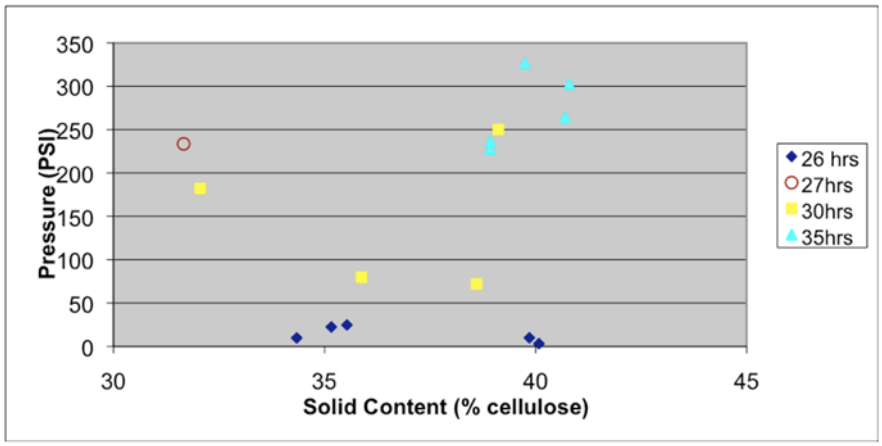

Figure 7.13: Impact of centrifugation times on solids content and pressure during fibre spinning.

7.5 Conclusions

This analysis leads to some important conclusions.

- There was substantial variation in solids contents between batches under the same centrifuge conditions and there appeared to be no predictable trends with dialysis time. It was hypothesized that this was due to variation in counterions

(particularly $CaCl_2$) in the tap water, which were found to vary significantly over time. This led to a decision to install a continuous reverse osmosis system to provide deionised water for dialysis to eliminate this source of variation;

- The variability in solids content at least partially explained some of the difficulties that were observed in trying to get gels that could produce a consistent fibre thread during spinning;

- The variation in solids content may also be a contributor to variability in fibre strength, which was observed in preliminary studies;

- A new more effective mixing process was required to ensure uniform gel structure and solids contents variation. This is discussed in more detail in Section 10.2.2;

- Mixing of these high viscosity gels has a major impact in reducing subsequent process variation;

- During spinning studies the micro scale variation in density led to big variations in pressure and fibre breakage during spinning.

8 PHASE BEHAVIOUR STUDIES

8.1 Introduction

In the literature review (Odijk, 1986) it was clear that the properties of liquid crystal suspensions are dependent upon a series of factors including:

- The length and diameter (aspect ratio) of the particles;
- The distribution of particle sizes (polydispersity);
- The surface charge of the particles;
- Ionic strength of the system.

It was also reported that it should theoretically be possible to fractionate cellulose suspensions by exploiting phase behaviour of these liquid crystal suspensions. So four methods to fractionate a cotton-based cellulose nano-fibril suspensions were investigated as a potential alternative to the use of centrifugation

8.2 Investigating alternatives to fractionation of cellulose nano-fibrils using centrifugation

A hypothesis was proposed that the smaller fibrillar debris after hydrolysis that were being removed through centrifugation in the standardized protocol in Section 3.2.6 could be separated from the main body of fibrils by drawing off shorter fibre fractions (which form different layers) in the "bi-phasic region" without resorting to expensive centrifugation techniques.

A first study involved the use of a Whatman No4 based cellulose suspension that had not been fractionated by centrifuge. The suspension was subjected to dialysis for 11 weeks against tap water to remove acid after hydrolysis. The sample was then separated into subsamples with a range of concentrations from to 2% to 10% in 1% intervals. Samples were then stored in 20 ml stoppered glass tubes for two weeks to determine the concentration range at which a bi-phasic system would form. None of the sub-samples showed phase separation although the suspension formed a thixotropic gel-like structure. In a concentration range from 4 to 8% this gel-like structure exhibited

increasing levels of birefringence (indicating alignment) under polarized light although there were no indications of the typical chiral nematic “finger print” structure. The structure observed had a characteristic crosshatch pattern (Fig 8.1)

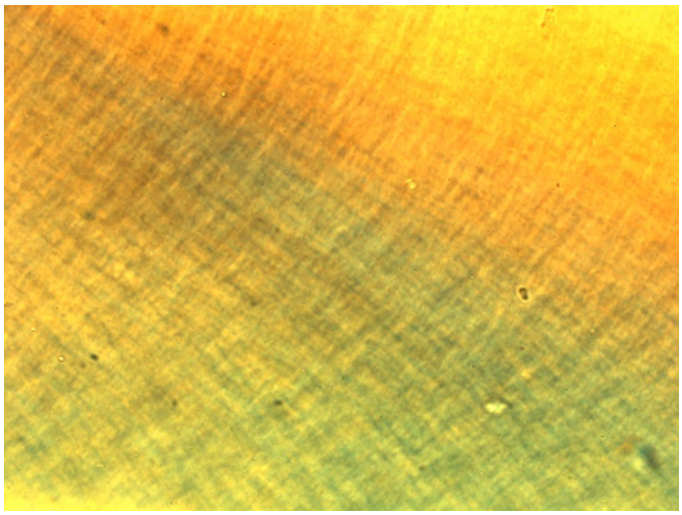

Figure 8.1: Crosshatch birefringent glassy phase pattern for an unfractionated cotton cellulose suspension (6.5% (w/w)).

This pattern was observed by Araki *et al.,* 2000 in relation to post-sulphated hydrochloric acid hydrolyzed cellulose. This configuration was termed the birefringent glassy phase. This structure was stable over time and was thus not an intermediate between isotropic and chiral nematic phases. This failure to phase separate may indicate that the charge on the nano-crystals had been masked by the presence of counterions introduced from the tap water during dialysis.

8.2.1 Preliminary investigation of uncentrifuged nano-fibril gels after the removal of counterions with cation exchange resin.

To determine whether counterions played a role in the phase behaviour of the gels a cation exchange resin (to remove the counterions) was added to a dilute suspension of the dialysed (gel prepared in Section 3.2.6) for 4 hours. The suspension was then filtered to remove resin and concentrated to 12%.

A series of suspensions with a concentration range of 5 to 10% cellulose by weight was then made by diluting this stock solution by the use of vortex mixing and subsequent treatment with ultrasound for 30 seconds. The actual post mixing cellulose

concentrations of the suspensions were determined gravimetrically. The suspensions were then left to phase separate for 12 days.

The cation exchanged material separated into two phases (in contrast to the untreated material), an upper isotropic layer and lower anisotropic layer. The volume fraction of the anisotropic phase was measured for each solution and is shown in Figure 8.2.

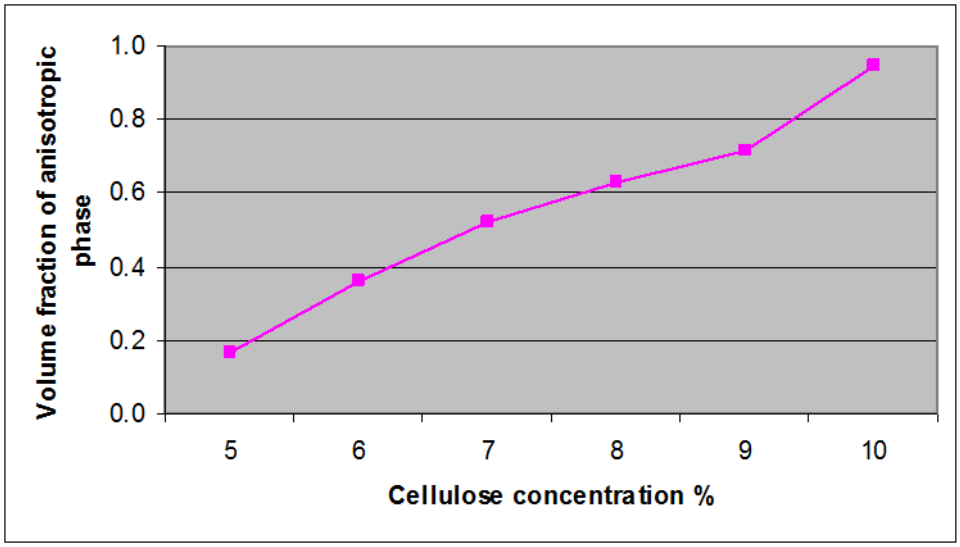

Figure 8.2: Volume fraction of anisotropic phase in relation to cellulose concentration of cotton cellulose for an un-centrifuged suspension after 11 weeks in dialysis.

Microscopic examination under polarised light showed that the anisotropic phase of these ion exchanged suspensions were chiral nematic (Fig. 8.3) except for the 5% cellulose concentration, which exhibited chiral nematic tactoids, but no coherent structure (Fig. 8.4). The presence of chiral nematic tactoids indicated the onset of formation of an anisotropic phase. The phenomenon is discussed in the literature review (Azaki and Kuga 2001).

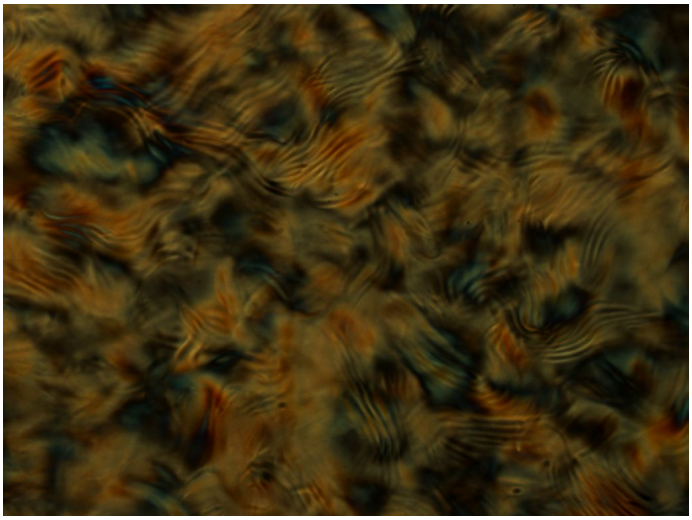

Figure 8.3: Typical chiral nematic "fingerprint" texture for a cotton cellulose suspension (7.07% (w/w)).

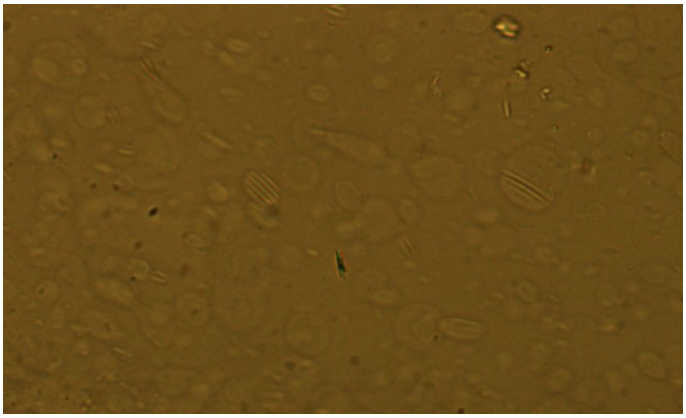

Figure 8.4: Anisotropic "tactoids" within isotropic layer for a cotton cellulose suspension (4.98% (w/w)).

When these results were compared with the non-ion exchanged suspensions in the same concentration range, it was concluded that cationic counterions from tap water were having an effect on the phase behaviour of the material.

Measurements were made to determine the chiral nematic pitch of these suspensions to determine if there was a concentration effect, the results are shown graphically in figure 8.5 where the pich decreases when the cellulose concentration increases. If the material forms a chiral nematic structure, the pitch of the structure can be approximately determined as being twice the distance between the lines of the observed "fingerprint texture" (Beck-Candanedo *et al.,* 2005).

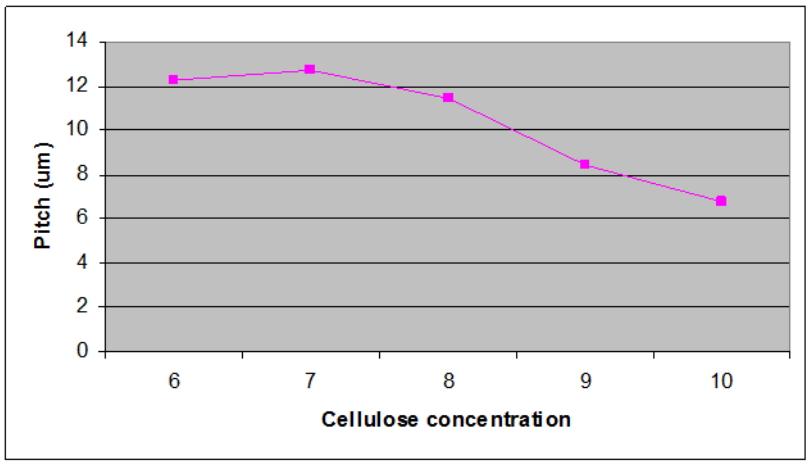

Figure 8.5: Effect of cellulose concentration on chiral pitch of cotton cellulose suspension (un-centrifuged, 11 weeks dialysis) where the pitch decreases when the cellulose concentration increases.

8.2.1.1 Conclusions

The conclusion from this preliminary work was that the counter ions present in tap water were having a significant impact on the phase behaviour of uncentrifuged cellulose nano-fibrils suspensions. The data supported the need to dialyze these suspensions against deionized water in order to induce the uncentrifuged material to fractionate. Section 8.2.2 provides a more detailed investigation into the phase behaviour of cation exchange resin treated gels.

8.2.2 Further phase behaviour studies using gels treated with cation exchange resin

8.2.2.1 Methodology

Whatman No4 cellulose preparations that had been centrifuged after hydrolysis and then dialysed for 7 weeks against tap water were selected for these studies. The cellulose suspension was agitated with cation exchange resin at a concentration of 1.5g resin to 1g of cellulose for 4 hours. The suspension was then filtered to remove the resin.

The exchanged material was centrifuged to concentrate to 20% cellulose by weight. A series of suspensions with an expected concentration range of 4 to 10% cellulose by weight was then made by diluting this stock suspension, vortex mixing and treating

each suspension with ultrasound for 30 seconds. The actual post mixing cellulose concentrations of the suspensions was determined gravimetrically.

8.2.2.2 Results

The suspensions were left to stand for 10 days in order for phase separation to occur. The suspensions separated into 2 phases (dependent on concentration) as shown in figure 8.6.

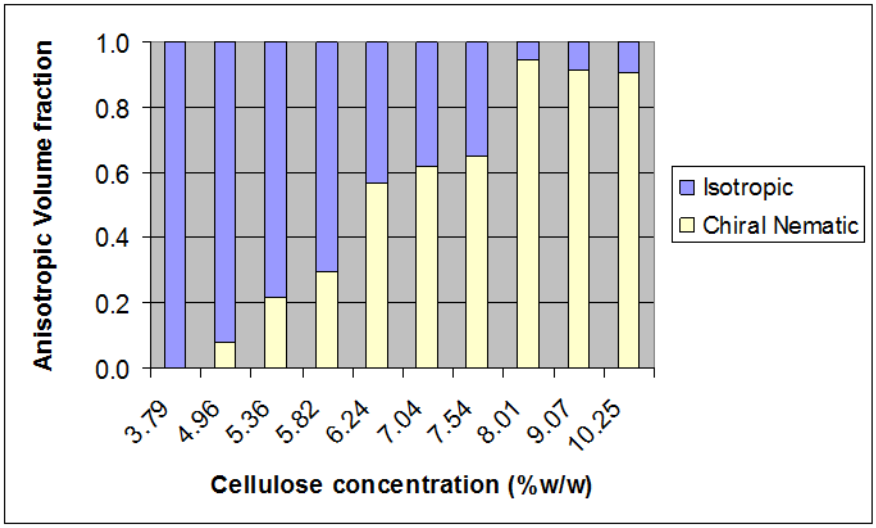

Figure 8.6: Phase behaviour of cation exchanged Whatman No4 based fibrils suspensions.

Under polarised light microscopy the uppermost layer could be seen to be isotropic (Fig 8.7) whilst the lower phase was anisotropic and showed the characteristic "finger print" structure of chiral nematic structure (Fig 8.8).

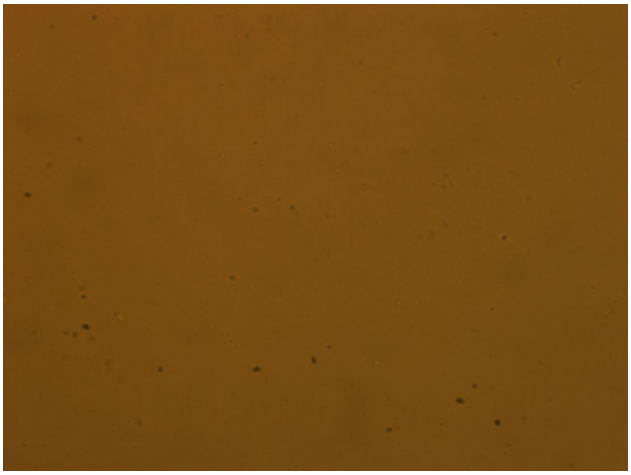

Figure 8.7: Isotropic layer for a cation exchanged Whatman No4 based fibrils (7.04% (w/w)).

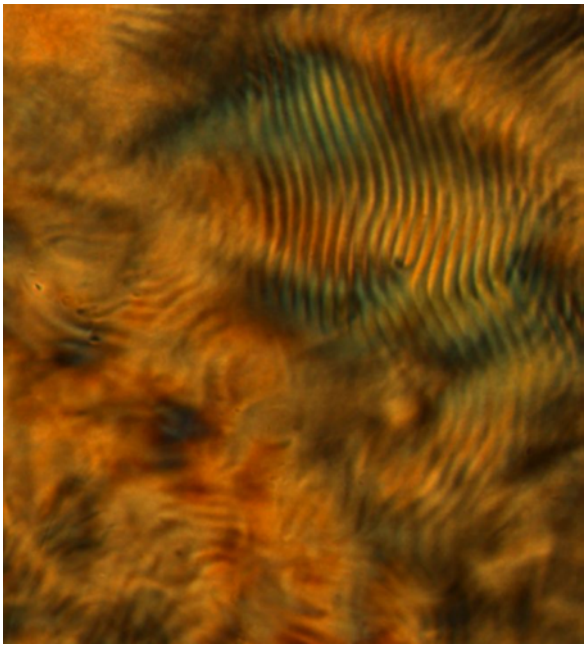

Figure 8.8: Chiral nematic anisotropic layer for a cation exchanged Whatman No4 based fibrils (7.04% (w/w)).

Observations were made of the chiral nematic pitch of the appropriate suspensions to determine the effect of concentration and the results are shown graphically in figure 8.9. The data indicates a trend of decreasing pitch with increasing concentration, which corresponds to data reported previously (Fig. 8.5).

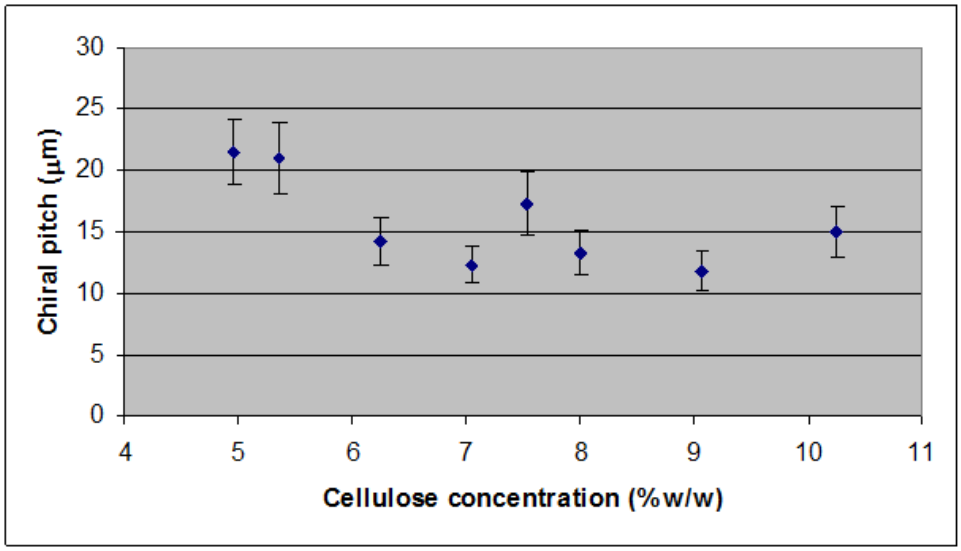

Figure 8.9: Effect of concentration on chiral pitch of chiral nematic layer of cation exchanged Whatman No4 based fibrils.

8.2.2.2.1 Particle size and zeta potential of isotropic/anisotropic layers

Samples were taken from each layer in each suspension. These samples were analysed utilising the Zetasizer to determine particle size and zeta potential. The difference in the particle size between layers is shown in figure 8.10.

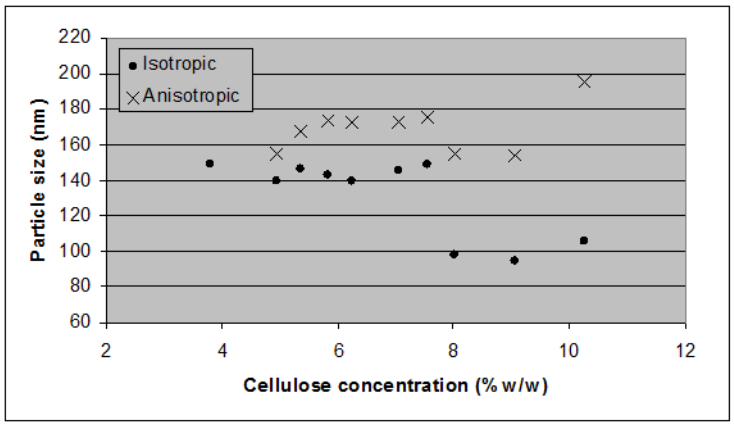

Figure 8.10: Particle size of isotropic and anisotropic layers of cation exchanged Whatman No4 based fibrils.

The data showed a clear difference in particle size between the layers (significant at p0.05 using a t-test), but with considerable variance especially in the last three concentration values. It is not known whether these three data points were unexplained outliers or if they genuinely reflected the extent of variation in the data. If these last three values are excluded from the statistical analysis the difference was still significant at p0.05.

The data for Zeta potential (figure 8.11) showed no significant differences between the 2 layers.

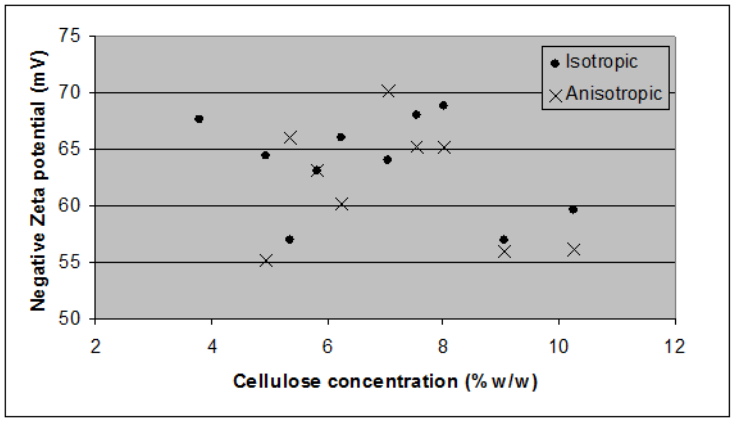

Figure 8.11: Zeta potential of isotropic and anisotropic layers of cation exchanged nano-fibrils from Whatman No4 filter paper.

The cellulose concentration of the individual layers was also determined and plotted against the average concentration of fibrils suspension (Fig. 8.12) with the data indicating a difference in concentration between the 2 layers. The spread of standard deviation (error bars) shows that the most significant differences were in the concentration range (5-8%) where the anisotropic volume fraction was between 0.2 and 0.8.

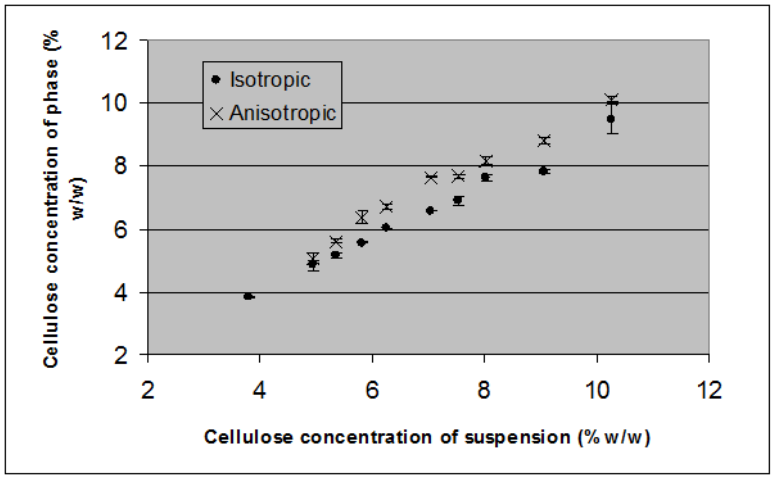

Figure 8.12: Cellulose content (% w/w) of isotropic and anisotropic layers of Whatman No4 based fibrils.

For comparison, a second batch was treated using cation exchange resin, using the method detailed above.

The suspension again separated into 2 phases – an isotropic and anisotropic layer. The comparison in change in volume fraction with concentration for the 2 batches (termed Cation 1 and Cation 2) is shown in figure 8.13.

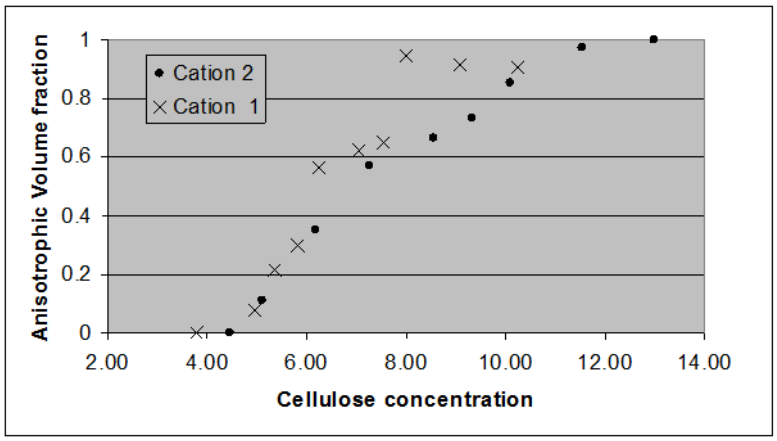

Figure 8.13: Comparison of concentration on anisotropic volume fraction for 2 batches of cation exchanged Whatman No4 based fibrils.

The data shows that the general trend for the phase separation was reproducible but that the second batch had less variance.

The particle size was also determined for the two batches of cation treated material. The particle size of the anisotropic layer was significantly higher (p0.05) than that of the isotropic layer. However, when the 2 batches were compared to each other (Fig. 8.14) there were clear and significant (p0.05) differences between the corresponding layers of each batch.

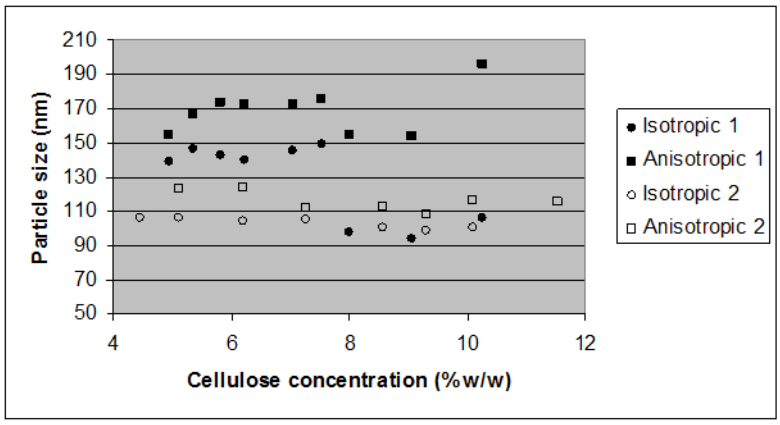

Figure 8.14: Comparison of layer particle sizes for cation exchanged batches 1 and 2.

There are a number of possible explanations for this observation. The batches may have had differing particle sizes due to differences during hydrolysis. It is also possible that during the ion exchange treatment certain fractions were removed. Also, although the batches were sonicated for equal times there may have been agglomeration taking place in batch 1. The sizing method would therefore seem to be highly sensitive to small changes and this will need to be taken into account during sample preparation and when analysing data.

The zeta potential of the layers for batch 2 showed a similar distribution pattern to that for batch 1, with no significant differences between the layers. However, the mean zeta potential obtained for batch 1 was significantly higher (at p0.05) than that of batch 2.

The cellulose concentration of the individual layers of batch 2 was also determined (Fig 8.15) and as in batch 1 (Fig. 8.11) there was a clear difference in concentration between the isotropic and anisotropic layers.

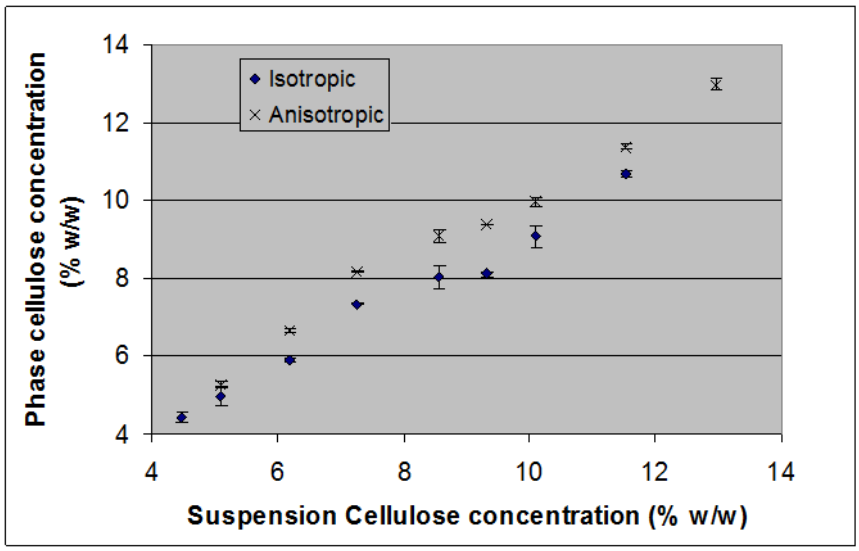

Figure 8.15: Cellulose concentration of isotropic and anisotropic layers of batch 2 of cation exchanged Whatman No4 based fibrils (error bars = standard deviation).

When the data for the two batches was compared graphically (Fig. 8.16 and 8.17) a consistent correlation between suspension concentration and phase concentration was observed. Linear relationships between the phase and suspension concentrations were determined with good R^2 values: Isotropic $R^2 = 0.9843$, Anisotropic $R^2 = 0.9841$.

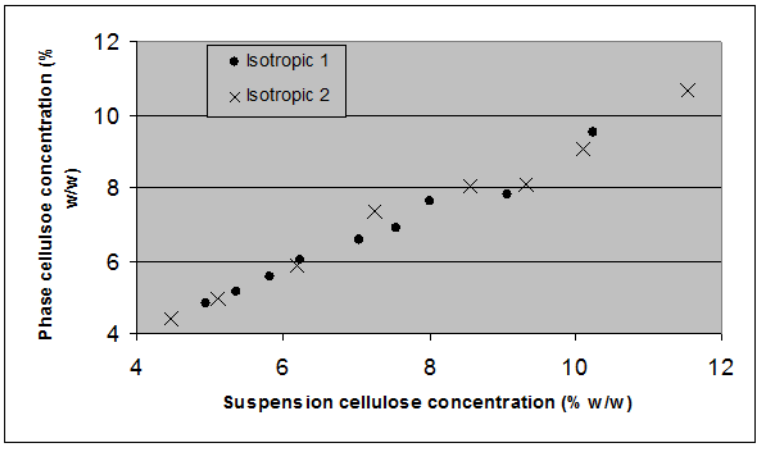

Figure 8.16: Concentration of isotropic phase of batches 1 and 2 of cation exchanged Whatman No4 based fibrils.

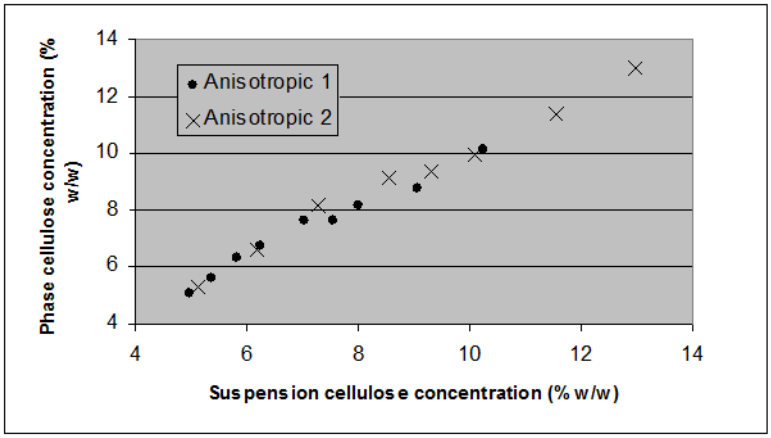

Figure 8.17: Concentration of anisotropic phase of batches 1 and 2 of cation exchanged Whatman No4 based fibrils.

The anisotropic layer of batch 1 and 2 was observed to be chiral nematic in nature. The chiral pitch was determined and as in batch 1 there was a trend of decreasing pitch with increasing concentration. When the 2 batches are compared (Fig. 8.18) similar values were seen with no significant difference (at p0.05) seen between them.

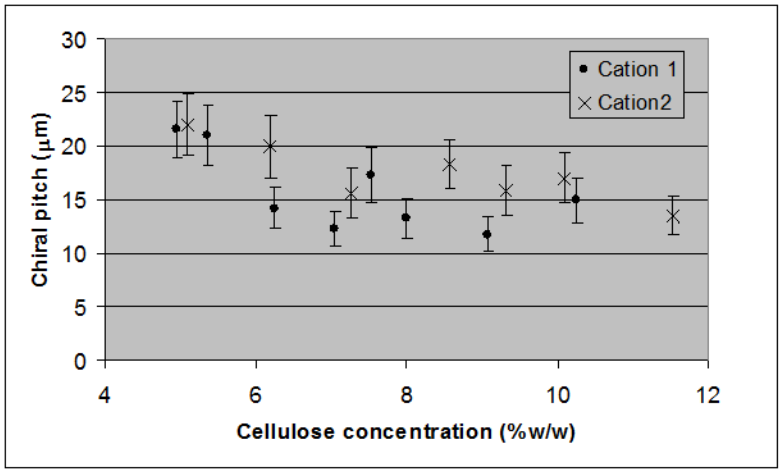

Figure 8.18: Comparison of chiral pitch of chiral nematic layers of cation exchanged Whatman No4 based fibrils (error bars = standard deviation).

8.2.2.2.2 Summary

- Good correlation between batches for effect of concentration on anisotropic volume fraction obtained.

- Different layers showed different particle size but there was poor correlation of particle size between batches.

- There appeared to be no difference in zeta potential between layers.

- Different layers had different cellulose concentrations with a consistent linear relationship observed between phase cellulose concentration and suspension concentration.

- A consistent trend of decreasing chiral pitch with increasing concentration was observed.

8.2.3 Fractionation studies for a suspension that was centrifuged but not treated to remove counterions

8.2.3.1 Three layer fractionation

Cotton cellulose preparations that had been centrifuged after hydrolysis and then dialysed for 7 weeks against tap water were selected for phase behaviour studies. The dialysed material was centrifuged to concentrate to 20% cellulose by weight. A series of suspensions with an expected concentration range of 4 to 12% cellulose by weight was then made by diluting this stock suspension, vortex mixing and treating each suspension with ultrasound for 30 seconds. The actual post mixing cellulose concentrations of the suspensions was determined gravimetrically.

The suspensions were left to stand for 10 days in order for phase separation to occur. The cellulose suspensions were seen to phase separate into 2 phases after 2 days (dependent on concentration). However, after the full 10 days a third phase was visible (Fig. 8.19) in some of the suspensions, again concentration dependent.

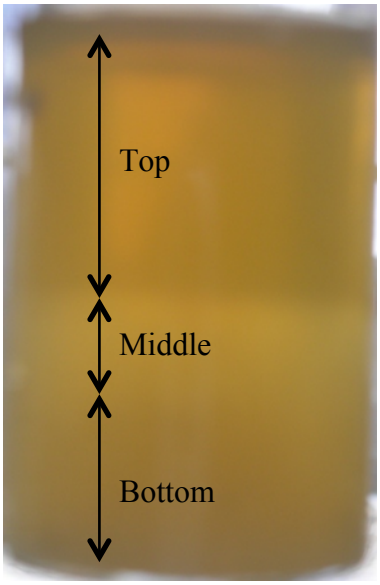

Figure 8.19: Tri-phasic solution.

The 3 phases were examined using polarised optical microscopy and the field emission scanning electron microscope (FEG-SEM). The top layer was identified as the non-birefringent isotropic layer. In some instances anisotropic tactoids were evident (Figure 8.20). Figure 8.21 shows the same suspension through the FEG-SEM at 25 000 times magnification.

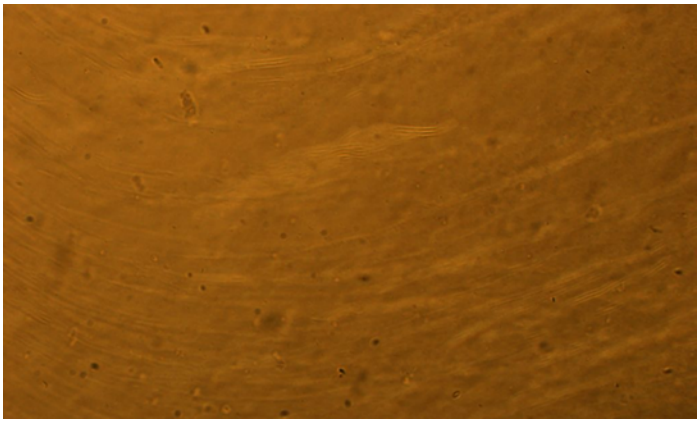

Figure 8.20: Isotropic top layer from cotton cellulose suspension of 7.27% w/w concentration. Anisotropic tactoids are present.

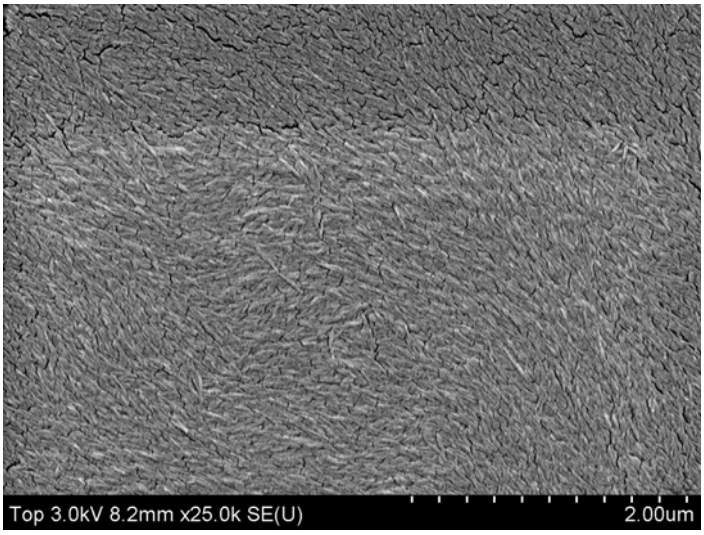

Figure 8.21: FEG-SEM image of nano-fibril suspension at 25 000 x magnification.

The second layer (where present) exhibited the classic "fingerprint" texture of the chiral nematic phase (Fig. 8.22)

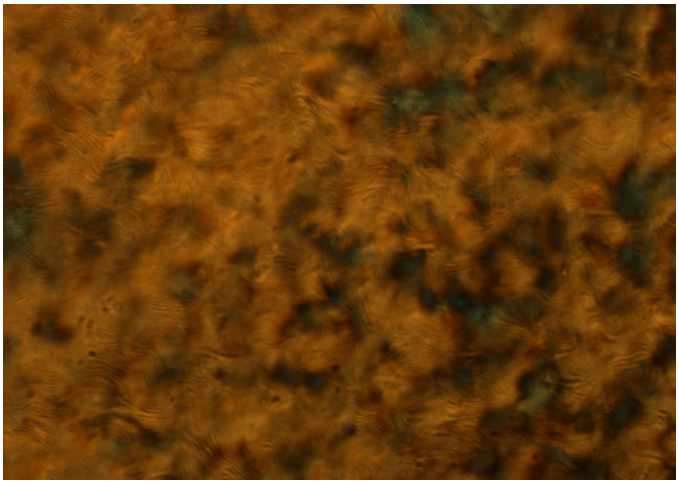

Figure 8.22: Second layer from cotton cellulose suspension of 7.27% w/w concentration. Characteristic "fingerprint" texture indicates chiral nematic anisotropic phase.

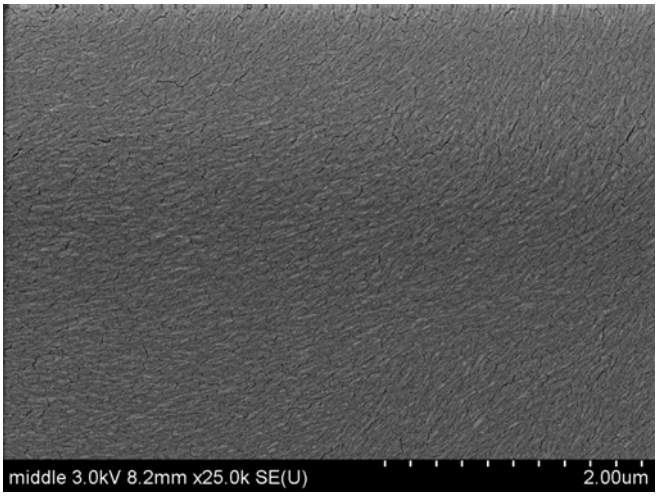

Figure 8.23: FEG-SEM image of the cellulose nano-fibrils at 25 000x magnification of the middle layer.

Figure 8.23 shows that the fibril size looks similar to that of the top layer although the structure of the fibrils looked more ordered. The third layer did not exhibit the same fingerprint structure as the second layer, although it was still birefringent under polarised light and therefore anisotropic (Fig. 8.24). At some concentrations (7.09-7.37%) some regions of the third layer showed small domains with the fingerprint texture but these disappeared with increasing concentration.

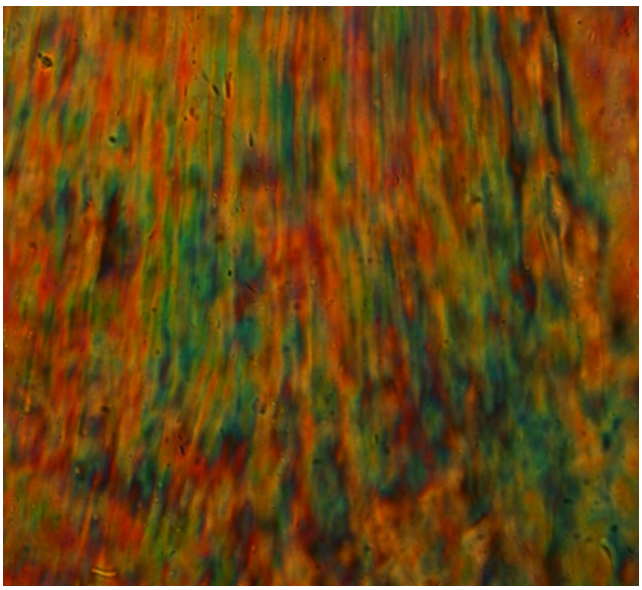

Figure 8.24: Third layer from cotton cellulose suspension of 7.27% w/w concentration. Birefringence indicates anisotropic phase but characteristic chiral nematic structures missing

Figure 8.25 shows a FEG-SEM image of the nano-fibrils in the bottom layer. The SEM image looks very similar to previous images of fibrillar debris with the presence of

amorphous cellulose. It is very difficult to discriminate between individual fibrils that are much smaller than in the top two layers. Surface cracks are also visible in the film due to damage by the electron beam indicating the presence of amorphous material as it is highly sensitive to the electron beams.

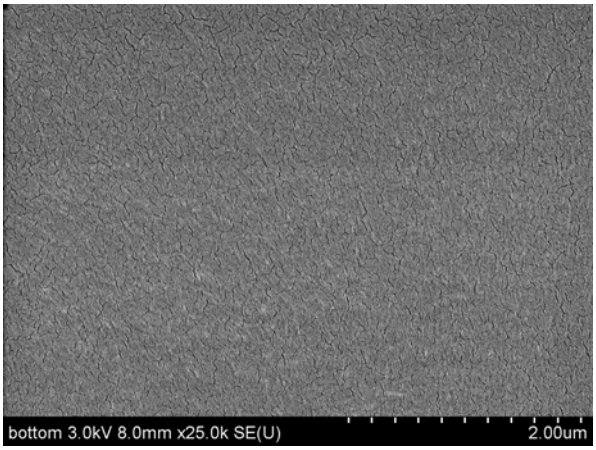

Figure 8.25: FEG-SEM image of nano-fibrils in the bottom layer.

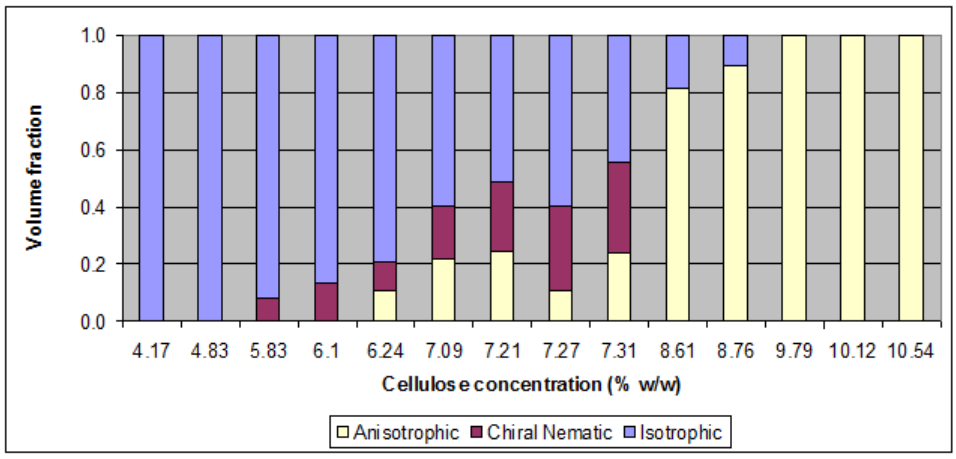

Figure 8.26: Volume fraction of different phases dependent on suspension concentration.

Figure 8.26 shows the volume fraction of the different phases dependent on suspension concentration. The data shown in figure 8.26 shows that at low concentrations the suspension was isotropic (albeit with anisotropic tactoids). As the concentration increased the suspension separated into 2 phases – with the second being chiral nematic anisotropic. As concentration increased further an anisotropic phase itself separated into a chiral nematic and a non-chiral phase. The non-chiral phase increased with increasing concentration, until at higher concentrations, 9.7% +, the suspension was 100% non-chiral anisotropic. The exact nature of this phase is yet to be determined. It is thought

that this phase would have been chiral nematic if the counterions had been removed from the gel.

A phase diagram was determined by combining the 2 anisotropic phases, and this is shown in figure 8.27.

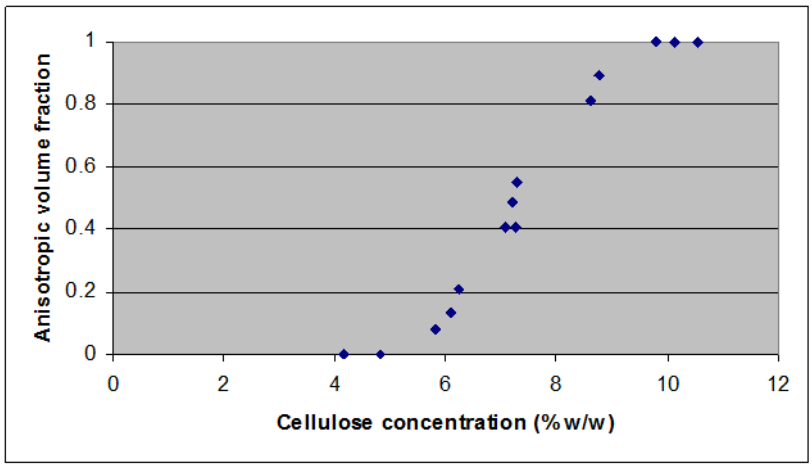

Figure 8.27: Phase separation diagram of standard material.

This phase separation can be compared to that of the uncentrifuged material (Fig. 8.28) and shows some slight differences in the shape of the curve. This is almost certainly due to the change in size distribution resulting from centrifugation.

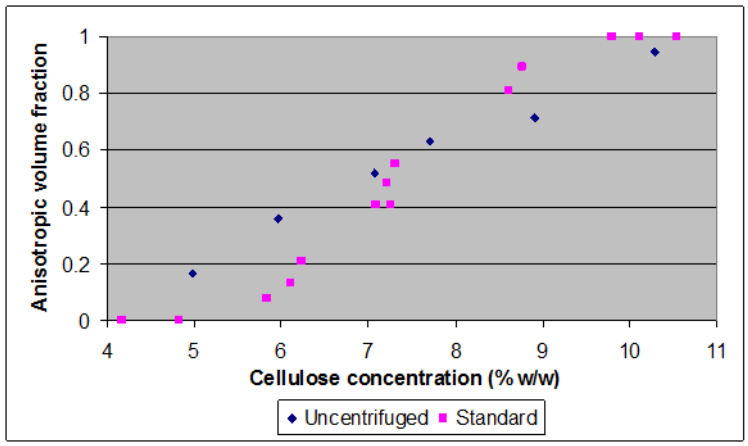

Figure 8.28: Comparison of phase separation between standard and uncentrifuged cotton cellulose.

8.2.3.1.1 Particle size distribution and zeta potential of isotropic/anisotropic layers

Samples were taken from each layer in each suspension and analysed using the Zetasizer to determine particle size and zeta potential.

The data for the mean particle size and zeta potentials for each layer is shown in table 8.1. Only data for those concentrations where phase separation occurred is included (i.e. high and low concentrations excluded)

Phase	Mean particle size nm	Mean Zeta potential mV
Isotropic	**102.99** *(8.17)*	**-37.89** *(2.21)*
Chiral nematic	**112.67** *(7.47)*	**-36.84** *(2.02)*
Non-chiral anisotropic	**120.48** *(9.33)*	**-36.53** *(1.68)*

Table 8.1: Mean particle size and zeta potentials for each layer (standard deviation).

The mean particle size data plotted in figure 8.29 showed differences between the particle size of the layers but with some variance (as shown by the standard deviations in table 8.1).

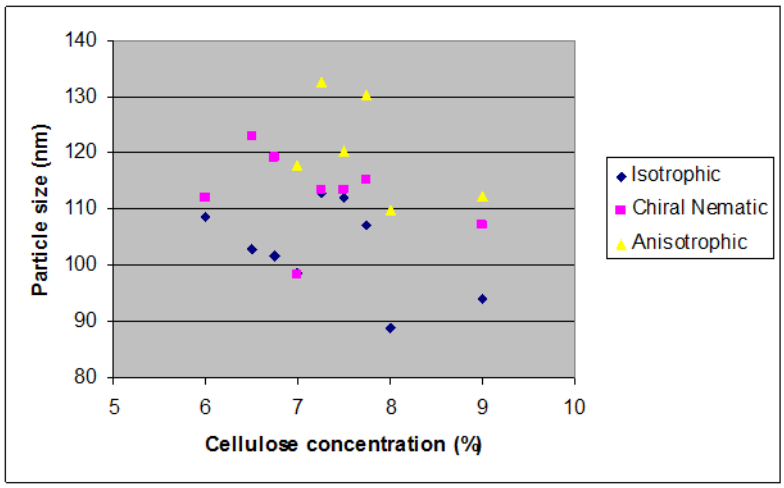

Figure 8.29: Mean particle size of layers dependent on concentration.

Analysis of the data using single factor ANOVA shows that there were significant differences between the layer sizes at p0.5 (p value = 0.018). Further analysis using 2 sample t-tests based on unequal variance (variance determined by f-test) shows there was significant difference (at p=0.05) between the particle sizes of the isotropic and chiral nematic layers (p-value = 0.009) and the isotropic and non-chiral anisotropic layers (p-value = 0.01) but not between the chiral and non-chiral anisotropic layers (p-value = 0.61) indicating very subtle differences in size can impact on the behaviour of the suspensions and the differentiation into different layers.

The plots of particle distribution between layers at different solid concentrations show different results; some show a more variable particle distribution as in figure 8.30 whilst

others show no observable difference in the particle distribution i.e. figure 8.31. This suggest that solids concentration has an impact on how the nano-fibrils self organise within the different layers.

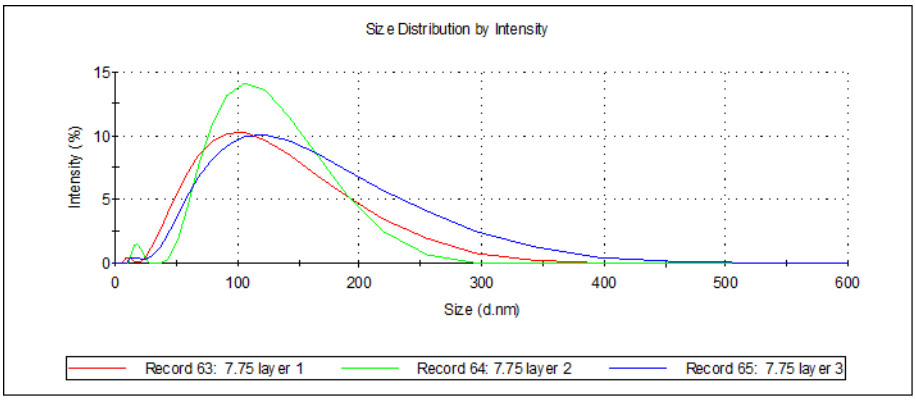

Figure 8.30: Particle distribution between layers – standard preparation 7.21% cellulose concentration.

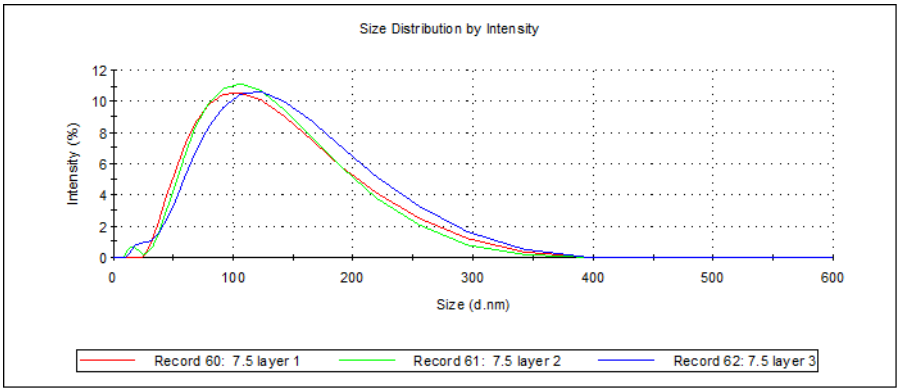

Figure 8.31: Particle distribution between layers- standard preparation 7.09% cellulose concentration.

Graphical plot (Fig. 8.32) and analysis for the Zeta potential shows that there was no significant difference (ANOVA p-value = 0.32) in average zeta potential of the particles between layers. However Fig. 8.33 shows that although the average zeta potential values are similar the different layers have a different zeta potential distribution.

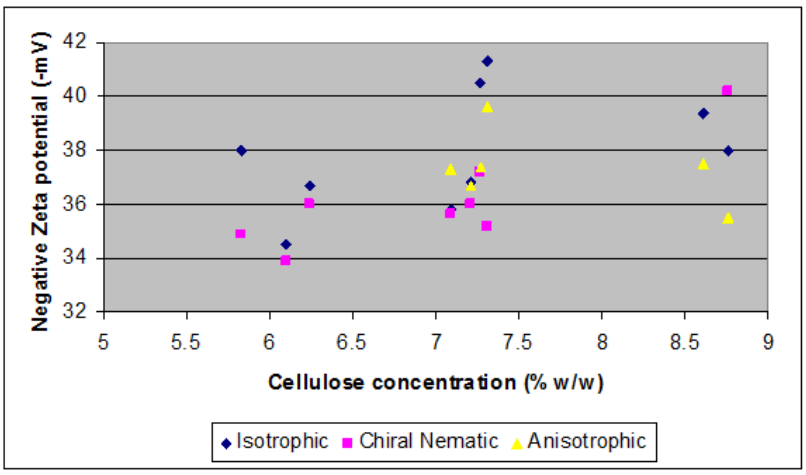

Figure 8.32: Zeta potential of particles within different layers dependent on concentration.

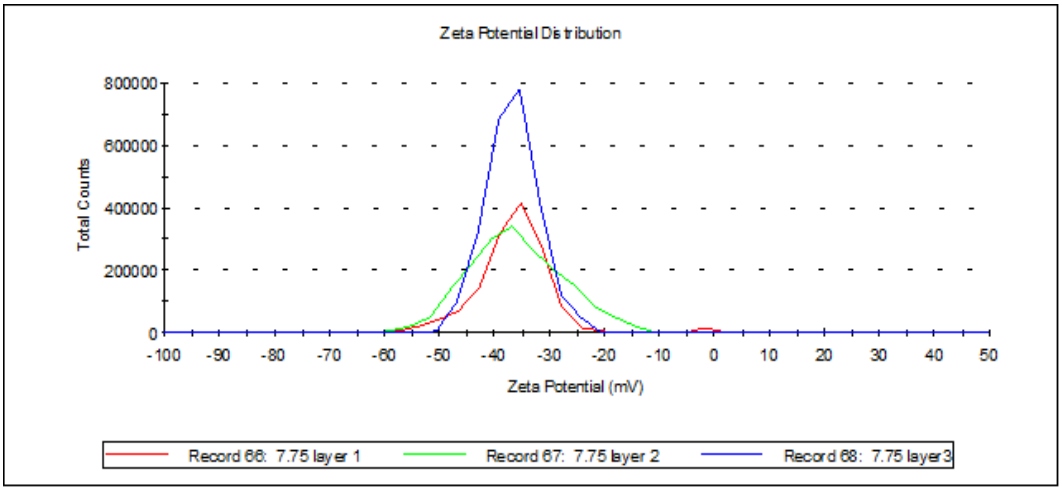

Figure 8.33: Zeta potential distribution across different layers – 7.21% cellulose concentration.

8.2.3.1.2 Cellulose concentration of layers

The percentage cellulose content for each layer for each suspension was determined. Comparative data for the cellulose content for those suspensions showing 3 phases is given in table 8.2.

Suspension cellulose content (%)	Layer Cellulose content (%)		
	Isotropic	**Chiral Nematic**	**Anisotropic**
7.14	6.75	7.19	7.5
7.21	6.98	7.38	7.48
7.27	6.84	7.31	7.57
7.31	6.11	6.68	7.25

Table 8.2: Comparison of cellulose content between layers.

ANOVA analysis of this data showed that there was significant differences (p-value = 0.015) within the data set. Further analysis using 2 sample t-test based on unequal variance (variance determined by f-test) showed that there was significant difference (at p = 0.05) between the non chiral anisotropic and the isotropic layers (p-value = 0.02) but not between the chiral nematic and the isotropic (p-value = 0.1) or the non-chiral anisotropic (p-value = 0.14).

8.2.3.1.3 Three layer fractionation summary

In the case of the standard material it would seem that a triphasic solution could be obtained dependent on concentration. The phases appeared to be fractionated by size rather than zeta potential although it must be remembered that any ions added during dialysis may also affect recorded zeta potentials.

8.2.3.2 Four layer fractionation

As an extension to the above work excess standard material used in the analysis above was concentrated to a starting concentration of 7.5%, vortex mixed and sonicated as above. Actual concentration was determined to be 7.09%. This suspension was then placed into a conical flask and left to separate. After 10 days four distinct layers could be discerned visually (Fig. 8.34)

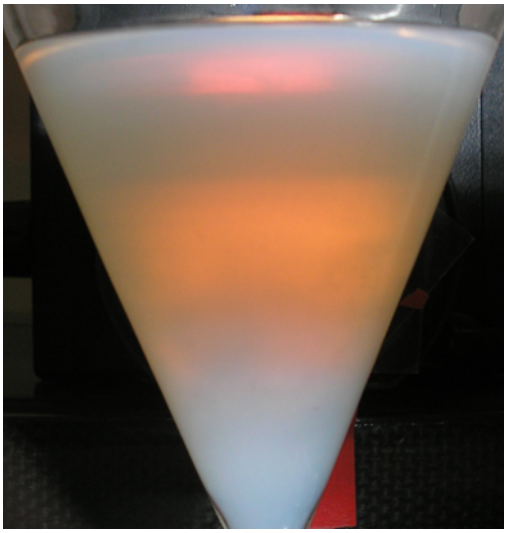

Figure 8.34: Four-phase separation of standard prepared material at 7.09% cellulose concentration.

Samples of each of the four layers were taken for microscopy, particle size and zeta potential analysis.

The microscopy showed that the upper layers were isotropic (Fig. 8.35 and 8.36) with layer 2 having anisotropic tactoids within it.

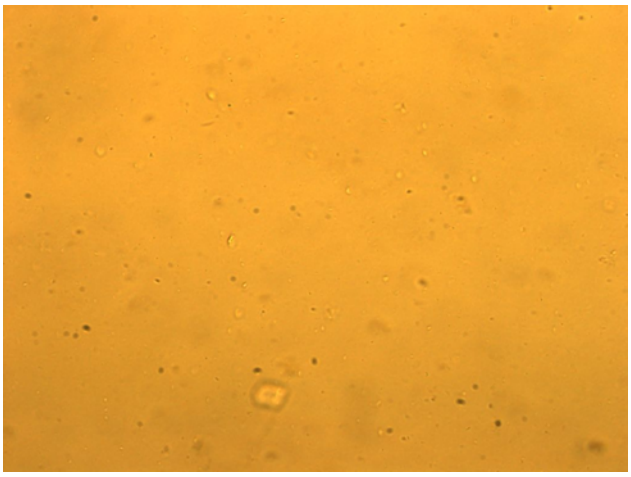

Figure 8.35: Upper isotropic layer of standard prepared material at 7.09% cellulose concentration.

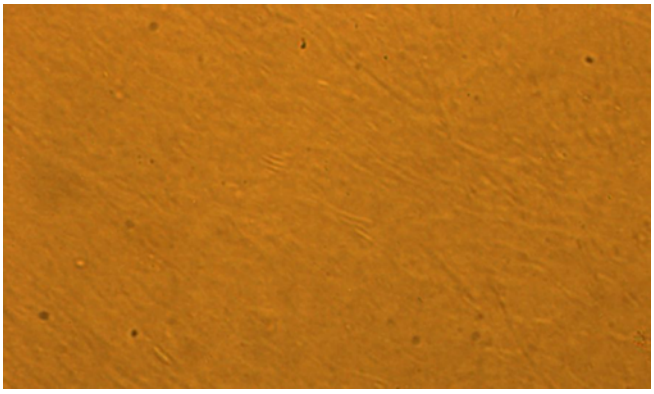

Figure 8.36: Upper isotropic layer with anisotropic tactoids of standard prepared material at 7.09% cellulose concentration.

Layers 3 and 4 showed the characteristic chiral nematic fingerprint texture (Fig. 8.37 and 8.38).

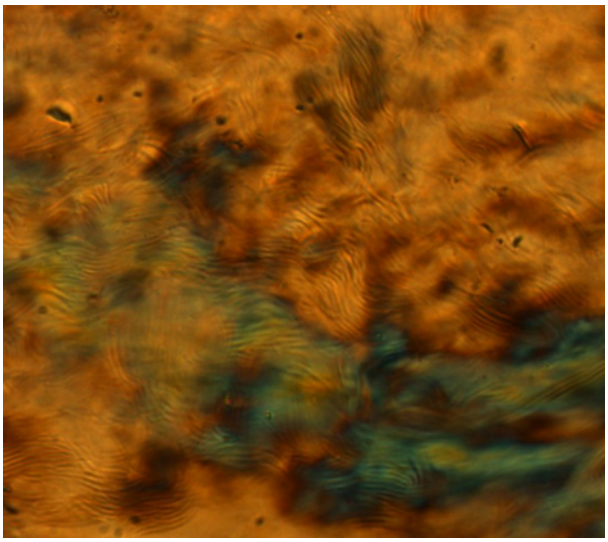

Figure 8.37: Anisotropic layer with the characteristic chiral nematic fingerprint texture of standard prepared material at 7.09% cellulose concentration.

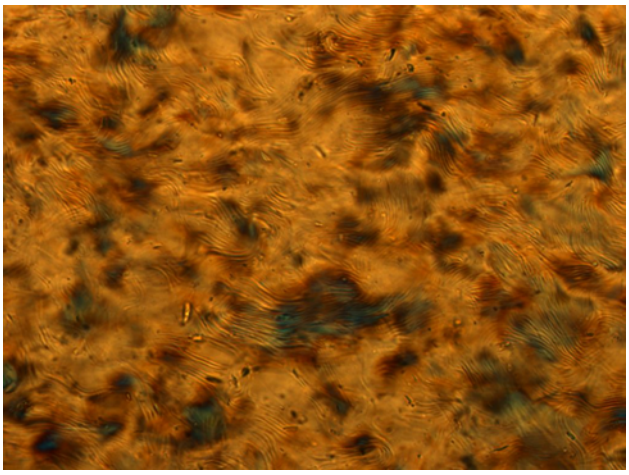

Figure 8.38: Lower anisotropic layer with the characteristic chiral nematic fingerprint texture of standard prepared material at 7.09% cellulose concentration.

The cellulose content, particle size and particle zeta potential of each layer are given in table 8.3. The data shows that cellulose content and particle size increases down the suspension. Zeta potential remained relatively constant.

Layer	Cellulose concentration (%)	Particle size nm	Zeta potential mV
1	6.89	146.0	-36.8
2	6.84	137.0	-39.8
3	7.46	171.4	-40.0
4	7.77	206.8	-37.9

Table 8.3: Layer analysis.

The particle size distribution graphs generated using the Zetasizer show that there was a general increase in size profile of the particles with the lower layers (Fig. 8.39).

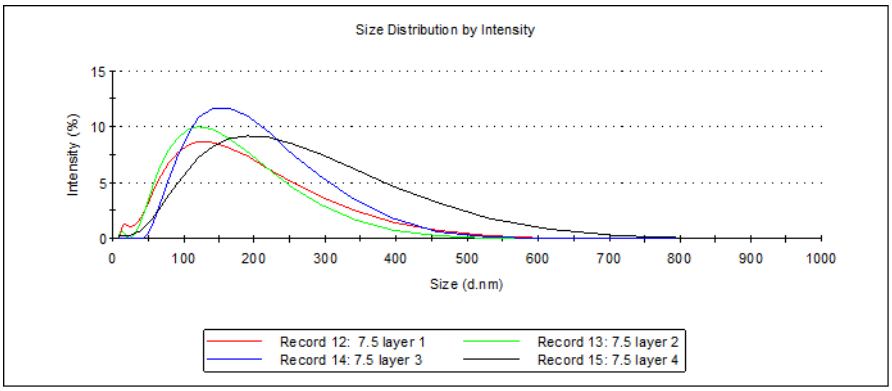

Figure 8.39: Particle size distributions of the 4 layers.

8.2.3.3 Conclusions

The phase behaviour of Whatman No4 cellulose nano-fibrils produced by the standard method and by a modified method where the suspensions were not centrifuged after hydrolysis show that:

- The suspensions that were not centrifuged following dialysis did not separate into different phases but showed an increase in levels of a characteristic birefringent glassy phase as suspension concentration increased;

- Upon treating the uncentrifuged material with a cation exchange resin the suspensions separated into upper isotropic and lower anisotropic phases, within certain suspension concentration ranges. The anisotropic phase was shown to be chiral nematic. Significant differences in particle size but not zeta potential were seen between the 2 phases;

- Suspensions produced in the standard manner (centrifuged but not treated to remove counterions) were shown to separate into 2 or 3 phases dependent on suspension concentration: An isotropic, a chiral nematic and an unidentified anisotropic phase. Again significant differences in particle size but not zeta potential were seen between phases;

- Removal of the amorphous material through centrifugation allowed the self-assembly of fibrils in the middle phase into a chiral nematic structure without the removal of counterions.

It appeared from these results that it might be possible to use phase behaviour to separate fibrillar debris (albeit rather crudely) from more desirable longer nano-fibrils by the simple use of settling tanks. Once the different phases have stabilized it should be possible to draw off the bottom layer of fibrillar debris leaving a more homogenous fibril suspension without using a centrifuge. However, when this setting process was scaled up to 1 litre batches, it took several days to fractionate, indicating that the process was not fast enough to be a practical process. So centrifugation technique was required for fractionation.

8.3 Overall conclusions of phase behaviour studies

- Without ion exchange resin uncentrifuged material does not form a chiral nematic layer.

- Without ion exchange resin, the standard material forms 3 rather than 2 phases. Counter ions from tap water dialysis are the most likely cause of this, as without the presence of counter ions i.e. removed by ion exchange, a biphasic (isotropic and a chiral nematic phase) suspension was formed.

- The pitch of the chiral nematic phase decreased with increasing concentration as shown in Fig. 8.5 for uncentrifuged and treated suspensions and Fig. 8.9 for centrifuged and treated suspensions.

- There was a linear relationship between cellulose concentration within the phases and the suspension as a whole.

- There is evidence to suggest that phase separation may be linked to particle size. However this phenomenon cannot be practically used for fractionation in a large

scale process because the phase separation process would take too long to be commercially practical.

- There is no evidence to suggest phase separation may be linked to zeta potential, however counter ions in the media may still be interfering with accurate measurement.

- This work confirms the need to control the ionic conditions of the gel more carefully and supports the decision to install a reverse osmosis dialysis system to remove counterions from tap water during the dialysis process.

9 DEVELOPMENT OF THE REVERSE OSMOSIS DIALYSIS PROCESS AND ITS IMPACT ON NANO-FIBRIL GEL SUSPENSION.

9.1 Introduction

Three dialysis tanks (Fig. 9.1) of 400 litres each were connected in series to a reverse osmosis unit (Osmotron QuadRO) capable of producing 260 litres of deionised water per hour. In preliminary analysis it was noted that cellulose suspensions reached a pH close to neutral within 48 hours. Compared with two to three weeks with the 10 – 25 litres containers into which the dialysis tubing were stored under continuous running tap water. This improvement was thought to be due to significant increases in water flow combined with much larger volumes of water (relative to the suspension volumes) in the larger tanks. This was confirmed by an observed reduction in rate of dialysis as the tanks become fulled with large volumes of cellulose nano-fibril gels.

Figure 9.1: De-ionized water tanks.

Following on from initial observations, a more detailed study was established to evaluate the impact of the new reverse osmosis dialysis system on pH, acid group content and Zeta potential (surface charge) of the cellulose nano-fibril suspensions. The raw material used for the nano-fibril suspensions was 92 alpha cellulose to allow comparison with the previous tap water dialysis experiment (Section 7.4). The two key variables considered included, the impact of dialysis time and the impact of storage time of the gels (stored in the fridge at 4^{o}C) once they have were taken out of dialysis, to determine the stability of the suspensions over time.

9.2 Methodology

Two batches (V55 and V57) of nano-fibril suspensions prepared by the standard process described in Section 5.2.2, were tested. Analysis of the suspensions included pH, acid group content and zeta potential.

9.3 Results and discussions

Due to time constraints the overall dialysis time was not as long as the original tap water study. Figure 9.2 illustrates the change in pH over a period from zero to 25 days. It can be seen that pH continued to increase over time.

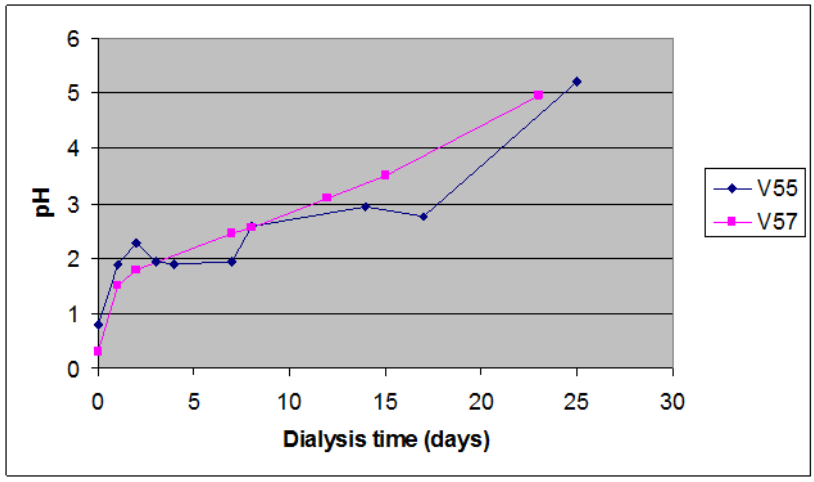

Figure 9.2: Mean pH of cellulose nano-fibril suspensions with dialysis time.

After dialysis the pH varied with storage time but not in a predictable way. However pH appeared to be more stable during storage with longer dialysis times (Fig. 9.3 and 9.4). These two graphs show how the pH changes with storage depending on the number of days in dialysis.

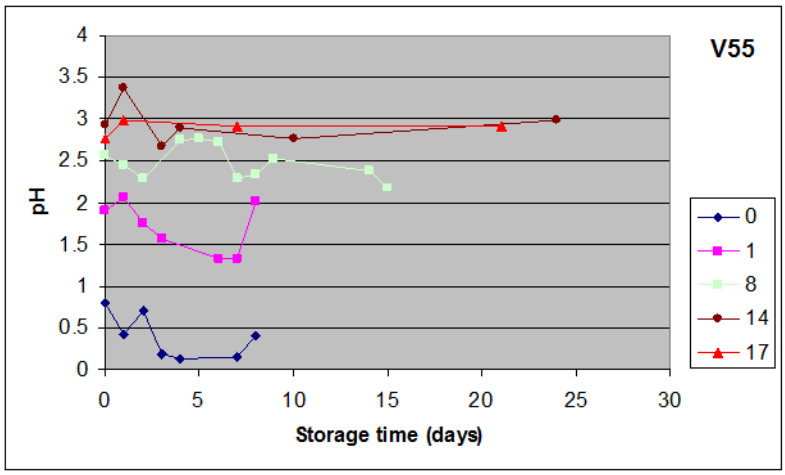

Figure 9.3: Stability of pH of cellulose nano-fibril suspensions with storage time after being taken at different times from the dialysis tank.

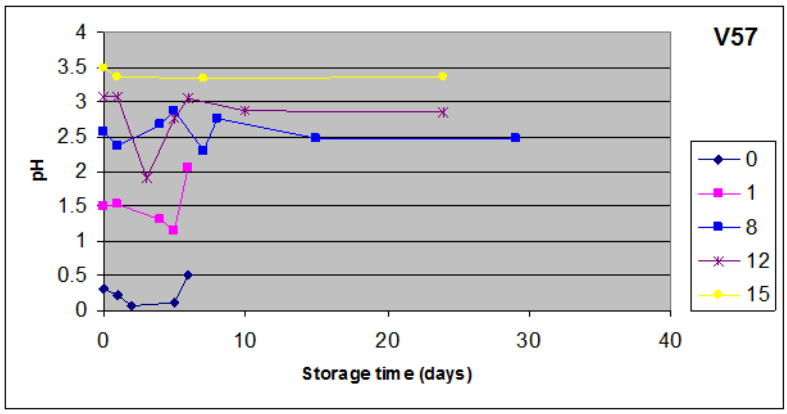

Figure 9.4: Stability of pH of cellulose nano-fibril suspensions with storage time after being taken from at different time from the dialysis tank.

Figure 9.5 shows how the acid group content declined with dialysis time for the two different batches of cellulose. The sulphate groups introduced through the hydrolysis process were slowly removed during dialysis. The trend was the inverse of that for pH.

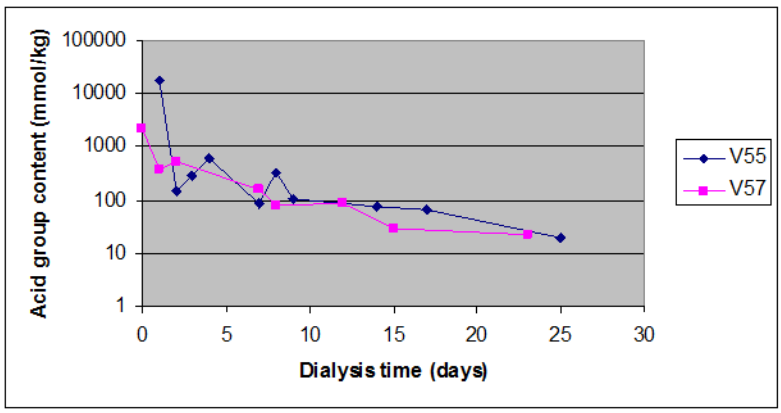

Figure 9.5: Impact of dialysis time on the acid group content of cellulose nano-fibril suspensions.

Figures 9.6 and 9.7 show the acid group content as it dropped during storage after dialysis of samples V55 and V57, with an initial large drop in the first few days of dialysis. The graphs show different trends depending how long the samples were originally in dialysis.

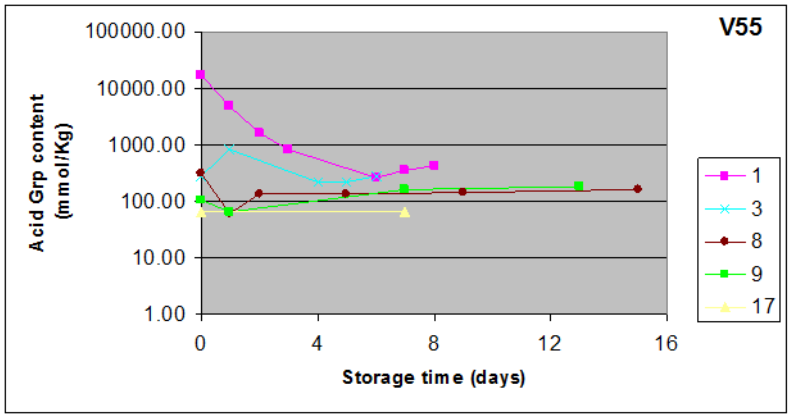

Figure 9.6: Stability of acid group content of cellulose nano-fibril suspensions with storage time after dialysis of sample V55.

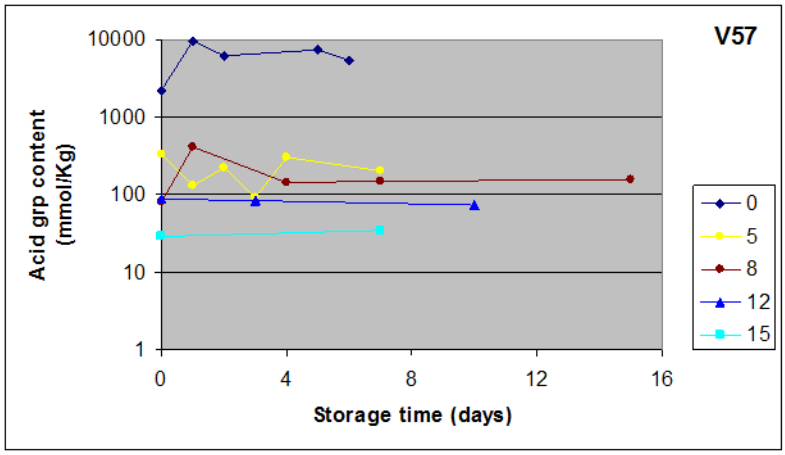

Figure 9.7: Stability of acid group content of cellulose nano-fibril suspensions with storage time after dialysis of sample V57.

Figure 9.8 indicates that there was a drop in Zeta potential for the two batches of fibrils within the first three to six days dialysis followed by a subsequent increase back up to the original levels of between 60-70 mV. It was not clear why this happened. However it is interesting to note that after 6 days storage after dialysis (Fig. 9.9) the three samples from batch V57 that had gone through dialysis stabilised at around -50/-60mV.

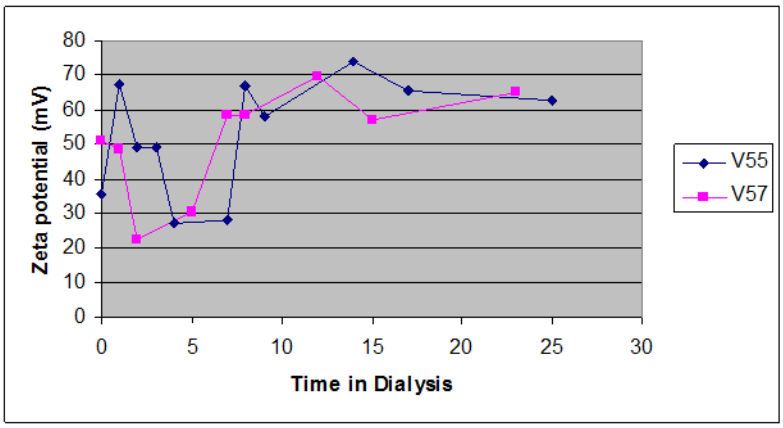

Figure 9.8: Impact of dialysis time on the zeta potential of cellulose nano-fibril suspensions.

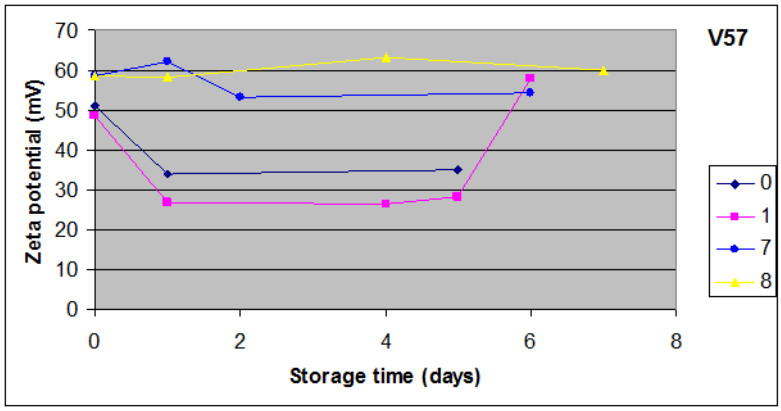

Figure 9.9: Stability of zeta potential of cellulose nano-fibril suspensions with storage time of sample V57.

9.4 Relationship between pH, acid group content and zeta potential

The relationship between the different parameters measured was tested graphically. Figures 9.10 to 9.12 illustrate the correlations between Acid group content (AGC), pH and Zeta potential. The objective was to highlight the extent of any relationships between these variables.

The data shows a good log relationship between AGC and pH (R^2= 0.92). This was expected but also confirmed accuracy and methodology of testing. With this strong correlation it was concluded that it was not necessary to measure acid group content in future.

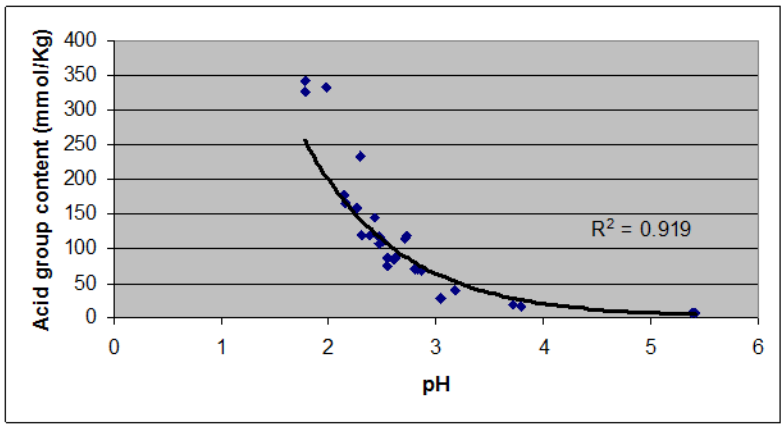

Figure 9.10: Correlation between acid group content and pH.

The data (Fig. 9.11) supported a strong log relationship between AGC and zeta potential (R^2= 0.823).

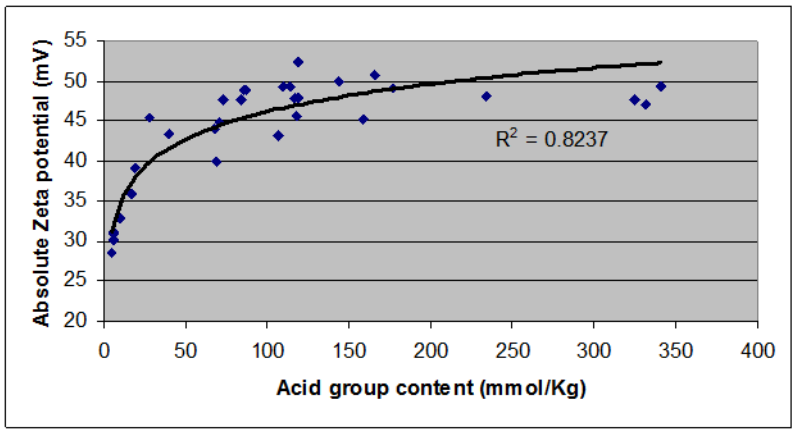

Figure 9.11: Correlation between absolute zeta potential and acid group content.

Figure 9.12 showed a linear good relationship between pH and the absolute zeta potential value (R^2= 0.87). Despite the reasonable fit the data was considered to have too great a scatter to enable pH to be used as a sufficient accurate indicator of zeta potential in routine analysis.

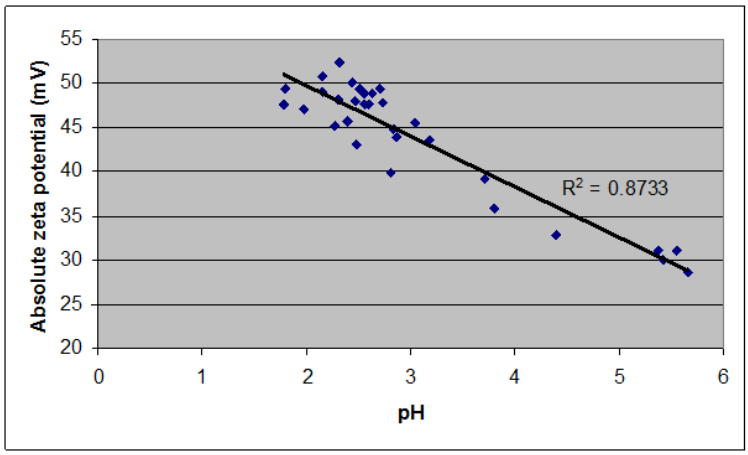

Figure 9.12: Correlation between absolute zeta potential and pH.

9.5 Reverse osmosis water characterization

The basic unit of conductivity is the Siemens (S). Conductivity was measured using conductio-metric titration. Since the geometry of the electrode used in measurements affects conductivity values, standardized measurements were expressed in specific conductivity units (S/cm) to compensate for variations in electrode dimensions.

Prior to measuring conductivity daily, the electrode was immersed in a weak solution (standard) of potassium chloride, to calibrate, i.e. with reference to the manual a conductivity of 1296 µS/cm at a temperature of 20.8°C would be deemed within calibrated range. With reference to the manufacturers of the RO tanks, fresh water direct from the tap should be approximately 6 µS/cm.

The three tanks were connected in series (Fig. 9.13), so the water flowed first through tank 3 and then to tank 5 via tank 4 before it was drained. The water for the analysis was taken at a position close to the exit of each tank to get an indication of conductivity at a distance away from the fresh running RO water.

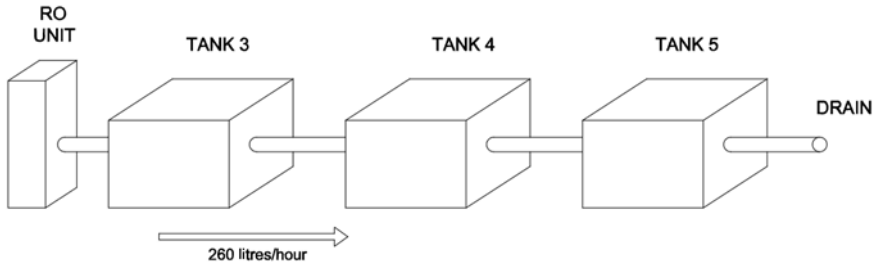

Figure 9.13: AutoCAD drawing representing the tanks configuration.

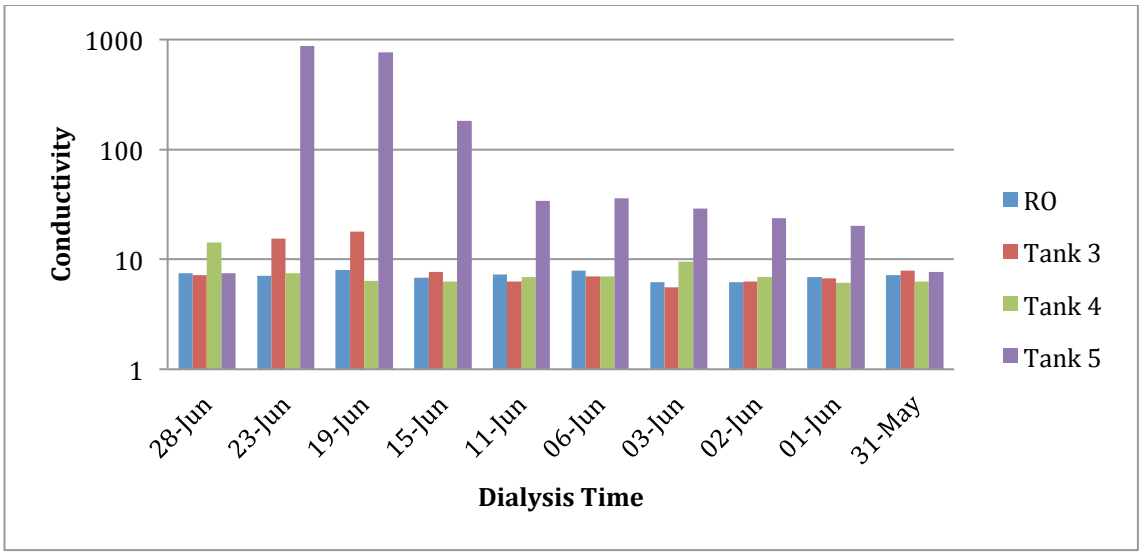

Figure 9.14: Conductivity variation over the time for samples placed in different tanks.

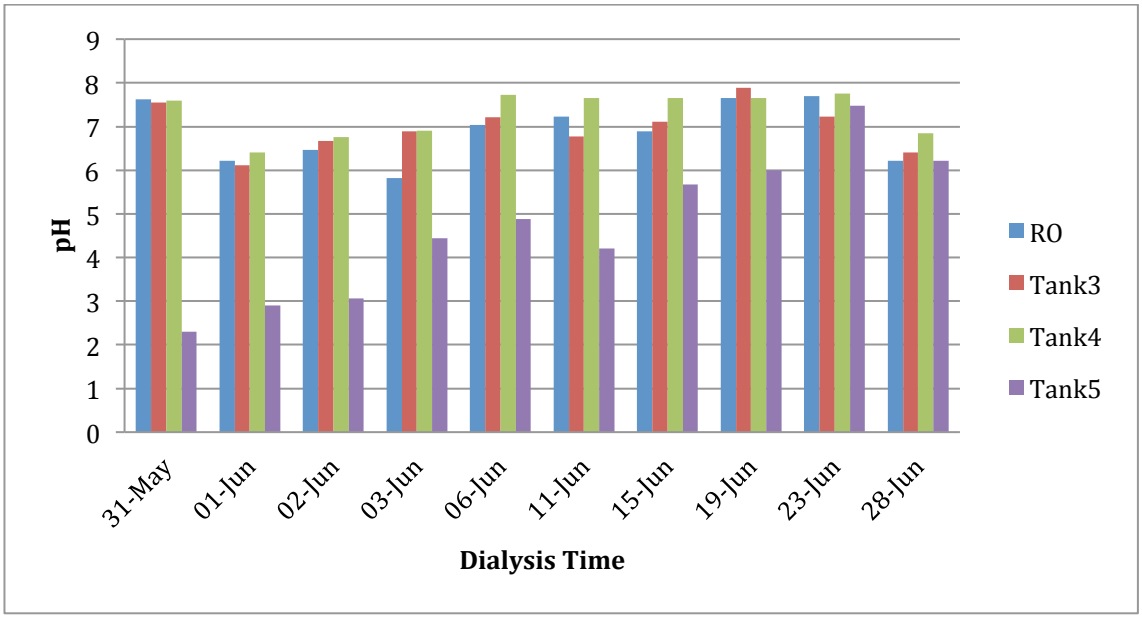

Figure 9.15: pH evolution over the time for samples placed in different tanks.

Tanks 3 & 4 did not vary to a significant degree in terms of conductivity (Fig. 9.15) of the reference point. However tank 5 did vary in conductivity quite considerably and this was reflected in pH variation (Fig. 9.14) in tank 5 over time.

The reason for the variation in conductivity and pH in tank 5 was related to the fact that in the first instance, all fresh batches of hydrolysed material were placed in tank 5 to remove the highest quantities of acid. The material was then moved to tank 4 and finally to tank 3 for final dialysis.

9.6 Problems with Reverse Osmosis (R.O.) dialysis: The impact of addition of counterions on the spinning of fibre.

9.6.1 Introduction.

After dialysis in R.O. water, a lack of coherence was observed in wet fibres during spinning due to a exessive surface charge (reflected as high zeta potential) on the nano-fibrils typically around -50 to -60mv. The phenomena led to lower viscosity gels and very low fibre cohesion during spinning. The low fibre cohesion prevented draw down of fibre during spinning. This problem didn't occur when nano-fibril suspensions were prepared using dialysis with tap water due to the introduction of counterions from the tap water during dialysis. The counterions reduced surface charge, but in an uncontrolled way, due to daily variation in the chemical composition of tap water. The result was large variation in the viscosity of gels produced for spinning. A study was carried out to investigate the introduction of counterions to mimick the counterions present in tap water. The objective was to add the counterions in a more controlled manner to avoid the variability in surface charge present in tap water and to determine the conditions required to produce a consistent (repeatable) gel from which it was possible to spin a coherent fibre that could be drawn down to smaller diameters.

9.6.2 Method

In the first instance NaOH was titrated into a suspension of cellulose nano-fibrils dialysed for 3 days against deionised water. NaOH was added until the pH reached neutrality as typically experienced with tap water. A larger sample of the cellulose

suspension was then treated at the same concentration with NaOH and concentrated using centrifugation in preparation for spinning.

It was found that centrifugation times to achieve high viscosities was lower than when no NaOH was added. This suggests that NaOH had an effect. However, although pH was considerably higher, Zeta potential changed very little and when spinning the concentrated gel, the fibre coherence improved only slightly compared with no treatment.

At this point it was decided to try three alternative counterions. The impact of $CaCl_2$, $BaCl_2$ and $MgCl_2$ at two different concentrations was investigated to determine which would have the biggest effect. It was found that the different counterions had similar effects on Zeta potential (Fig. 9.15) and so a decided was made to focus on $CaCl_2$. This choice was supported by an analysis of the tap water using ICP-MS and ICP-AES technique, which showed the predominant element to be calcium. A full analysis is attached as a separate PDF document in Appendix A.

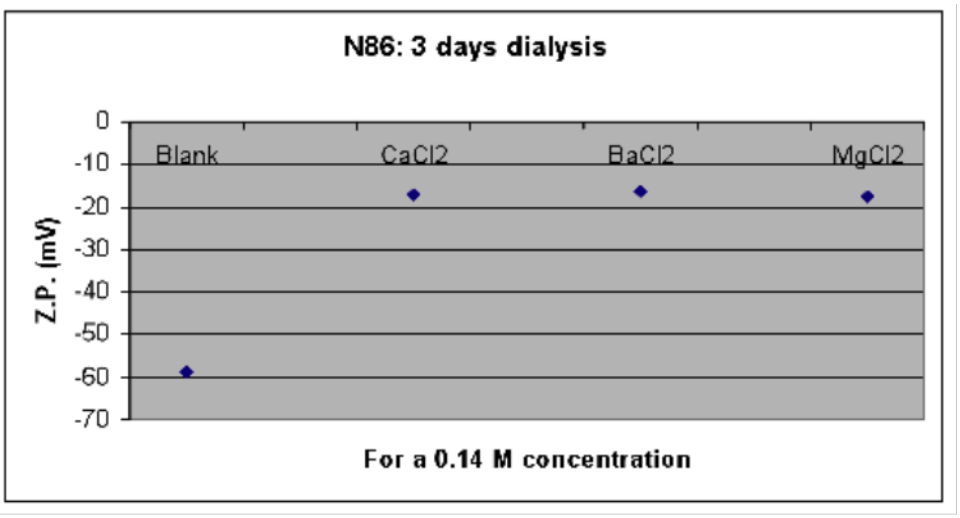

Figure 9.16: Impact of $CaCl_2$, $BaCl_2$ and $MgCl_2$ at 0.14M concentration.

9.6.3 Investigation of the impact of $CaCl_2$ addition on zeta potential

9.6.3.1 Methodology

A standardised method was developed in which a range of calcium chloride concentrations were added to small subsamples of a number of batches of cellulose

nano-fibril suspensions at 3% solids content immediately after 3 days dialysis. The suspensions were prepared from a standard sample of 92α grade pulp. Five zeta potential measurements were made on each subsample. Then a calcium chloride level was selected that resulted in an average zeta potential level close to targeted levels between -30 and -32mV. The larger batch of material from which the subsample was taken was then treated with the same level of calcium chloride. The larger batches were re-analysed for zeta potential (5 replicates) before concentrating under constant conditions for 28 hours in a centrifuge at 11 240 RCF. Zeta potential of the concentrated samples were then measured again immediately prior to spinning in the spin-line rheometer.

9.6.3.2 Results

Gels with an average zeta potential below -30mV were unusable due to problems with consistency of flow of the extrudate during spinning. Shear thickening thought to be due to cellulose nano-fibril aggregation was such a problem that it was not possible to spin a fibre for any significant period of time before flow was interrupted.

When the average zeta potential was above -34.5mV, the problem of fibre cohesiveness was observed, which prevented any application of tension or draw to the fibre.

9.6.3.3 Conclusions

A narrow window of between -30 to -34 mV was found to produce spinnable fibres. The results demonstrated the principle that addition of counterions directly to the cellulose suspensions was a workable solution.

10 FURTHER DEVELOPMENT OF THE FIBRE SPINNING PROCESS

10.1 Introduction

The spinning of a continuous fibre with the spin-line rheometer conceptually consisted of three phases.

Phase 1 involved threading of the extruded wet fibre onto a take up wheel. The extruding rate being the same as that of the take up wheel with no draw down of the fibre. The standard threading speed was 30m/min.

Phase 2 involved ramping up the speed of fibre extrusion and take up wheel until the required spinning speed was achieved. Theoretically, the higher shear and extensional forces associated with higher spinning speeds should lead to better alignment of the nano-fibrils and increased fibre strength. Once the fibre was spooling smoothly the fibre required drying. The dryer temperature had to be set at a level sufficient to ensure complete drying of the fibre as it exited the dryer. The drying temperature should theoretically be dependent upon the following key variables:

- Die/needle diameter;
- The spinning speed;
- Fibre diameter (dependent on die diameter and draw down ratio);
- Solids content of the gel.

Phase 3 involved maintaining the fibre extrusion rate at a constant level whilst ramping up the speed of the take up wheel until the required draw down ratio was achieved. The draw down was required to stretch the fibre to give maximum alignment of the nano-fibrils and to achieve the final diameter required.

10.2 Preliminary fibre spinning studies with a rheometer.

10.2.1 Hand pulled fibres

In initial work (before the development of a fibre drying protocol) the manufacture of fibres was limited to a hand drawing process. The extruded gels were drawn wet from a 240 micron needle at a spinning speed of 60 m/min and layed on a rack to air dry in short lengths of around 15 cm. The properties of the gel used for this study are recorded in Table 10.1. Electron micrographs (e.g. Fig. 10.1) indicated that the hand drawn-fibres provided some orientation to the fibrils but the chiral twist could still be seen (alignment was not visibly as good as those spun with the first prototype equipment due to zero draw down). In order to obtain some baseline strength data on these early fibres without draw, the spun fibres were sent to Cambridge University for strength testing, fibre tenacity and Initial modulus values are reported in Table 10.2.

Cellulose source	Whatman No4
Cellulose content	30.12%
Zeta Potential	- 31.2 mV
Size distribution of the nano-fibrils	120nm

Table 10.1: Gel properties from the hand pulled fibres.

Modulus	Tenacity	Linear Density
cN/tex	cN/tex	tex
1869	9	2.1
681	11	3.6
6565	**16**	**1.4**
1559	10	3.3
1155	22	3.7
1989	18	4.1
2303	**14**	**3.0**
586	6	3.5
4209	**44**	**3.4**
1448	11	3.6
1321	23	3.3
1241	10	3.3
1832	8	3.0
2419	26	2.9
1865	**18**	**3.3**

Table 10.2: Mechanical results from the fibre pulled by hand from the rheometer.

The results from Cambridge on these first fibres were variable. This was to be expected since the spinning process was not carried out under controlled conditions. In addition, SEM images (Fig. 10.1) indicated to a chiral twist in the nano-fibrils, which would lead to weakness in the fibre when the oriented nano-fibrils change direction.

The fibre values quoted in Table 10.2 show a range of strength properties in two separate fibre batches. The average Initial modulus values were 2303 cN/tex and 1865 cN/tex for the two batches. However it was interesting to note some of the higher individual values of 6565 and 4209 cN/tex. These values were close to the range of typical Kevlar fibres. Looking at tenacity, the average values were 14 and 18 cN/tex. As with Initial modulus, there were some interesting individual values as high as 44 cN/tex (for reference, viscose has a tenacity of 20 cN/tex and lyocell a tenacity of 40 cN/tex). With regards to % extension at failure these fibres exhibited around 0.1% strain,

indicating that they would not be suitable for conventional textiles being more closely related to that of high tenacity carbon fibre, which typically exhibits less than 1% strain to failure.

These first fibres showed some interesting fibre strength and stiffness potential.

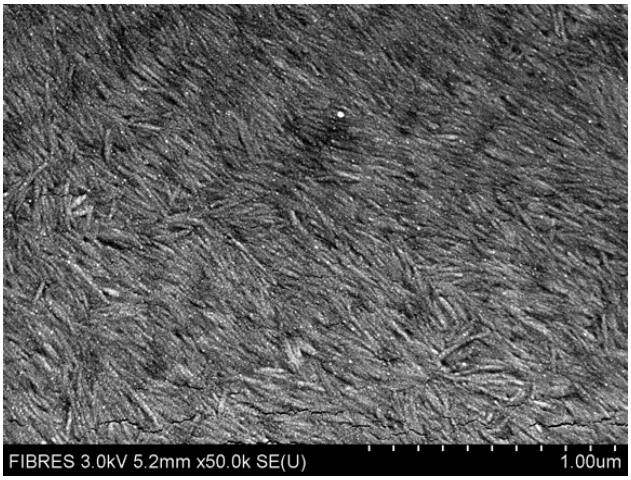

Figure 10.1: FEG-SEM photographs at 50 000x magnification where the chiral twist can be seen.

Having demonstrated that fibres could be produced from the rheometer with promising fibre characteristics at 60 m/min spinning speeds, the next step was to address some issues of gel consistency. A key challenge was to be able to spin fibre on a continuous basis without breakage. Unfortunately it was found that the gel exhibited regular breaks, which prevented the development of a fibre drying regime.

The trial was repeated several times with similar results. It was decided to evaluate the reasons for the breakage before progressing with further spinning.

The problem had two origins:

a. Some of the breaks were due to air pockets (it was possible to hear the bubble a burst under pressure). A single air bubble in the suspension will lead to fibre fracture and the spinning process would then have to be restarted from phase 1. A visual assessment was systematically done to check the removal of air pockets in the gel. It was apparent that there were microscopic air pockets, which required more centrifugation to be removed.

As a result, the degassing process was extended from 10 minutes at 17 000RCF to 20 minutes at 22 600 RCF using the new ultra speed centrifuge;

b. A more problematic issue was related to previously unobserved inconsistencies in the gel structure. It was thought that the problem was related to the way in which the gel was concentrated down using centrifugation. As part of this process a gradient of particle size and gel density should take place. The larger nano-fibrils fall out of suspension first and should be expected to become more densified over the duration of centrifugation compared to the top of the centrifuge tube. As a result when a gel was decanted into a syringe ready for injecting into the rheometer it was possible that there would be abrupt transitions between domains within the gel. It is highly probable that these transitions led to weak points, resulting in fibre fracture during spinning.

As a result of these concerns, the nano-fibril distribution within the gel (after it had been concentrated) was investigated. The results confirmed a gradient within the centrifuge tube meaning there was a requirement to look at mechanisms to mix the gel to remove abrupt transition points in the gel structure.

A mixing process with a spatula was tested but this was time consuming and potentially a source of variation. Different individuals may apply different levels of effort in a highly subjective process. In addition it was clear that this approach did not meet the need to effectively re-distribute the nano-fibril size range evenly throughout the gel at the micro-scale.

A number of mixing options were considered to resolve the problem. However, the most appropriate for the project needs was an Ekakt 3-roll mill. The 3-roll mill is a standard batch production machine (Fig. 10.2) commonly used to mix paints and pigments. It creates a high shear and tensile stress in material trying to flow between two rotating rollers. The material passes through a nip, and then experiences a second nip at a different flow rate. The nip distance can be set by the user. In this case the first nip was set at 15 microns and the second nip at 5 microns. (The smallest gap practical). As a gel is fed through the roll mill a 5 micron sheet of cellulose gel on the third roller

would then be scraped off with a knife and then re-passed through the roll mill until good distributive mixing has been achieved.

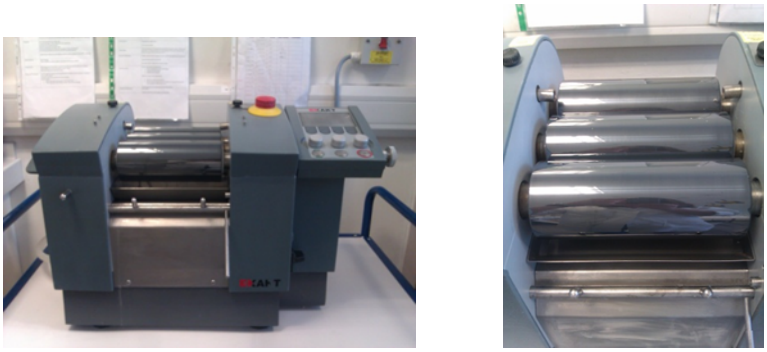

Figure 10.2: Ekakt three roll mill.

10.2.2 Gel mixing studies with the three roll mill

10.2.2.1 Initial study

Initial trials with a high viscosity cellulose nano-fibril gel into which a food die was injected appeared to give a very good distribution of the die though the gel after 10 cycles through the roll mill (Fig. 10.3).

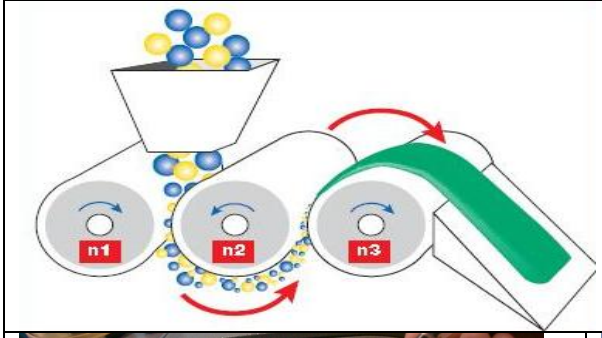

The flow is created by dragging the fluid through the nip.

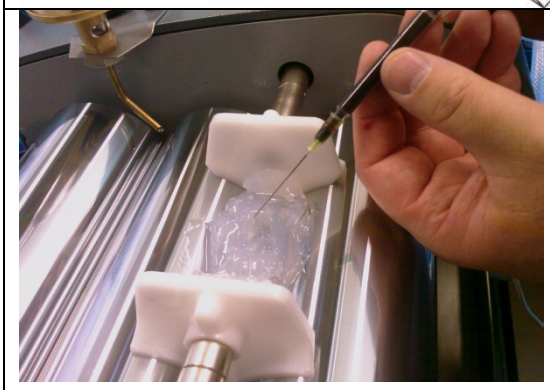

Some food dye was introduced into the sample while it was loaded into the feed area to give a visual (subjective) indication of the level of mixing achievable with the roll mill.

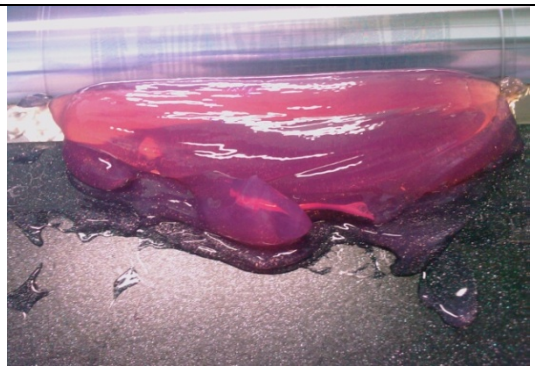

As the sample passed through the two rolls and onto the scraper, it was evident from the distribution of the food dye that a high degree of mixing had taken place. The fluid collecting on the scraper plate was put back into the feeding area for multiple passes. The final collected material was well distributed.

Figure 10.3: Distributive mixing through the addition of a small sample of food dye to the gel.

A further mixing trial (on a 30% solids content gel) and subsequent spinning study with the rheometer demonstrated a dramatic improvement in gel consistency and fibre flow. A decision was taken to incorporate this mixing procedure into the standardized fibre manufacturing process.

10.2.2.2 Assessment of roll mill repeatability

As part of the roll mill assessment process a more detailed study was carried out to assess the repeatability of mixing nano-cellulose gel using the Ekakt Three Roll Mill.

A 92α cellulose gel was passed through the three roll mill at a fixed roll pressure and nip gap of 10 µm. Samples of mixed gel were taken for solids content uniformity assessment after 10, 15, 20, 25, 30 and 35 cycles.

For the purpose of this study a batch of gel (Batch D1v5) was split into three equal samples. Each gel was loaded on the roll mill and processed for ten cycles. Any crystalline material formed at the edges was removed after each cycle. A sample was taken from the centre of the gel for solids content measurements. The solids content was measured three times and an average value and standard deviation recorded. Similar samples were then taken every subsequent 5 cycles until the end point was reached. No sample was taken for D1v5C at 35 cycles because the gel was very dry and sticking to the rollers. The average solids content values and standard deviations are shown in table 10.3. Figure 10.4 shows the same data in graph form.

10.2.2.3 Results

Sample ID	No. Cycles	Average % Solids content	Standard Deviation
D1v5 A	10	29.22	0.18
	15	30.50	0.13
	20	32.80	0.16
	25	34.64	0.18
	30	37.17	0.52
	35	40.76	0.39
D1v5 B	10	29.07	2.20
	15	29.77	0.25
	20	32.35	0.22
	25	35.07	0.18
	30	38.25	0.25
	35	43.07	0.23
D1v5 C	10	29.00	0.13
	15	31.20	0.08
	20	34.73	0.14
	25	38.49	0.24
	30	44.35	0.21

Table 10.3: Average of solid content and standard deviation for batch.

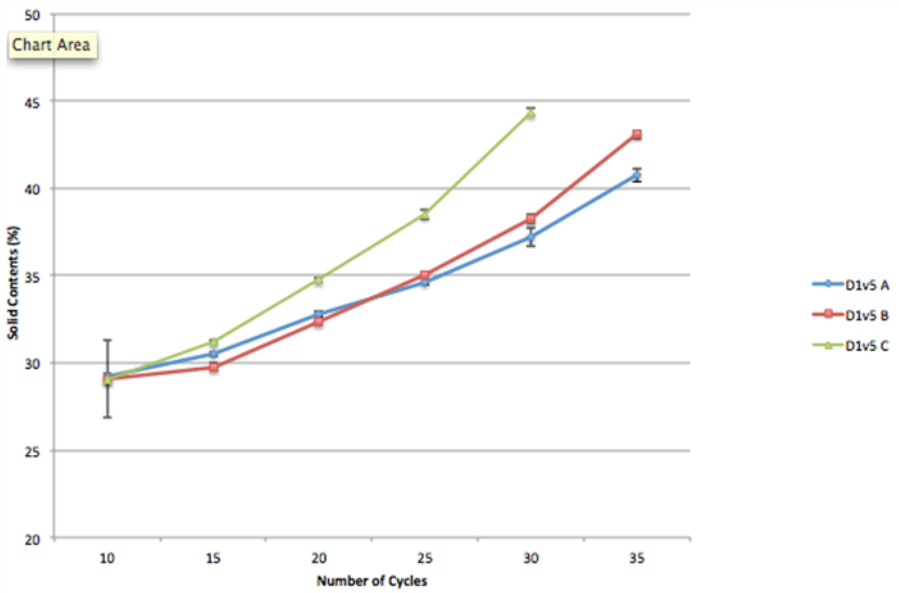

Figure 10.4: Average solid content per cycle. Error bars indicate standard deviation.

10.2.3 Discussions and conclusions

Variation in solids content dropped significantly between 10 and 15 cycles after which variation was very low and consistent. As the number of cycles increased the variation in solid content increased. It was concluded that the only reason to go beyond 15 cycles would be if a greater solids concentration was required as no further improvements in solids content consistencies would result.

10.3 Evaluating the impact of very high aspect ratio cellulose nano-fibrils on fibre spinning using bacterial cellulose.

10.3.1 Introduction

As part of the ongoing process to improve the fibre spinning process one important criteria to assess was the impact of aspect ratio on fibre spinning. The most effective way to do this was by changing the source of nano-fibrils. Bacterial cellulose was chosen for this study as it had one of the highest reported aspect ratios of any source of cellulose. For this reason bacterial cellulose should theoretically be capable of forming a very strong fibre if the nano-fibrils could be aligned in the fibre.

Bacterial cellulose preparations were centrifuged after hydrolysis (70% H_2SO_4 for 90 minutes at 46°C) as described in Section 3 and then dialysed for 4 weeks. Fibre spinning trials were carried out using a 90 micron needle with gels covering a range of solids content from 10% to 35% SC and zeta potential from -30 mV to -35mV.

10.3.2 Results

In all cases, irrespective of gel conditions, it was not possible to spin a fibre at anything other than very slow threading speeds of 15m/min. Above this speed, shear thickening was observed, presumably due to entanglement and aggregation of the nano-fibrils.

Figure 10.5 shows a close up of the very high aspect ratio of this form of cellulose at a low magnification (25K) and figure 10.6 shows the fractured surface of a fibre spun from these fibrils.

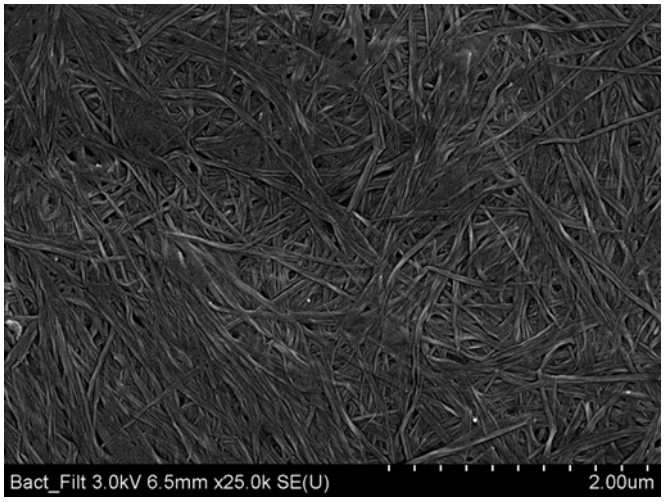

Figure 10.5: FEG-SEM image of bacterial cellulose on the surface of a spun fibre.

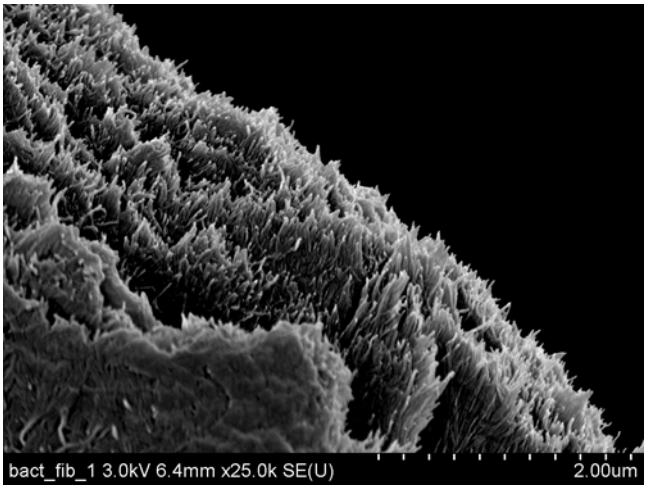

Figure 10.6: FEG-SEM image of a fracture surface of a bacterial based fibre.

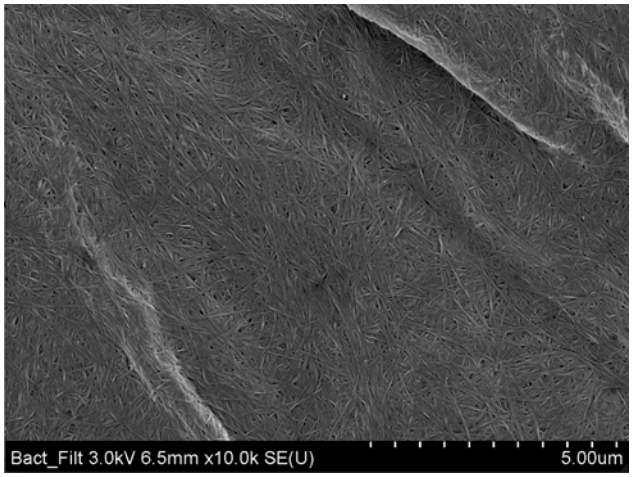

Figure 10.7: FEG-SEM image of the ramdom surface of a bacterial based fibre.

Figure 10.7 shows an image of a dried fibre surface spun from bacterial cellulose. The folded structure reflects the disrupted, random internal structure of the fibre showing lack of alignment. Preliminary strength data indicated that the fibres spun from bacteria cellulose were lower than with previously studied wood and cotton based nano-fibrils. Tenacity values were in the region of 5 cN/tex. This appeared to confirm the very poor alignment of the fibrils within the fibres.

10.3.3 Conclusions

It is suggested that the extremely high aspect ratio of bacterial cellulose nano-fibrils is a significant constraint in ensuring alignment. Fibril entanglement at anything other than very slow spinning speeds resulted in an effective “log jam” exiting the needle before

they have had chance to align. The poor alignment of the fibrils led to poor fibre strength and poor surface quality of the spun fibres.

It was concluded that the aspect ratio of bacterial cellulose was too high to spin a useable fibre with an aligned internal structure. This lack of alignment and flow blockage during spinning may be also due to the lack of rigidity of the fibrils. A rigid rod is as essential prerequisite for a stable liquid crystal suspension (Donald *et al.*, 2006). The study demonstrates the point that there is a balance between alignment and fibril length. Further studies are required to determine what the optimal fibril length might be for optimal spinning conditions.

10.4 The impact of zeta potential on gel shear viscosity

10.4.1 Introduction

Having demostrated that it was possible to add counterions to control zeta potential the next step was to determine an optimal viscosity for spinning of fibre that gave the best possible draw down. It has already been reported that zeta potential has an important impact on viscosity. The focus of work in this section was to determine the impact of zeta potential on viscosity more precisely. Shear viscosity was measured directly using the spinline rheometer. A series of fibre spinning trials with a range of gels with different zeta potential values were carried out, all gel samples were mixed for 20 cycles using a three roll mill. A number of different extrusion speeds were selected along with two different needle diameters, as the high viscosity gels were influenced by shear forces. As shear viscosity is shear dependent it is important to know the impact of zeta potential on viscosity at a constant shear rate.

It was previously reported (Section 9.6.3.2) that the range of zeta potential values that practically allow spinning was relatively narrow. However, for this work a broader range of values (including values outside the range that would normally be considered for spinning fibres) were looked at in order to determine the bigger picture impact of zeta potential on viscosity. The gels were prepared as described in Section 3.2.6 with zeta potential being determined by the addition of $CaCl_2$.

10.4.2 Results and discussions

Figure 10.7 shows the results of the first trial using a 140 micron needle with 3 gels with ZP values from -39 to -33.1mV. There was a clear increase in viscosity with decrease in zeta potential (ZP) at a constant shear rate of 28571 s^{-1}. Figure 10.8 includes the addition of further 3 gels which extended the ZP range down to -31.6mV and provided additional data within the range using 90 micron needle. The shear rate was approximately double that shown in figure 10.7. Again there was a clear relationship of increasing viscosity with decreasing ZP. However, the viscosity level at a specific ZP was notably lower, particularly at -38.3mV (dropped from 19 to 11 mPa.s) and -33.1mV (dropped from 25 to 14mPa.s). This data clearly highlights the shear thinning characteristic of the gels.

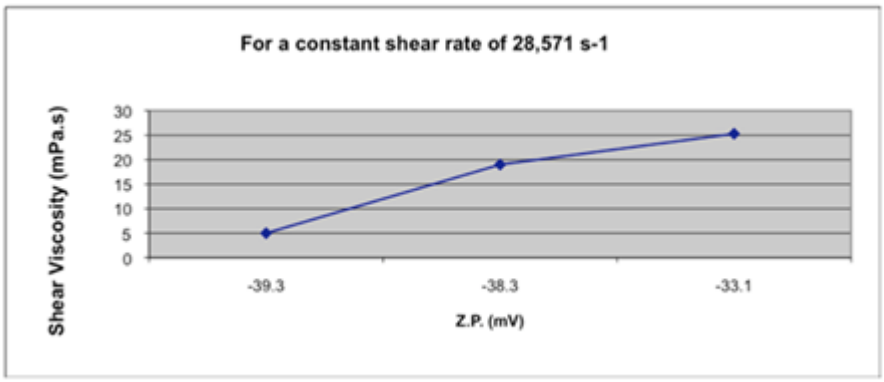

Figure 10.8: ZP vs. shear viscosity for a constant shear rate of 28,571 s^{-1} (140μm).

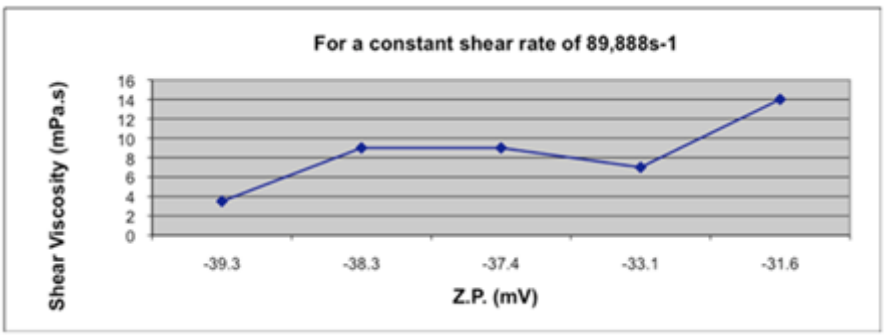

Figure 10.9: ZP vs. shear viscosity for a constant shear rate of 57,143 s^{-1} (90μm).

Figure 10.10 confirmed the general trend of increasing viscosity with decreasing ZP using a 45 micron needle. The smaller needle resulted in a further increase in shear rate and a further drop in viscosity at a specific ZP value.

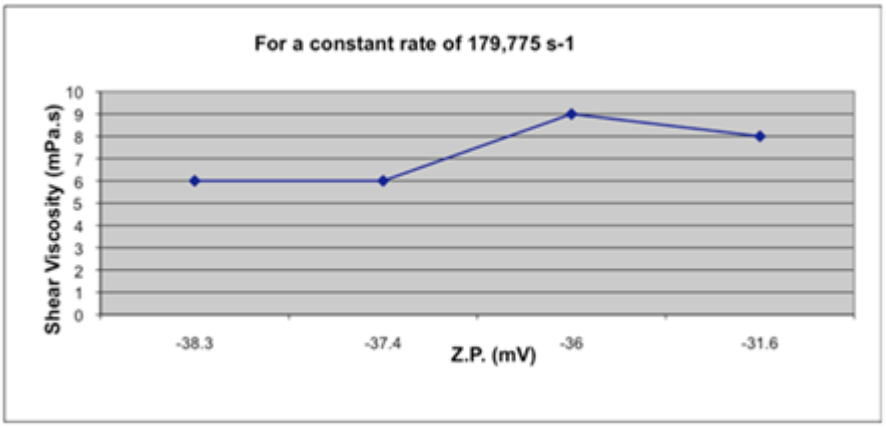

Figure 10.10: ZP vs. shear viscosity for a constant shear rate of 179,775 s^{-1} (45µm).

10.4.3 Conclusions

The results highlight the interaction between zeta potential, shear rate and viscosity. It is essential that ZP/viscosity relationship is quoted at a specific shear rate. On a number of occasions outside of this study shear thickening was observed. However this was usually a zeta potential levels below -30mV where floculation can take place. This data shows that within the range of conditions evaluated in this work i.e. zeta potential above -30mV the gels are shear thinning. With respect to fibre spinning it is preferrable to have shear thinning properties.

10.5 Determining the impact of drying temperature and extrusion speed on draw down

10.5.1 Introduction

As part of the ongoing establishment of a standard fibre spinning process a trial was conducted to determine the most appropiate fibre drying conditions. The objective was to determine the temperatures required to produce dry fibres at a range of draw down levels.

It was hypothesised that there should be an optimum temperature for maximising draw down under a standard set of conditions. If temperature is too high then the internal structure of a fibre could theoretically dry too quickly, limiting the amount of inter-fibril

slip and subsequent fibre draw down. The higher the draw down, the less energy required to dry the fibre.

10.5.2 Experimental work

The draw down studies involved the use of the standard protocols explained in Section 10.1. A 90 micron needle was used for spinning. The first step was to attain an extrusion speed of 60m/min with the take up wheel rotating at the same speed. Once this speed was reached, the take up wheel was increased over a 10 second period to a speed double that of the extrusion rate. The point at which the fibre broke was then recorded as a percentage value of the final speed of the take up wheel. In all cases, the draw down run was repeated 10 times so that average draw down values could be determined.

Temperatures for the fibre dryer were evaluated in the range from 470 to 530°C in 10 degree intervals (approx) as this was found to give completely dry fibres for the range of draw down values achieved. Below a temperature of 470°C incompleted fibre drying was observed at a spinning speed of 60m/min.

10.5.3 Results

Figure 10.12 indicates the impact of drying temperature on draw down (%). The results were generated on a single batch of material at a zeta potential of -32mV and a solids content of 30%. The graph shows how the average draw down gradually increased from 44% at 532^{o}C to 60% at 470^{o}C.

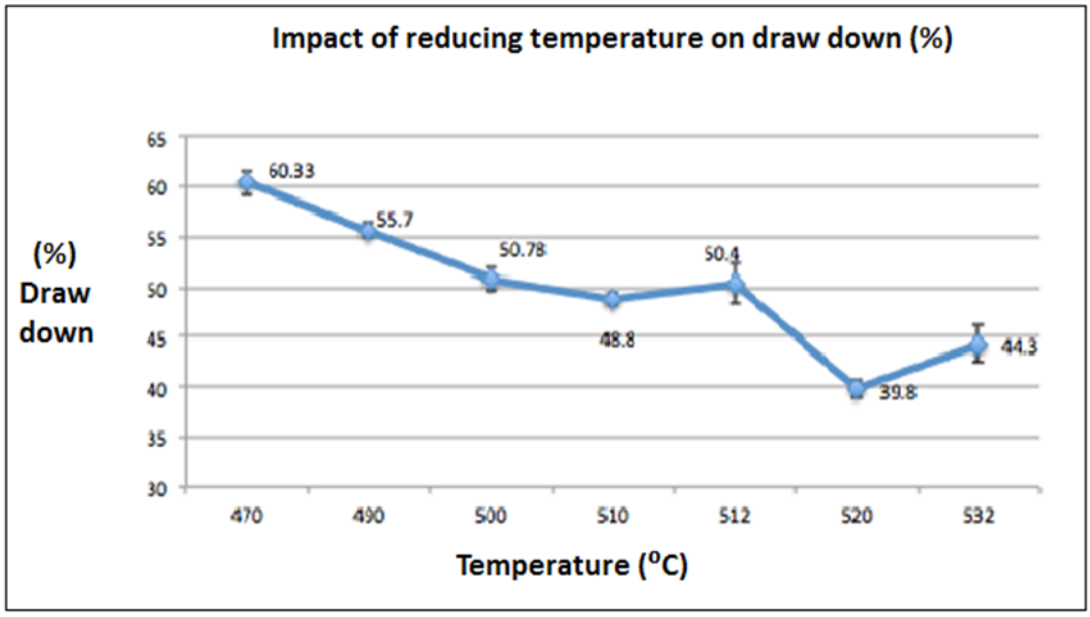

Figure 10.11: The impact of reducing temperature on increasing % fibre draw down. Error bars indicate standard deviation.

10.5.4 Conclusions

Data confirmed the hypothesis that better draw down should theoretically occur at lower drying temperatures. If the fibre dryer is too hot the structure of the fibre freezes, limiting the inter-fibril slip and subsequent fibre draw down. From this set up (90 micron needle and 60 m/min spinning speed) temperatures lower than 470°C didn't produce dry fibres.

10.6 Determining the impact of the extrusion speed on draw down

10.6.1 Introduction

It is known from SEM images that the nano-fibril structure within the fibre at the slow threading speed was chiral (twisted), with the nano-fibrils at an angle to the main fibre axis. It was hypothesized that at the slow feed speed, as the drying begins, the chirally twisted fibrils are drawn together shortening the fibre. As moisture loss progresses the fibrils, which are at an angle to the main fibre axis move closer together causing shrinkage in both, diameter and length. This will open up defects in the fibre leading to

fibre breakage more readily than if the fibrils were aligned parallel to the fibre where the fibres could more easily slip between each other.

The objective of this study was to investigate the impact of the extrusion speed on draw down. It has already been reported in Section 10.4 that the cellulose nano-fibril gels are shear thinning. This is thought to be due to the unwinding of chiral pitch (Fig. 10.13), the two models indicating different levels of pitch or twist. It is apparent that the greater the level of twist the more difficult this unwinding process and the more difficult it is for nano-fibrils to slide across one another and facilitate better draw down.

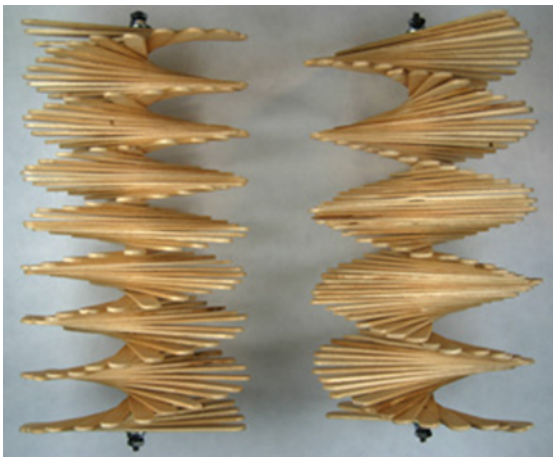

Figure 10.12: Models indicating the principle of chiral pitch. Short on the left and long on the right.

This section looked at the potential to improve draw down through better alignment of the fibres at higher extrusion rates. If the fibrils are aligned in the fibre direction, better mobility then theoretically facilitate slip between fibres and better draw down before fracture.

10.6.2 Experimental work and discussions

Trials were run with a standard 92α cellulose based gel at 40% solids after 4 weeks dialysis and 30 hours centrifugation at 20 000RCF.

A first trial looked at the base line drawdown that could be achieved. The work was started with % draw down measurements at a standard threading speed of 30m/min and a take up wheel speed to match, the fibre dryer was not switched on. Once the threading

process was stabilized the take up wheel speed was programmed to gradually increase to double that of the extrusion speed over a period of 5 minutes to ensure that there was no shock to the fibre. The trial was repeated three times. At 30m/min the fibre consistently broke when the wheel speed reach 5% of the final speed (31.5m/m). It should be noted that the fibre whilst being spun onto the take up wheel moved around the take up wheel due (it was thought) to the inherent nano-fibril twist within the fibre.

The second step involved a repeat of the first stage, of establishing a stable threading speed onto the take up wheel. Extrusion speed and take up speed were then ramped up at the same rate to 180m/minute over a period of 5 min to allow the nano-fibril structure time to respond to the higher spinning speed. It was noticeable that the fibre movement on the take up wheel was eliminated with the fibre being laid down very precisely over a footprint of less than 1 mm. The next stage involved repeating the draw down cycle in the first set of trials in which the take up wheel was programmed to increase to a speed of double that of the extrusion speed (360 m/minute) over 5 minutes. The trial was repeated three times. The difference in draw down was significant, with the fibre consistently breaking when the take up wheel reached 25% of the final speed.

The trial was repeated again by doubling the extrusion speed to 360m/minute and the results were the same as those at 180m/minute indicating that no further improvements in nano-fibril alignment occurred above 360m/minute.

10.6.3 Conclusions

The trial confirmed that the better alignment of nano-fibrils at higher extrusion speeds could give improved drawdown whilst the fibre is still wet.

One negative finding from spinning at anything above 60m/min was that the fibre drier set at its highest temperature of 540°C was only partially drying the fibre making it impossible to test the physical properties of these fibres. It was concluded that the only way to test higher extrusion rates (or higher shear rate in general) would be to spin fibre with a smaller diameter needle.

11 STUDY TO DETERMINE THE IMPACT OF KEY VARIABLES ON FIBRE DRAW DOWN AND END PRODUCT CHARACTERISTICS.

11.1 Introduction

In Section 10 a series of trials were carried out to support a better understanding of the range of factors that could impact on fibre spinning and end properties. The first of these assessed was drying temperature. For the purpose of this investigation, a drying temperature of 470°C was used as the standard, as this gave the best draw down whilst ensuring a dry fibre. The second factor analysed was extrusion rate. This was kept at 60m/min as significantly faster spinning speeds could not be dried with the fibre dryer available. Having established some fixed process variables, this section reports on a second more structured investigation to identify the conditions that would lead to best possible draw down of the fibre. The hypothesis was that as fibre diameter decreases, the number of defects per unit length of fibre will decrease leading to an overall increase in strength properties. It was also thought that higher levels of draw down of the fibre would lead to improved alignment of fibrils. This phenomenon is common in other fibres such as Lyocell. Figure 11.1 compares the uniform structure of a drawn lyocell fibre under crossed polars with an undrawn in which birefrigerent domains can be observed.

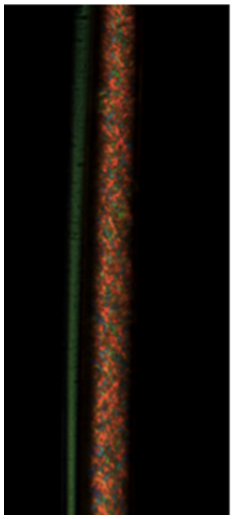

Figure 11.1: Shows on the right hand an undrawn Lyocell fibre where domains can be observed under crossed polars and on the left hand a drawn fibre, which is by contrast, uniform in structure. It is interesting to note that the granular domain like structure of the undrawn fibre is remarkably similar to that of the fibres prepared from cellulose nano-fibrils (see Fig. 11.11B)

It was noted in earlier work (Section 10) that the concentrated gels have low extensional viscosity compared to many precursor dopes such as that used in the production of lyocell. This made large draw down challenging to achieve.

All experimental work was carried out using a single batch of viscose grade 92 alpha cellulose as the raw material base. Gel preparation was the same as that described in section 5.2. The work took the form of two separate stages in the spinning process.

The objective of the first stage was to understand the conditions that would lead to smallest diameters (tex) without significant physical draw down, i.e. low levels of tension on the take up wheel. Preliminary observations indicated that fibre diameter varied substantially with conditions and this needed to be better understood. In principle it appeared logical to begin draw down on a fibre that was already the smallest diameter possible as a starting point.

The objective of the second stage was to determine the conditions that would allow the best draw down under tension (which may potentially have been different from stage 1). The draw down studies involved increasing the take up wheel from standard draw down speeds of 60m/min through to 120m/min over a period of 60 seconds. At the point of fibre breakage the trial was stopped, then repeated to produce three replicate runs per experimental condition. For each experimental condition 10 fibres per fibre batch were selected for testing.

The key variables selected for this study included zeta potential (which affects inter fibril repulsion and fibril mobility) and solid content. Solid content is to some degree affected by zeta potential and this impacts on solid content in the centrifuge. However, it was determined from earlier work that solid content can have an important impact on the rheology of the gel independent of zeta potential and for this reason it was considered as a separate variable.

11.2 Experimental design for 90 micron needle

A zeta potential and solid content range were selected based on what was thought to be the practical limits of spinning conditions. A zeta potential of -25mV was selected at the low end, as a stable colloid had not been previously observed below this level. At the high end a value of -36mV was selected. Previous results indicated that it was very difficult to spin a coherent fibre at a value higher than -34mV so a value of -36mV was seen as a realistic higher value.

It was not possible to carry out an investigation of all solid content/zeta potential combinations within the ranges selected (a full factorial design). The experimental design selected aimed for an even distribution of combinations across the two ranges in an approximation to a chessboard design (a partial factorial design). All the fibres were spun using a 90 micron needle. Once the fibres had been spun they were tested for tenacity, Initial modulus and extension to failure using a Favimat fibre tester at Edinburgh Napier University.

11.2.1 Results

The first point to note is that the original experimental design was difficult to follow precisely as the zeta potential was difficult to accurately target. The problem was related to the inherent in-stability of zeta potential in the preparation process described in Section 9.6.3. The preparation involved hydrolysis followed by four washing and centrifugation cycles and dialysis. After this the zeta potential was measured and modified by the addition of $CaCl_2$ to a target zeta potential, then centrifuged down to the targeted solids content. After concentration the gels were mixed using 20 cycles of the roll mill before centrifugation to remove air bubbles from the gel. The gel was then stored in the fridge from 24 to 72 hours. From the addition of $CaCl_2$ to the final gel, ready for spinning, the zeta potential varied to the extent that it was not possible to precisely target a specific zeta potential. As a result it was decide to take the approach of targeting an approximate zeta potential range and then run each gel through the spinning process. Immediately after spinning, zeta potential and solid content of the gel were measured and recorded. This approach meant that a fully balanced range of zeta potential values and solids content (that are partially dependent on zeta potential) was

not achieved. The unbalanced data set, put some limitations on our ability to carry out a robust statistical analysis. Figure 11.2 shows the actual zeta potential/solids content combinations that were produced. The figure also shows the average tex values per trial and standard deviations of the fibres that were subsequently tested. A third value (n) indicates the number of batches of ten fibres that were tested in each combination.

90 µm Needle AVG + S.D.	Zeta Potential												
Solid content	-24	-25	-26	-27	-28	-29	-30	-31	-32	-33	-34	-35	-36
38									Avg=2.57 S.D.= 0.2015 n=2	Avg= 2.93 S.D.= 0.1527 n= 2			
37									Avg=2.44 S.D.= 0.2498 n=2				
36					Avg= 2.25 S.D.= 0.4203 n=3		Avg=2.51 S.D.= 0.1443 n=2	Avg=3.7 S.D.= 0.1928 n=3					
35		Avg= 2.37 S.D.= 0.3785 n=2		Avg= 2.13 S.D.= 0.1632 n=3			Avg=2.45 S.D.= 0.2498 n=5						
34			Avg= 2.45 S.D.= 0.2121 n=2				Avg= 2.57 S.D.= 0.0957 n=4						
33							Avg=2.21 S.D.= 0.1121 n=3					Avg=2.41 S.D.= 0.2128 n=2	
32	Avg= 2.41 S.D.= 0.1792 n=2	Avg= 2.2 S.D.= 0.1341 n=2		Avg= 2.4 S.D.= 0.1414 n=2							Avg= 2.8 S.D.= 0.3618 n=4	Avg= 2.53 S.D.= 0.1527 n=2	
31		Avg= 2.13 S.D.= 0.2765 n=2	Avg= 2.1 S.D.= 0.2113 n=2			Avg= 2.18 S.D.= 0.1464 n=6	Avg= 2.16 S.D.= 0.2704 n=5	Avg=2.1 S.D.= 0.2213 n=3				Avg= 2.3 S.D.= 0.1414 n=2	
30			Avg= 2.1 S.D.= 0.1712 n=2			Avg=1.97 S.D.= 0.1532 n=2	Avg= 2.59 S.D.= 0.3984 n=6	Avg= 2.42 S.D.= 0.2787 n=2					
29			Avg= 1.8 S.D.= 0.2390 n=2	Avg= 2. 19 S.D.= 0.1872 n=3									Avg= 1.75 S.D.= 0.3209 n=2
28					Avg= 1.925 S.D.= 0.05 n=2	Avg= 2.03 S.D.= 0.0577 n=3		Avg=1.5 S.D.= 0.2612 n=2	Avg= 2 S.D.= 0.1414 n=2	Avg=1.9 S.D.= 0.2254 n=2	Avg= 2.3 S.D.= 0.2 n=3		
27					Avg= 1.4 S.D.= 0.121 n=3			Avg= 1.817 S.D.= 1.1941 n=3		Avg= 2.08 S.D.= 0.1923 n=3	Avg=1.4 S.D.= 0.2618 n=2		
26			Avg= 1.5 S.D.= 0.1383 n=2	Avg= 2.457 S.D.= 0.1521 n=2	Avg=1.34 S.D.= 0.098 n=2	Avg= 1.75 S.D.= 0.0707 n=2		Avg=1.8312 S.D.= 0.1182 n=2					
25			Avg= 1.67 S.D.= 0.0577 n=2	Avg= 2.65 S.D.= 0.1767 n=2	Avg=1.65 S.D.= 0.1543 n=2	Avg= 1.85 S.D.= 0.0707 n=2		Avg= 1.875 S.D.= 0.05 n=2	Avg= 1.5 S.D.= 0.1967 n=2				
24												Avg=1.3 S.D.= 0.2311 n=2	
23					Avg=1.9 S.D.= 0.1324 n=2				Avg= 1.8 S.D.= 0.1765 n=2		Avg= 1.25 S.D.= 0.2121 n=2		

Figure 11.2: The figure shows the average tex values and standard deviations of the fibres spun through a 90 micron needle for each zeta potential/solid content combination tested. n=the number of batches of fibres tested.

11.2.1.1 Tenacity and initial modulus

Figure 11.3 shows an overview of the mean values for the two most important fibre properties for all fibres tested. The graph indicates an increase in modulus with increasing tenacity with a reasonably good correlation between the two values (r=0.7). It is noticeable that the mean values were relatively low with highest tenacity values

around 13cN/tex and Initial modulus of 5000cN/tex. However the mean values don't tell the full story. Figure 11.4 shows the 1410 raw data points generated from this trial.

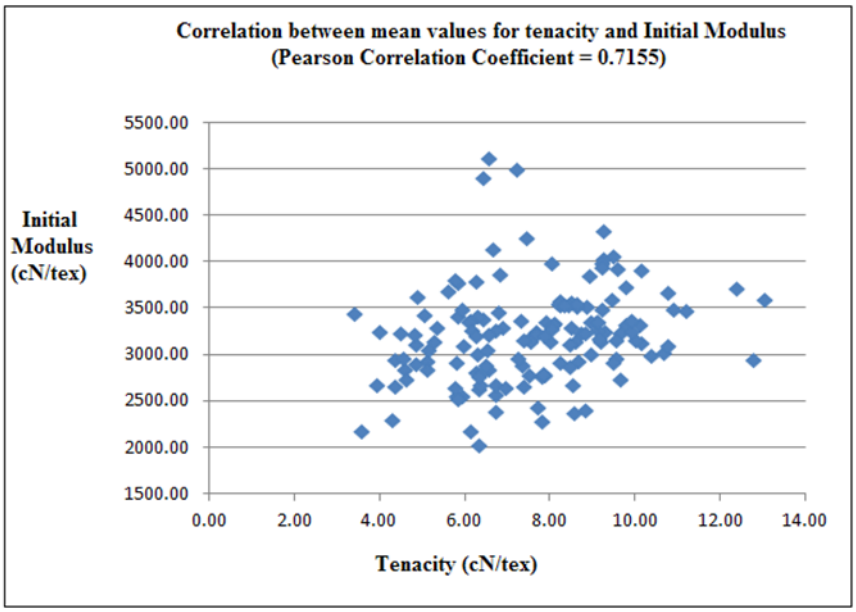

Figure 11.3: Shows the relationship between mean values (at least 10 replicates per data point) for tenacity and initial modulus of fibres produced from a viscose grade pulp (92 alpha cellulose from Saiccor).

Figure 11.4 reveals that within the average data from figure 11.3 there are some higher tenacity fibres with values reaching over 40cN/tex. It is also interesting to note that some of the Initial modulus values reached over 5000cN/tex, which is approaching the stiffness levels of carbon fibre.

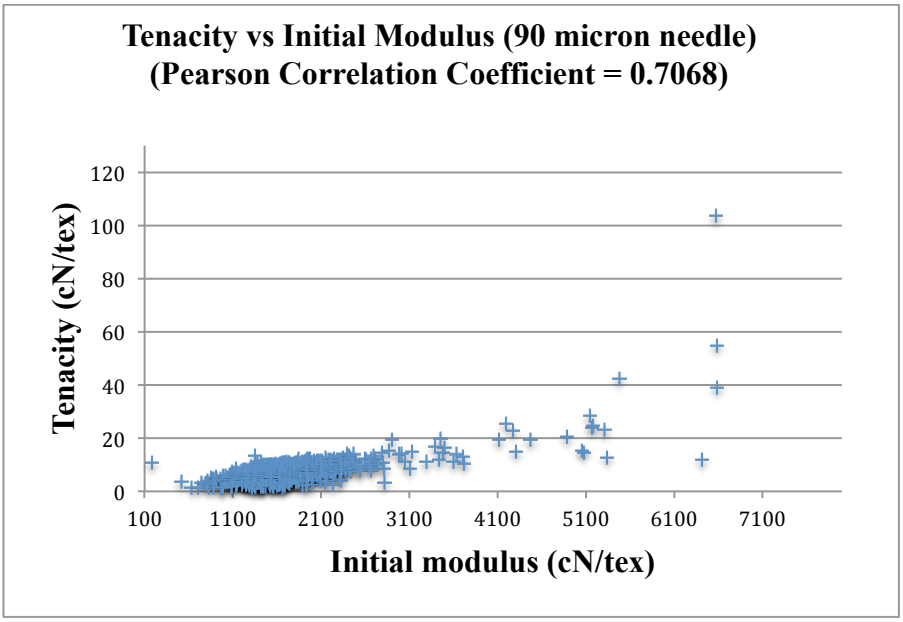

Figure 11.4: The relationship between tenacity and initial modulus (all data).

It is proposed that the higher values for tenacity and initial modulus are a result of some of the better draw down values that were obtained when trying to stretch the fibre. The wide variation in tex and subsequent physical properties is related to the way in which the fibres were manufactured in this study. From a starting point of very low tension, the take up wheel was ramped up at a rate of 1m/second until the fibre broke. During this drawing process the fibre decreased in diameter on a continuous basis as the take up wheel speed increased. The net result was only short lengths of fibre (of 5 to 6 cm.) of any one particular diameter. Inevitably only short lengths of fibre were formed at the very smallest tex values just before fibre breakage. The above explanation for only a small number of fibres at high draw down and high strength is supported by Figures 11.5 and 11.6, which show the correlation between linear density (g/Km) and tenacity and Initial modulus. The small amounts of low linear density fibre made the fibre production process at the smaller linear density values very difficult to validate through replication. A number of factors could contribute to fibre breakage; as a result it was difficult to draw accurate conclusions about what conditions led to the lowest tex (and highest strength) values. However the work does give some indication of what the strength potential might be if the draw down process could be improved. What is perhaps most important from these results is that it was possible to view general trends that influenced the fibre draw down process.

The data (Fig. 11.5) suggests that below linear density of around 1 Tex, the tenacity of the fibre starts to increase markedly. A similar trend is noted for initial modulus with tex (Fig. 11.6) which shows a very clear increase in initial modulus with decreasing tex from about 1.6 tex and lower.

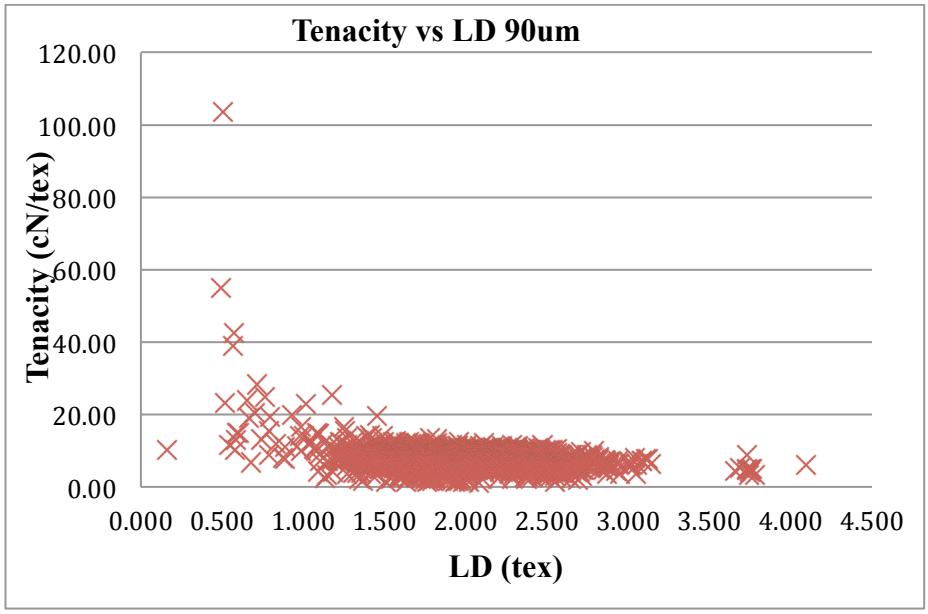

Figure 11.5: The relationship between tenacity and liner density (all data).

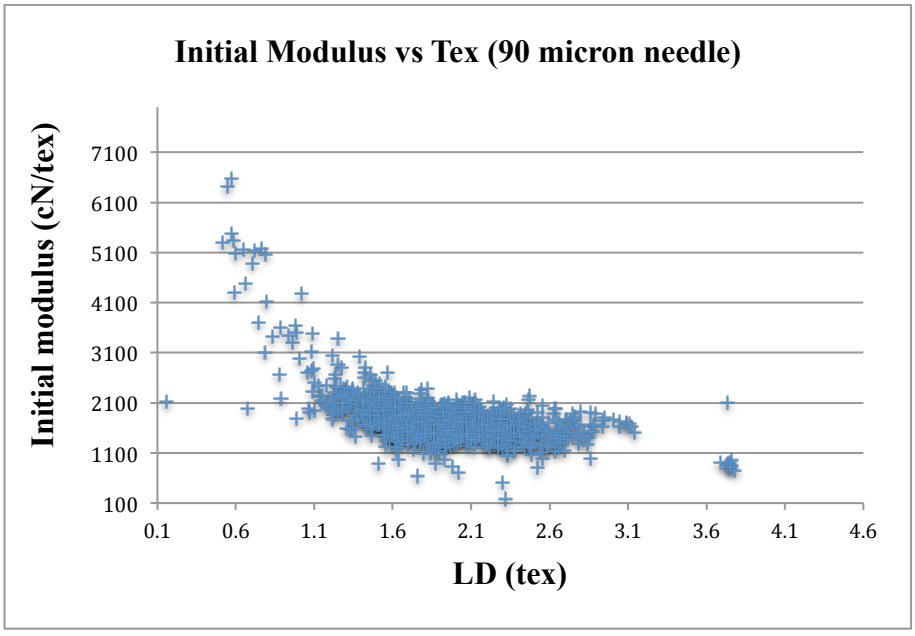

Figure 11.6: Graph showing the correlation between initial modulus and tex.

A multiple regression analysis (Table 11.1) indicates that decreasing linear density is the largest contributor to both, tenacity and initial modulus contributing almost 60% of

the total raw data. The second most important contributor was solid content (15% for tenacity and 14% for initial modulus). Zeta potential had a small (less than 2%) contribution to both fibre characteristics.

90 µm needle: Tenacity		**90 µm needle: Modulus**	
VARIABLES	**% Contribution**	**VARIABLES**	**% Contribution**
LD (tex)	59.4% (P<0.001)	LD (tex)	58% (P<0.001)
SC (%)	15% (P<0.001)	SC (%)	14% (P<0.001)
ZP (mV)	(P<0.003)	ZP (mV)	(P<0.006)
Total = 77%		Total = 73%	

Table 11.1: The contribution of variables to the tenacity and initial modulus of fibres spun from a 90 micron needle.

The data supports the hypothesis, that the lower diameter fibres with lower linear densities give higher strength. Further analysis (Fig. 11.7) indicates that solids content accounts for 74% of the variation in linear density. Lower solids content has a positive effect on lower linear density. Two factors can explain this; lower solids content means more water within the fibre which when removed during drying will lead to a smaller diameter as the starting diameter was fixed at 90 microns. However when moisture content volume was corrected for, the trend of decreasing linear density with decreasing solids content remained the same. The second factor contributing to lower linear density with decreasing solids content was thought to be the increased mobility of the fibrils. This should facilitate draw down. However there is a point at which lower solids becomes a constraint due to very poor wet fibre coherence. This means that no tension can be put on the fibre and it often breaks under its own weight at relatively short lengths. Fibre coherence is also affected by repulsive forces, which are driven by zeta potential.

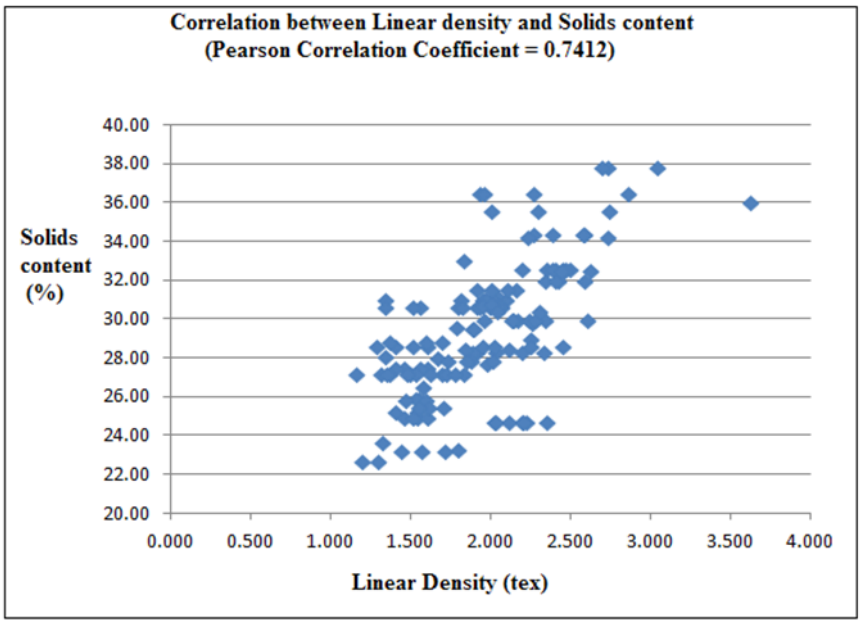

Figure 11.7: Correlation between linear density and solid content with a Pearson correlation coefficient of 0.7412).

Figure 11.8 provides a 3D graph representing the impact of both zeta potential and solids content on linear density after stage 2 of the spinning process i.e. before draw down. The highest linear density can be found at higher zeta potential and higher solids content. As discussed in the multiple regression analysis, as solids content decreased the linear density decreased to a level of around 2 tex. Zeta potential had a small impact with a lower zeta potential leading to a slight reduction in linear density.

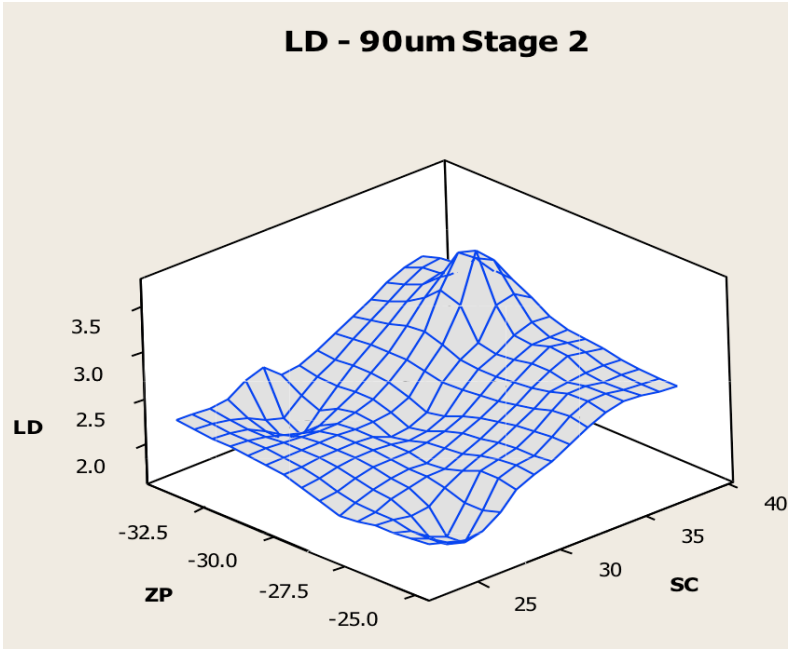

Figure 11.8: The relationship between linear density, zeta potential and solids content for fibres without draw down.

Figure 11.9 shows a 3D graph of impact of zeta potential and solid contents on linear density after stage 3 (draw down). The graph shows an overall decrease in linear density as draw down of the fibre was applied, with the largest fibres dropping from 3.5 to 2.5 tex. Overall the smallest diameter fibres in figure 11.8 around 2 tex dropped to below 1 tex after draw down. It was notable that the smallest fibres with draw down (Fig. 11.9) were at the higher end of the zeta potential range where an interesting phenomena was observed. For most of the fibres at the beginning of the draw down process the fibre was relatively taut as it was fed onto the take up wheel. However, at the lower solids contents and higher zeta potential, the fibre extended so that the take up wheel speed had to be increased significantly (between 30% to 70%) just to maintain a taut fibre. The hypothesis is that at this point of extension, the fibrils were beginning to align within the spinneret allowing more mobility of the fibres. As they shifted from an angle to the main axis, to parallel to the main axis, the fibre diameter should be expected to drop and extend in length proportionately. A key concern was that whilst the fibre extension trend was observed at high zeta potential and low solid content it was not completely predictable. Before further progress could be made with capillary die spinning, in reducing fibre diameter (using a 90 micron needle), this phenomena needs to be understood better. Proposals for this are discussing in section 12.

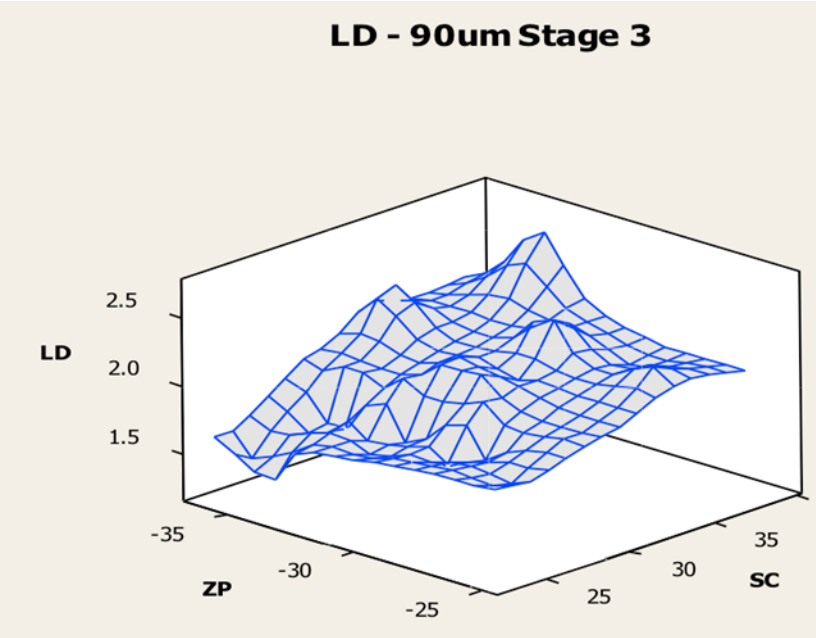

Figure 11.9: The relationship between linear density, zeta potential and solids content for draw down fibres.

11.2.1.2 Extension to failure

It was noted that the extension to failure of these fibres was low. Figure 11.10 shows mean values of up to 1.7%, these values are in line with high tenacity carbon fibre. Multiple regression analysis indicated that only one variable (tenacity) correlated with this value. The correlation with Tenacity was rather poor (r=0.5) due to the broadening of the spread of data as the two variables increase. However, figure 11.10 shows a trend, suggesting that as tenacity improves there is some improvement in extension to failure. Interestingly there was no correlation between Initial modulus and extension to failure.

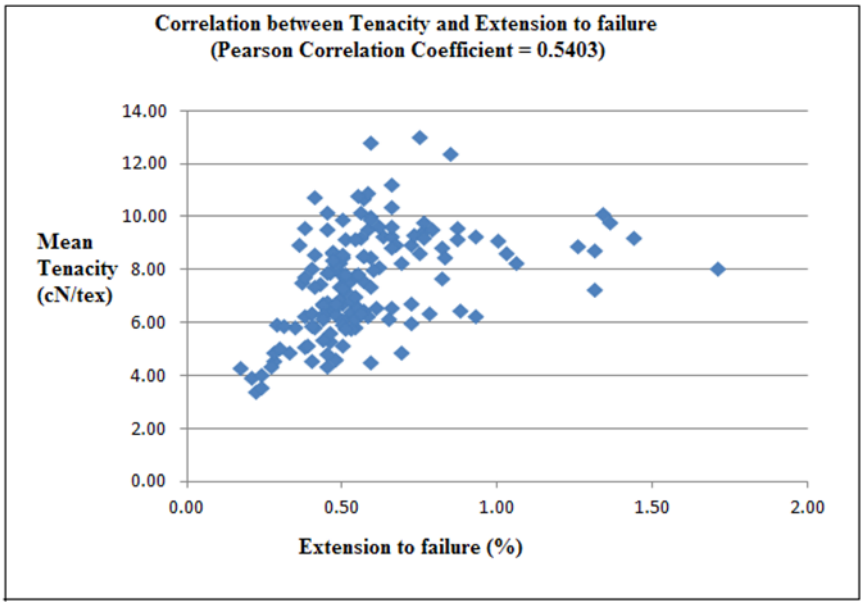

Figure 11.10: Extension to failure vs. tenacity.

11.3 Spinning from 45 micron needles

As part of the process of continuing to reduce the diameter of the fibre it was concluded that without a better understanding of what was causing alignment and draw down in the fibre it was difficult to make significant further progress with the 90 micron needle. The next approach was to try spinning with a 45 micron needle.

20 micron fibres were successfully produced from a 45 micron needle but not without challenges. Spinning from a 45 micron needle posed practical problems. The fibre was so light that it initially proved difficult to control, often floating upwards on the

thermals from the fibre drier (and not on the take up wheel). The problem was partially solved by drawing a vacuum below the take up wheel. This had the effect of overcoming any thermal effects or other airflow within the room that could disturb the fibre.

A second challenge when spinning from the 45 micron needle was of itself, quite revealing when compared to a 90 micron needle. In a number of cases the fibre was incoherent as it came out of the needle almost as a spray and when it was a coherent fibre it was only just stable and extended in the same way as observed with some of the fibres at low solids content and high zeta potential using the 90 micron needle. The explanation for this phenomena was thought to be the higher shear forces associated with the smaller diameter needle leading to better alignment and shear thinning to a point were in some cases the fibrils were incoherent. The hypothesis for better alignment was supported by the image shown of a 16 micron fibre under cross polarised light (Figure 10.11A), which shows banding typically associated with relaxation in lyotropic fibres such as Kevlar shown in Figure 2.6 in the literature review. The pleated structure suggests that the fibrils were aligned but subsequently partially relaxed into the pleated structure as the fibre dried. The pleated structure makes an interesting comparison with the typical domain like structure in 90 micron needle fibres as seen in Figure 10.11B when viewed through cross polarizers. This observation confirms the findings of Brecea *et al*. (1996) and Brecea and Navaral (2000) who observed that cellulose nano-fibril suspensions show fast inception and relaxation when compared to conventional liquid crystalline polymer solutions.

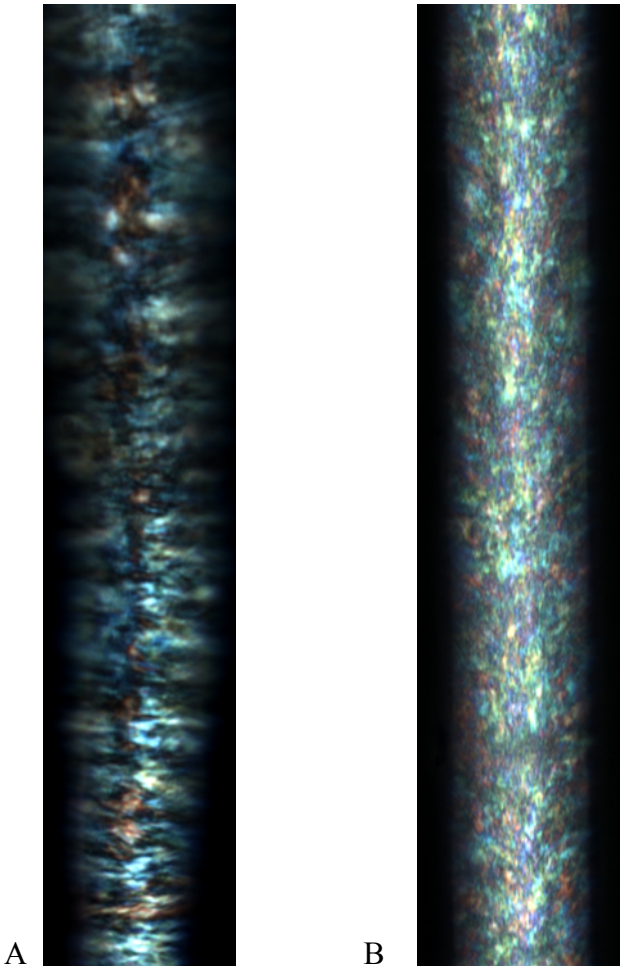

Figure 11.11: Shows the domain structure through the light microscope of A: a 16 micron fibre spun from a 45 micron needle. B*: a 50 micron fibre spun from a 90 micron needle.*

When these 16 micron fibres were tested they were found to be no stronger than the larger fibres with a tenacity in the range of 10cN/tex. At the time it was decided that these fibres were not particularly interesting because of the low strength. However, in hindsight it seems that if the fibre drier had been more efficient, it may have been possible to freeze the nematic structure, which should theoretically have resulted in a higher strength fibre.

11.3.1 Conclusions

Spinning from 45 micron needles produced higher shear and extensional stresses in smaller diameter dies. It appears that this resulted in better alignment of the fibrils and subsequent fibre extension. However because of subsequent partial relaxation of the fibril orientation before drying, fibre strength was still low. Proposals to address this in

future work could include heating gels to higher temperature to allow more rapid drying and/or better optimization of drying conditions to ensure drying before relaxation can take place.

11.4 Hyperbolic die (HD)

A third approach to improving fibre alignment involved the design and manufacture of a hyperbolic die that was used in spinning trials. Gao-yuan Chen *et al.*, 1992 reported that an optimal hyperbolic die is critical to ensuring the best possible draw down and alignment of the internal structure of a fibre.

11.4.1 Rheology studies

In order to design the hyperbolic die required to ensure maximum alignment of cellulose nano-fibrils, an evaluation of the rheological properties of the cellulose suspension was required. The basic properties measured included shear and extensional viscosity. Shear flow involves molecules (or domains) rotating and extensional flow involves molecules (or domains) stretching.

The capillary rheometer (Fig. 6.14) was used to measure the extensional and shear viscosity of a number of cellulose nano-fibrils based gels. This work was undertaken as a separate study that fell outside the remit of the PhD studies.

The data generated from this study was sent to a specialist external contractor (Dr. Rheology) for the design of the profile of the hyperbolic die. The die design was based upon a gel with a zeta potential of -30mV and 30% solids content.

11.4.2 HD manufacturing

The hyperbolic dies were produced by casting epoxy resin around a re-useable, tool steel core of the desired hyperbolic profile (Fig. 11.12A). The casting was carried out within a modified brass standpipe adaptor (Fig. 11.12B), which acted as a housing for

the die. This adaptor also allowed the finishing of the die exit with a 45° angle (Fig. 11.12C) on a standard engineering lathe and allowed convenient fitting of the assembly to spinning equipment. Once physically complete the epoxy die was chemically treated so that the surfaces exposed to the spun material were hydrophobic in nature.

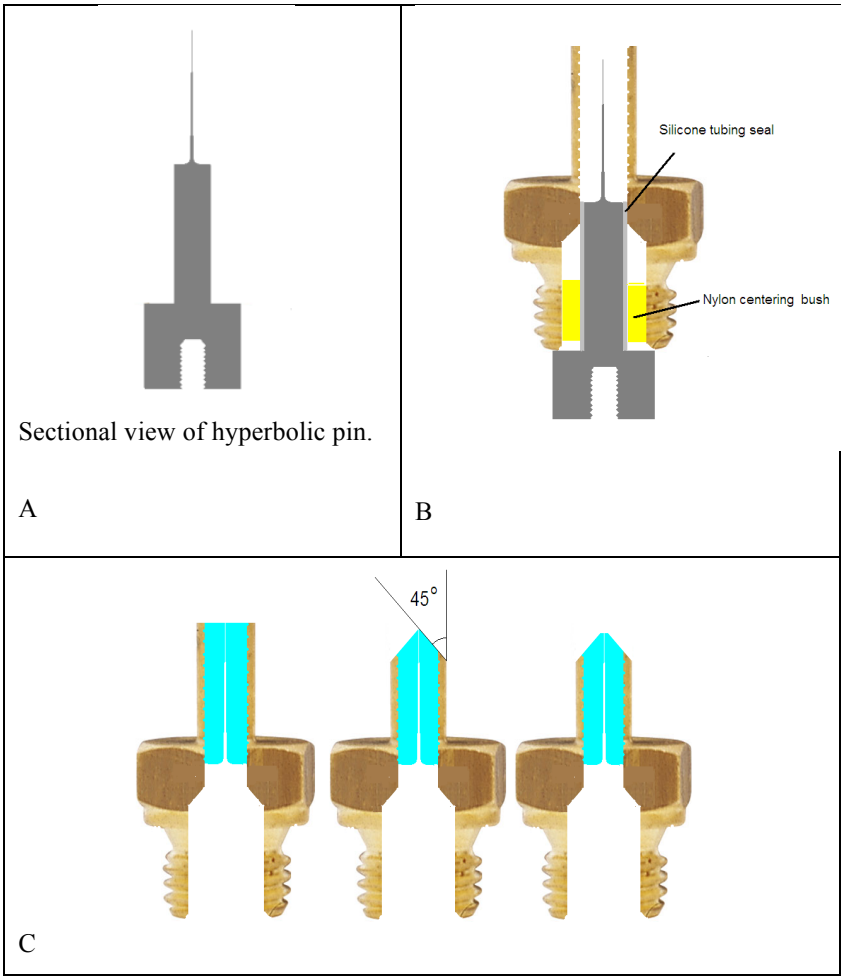

Figure 11.12: Various processes on the hyperbolic die manufacturing.

The hyperbolic pin was fitted with a custom made nylon centering bush and a silicone tubing seal (Fig. 11.12B), dipped in Buehler mould release fluid. The epoxy resin and hardener was dispensed into a centrifuge tube in equal volumes and mixed. The mixed resin was then centrifuged to remove any entrained air. The resin was cast into the pin/fitting assembly by carefully inserting the cannula over the hyperbolic pin and injecting the resin in a pulsed fashion so that the resin overflowed from the assembly. When the overflowing resin appeared to be air bubble free, the cannula was slowly withdrawn while still injecting resin, preventing any air being drawn into the assembly upon withdrawal of the cannula. The casting assembly was set aside at elevated

temperature (~ 55^{o}C) until the resin has cured sufficiently to feel glassy when tapped with a fingernail. The pin/seal/spacer was removed by means of the puller assembly and the revealed cast surface checked by microscopic inspection. The brass fitting was screwed into a custom holder and centered on an engineering lathe. The tip of the die was machined at high speed with no cutting lubricant to a 90^{o} point (Fig. 6.13C). The point of the tip of the die was ground/polished flat using very fine wet/dry abrasive paper on a metallurgical polishing wheel such that the die exit hole was within the flattened area. The die was placed on clean dry absorbent paper in a fume cupboard and a hydrophobic chemical (dichlorodimethylsilane) was injected into the exit hole of the die. The die was left overnight in a fume-cupboard before a final wash with distilled water and blow dried with compressed air. Figure 11.13 shows a cross section of one of the hyperbolic dies.

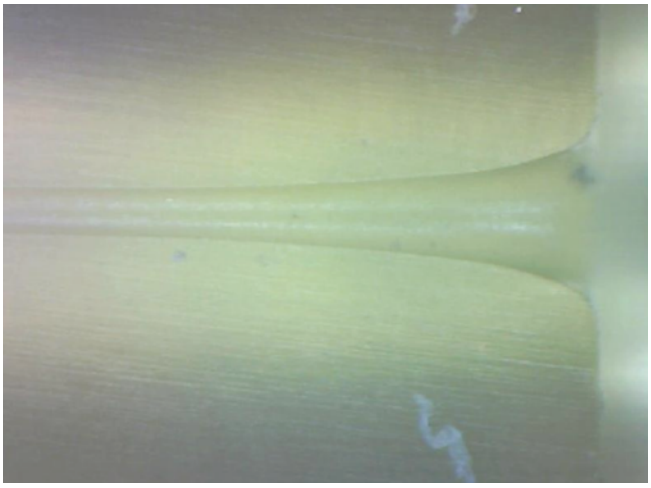

Figure 11.13: Cross section of one of the epoxy hyperbolic dies.

11.4.3 Experimental design for hyperbolic die studies

The objective of spinning with a hyperbolic die was to determine if it was possible to improve on the alignment, draw down and subsequent strength of the fibre compared with the 90 micron needle studies. The experimental design was similar to that with the 90 micron needle. The intention was to select a zeta potential around -26mV to -35mV. The solids content range was from 24% to 39%.

The spinning regime was carried out in the same way as with the 90 micron needle. 10 fibres per set of spinning conditions were tested for tenacity, Initial modulus and

extension to failure. Figure 11.14 shows the actual combinations of zeta potential and solids content selected.

Hyperbolic Die AVG + SD		Zeta Potential													
		-22	-23	-24	-25	-26	-27	-28	-29	-30	-31	-32	-33	-34	-35
	43									Avg= 3.06 SD=0.12 n=6					
	42														
	41														
	40														
	39										LD= 2.46 n=1				LD= 2.35 n=1
	38														
	37									Avg= 3.24 SD=0.11 n=2					
	36														
	35							Avg= 3.42 SD=0.84 n=3					LD= 3.59 n=1		
Solid content	34						Avg= 2.42 SD=0.75 n=3	Avg= 3.92 SD=0.48 n=3	NF		Avg= 2.68 SD=0.07 n=8	Avg= 3.28 SD= 0.66 n=10			
	33						LD= 3.08 n=1	LD= 2.12 n=1	Avg= 3.06 SD=0.36 n=2	Avg= 2.95 SD=0.45 n=2			Avg= 3.87 SD=0.88 n=2		
	32	Avg= 2.40 SD=0.45 n=2							NF						Avg= 2.40 SD=0.13 n=2
	31					Avg= 2.31 SD=0.10 n=2			Avg= 2.27 SD=0.03 n=2	Avg= 2.37 SD=0.25 n=4	Avg= 2.47 SD=0.14 n=3	Avg= 2.39 SD=0.16 n=2	Avg= 2.61 SD=0.12 n=2		Avg= 2.31 S.D.= 0.0986 n=2
	30								Avg= 2.29 SD=0.15 n=2	2.23	Avg= 1.62 SD=0.14 n=2				Avg= 2.45 S.D.= 0.0577 n=2
	29								NF	Avg= 2.25 SD=0.06 n=5					
	28							NF	NF	LD= 2.26 n=1					NF
	27							Avg= 2.31 SD=0.10 n=3	Avg= 1.61 S.D.= 0.4140 n=2						
	26						Avg= 1.79 SD=0.01 n=2		Avg=1.8 S.D. = 0.145 n=4						
	25			NF				Avg=2.3 SD=1.17 n=3		NF					
		-22	-23	-24	-25	-26	-27	-28	-29	-30	-31	-32	-33	-34	-35

Figure 11.14: The figure shows the average tex values and standard deviations of the fibres spun thought the hyperbolic die for each zeta potential/solid content combination tested.

11.4.4 Results

Figure 11.15 shows a trend of increasing tenacity with increasing Initial modulus for all fibres tested. The trend was the same as that for the fibres spun with a 90 micron needle.

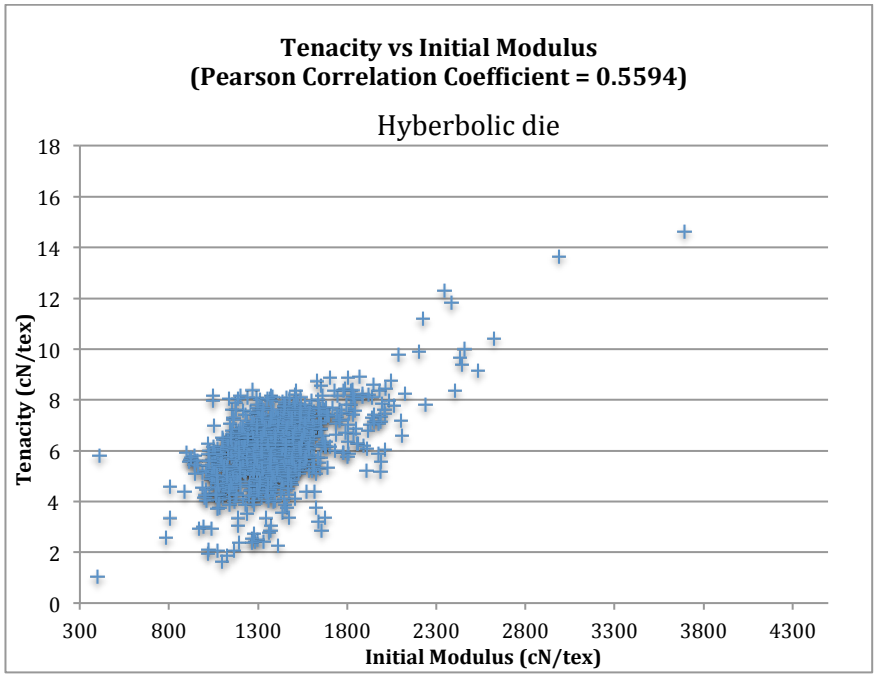

Figure 11.15: The figure shows the correlation between tenacity and Initial modulus for fibres spun with hyperbolic die.

Figure 11.16 shows the plot of linear density versus tenacity and it compares fibres spun using the hyperbolic die with those spun with the 90 micron needle. The two sets of data overlap. However, the fibres spun with the hyperbolic die do not reach as low a linear density or offer, some of the higher strength values associated with the lower linear density values. The lack of strength fibres spun from the hyperbolic die could be attributable to the design of the die.

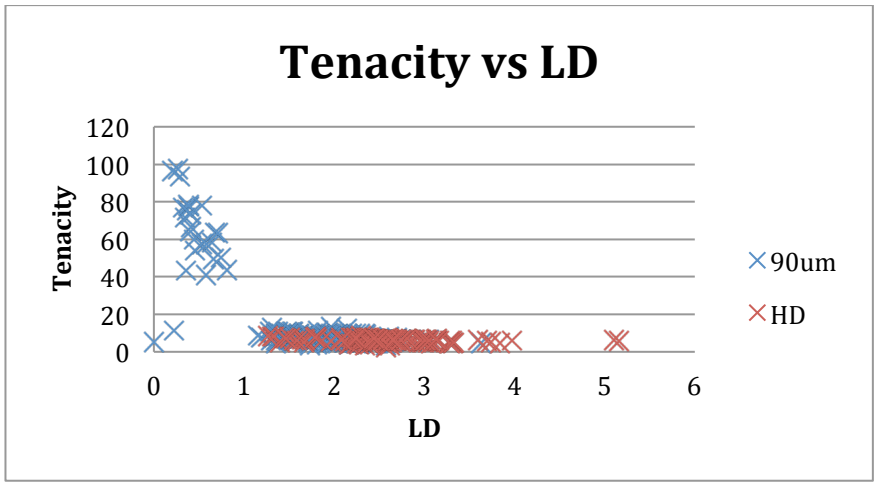

Figure 11.16: Tenacity vs. linear density for fibres spun from a 90 micron needle (blue) and from a hyperbolic die (red).

Figure 11.17 summarizes the mean values (error bars representing standard deviation) for tenacity for both the 90 micron needle and hyperbolic die. Table 11.2 summarizes data for both tenacity and Initial modulus. The lowest tex values are 0.8 for hyperbolic die fibres with a strength around 14cN/tex. The figure shows the lower linear density values for the 90 micron needle spun fibres. What is interesting to note is that there were no significant differences between the two types of fibres at a specific linear density suggesting that the hyperbolic die was not having a significant input on alignment. It is proposed that the lack of any significant effect could be attributable to design of the die, which was optimized for a gel with a solids content of 30% and a zeta potential of -30mV. In practice the gels that showed best propensity for draw down had a zeta potential of -33mV and a solids content of 27%. It seems possible that it was only under these specific conditions that the gels were able to respond to shear and alignment forces. It is may therefore be concluded that the die was not optimally designed for gels which gave the best draw down.

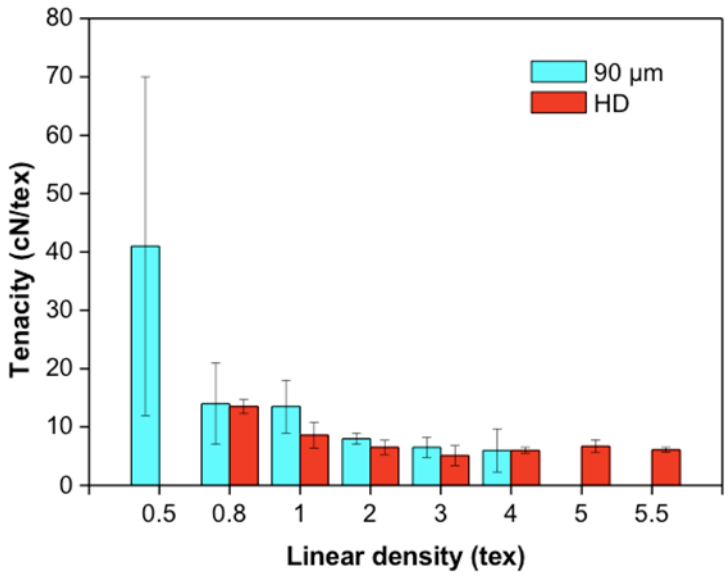

Figure 11.10: Tenacity vs. linear density for both, 90 micron needle and hyperbolic die.

	90 µm needle		H.D.	
LD (tex)	**Tencity (cN/tex)**	**Modulus (cN/tex)**	**Tencity (cN/tex)**	**Modulus (cN/tex)**
0.5	41 (29)	6041 (581)	---	---
0.8	14 (7)	3669 (1313)	13.5 (1.2)	3009 (674)
1	13.5 (4.5)	2848 (781)	8.6 (2.2)	2000 (495)
2	8 (1)	1541 (198)	6.5 (1.2)	1534 (229)
3	6.5 (1.7)	1666 (99)	5.1 (1.7)	1294 (80)
4	6 (3.7)	1228 (273)	6 (0.5)	1176 (47)
5	---	---	6.7 (1.1)	1200 (158)
5.5	---	---	6.1 (0.4)	1003 (140)

Table 11.2: Summarizes data for hyperbolic die and 90 micron needle for tenacity and Initial modulus.

Table 11.3 shows a summary of variables contributing to tenacity and Initial modulus for the hyperbolic die fibres. As previously, linear density and solids content were the significant contributors with zeta potential having a very small contribution.

What is more interesting is that the two multiple regression models only explain 15% and 31% of total variation for tenacity and Initial modulus. This is almost certainly explained by the narrow range of strength values compared with the 90 micron fibres. Zeta potential and solids content only started playing a significant role on linear density once linear density dropped below 2 tex. At the same time tenacity only starts to increase noticeable below 2 tex and only really begins to take off below 1 tex.

HD: Tenacity		HD: Modulus	
VARIABLES	% Contribution	VARIABLES	% Contribution
LD (tex)	P <0.003	LD (tex)	P <0.001
SC (%)	P<0.003	SC (%)	P <0.001
ZP (mV)	P <0.011	ZP (mV)	P <0.014
	Total = 15%		Total =31%

Table 11.3:The table shows the contribution of some variables to the tenacity and initial modulus of fibres spun from hyperbolic die.

11.5 Conclusions

Linear density plays a key role in fibre characteristics with smaller linear density values leading to higher strength and stiffness. It is thought that this is due to better interfibril alignment within the fibre at it is drawn to a smaller diameter. However, this trend only really starts to take effect below 1 tex for tenacity.

Lower solids content had the single biggest effect on linear density (even after correcting for moisture loss). The impact of solids content is related to the shear viscosity of the gels. As shear viscosity declines the fibril mobility goes up supporting better intra-fibril flow and better draw down.

There appeared to be a fine balance between fibril mobility and fibre coherence. If fibre mobility increased above a certain level then the gel didn't spin as a coherent fibre, being rather more analogous to a stream of water.

Fibril mobility can be influenced by the following:

- Solids content;
- Zeta potential;

- Shear force applied determined by extrusion rate (or spinning speed), as the gels are shear thinning. This can also be driven by die size (as seen with 45 micron needle) and design;
- The hyperbolic die design was not optimal for the lower viscosity fibres that were subsequently found to give better draw down. Once the optimal gel has been identified a new optimised hyperbolic die design should be considered;
- Under spinning conditions it is clear that insufficient shear force was applied to ensure alignment of the fibrils during spinning. This resulted in fibres in which the chiral nematic domains were clearly visible under cross polarized light;
- The gels manufactured in this study had inherently low extensional viscosity and as a result only allowed a limited amount of draw under tension from the take up wheel before failure. However when fibril mobility was higher (through low solids content and high zeta potential) the subsequent fibre extended by up to 70% in some cases without significant tension on the take up wheel;
- The limited amount of work on the impact of aspect ratio on the spinning properties of gels using bacterial cellulose highlighted a problem when fibrils are too long. Further work would be required with different sources of cellulose to determine if there is an optimum fibril length for fibre spinning.

More work is required to better understand the impact of fibril mobility on alignment if significant progress is to be made in achieving the draw down levels required to achieve the full strength potential of these fibres.

12 OVERALL CONCLUSIONS

The thesis describes a programme of work to develop a new approach to the spinning of a cellulose fibre. The results demonstrated that in principle it was possible to spin a continuous fibre from a chiral nematic suspension of cellulose nano-fibrils.

A set of hydrolysis conditions, initially based upon literature was developed as a standard preparation process for the extraction of cellulose nano-fibrils. The degree of sulphonation had an important impact on repulsive forces between the fibrils, which was reflected in the zeta potential of suspensions. Zeta potential had an important impact on solids content, viscosity and nano-fibrils mobility. A Zetasizer was important to characterize the particle size distribution and zeta potential of the cellulose nano-fibril gels.

In order to remove sulphuric acid from hydrolysed fibrils and to produce a gel with consistent properties, dialysis treatment of cellulose nano-fibrils after hydrolysis with deionised water was found to be essential. Addition of counterions was then required to control zeta potential of the subsequent gels.

A hypothesis was set that it may be possible to fractionate cellulose nano-fibril gels using the biphasic behaviour properties of the gels. In principle, this approach appeared plausible on a small scale. However, in practice phase separation on an industrial scale would take too long and proved impractical.

Concentrating gels after dialysis required centrifugation, which led to gradation of solids content and particle size. To produce a homogeneous gel a distributive and dispersive mixing process using a three roll mill was required for fibre spinning.

The strength and stiffness of some of the fibres showed interesting potential but did not reach the levels originally hoped for. This was thought to be primarily due to the fact that it was not possible to completely unwind the chiral twist in the suspension. The chiral nematic domains in spun fibres could clearly be seen under cross polarised light.

Only a narrow range of zeta potential values (-25 to -34mV) allowed practical spinning of fibres. Values below -25mV led to fibril flocculation whilst values above -34mV resulted in lack of fibre coherence making fibre draw down impossible.

Work has shown that in a stable suspension, cellulose nano-fibril based gels are shear thinning. This meant that fibril mobility and potential alignment could be improved through higher extrusion rate or using smaller diameter dies to increase shear and extensional forces. It appeared that there was a fine balance between factors increasing fibril mobility and being able to form a coherent gel that could be drawn into a small diameter fibre.

Spinning at higher shear levels using a 45 micron needle did give some indications that alignment was possible giving sufficient shear and extensional force. However the results also indicated that the relaxation time was very short and was partially relaxed before fibre drying could take place.

13 FUTURE WORK

Fibre drying temperature had a significant impact on draw down. In practice the results indicate that best draw down was at a temperature that was just sufficient to dry the fibre. This would suggest that in future work, efforts should focus on fibril alignment and maximum draw before the drying process is considered.

Linear density has a major role to play in fibre strength and stiffness. It was only in fibres below 1 tex that fibre strength began to increase significantly. Future work will have to focus on achieving tex values in the region of 0.1 tex (5-10 micron fibre diameters) if high performance fibres are to result. Results to date have indicated that the factor that had the biggest impact on linear density was solids content, which is indirectly related to viscosity or inter-fibril mobility. Future work will have to focus on how to maximize fibrils mobility whilst maintaining fibre coherence. This will require a careful balancing act. It is thought that the factors in this scenario will be:

- Level of sulphonation;
- Zeta potential;
- Shear and extensional force applied through extrusion speed and die design (geometry);
- Impact of addition of counterions;
- Gel temperature;
- Ionic concentration of the suspension.

Apart from studies to look at the impact of levels of sulphonation on fibril alignment under flow it is important to determine if the degree of sulphonation has an impact on inter fibril bonding.

As part of ongoing work it will also be important to build on the findings in Section 4, to explore the extent of variation in fibre size distribution amongst different sources of cellulose and determine which sources offer the best potential for the manufacture of fibre. It will be important to look at the impact of size distribution on both, ability to align under flow but also impact on relaxation times before drying. Longer fibrils are more problematic to align but they may also take longer to relax once aligned. Finding the balance may be an important factor in achieving nematic order in a dried fibre.

Longer fibrils should also theoretically have a positive impact on fibre strength. However, as demonstrated with bacterial cellulose, longer fibrils are of no benefit without alignment.

A comprehensive study of the relative impact of all the above factors on alignment of fibres under flow is recommended using birefringence as a mechanism to determine alignment of fibrils under spinning conditions in a transparent flow cell. Such a study would assist in identifying which variables to explore in more detail in ongoing fibre spinning experiments.

A further area of ongoing investigation should look at improving the efficiencies of fibre drying. There is evidence to suggest the relaxation time of aligned fibres is rapid. A system needs to be developed that can very rapidly dry the fibres as the emerge from the extrusion process.

REFERENCES

ABE, A. AND FLORY, P. J. (1978)
Statistical thermodynamics of mixtures of rod-like particles. 2. Ternary systems.
Macromolecules 11, 1122-1126.

ACIERNO, D. ; LA MANTIA, F. ; POLIZZOTTI, G. ; CIFERRI, A. AND VALENTI, B. (2009)

Ultrahigh modulus liquid crystalline polyesters. P-Hydroxybenzoic acid copolyesters.
Macromolecules 15, 1455-1460.

ANDRESEN, E. AND MITCHELL, G. (1998)
In situ X-ray scattering investigations of solutions of cellulose in N-methylmorpholine-N-oxide during shear flow.
Polymer 39, 712-7129.

APPAW, C. (2004)
Rheology and microstructure of cellulose acetate in mixed solvent systems.
PhD etd-01102005-140944
North Carolina State University.

ARAKI, J.; WADA, M.; KUGA, S. AND OKANO, T. (1998)
Flow properties of microcrystalline cellulose suspension prepared by acid treatment of native cellulose.
Colloids Surfaces A 142:75-82.

ARAKI, J.; WADA M.; KUGA S. AND OKANO T. (1999)
Influence of surface charge on viscosity behaviour of cellulose microcrystal suspension.
Journal of Wood Science 45(3), 258-261.

ARAKI, J.; WADA, M.; KUGA, S. AND OKANO, T. (2000)
Birefringent glassy phase of a cellulose micro-crystal suspension.
Langmuir 16(6), 2413-2415.

ARAKI, J. AND KUGA, S. (2001)
Effect of Trace Electrolyte on Liquid Crystal Type of Cellulose Microcrystals.
Langmuir (Letter), 17(15), 4493-4496.

ASAKURA, T.; UMEMURA, K.; NAKAZAWA, Y.; HIROSE, H.; HIGHAM, J. AND KNIGHT, D. (2007)
Some observations on the structure and function of the spinning apparatus in the silkworm Bombyx mori.
Biomacromolecules 8, 175-181.

ATALLA, R.H. (1999)
The structure of native celluloses, and the origin of their variability.
MIE Bioforum. 227, 1-13. Suzuka, Japan: UNI Publisher Co.

AZIZI SAMIR, M.; ALLOIN, F.; SANCHEZ, J.; KISSI, N. AND DUFRESNE, A. (2004)

Preparation of cellulose whiskers reinforced nanocomposites from an organic medium suspension.
Macromolecules 37, 1386-1393.

AZIZI SAMIR, M.A.S.; ALLOIN F. AND DUFRESNE, A. (2005)
Review of recent research into cellulosic whiskers, their properties and their application in nanocomposite field.
Biomacromolecules 6, 212-226.

BANG, Y.; LEE, S.; PARK, J. AND CHO, H. (1999)
Effect of coagulation conditions on fine structure of regenerated cellulosic films made from cellulose/N-methylmorpholine-N-oxide/H_2O systems.
J. Appl. Polym. Sci. 73, 2681-2690.

BARNES, H.; HUTTON, J. AND WALTERS, K. (1997)
An Introduction to Rheology. 5th impression. Elsevier, Amsterdam, Netherlands.
ISBN 0-444-87140-3.

BATCHELOR, G. (1970)
The stress system in a suspension of force-free particles.
J. Fluid Mech. 41, 545-570.

BATCHELOR, G. (1971)
The stress generated in a non-dilute suspension of elongated particles in pure straining motion.
J. Fluid Mech. 46, 813-829.

BATTISTA, O.A. AND COPPICK, S. (1947)
Hydrolysis of native versus regenerated cellulose structures.
Textile Research Journal 17, 419-422.

BATTISTA, O.A.; COPPICK, S.; HOWSMON, J.A,; MOREHEAD, F.F. AND SISSON, W.A. (1947)
Industrial and Engineering Chemistry 48, 333-335.

BATTISTA, O. A. (1950)
Hydrolysis and crystallization of cellulose.
Industrial and Engineering Chemistry 42(3), 502-507.

BATTISTA, O. A. (1955)
Level-off degree of polymerization. Relation to polyphase structure of cellulose fibers.
Ind. Eng. Chem. 48, 333-335.

BATTISTA, O. A.; COPPICK, S.; HOWSMON, J. A.; MOREHEAD, F. F. AND SISSON, W. A. (1956)
Level-off degree of polymerisation. Relation to polyphase structure of cellulose fibers.
Industrial and Engineering Chemistry 48(2), 333-335.

BATTISTA, O.A.; HILL, D AND SMITH P.A. (1961)
Level-off D.P. Cellulose Products. US Patent 2,978,446.

BATTISTA, O.A. (1975)
Journal of Polymer Science: Polymer Letters Edition.
Microcrystal polymer science, McGraw-Hill, New York, N.Y., 208.

BECK-CANDANEDO, S; ROMAN, M. AND GRAY D.G. (2005)
Effect of reaction conditions on the properties and behaviour of wood cellulose nanocrystal suspensions.
Biomacromolecules 6, 1048-1054.

BEL-BERGER, P., VON HOVEN, T., RAMASWAMY, G. N., KIMMEL, L. AND BOYLSTON, E. (1999)
Textile Technology: Cotton/Kenaf Fabrics: a Viable Natural Fabric.
Journal of Cotton Science, 3:60–70

BELLOMO, E.; DAVIDSON, P.; IMPEROR-CLERC, M. AND DEMING, T. (2004)
Aqueous cholesteric liquid crystals using uncharged rodlike polypeptides.
J. Amer. Chem. Soc. 126, 9101-9105.

BELTON, P.S.; TANNER, S.F.; CARTIER, N. AND CHANZY, H. (1989)
High-resolution solid-state carbon-13 nuclear magnetic resonance spectroscopy of tunicin, an animal cellulose.
Macromolecules 22(4); 1615-1617.

BERCEA, M.; NAVARD, P.; CAVAILLE, J. Y. AND ERNST, B. (1996)
Etude thermodynamique des suspensions aqueuses de whiskers cellulosiques.
Synthetic Polymer Journal III(1-2), 50-59.

BERCEA, M. AND NAVARD, P. (2000)
Shear dynamics of aqueous suspensions of cellulose whiskers.
Macromolecules 33(16), 6011-6016.

BRAZINSKY, I.; WILLIAMS, A. AND LANIEVE, H. (1975)
The dry spinning process: Comparison of theory with experiment.
Polymer Engineering and Science 15, 834-841.

BRENNER.F.C.; FRILETTE, V.; MARK, H. (1948)
Crystallinity of hydro-celluloses (Communications to the Editor).
J.Am.Chem.Soc. 70, 877.

BUINING, P.A, AND LEKKERKERKER, H.N.W. (1993)
Isotropic-nematic phase separation of a dispersion of organophillic boehmite rods.
J.Phys.Chem. 97, 11510-11516.

BUINING, P.A,; PHILIPSE A.P. AND LEKKERKERKER, H.N.W. (1994)
Phase Behavior of Aqueous Dispersions of Colloidal Boehmite Rods
Langmuir 10, 2106.

CALVET, E. AND HERMANS P. H. (2003)
Heat of crystallization of cellulose.
Journal of Polymer Science 6(1), 33-38.

CARRILLO, F.; COLOM, X.; SUÑOL, J. AND SAURINA, J. (2004)
Structural FTIR analysis and thermal characterisation of lyocell and viscose-type fibres.
Eur. Polym. J. 40, 2229-2234.

CHAE, D.; KIM, B. AND LEE, W. (2002)
Rheological characterization of cellulose solutions in N-methyl morpholine N-oxide monohydrate.
J. Appl. Polym. Sci. 86, 216-222.

CHAE, H. AND KUMAR, S. (2006)
Rigid-rod polymeric fibers.
J. Appl. Polym. Sci.100, 791-802.

CHAKRABORTY, A.; SAIN, M. AND KORTSCHOT, M. (2005)
Cellulose microfibrils: A novel method of preparation using high shear refining and cryocrushing.
Holzforschung 59(1), 102- 107.

CHANZY, H. AND DUBE, M. (1979)
Crystallisation of cellulose with N-methyl-morpholine n- oxide: a new method for texturing cellulose.
J. Poly. Sci. Lett. 17, 219.

COLLIER, J.; ROMANOSCHI, O. AND PETROVAN, S. (1998)
Elongational rheology of polymer melts and solutions.
J. Appl. Polym. Sci. 69, 2357-2367.

COLLIER, B.; DEVER, M.; PETROVAN, S.; COLLIER, J.; LI, Z. AND WEI, X. (2000A)
Rheology of lyocell solutions from different cellulose sources.
J. Polymers and Environ. 8, 151-154.

COLLIER, J.; NEGULESCU, I. AND COLLIER, B. (2000B)
Process for manufacturing cellulose microfibers. US Patent 6,153,136.

COLLIER, J.; NEGULESCU, I. AND COLLIER, B. (2003)
Cellulosic microfibers. US Patent 6,511,746.

COLLIER, J.; PETROVAN, S.; PATIL, P. AND COLLIER, B. (2005)
Elongational rheology of fiber forming polymers.
J. Mat. Sci., 40, 5133-5137.

COLLIOPOULOS, J. A.; DELL, S. M.; BULIGA, G. S. AND VENABLES, A. C. (1998)
Ultra-fine microcrystalline cellulose compositions and process for their manufacture, WO9856826

COULSEY, H. AND SMITH, S. (1996)
The formation and structure of a new cellulosic fibre.

Lenzinger Berichte 75, 51-61.

COWIE, J.; ARRIGHI, V.; CAMERON, J.; MCEWEN, I. AND MCEWEN, I. (2001)
Lyotropic liquid crystalline cellulose derivatives in blends and molecular composites.
Polymer 42, 9657-9663.
CRANSTON, E. AND GRAY, D. (2006)
Morphological and optical characterization of polyelectrolyte multilayers incorporating nanocrystalline cellulose.
Biomacromolecules 7, 2522-2530.

DALE, E.B. AND TSAO, G.T. (1982)
Crystallinity and heats of crystallization of cellulose: A microcalorimetric investigation.
J Applied Polymer Science 27, 1233-1241.

DAVÉ, V. AND GLASSER, W. (1992)
In: Viscoelasticity of Biomaterials. Glasser, W.G. and Hatakeyama, H. Eds. ACS Symposium Series 489, American Chemical Society, Washington DC, 144-165.

DAVÉ, V. AND GLASSER, W. (1993)
Cellulose-based fibers from liquid crystalline solutions. III Processing and morphology of cellulose and cellulose hexanoate esters.
J. App. Polym. Sci. 48, 683-699.

DAVIDSON, G. F. (1943)
The rate of change in the properties of cotton cellulose under the prolonged action of acids.
The Journal of the Textile Institute-Transactions 34, P. T87-T96

DE SOUZA LIMA, M.M AND BORSALI, R. (2002)

Static and Dynamic Light Scattering from Polyelectrolyte Microcrystal Cellulose.

Langmuir 18(4), 992-996.

DE SOUZA LIMA, M. M.; WONG, J. T.; PAILLET, M.; BORSALI, R. AND PECORA, R. (2003)
Translational and rotational dynamics of rodlike cellulose whiskers.
Langmuir 19(1), 24-29.

DE SOUZA LIMA, M. M.; BORSALI, R. (2002)
Rodlike cellulose microcrystals: Structure, properties, and applications,
Macromolecular Rapid Communications 25(7), P. 771-787

DINAND E.; CHANZY H. AND VIGNON R.M. (1999)
Suspensions of cellulose microfibrils from sugar beet pulp.
Food Hydrocolloids 13(9), 275-283.

DOBB, M., JOHNSON, D. AND SAVILLE, B. (1977)
Supramolecular structure of a high-modulus polyaromatic fiber (Kevlar 49).
J. Polym. Sci., Polym. Phys. Ed. 15, 2201-2211.

DOI, M. AND EDWARDS, J. (1986)

The Theory of Polymer Dynamics. Clarenden Press, Oxford UK.

DONALD, A.; WINDLE, A. AND HANNA, S. (2002)
Liquid Crystalline Polymers. 2nd edition, Cambridge University Press. ISBN 0-521-58001-3

DONALD, A.M.; ZHANG, S. AND TERENTJEV, E.M. (2005).

Nature of disclination cores in liquid crystals.

Liq Cryst 32, 69-75.

DONG, X. M.; KIMURA, T.; REVOL, J.F. AND GRAY, D.G. (1996)
Effects of ionic strength on the isotropic-chiral nematic phase transition of suspensions of cellulose crystallites.
Langmuir 12(8), 2076-2082.

DONG, X.M. AND GRAY, D.G. (1997)
Induced circular dichroism of isotropic and magnetically-oriented chiral nematic suspensions of cellulose crystallites.
Langmuir 13(11), 3029-3034.

DONG, X.M. AND GRAY, D.G. (1997)
Effect of counterions on ordered phase formation in suspensions of charged rod-like cellulose crystallites.
Langmuir 13(8), 2404-2409.

DONG, X.M.; REVOL, J.F. AND GRAY, D.G. (1998)
Effect of microcrystallite preparation conditions on the formation of colloid crystals of cellulose.
Cellulose 5(1), 19-32.

DUFRESNE, A.; CAVAILLE, J.Y. AND VIGNON, M.R. (1997)
Mechanical behaviour of sheets prepared from sugar beet cellulose microfibrils.
J. Appl Polym Sci 6, 1185-1194.

EBELING, T.; PAILLET, M.; BORSALI, R.; DIAT, O.; DUFRESNE, A.; CAVAILLE, J. Y. AND CHANZY, H. (1999)
Shear-induced orientation phenomena in suspensions of cellulose microcrystals, revealed by small angle X-ray scattering.
Langmuir 15(19), 6123-6126.

EDGAR, C. D. AND GRAY, D. G. (2001)
Induced circular dichroism of chiral nematic cellulose films.
Cellulose 8(1), 5-12.

EDGAR, C. D. AND GRAY, D. G. (2003)
Smooth model cellulose I surfaces from nanocrystal suspensions.
Cellulose 10(4), 299-306.

EICHHORN, S.J.; BAILLIE, C.A.; ZAFEIROPOULOS, N.; MWAIKAMBO, L.Y.; ANSELL, M.P.; DUFRESNE, A.; ENTWISTLE, K.M.; HERRERA-FRANCO, P.J.;

ESCAMILLA, G.C.; GROOM, L.; HUGHES, M.; HILL, C.; RIALS, T.G. AND WILD, P.M. (2001)
Review: Current international research into cellulosic fibres and composites.
Journal of material science. 36(9), 2107-2131.

FAVIER, V.; CHANZY, H. AND CAVAILLE, J.Y. (1995)
Polymer nanocomposites reinforced by cellulose whiskers.
Macromolecules 28(18), 6365-6367.

FENGEL, D.; WEGENER, G. (1984)
Journal of Polymer Science Part C: Polymer Letters
Wood - chemistry, ultrastructure, reactions, Walter de Gruyter, Berlin and New York, 1984, 613 pp

FLEMING, K.; GRAY, D.; PRASANNAN, S. AND MATTHEWS, S. (2000)
Cellulose crystallites: A new and robust liquid crystalline medium for the measurement of residual dipolar couplings.
Journal of the American Chemical Society 122(21), 5224-5225.

FLEMING, K.; GRAY, D. G. AND MATTHEWS, S. (2001)
Cellulose Crystallites.
Chemistry – A European J. 9, 214-218.

FLORY, P.J. (1956)
Statistical Thermodynamics of Semi-Flexible Chain Molecules.
Proc. R. Soc. London Ser. A 1956, 234, 7.3

GINDL, W. AND KECKES, J. (2006)
Strain hardening in regenerated cellulose fibres.
Composites Science and Technology, 66, 2049-2053.

GOPALAN NAIR, K. AND DUFRESNE, A. (2003a)
Crab shell chitin whisker reinforced natural rubber nanocomposites. 1. Processing and swelling behaviour.
Biomacromolecules 4(3), 657-665.

GOPALAN NAIR, K. AND DUFRESNE, A. (2003b)
Crab shell chitin whisker reinforced natural rubber nanocomposites. 2. Mechanical behavior.
Biomacromolecules 4(3), 666-674.

GOPALAN NAIR, K.; DUFRESNE, A.; GANDINI, A. AND BELGACEM, M. N. (2003)
Crab shell chitin whiskers reinforced natural rubber nanocomposites. 3. Effect of chemical modification of chitin whiskers.
Biomacromolecules 4(6), 1835-1842.

GOUSSE, C.; CHANZY, H.; EXCOFFIER, G.; SOUBEYRAND, L. AND FLEURY, E. (2002)
Stable suspensions of partially silylated cellulose whiskers dispersed in organic solvents.

Polymer 43(9), 2645-2651.

GRAY, D. (1993)
Liquid crystalline and mesomorphic polymers.
Shibaev, V, Lam, L. (Eds.), Springer, Berlin.

GRELET, E. AND FRADEN, S. (2003)
What is the origin of chirality in the cholesteric phase of virus suspensions?
Physical Review Letters 90, 19, 198302

HANLEY, S.J.; GIASSON, J.; REVOL, J.-F. AND GRAY, D.G. (1992)
Atomic force microscopy of cellulose microfibrils: comparison with transmission electron microscopy.
Polymer 33, 4639-4642

HANLEY, S.J.; REVOL, J.-F.; GODBOUT, L. AND GRAY, D.G. (1997)
Atomic force microscopy and transmission electron microscopy of cellulose from Micrasterias denticulate; evidence for a chiral helical microfibril twist.
Cellulose, 4, 209-220.

HERMANS, P.H. AND WEIDINGER, A. (1949)
Changes in crystallinity upon heterogeneous acid hydrolysis of cellulose fibres.
J.Polymer Sci., 4, 317-22.

HERMANS, P.H. (1951)
X-ray investigations on the crystallinity of cellulose.
Makromol. Chem. 6, 25-29.

HERMANS, J. (1963)
Reflections On Theories Of Polymer Solutions.
J. Polymer Sci., Part C:Polym. Symp, 2, 129-144.

HERRICK, F.W.; CASEBEIR, R.L.; HAMILTON, J.K. AND SANDBERG, K.R. (1983)
J. Appl.Polymer Sci.: Appl. Polymer Symp. 37, 797-813.

HERRICK, F.W. (1984)
Process for preparing microfibrillated cellulose.
US Patent 4,481,077.

HEUX, L.; CHAUVE, G. AND BONINI, C. (2000)
Non-flocculating and chiral-nematic self-ordering of cellulose microcrystals suspensions in nonpolar solvents.
Langmuir 16(21), 8210-8212

HEUX, L.; D'URIAGE, S-M. AND BONINI, C. (2005)
Microfibrillated and/or microcrystalline dispersion, in particular of cellulose, in an organic solvent.
US Patent 6,967,027 B1

HON, D. N.-S. AND SHIRAISHI, N. (Eds.) (2001)
Wood and Cellulosic Chemistry 2nd Ed. New York and Basel: Marcel Dekker, 914.

HONGLADAROM, K.; UGAZ, V.; CINADER, D.; BURGHARDT, W.; QUINTANA, J.; HSIAO, B.; DADMUN, M.; HAMILTON, W. AND BUTLER, P. (1996)
Macromolecules 29, 5346-5355.

HOWSMOON, J.A. (1949)
Water sorption and the poly-phase structure of cellulose fibres.
Textile Research J. 19,152-62

IMAI, T.; BOISSET, C.; SAMEJIMA, M.; IGARASHI, K. AND SUGIYAMA, J. (1998)
Unidirectional processive action of cellobiohydrolase Cel7A on Valonia cellulose microcrystals.
FEBS Letters 432(3), 113-116.

INGERSOL, H.G. (1946)
Fine structure of viscose rayon.
J.Applied Phys., 17(11), 924-39.

JANARDHNAN, S AND SAIN, M.M. (2006)
Isolation of cellulose microfibrils – an enzymatic approach.
BioResources 1(2), 176-188.

JOHANSSON, B.; WIKBERG, M.; EK, R. AND ALDERBORN, G. (1995)
Compression behaviour and compactability of microcrystalline cellulose pellets in relationship to their pore structure and mechanical properties.
Int. J. Pharm. 117, 57–73.

JONES, M. AND MARTIN, D. (1995)
Molecular stress and strain in an oriented extended chain polymer of finite molecular length.
Macromolecules 28, 6161-6174.

KEATES, P., MITCHELL, G., PEUVREL-DISDIER, E. AND NAVARD, P. (1996)
Time-resolved in situ X-ray scattering studies of aqueous hydroxypropylcellulose solutions.
Polymer 37, 893-901.

KIM, N.H.; HERTH, W.; VUONG, R. AND CHANZY, H. (1996)
The cellulose system in the cell wall of Micrasterias.
Journal of Structural Biology 117(3), 195-203.

KIM, D.; LEE, W.; JO, S.; LEE, Y. AND KIM, B. (2002)
Physical properties of lyocell fibers spun from different solution-dope phases.
J. Appl. Polym. Sci. 83, 981-989.

KIM, D.; PAK, J.; JO, S. AND LEE, W (2005)
Dry jet-wet spinning of cellulose/N-methylmorpholine N-oxide hydrate solutions and physical properties of lyocell fibers.
Textile Research Journal 75, 331.

KIMURA, F.; KIMURA, T.; TAMURA, M.; HIRAI, A.; IKUNO, M. AND HORII, F. (2005)
Magnetic alignment of the chiral nematic phase of a cellulose microfibril suspension.
Langmuir 21, 2034-2037.

KONDO, T.; NOJIRI, M.; HISHIKAWA, Y.; TOGAWA, E.; ROMANOVICZ, D. AND BROWN, R. (2002)
Biodirected epitaxial nanodeposition of polymers on oriented macromolecular templates.
Proc. Natl. Acad. Sci. USA 99, 14008-14013.

KONDO, T.; KASIA, W. AND BROWN, R. (2004)
Formation of nematic ordered cellulose and chitin.
Cellulose 11, 463-474.

KRÄSSIG, H. A. (1996)
Cellulose. Structure, Accessibility and Reactivity
2nd Ed. In: Polymer Monographs, 11. Yverdon, Switzerland: Gordon and Breach Science, Publishers S.A., 376p

LARSON, R.G. (1999)
The Structure and Rheology of Complex Fluids.
Oxford University Press: New York.

LARSSON, T.; NOCANDA, X.; SPARK, A.; BUSH, T.; OLSSON, A.; MADIKANE, M.; BISSESSUR, A. AND IVERSEN, T. (2007)

Cross polarisation/magic angle spinning 13 C-NMR spectroscopic studies of cellulose structural changes in hardwood dissolving pulp process

Holzforschung 61 (6), 675-679.

LEWANDOWSKI, Z. (2001)
Rheological aspects of fiber spinning from cellulose solutions in N-methylmorpholine-N-oxide.
J. Appl. Polym. Sci. 79, 1860-1869.

LI, J.; REVOL, J. F. AND MARCHESSAULT, R. H. (1996)
Rheological properties of aqueous suspensions of chitin crystallites.
Journal of Colloid and Interface Science 183(2), 365-373.

LI, J.; REVOL, J. F. AND MARCHESSAULT, R. H. (1997)
Effect of N-sulfonation on the colloidal and liquid crystal behaviour of chitin crystallites.
Journal of Colloid and Interface Science 192(2), 447-457.

LIU, R.; SHAO, H. AND HU, X. (2001)
The online measurement of lyocell fibers and investigation of elongational viscosity of cellulose N-methylmorpholine-N-oxide monohydrate solutions.
Macromol. Mater. Eng. 286, 179-186.

LIU, R. AND HU, X. (2006).

Precipitation kinetics of cellulose in the lyocell spinning process.
Ind. Eng. Chem. Res. 45, 2840-2844.

LOUBINOUX, D. AND CHAUNIS, S. (1985)
An experimental approach of spinning new cellulose fibres with NMMO (N-Methylmorpholine-oxide) as solvent of cellulose.
Lenzinger Berichte 59, 105-110.

MANNING, G. AND ZIMM, B. H. (1965)
Cluster theory of polyelectrolyte solutions I Activity coefficients of the mobile ions.
J. Chem. Phys. 43, 4250-4259.

MARCHESSAULT, R. H.; MOREHEAD, F. F. AND WALTER, N. M. (1959)
Liquid crystal systems from fibrillar polysaccarides.
Nature 184, 632-633.

MARCHESSAULT, R. H.; MOREHEAD, F. F. AND KOCH, M. J. (1961)
Some hydrodynamic properties of neutral suspension of cellulose crystallites as related to size and shape.
Journal of Colloid Science 16, 327-344.

MARSANO, E.; CORSINI, P.; AROSIO, C.; BOSCHI, A.; MORMINO, M. AND FREDDI, G. (2005)
Wet spinning of Bombyx mori silk fibroin dissolved in N-methyl morpholine N-oxide and properties of regenerated fibres.
Int. J. Biol. Macromol. 37, 179-188.

McCLEMENTS, D.J. AND DEMETRIADES, K. (1998)
An integrated approach to the development of reduced fat food emulsions.
Crit. Rev. Food Sci. Nutr. 38, 511-536.

MILLER, A. AND DONALD, A. (2002)
Surface and interfacial tension of cellulose suspensions.
Langmuir 18, 10155-10162.

MILLER, A. AND DONALD, A. (2003)
Imaging of anisotropic cellulose suspensions using environmental scanning electron microscopy.
Biomacromolecules 4, 510-517.

MORIN, A. AND DUFRESNE, A. (2002)
Nanocomposites of chitin whiskers from Riftia tubes and poly(caprolactone).
Macromolecules 35(6), 2190-2199.

MORTIMER, S. AND PÉGUY, A. (1996A)
Methods for reducing the tendency of lyocell fibers to fibrillate.
J. Appl. Polym. Sci. 60, 305-316.

MORTIMER, S. AND PÉGUY, A. (1996B)
The influence of air-gap conditions on the structure formation of lyocell fibers.

J. Appl. Polym. Sci. 60, 1747-1756.

MORTIMER, S. AND PEGUY, A. (1996C)
The formation of structure in the spinning and coagulation of lyocell fibres.
Cel. Chem. Technol. 30, 117-132.

MORTIMER, S. AND PEGUY, A. (1996D)
Influence of the physical process parameters on the structure formation of lyocell fibres.
Cel. Chem. Technol. 30, 251-256.

MOSS, C.; BUTLER, M.; MULLER, M. AND CAMERON, R. (2002)
Microfocus small-angle X-ray scattering investigation of the skin-core microstructure of lyocell fibers.
J. Appl. Polym. Sci. 83, 2799-2816.

MUKHERJEE, S. M. AND WOODS, H. J. (1953)
X-ray and electron microscope studies of the degradation of cellulose by sulphuric acid.
Biochimica et Biophysica Acta 10, 499-511.

NAGARKAR, S.; OJHA, R.; MANKAD, J.; PATIL, P.; SONI, V. AND LELE, A. (2006)
Measuring the elongation viscosity of lyocell using a semi-hyperbolic die.
Rheologica Acta 45, 260-267.

NEVELL, T.P. AND ZERONIAN, S.H.
Cellulose chemistry and its applications.
Ellis Horwood series chemical science, 1985, England.
ISBN 0-85312-704-2

NICKERSON F. AND HABRLE J.A. (1947)
Cellulose intercrystalline structure.
Industrial and Engineering chemistry 39(11), 1507-12.

NISHIYAMA, Y.; KUGA, S.; WADA, M. AND OKANO, T. (1997)
Cellulose microcrystal film of high uniaxial orientation.
Macromolecules 30(20), 6395-6397.

ODIJK, T. AND LEKKERKERKER, H. N. W. (1985)
Theory of the isotropic-liquid crystalline phase separation for a solution of bidisperse rodlike macromolecules.
J. Phys. Chem. 89, 2090-2096.

ODIJK, T. (1986)
Theory of lyotropic polymer liquid crystals.
Macromolecules 19, 2219-2313.

OHZAWA, Y.; NAGANO, Y. AND MATSUO, T. (1969)
Studies of dry spinning. I Fundamental equations.
J. Appl. Polym. Sci. 13, 257-283.

O'NEIL, A.J.; JEE, R.D. AND MOFFAT, A.C. (1998)

Measurement of the cumulative particle size distribution of microcrystalline cellulose using near infrared reflectance spectroscopy.
Analyst; 124 (1), 33-36.

ONOGI AND ASADA (1980)
Rheology and Rheo-Optics of Polymer Liquid Crystals, in Rheology, Ed. Astarita, G and Nicolais, Plenum, NY., pp. 127-147.

ONSAGER, L. (1949)
The effects of shape on the interaction of colloidal particles.
Ann.N.Y.Acad.Sci. 51, 627-659

ORTS, W. J.; GODBOUT, L.; MARCHESSAULT, R. H. AND REVOL, J. -F. (1995)
Flow-Induced structure in polymers;
Nakatani, A.I., Dadmun, M.D., Eds.; ACS Symposium Series, Vol 597; American Chemical Society: Washington, DC, p335

ORTS, W. J.; GODBOUT, L.; MARCHESSAULT, R. H. AND REVOL, J. -F. (1998)
Enhanced ordering of liquid crystalline suspensions of cellulose microfibrils: A small angle neutron scattering study.
Macromolecules 31(17), 5717-5725.

PADMANABHAN, M. (1995)
Measurement of extensional viscosity of viscoelastic liquid foods.
J. Food Engineering 25, 311-327.

PAILLET, M. AND DUFRESNE, A. (2001)
Chitin whisker reinforced thermoplastic nanocomposites.
Macromolecules 34(19), 6527-6530.

PETRIE, C. (1999)
The rheology of fibre suspensions.
J. Non-Newtonian Fluid Mech. 87, 369-402.

PETROVAN, S.; COLLIER, J. AND NEGULESCU, I. (2001)
Rheology of cellulosic N-methylmorpholine oxide monohydrate solutions of different degrees of polymerisation.
J. Appl. Polym.Sci., 79, 396-405.

RANBY, B.G. (1949)
Aqueous colloidal solutions of cellulose micelles.
Acta Chem. Stand 3, 649-650.

RANBY, B. G. AND RIBI, E. (1950)
The fine structure of cellulose
Experimentia, 6,12-14

RANBY, B. G. (1951)
The collodial properties of cellulose micelles.
Discussions of the Faraday Society 11, 158-164.

REES, L.H. (1974)
Evaluating homogenizers for chemical processing.
Chemical Engineering 86-92.

REVOL, J. –F. (1982)
On the cross sectional shape of cellulose crystallites inValonia ventricosa.
Carbohydrate Polymer 2, 123–134.

REVOL, J. -F.; BRADFORD, H.; GIASSON, J.; MARCHESSAULT, R. H. AND GRAY, D. G. (1992)
Helicoidal self-ordering of cellulose microfibrils in aqueous suspensions.
International Journal of Biological Macromolecules 14, 170-172.

REVOL, J. -F.; GODBOUT, L.; DONG, X. -M.; GRAY, D. G.; CHANZY, H. AND MARET, G. (1994)
Chiral nematic suspensions of cellulose crystallites; phase seperation and magnetic field orientation.
Liquid Crystals 16(1), 127-134.

REVOL, J.-F. AND MARCHESSAULT, R.H. (1996)
Single crystals and crystalline morphology of racemic poly(β-hydroxybutyrate).
Macromolecules 29, 2467-2471.

REVOL, J. -F.; GODBOUT, L.; DONG, X. M. AND GRAY D. G. (1997)
Solid liquid crystals of cellulose with optically variable properties.
US Patent 5,629,055

REVOL, J. -F.; GODBOUT, L. AND GRAY, D. G. (1998)
Solid self-assembled films of cellulose with chiral nematic order and optically variable properties.
Journal of Pulp and Paper Science 24(5), 146-149.

ROMAN, M. AND WINTER, W. T. (2004)
Effect on sulfate groups from sulphuric acid hydrolysis on the thermal degradation behaviour of bacterial cellulose.
Biomacromolecules 5, 1671-1677.

ROMO-URIBE, A. AND WINDLE, A. (1999)
A rheo-optical and dynamic X-ray scattering study of flow-induced textures in main-chain thermotropic liquid-crystalline polymers. The influence of molecular weight.
Proc. Roy. Soc. London A, 455, 1175-1201.

ROSEVEARE, W.E.; WALLER, R.C. AND WILSON, J.N. (1948)
Structure and properties of regenerated cellulose.
Textile Research Journal 18, 114-23

SAIN, M AND BHATNAGAR, A. (2005)
Manufacturing of nano-fibrils from natural fibres, agro based fibres and root fibres.
Canadian Patent CA 2,437,616

SASSI J.-F. AND CHANZY H. (1995)
Ultrastructural aspects of the acetylation of cellulose.
Cellulose 2, 111-127.

SASSI, J. -F.; CHANZY H.; FLEURY E. AND CAVAILLE J.- Y. (1997)
Surface-modified cellulose microfibrils, method for making the same, and use thereof as a filler in composite materials, WO9712917.

SATO, T. AND TERAMATO A. (1991)
Statistical Mechanics and its Applications
A. Physica, 176, 72-86.

SCHUSTER, K.; ALDRED, P.; VILLA, M.; BARON, M.; LOIDL, R.; BIGANSKA, O.; PATLAZHAN, S.; NAVARD, P.; RUF, H. AND JERICHA, E. (2003)
Characterising the emerging lyocell fibres structures by ultra small angle neutron scattering (USANS).
Lenzinger Berichte 82, 107-117.

SEMENOV, A.N. AND KOKHLOV, A.R. (1988)
Statistical physics of liquid-crystalline polymers.
Sov.Phys. Usp 31(11), 988-1014.

SHAHIN, M. (2003).
Optical microscopy study on poly(p-phenylene terephthalamide) fibers.
J. Appl. Polym. Sci., 90, 360-369.

SHAO, Z.; VOLRATH, F.; YANG, Y. AND THARGERSEN, H. (2003)
Structure and behaviour of regenerated spider silk.
Macromolecules 36, 1157-1161.

SJOSTROM, E. (1981)
Word chemistry: Fundamentals and Applications, 2nd ed.; Academic press: New York

SONG, W. AND WINDLE, A. (2005)
Isotropic-nematic phase transition of dispersions of multi-wall carbon nanotubes.
Macromolecules 38, 6181-6188.

SPREY, B. AND BOCHEM, H. P. (1991)
Electron microscopic observations of cellulose microfibril degradation by endocellulase from Trichoderma reesei, FEMS Microbiology Letters 78, 183-188.

STROOBANTS, A,; LEKKERKERKER, H.N.W. AND ODIJK, T. (1986)
Effects of Electrostatic Interaction on the Liquid Crystal Phase Transition in Solutions of Rodlike Polyelectrolytes.
Macromolecules 19, 2232-2238.

SUGIYAMA, J.; HARADA, H.; FUJIYOSHI, Y. AND UYEDA, N. (1984)
High resolution observations of cellulose microfibrils.
Mokuzai Gakkaishi 30(1), 98-99.

SUGIYAMA, J.; CHANZY, H. AND MARET, G. (1992)
Orientation of cellulose microcrystals by strong magnetic fields.

Macromolecules 25, 4232-4234.

SUGIYAMA, J.; CHANZY, H. AND REVOL, J.F. (1994)
On the polarity of cellulose in the cell wall of Valonia.
Planta 193, 260.

TANIGUCHI, T. AND OKAMURA, K. (1998)
New Films Produced from Microfibrillated Natural Fibres.
Polymer Int. 47, 291-294.

TERECH, P.; CHAZEAU, L. AND CAVAILLE, J.Y. (1999)
A small-angle scattering study of cellulose whiskers in aqueous suspensions.
Macromolecules 32(6), 1872-1875.

TURBAK, A.F.; SNYDER, F.W. AND SANDBERG, K.R. (1983)
Microfibrillated Cellulose. US Patent 4,374,702.

TURNER, P.; HERNANDEZ, Z. AND CALLUM, H. (2010) (2011)
Process for the manufacture of cellulose-based fibres and the fibres thus obtained.
PCT/GB2009/051356
P116339 GB 01/EBA/SCR

WARNER, S. (1983)
On the radial structure of Kevlar.
Macromolecules 16, 1546-1548.

WESTERMARCK, S.; JUPPO, A.M.; KERVINEN, L. AND YLIRUUSI, J. (1999)
Microcrystalline cellulose and its microstructure in pharmaceutical processing.
Eur. J. Pharm. Biopharm. 48(3), 199-206.

WOODINGS, C. (1995)
The development of advanced cellulosic fibres.
Int. J. Biol. Macromol. 17, 305-309.

XU, J.; CHATTERJEE, S.; KOELLING, K.; WANG, Y. AND BECHTEL, S. (2005)
Shear and extensional rheology of carbon nanofiber suspensions.
Rheol. Acta. 44, 537-562.

YOSHIHARU, N.; SHIGENORI, K.; MASAHISA W. AND TAKESHI, O. (1997)
Cellulose microcrystal film of high uniaxial orientation.
Macromolecules 30, 6395-6397.

ZABRISKIE D.W. (1984)
Enzymatic preparation of particulate cellulose for tablet making.
US Patent 4,427,778

ZIMMERMANN, T.; POHLER, E.; GEIGER, T. (2004)
Cellulose fibrils for polymer reinforcement.
Advanced Engineering Materials 6(9).

ZUGENMAIER, P. (1994)
Cellulose derivatives systems, in cellulosic polymers, blends and composites.
Gilbert, R.D. Ed., Hanser, NY., 71-94.

ZULUAGA , R.; PUTAUX, J-L.; RESTREPO, A.; MONDRAGON, I.; GANAN, P. (2007)
Cellulose microfibrils from banana farming residues: isolation and characterisation.
Cellulose 14, 585–592.

Appendix A

Test Report: **EH8371**

The Analysis of a Water Sample for a 70-Element Scan by ICP-MS and ICP-AES

Prepared for Zurine Hernandez

Centre for Timber Engineering

August 2009

scientifics

The Analysis of a Water Sample for a 70-Element Scan by ICP-MS and ICP-AES

Customer:	Zurine Hernandez Centre for Timber Engineering Napier University Merchiston Campus 10 Colinton Road Edinburgh EH10 5DT
Testing Facility:	Scientifics Ltd, Harwell Laboratory 551 South Becquerel Avenue Harwell Science and Innovation Campus Didcot Oxfordshire OX11 0TB
Laboratory Reference:	EH8371
Customer Reference:	Tap Water from Edinburgh Napier University
Quote Number:	MET-HAR-5831
Samples Received:	10 August 2009
Sample Condition:	Good
Analysis Completed:	19 August 2009
Approved by:	PHOLP
Date:	24/08/2009
Approver's name:	Phil Holdship
Job Title:	Senior Analyst
Checked by:	Rebeca Zorrilla
Date:	24/08/09
Checker's name:	Rebeca Zorrilla
Job Title:	Senior Analyst
Report Date:	24 August 2009

UKAS TESTING
1015

scientifics

Introduction

One sample of water was received for the measurement of a 70 Element Scan. The liquid sample was within a plastic vial. This vial was received in good condition. The sample was logged into our system upon receipt and then stored in a secure sample store, prior to analysis.

Experimental

This sample was analysed by ICP-MS and ICP-AES, following methods HS/WI/1002 *'Operation and maintenance of inductively coupled plasma mass spectrometers (ICP-MS)'* issue 18 and HS/WI/1075 *'Operation and Maintenance of Perkin Elmer Optima 4300 Inductively Coupled Plasma Atomic Emission Spectrometer (ICP-AES)'*, issue 8, respectively.

Measurements of all 70 elements, were conducted using a combination of ICP-MS and ICP-AES- which were calibrated using assayed standards, containing the 70 elements of interest.

ICP-MS

Portions of the sample were diluted in 2% nitric acid; containing de-ionised water of resistivity 18.2 MΩ.cm and concentrated nitric acid (Romil SpA grade, batch: R539428).

Indium was also added to the sample solutions as an internal standard to monitor and correct for instrument drift. Subsequent semiquantification calculations were conducted using the ICP-MS software (Chemstation G1834B).

scientifics

Results

The results for the samples are detailed in the table attached.

Results for the samples are expressed as $\mu g.L^{-1}$.

The LOD is the limit of detection and is defined as three times the standard deviation obtained from the measurement of a series of at least five instrument blanks. Measurement uncertainty for those results significantly above the LOD is estimated to be ± 20%.

The measurement of a 70-Element Scan in solution by ICP-MS and ICP-AES is accredited by UKAS.

Any opinions and interpretations expressed herein are outside the scope of our UKAS accreditation.

scientifics

Results from the Analysis of a Water Sample for a 70-Element Scan by ICP-MS and ICP-AES

Customer Reference		Tap Water from Edinburgh Napier University
Laboratory Reference	LOD	EH8371
Li	0.3	0.3
Be	10	<10
B	50	<50
Na	20	2300
Mg	1	1500
Al	10	<10
Si	700	<700
P	70	600
K	20	230
Ca	1	9700
Sc	0.08	1.1
Ti	1	<1
V	2	<2
Cr	1	<1
Mn	4	<4
Fe	1	<1
Co	10	<10
Ni	10	<10
Cu	20	<20
Zn	3	<3
Ga	1	2
Ge	0.2	0.5

1. Results are expressed as $\mu g.L^{-1}$ in the sample as received.
2. Results over an order of magnitude above the LOD are estimated to have an uncertainty of ±50%.
3. Results within an order of magnitude of the LOD have a high uncertainty and are reported to one significant figure.

UKAS TESTING
1015

scientifics

Results from the Analysis of a Water Sample for a 70-Element Scan by ICP-MS and ICP-AES

Customer Reference		Tap Water from Edinburgh Napier University
Laboratory Reference	LOD	EH8371
As	10	<10
Se	10	<10
Rb	0.7	3
Sr	10	30
Y	0.006	0.06
Zr	0.02	0.2
Nb	0.03	<0.03
Mo	10	<10
Tc	0.3	0.5
Ru	0.03	0.03
Rh	0.005	0.005
Pd	0.05	0.05
Ag	0.01	0.01
Cd	10	<10
In	10	<10
Sn	10	<10
Sb	20	<20
Te	20	<20
Cs	0.008	0.009
Ba	10	30
La	1	2
Ce	0.03	0.05
Pr	0.009	0.01
Nd	0.2	<0.2
Sm	0.09	<0.09

1. Results are expressed as $\mu g.L^{-1}$ in the sample as received.
2. Results over an order of magnitude above the LOD are estimated to have an uncertainty of ±50%.
3. Results within an order of magnitude of the LOD have a high uncertainty and are reported to one significant figure.

UKAS TESTING
1015

scientifics

Results from the Analysis of a Water Sample for a 70-Element Scan by ICP-MS and ICP-AES

Customer Reference		Tap Water from Edinburgh Napier University
Laboratory Reference	LOD	EH8371
Eu	0.01	0.01
Gd	0.06	<0.06
Tb	0.003	0.007
Dy	0.006	0.008
Ho	0.006	<0.006
Er	0.02	<0.02
Tm	0.005	<0.005
Yb	0.02	0.03
Lu	0.007	0.01
Hf	0.03	0.04
Ta	0.008	0.01
W	0.6	<0.6
Re	0.03	<0.03
Os	0.03	0.07
Ir	0.02	0.02
Pt	0.04	<0.04
Au	0.08	<0.08
Hg	70	<70
Tl	0.03	0.03
Pb	10	<10
Bi	0.05	<0.05
Th	0.008	0.01
U	0.01	0.03

1. Results are expressed as $\mu g.L^{-1}$ in the sample as received.
2. Results over an order of magnitude above the LOD are estimated to have an uncertainty of ±50%.
3. Results within an order of magnitude of the LOD have a high uncertainty and are reported to one significant figure.

UKAS TESTING
1015